International Journal of Photoenergy

Photobiomodulation

Guest Editors: Timon Cheng-Yi Liu, Rui Duan, and Lutz Wilden

Photobiomodulation

International Journal of Photoenergy

Photobiomodulation

Guest Editors: Timon Cheng-Yi Liu, Rui Duan, and Lutz Wilden

Editorial Board

Contents

Photobiomodulation, Timon Cheng-Yi Liu, Rui Duan, and Lutz Wilden
Volume 2012, Article ID 352582, 1 page

Photobiomodulation on Stress, Timon Cheng-Yi Liu, Yan-Ying Liu, En-Xiu Wei, and Fang-Hui Li
Volume 2012, Article ID 628649, 11 pages

Photobiomodulation Process, Yang-Yi Xu, Timon Cheng-Yi Liu, and Lei Cheng
Volume 2012, Article ID 374861, 7 pages

Efficacy of Proliferation of HeLa Cells under Three Different Low-Intensity Red Lasers Irradiation, H. Q. Yang, Y. H. Wang, J. X. Chen, X. G. Chen, Y. M. Huang, H. Li, S. S. Xie, and L. Q. Zheng
Volume 2012, Article ID 290796, 5 pages

Low-Dose UVA Radiation-Induced Adaptive Response in Cultured Human Dermal Fibroblasts, Zhongrong Liu, Hulin Chen, Huilan Yang, Jie Liang, and Xuemei Li
Volume 2012, Article ID 167425, 11 pages

LED Light-Activated Hypocrellin B Induces Mitochondrial Damage of Ovarian Cancer Cells, Yuan Jiang, Albert Wingnang Leung, Junyan Xiang, and Chuanshan Xu
Volume 2012, Article ID 186752, 5 pages

Inhibitory Effects of Far-Infrared Ray-Emitting Belts on Primary Dysmenorrhea, Ben-Yi Liau, Ting-Kai Leung, Ming-Chiu Ou, Cheng-Kun Ho, Aiga Yang, and Yung-Sheng Lin
Volume 2012, Article ID 238468, 6 pages

Assessing the Therapeutic Effect of 630 nm Light-Emitting Diodes Irradiation on the Recovery of Exercise-Induced Hand Muscle Fatigue with Surface Electromyogram, Dandan Yang, Xiaoying Wu, Wensheng Hou, Xiaolin Zheng, Jun Zheng, and Yingtao Jiang
Volume 2012, Article ID 652040, 8 pages

TiO_2 and N-Doped TiO_2 Induced Photocatalytic Inactivation of Staphylococcus aureus under 405 nm LED Blue Light Irradiation, Hongfei Chen, Zhong Xie, Xiujuan Jin, Chao Luo, Chao You, Ying Tang, Di Chen, Zhengjia Li, and Xiaohong Fan
Volume 2012, Article ID 848401, 5 pages

Nd:YAG Lasers Treating of Carious Lesion and Root Canal In Vitro, Danqing Xia, Zenggui Mo, Gang Zhao, Fei Guo, Chao You, Ze Chen, Xiao Zhu, Zhengjia Li, Di Chen, and Xiaohong Fan
Volume 2012, Article ID 584079, 5 pages

Laser Acupuncture Reduces Body Fat in Obese Female Undergraduate Students, Xiao-Guang Liu, Juan Zhang, Jian-Liang Lu, and Timon Cheng-Yi Liu
Volume 2012, Article ID 730351, 4 pages

Aquaporin-1-Mediated Effects of Low Level He-Ne Laser Irradiation on Human Erythrocytes, Gang-Yue Luo, Li Sun, and Timon Cheng-Yi Liu
Volume 2012, Article ID 275209, 5 pages

Randomized, Double-Blind, and Placebo-Controlled Clinic Report of Intranasal Low-Intensity Laser Therapy on Vascular Diseases, Timon Cheng-Yi Liu, Lei Cheng, Wen-Juan Su, Yi-Wen Zhang, Yun Shi, Ai-Hong Liu, Li-Li Zhang, and Zhuo-Ya Qian
Volume 2012, Article ID 489713, 5 pages

Light-Emitting Diode-Based Illumination System for *In Vitro* Photodynamic Therapy, Defu Chen, Huifen Zheng, Zhiyong Huang, Huiyun Lin, Zhidong Ke, Shusen Xie, and Buhong Li
Volume 2012, Article ID 920671, 6 pages

Effects of Low-Intensity Laser Irradiation on Wound Healing in Diabetic Rats, Hui Ma, Ying-xin Li, Hong-li Chen, Mei-ling Kang, and Timon Cheng-Yi Liu
Volume 2012, Article ID 838496, 7 pages

Hindawi Publishing Corporation
International Journal of Photoenergy
Volume 2012, Article ID 352582, 1 page
doi:10.1155/2012/352582

Editorial

Photobiomodulation

Timon Cheng-Yi Liu,[1] Rui Duan,[2] and Lutz Wilden[3]

[1] *Laboratory of Laser Sports Medicine, South China Normal University, Guangzhou 510006, China*
[2] *Department of Molecular Biology and Genetics, Johns Hopkins University School of Medicine, Baltimore, MD 21205, USA*
[3] *Privatpraxis für Hochdosierte Low Level Lasertherapie, Wilden, L. Kuralle 16, 94072 Bad Füssing, Germany*

Correspondence should be addressed to Timon Cheng-Yi Liu, liutcy@scnu.edu.cn

Received 5 August 2012; Accepted 5 August 2012

Traditionally, lasers have been utilized in many aspects of medicine, such as surgery, cancer treatment, and cosmetic applications. The laser irradiation that was commonly used in cosmetic surgery or cancer therapy is high intensity laser irradiation which can cut through the human bodies and burn the tissues. Except this well-known high intensity laser therapy, there is another type of laser therapy, photobiomodulation (PBM), in which a low level/intensity/power laser irradiation or monochromatic light is used to modulate biological functions without irreversible damage. It has been widely used to reduce pain and inflammation, accelerate wound healing and hair growth, prevent cell death and tissue damage, and improve blood circulation since the invention of lasers in the 1960s. Currently, PBM is not only used to treat diseases, but also used to promote health.

Despite many laboratory experiments and clinical trials, the cellular and molecular mechanisms of PBM continue to be elusive. In this special edition, we present peer-reviewed up-to-date studies which focused on the mechanisms of PBM and its clinical applications.

The original research articles covered many aspects of PBM, from basic biomedical research to clinic applications, from *in vitro* cell-based studies to *in vivo* human tissues. In the two review papers, the authors proposed an interesting theory of PBM based on the function-specific homeostasis, which is a negative feedback response for a function to be perfectly performed. Besides the studies on PBM, we also selected several papers on photodynamic therapy and laser surgery in the current issue.

We highly appreciate the quality, originality, and novelty of the studies submitted to this special issue, and we welcome the proposal of the journal to publish a second special issue dedicated to the field of PBM in the near future.

Timon Cheng-Yi Liu
Rui Duan
Lutz Wilden

Hindawi Publishing Corporation
International Journal of Photoenergy
Volume 2012, Article ID 628649, 11 pages
doi:10.1155/2012/628649

Review Article

Photobiomodulation on Stress

Timon Cheng-Yi Liu,[1,2] Yan-Ying Liu,[1,2] En-Xiu Wei,[1,2] and Fang-Hui Li[1,2]

[1] *Laboratory of Laser Sports Medicine, South China Normal University, Guangzhou 510006, China*
[2] *The Key Laboratory of Laser Life Science of Ministry of Education of China, South China Normal University, Guangzhou 510631, China*

Correspondence should be addressed to Timon Cheng-Yi Liu, liutcy@scnu.edu.cn

Received 17 February 2012; Revised 17 June 2012; Accepted 25 June 2012

Academic Editor: Rui Duan

Photobiomodulation (PBM) is a nondamaged modulation of laser irradiation or monochromatic light (LI) on a biosystem function. It depends on whether the function is in its function-specific homeostasis (FSH). An FSH is a negative-feedback response of a biosystem to maintain the function-specific conditions inside the biosystem so that the function is perfectly performed. A function in its FSH is called a normal function. A function far from its FSH is called a dysfunctional function. The process of a function from dysfunctional to normal is called a functional normalization. For a normal function in its FSH, there are FSH-essential subfunctions (FESs), FSH-nonessential subfunctions (FNSs), and an FES/FNS-specific homeostasis (FESH/FNSH). A FSH can resist internal/external disturbances under the threshold, but can be disrupted by an FSH-specific stress (FSS). A normal/dysfunctional FSS is called a successful/chronic stress. An FESH/FNSH-specific stress was called an extraordinary/ordinary stress. A low level LI (LLL) cannot directly affect a normal function, but can modulate a chronic stress. A normal function may have a chronic ordinary stress, and an LLL may modulate the chronic ordinary stress so that it promotes the normalization of the dysfunctional FNS and then upgrades the normal function. A high level LI can modulate a normal function and may be a successful stress.

1. Introduction

The human mind and body respond to stress [1, 2], a state of perceived threat to homeostasis, by activating the sympathetic nervous system and secreting the catecholamines adrenaline and noradrenaline in the "fight-or-flight" response. The stress response is generally transient because its accompanying effects (e.g., immunosuppression, growth inhibition, and enhanced catabolism) can be harmful in the long term. When chronic, the stress response can be associated with disease symptoms such as peptic ulcers or cardiovascular disorders and leads to DNA damage [3]. Stress is also broadly defined as a noxious factor (physical, chemical, or biological), which triggers a series of cellular and systemic events, resulting in restoration of cellular and organismal homeostasis [4, 5]. It was re-defined from the viewpoint of our function-specific homeostasis (FSH) [6–8] and its photobiomodulation (PBM) was discussed in this paper.

2. Function-Specific Homeostasis

Negative feedback is common in biological processes and can increase a system's stability to internal and external perturbations [9]. An FSH is a negative-feedback response of a biosystem to maintain the function-specific conditions inside the biosystem so that the function is perfectly performed [6–8]. A function in its FSH is called a normal function. A function far from its FSH is called dysfunctional function. The process of a function from dysfunctional to normal is called functional normalization. A normal function is better performed than all the dysfunctional functions so that the normal function is locally the best performed one. A biosystem in an FSH means its normal function is in its FSH. A biosystem far from an FSH means its dysfunctional function is far from its FSH. Youk et al. have studied log-phase growth rates of single-HXT2 (hexose transporter 2) strain of yeasts at varying [glucose] but constant [doxycycline] (2.5 μg/mL) and

found the growth rate peaked in glucose between 0.06% and 0.20%, which corresponded to the normal growth that resists the concentration change of glucose between 0.06% and 0.20% [10]. We also have found that these are the best concentrations of glucose, normal glucose, in which C2C12 cells proliferated in their optimal rate and between which there was no significant difference of the proliferation rate, and the low/high glucose whose concentration was lower/higher than the one of normal glucose, and in which the C2C12 cells proliferated in a rate lower than the optimal rate [11–13]. In other words, the C2C12 cell proliferation in normal glucose was a normal proliferation which resisted the concentration change in the normal glucose.

The quality of an FSH, the functional fitness of a normal function, includes function complexity and function stability. At the molecular level, control loops always involve signalling steps with finite rates for random births and deaths of individual molecules. Lestas et al. have shown that seemingly mild constraints on these rates place severe limits on the ability to suppress molecular fluctuations [9]. Specifically, the minimum standard deviation in abundances decreases with the quartic root of the number of signalling events. In other words, the higher the function complexity, the higher the function stability. Let Q be the functional fitness of a normal function. A biosystem might simultaneously have many kinds of normal functions, $\{\mathrm{FSH}_i,\ i = 1, 2, \ldots, n\}$, and then have functional fitness set, $\{Q_i,\ i = 1, 2, \ldots, n\}$. Let $Q\max = \max\{Q_i,\ i = 1, 2, \ldots, n\}$, and Fmax and FmaxSH denote the corresponding normal function and its homeostasis, respectively. For proliferative cells in 10% fetal calf serum (FCS), proliferation and its PlSH may be generally Fmax and FmaxSH, respectively.

3. Stress

The response of a biosystem in an FSH to internal/external disturbances depends on the disturbance level. A normal function in its FSH can resist a low level disturbance, but cannot resist a high level disturbance. The high level disturbance is defined as a stressor, an FSH-specific stressor (FSSor), in this paper. In other words, a FSSor is so defined that it disrupts its corresponding FSH. A psychological/physiological/cellular stressor disrupts its corresponding psychological/physiological/cellular-function-specific homeostasis. An oxidative stressor disrupts a redox-specific homeostasis. The FSSor dose depends on its intensity and its action time. A strong FSSor can disrupt its corresponding FSH in a short time, but a weak FSSor can also disrupt its corresponding FSH in a long time. Burd et al. found that low-load high volume resistance exercise is more effective in inducing acute muscle anabolism than high-load low volume or work-matched resistance exercise modes [14].

3.1. FSH-Specific Stress. The response of a biosystem in a FSH to internal/external disturbance is FSH-specific. Fibroblasts from long-lived mutant mice are resistant to many forms of lethal injury as well as to the metabolic effects of rotenone and low-glucose medium. Salmon et al. have evaluated fibroblasts from young adult naked mole-rats (NMR) [15], a rodent species in which maximal longevity exceeds 28 years. Compared to mouse cells, NMR cells were resistant to cadmium, methyl methanesulfonate, paraquat, heat, and low-glucose medium, consistent with the idea that cellular resistance to stress may contribute to disease resistance and longevity. Surprisingly, NMR cells were more sensitive than mouse cells to H_2O_2, ultraviolet (UV) light, and rotenone. NMR cells, like cells from Snell dwarf mice, were more sensitive to tunicamycin and thapsigargin, which interfere with the function of the endoplasmic reticulum (ER). The sensitivity of both Snell dwarf and NMR cells to ER stress suggests that alterations in the unfolded protein response might modulate cell survival and aging rate.

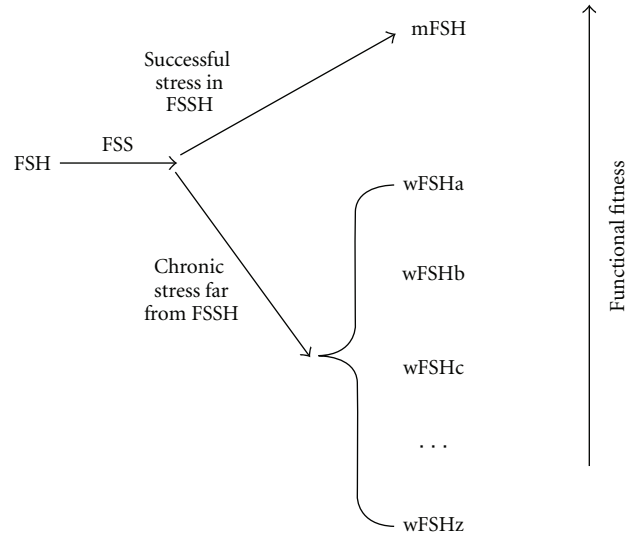

Figure 1: Successful stress and chronic stress. After the existing FSH is disrupted, many possible kinds of wFSH would be established. Among them, the wFSH of the highest functional fitness, mFSH, would be established by the FSS in its FSSH so that the normal FSS is called a successful stress; the other kinds of wFSH, wFSHa, wFSHb, wFSHc, …, or wFSHz would be established by the FSS far from FSSH so that the dysfunctional FSS is called a chronic stress.

3.2. Successful Stress and Chronic Stress. An FSH-specific stress (FSS) is defined as a response of a biosystem in its FSH to an FSSor. It is also a function of a biosystem and there is an FSS-specific homeostasis (FSSH). After the existing FSH is disrupted by a FSS, many possible kinds of would-be FSH (wFSH) would be established (Figure 1). Among them, the wFSH of the highest functional fitness, mFSH, would be established by the FSS in its FSSH so that the normal FSS is called a successful stress such as self-limiting/limited conditions [16, 17]; the other kinds of wFSH, wFSHa, wFSHb, wFSHc, …, or wFSHz would be established by the FSS far from FSSH so that the dysfunctional FSS is called a chronic stress such as the delayed self-limiting/limited conditions. In protein folding and secretion disorders, successful activation of ER stress signaling protects cells, alleviating stress that would otherwise trigger apoptosis. Studies in chondrocytes, which abundantly secrete collagens, have shown that dedifferentiation away from a secretory cell

phenotype may play a role in adaptation to chronic ER stress [18]. This suggests that the pathogenic features of chronic ER stress may be played out not only at the level of cell death but also at the level of altered cell function.

Self-limited/limiting conditions [16, 17] are examples of successful stress unless they are compromised. In immunocompetent hosts, the infection is self-limiting [19]. Inflammation involves a coordinated, sequential, and self-limiting sequence of events controlled by positive and negative regulatory mechanisms [20]. Bazzoni et al. found Toll/interleukin (IL)-1 receptor activated nuclear factor (NF) kappaB rapidly increases the expression of miR-9 that operates a negative feedback control of the NF-kappaB-dependent responses by fine tuning the expression of a key member of the NF-kappaB family [20]. Photoparoxysmal responses (PPRs) are generalized epileptiform abnormalities occurring during photic stimulation. Prolonged PPRs, which outlast the stimulus, can be distinguished from self-limited PPRs, which cease spontaneously or when the flashes stop. Comparing PPR groups, Puglia et al. found that a prolonged PPR was associated with a higher incidence of seizures than a self-limited response, and patients with a prolonged PPR more often had other epileptiform abnormalities than the self-limited group [21]. Kumar et al. infected mice with sublethal influenza A virus [22]. Despite early damage to lungs after infection, they had essentially returned to normal 3 months later. Repair was initiated by stem cells that proliferated in the bronchiolar epithelium and migrated to sites of damage, where they formed clusters around bronchioles and differentiated into alveolar structures destroyed by the infection. This is a typical self-limited condition. Its delayed cases can cause extensive, life-threatening lung pathology in humans.

Generally, the functional fitness of a normal function is higher than the one of a successful stress. A successful stress is easily disrupted by other stressors. The training program plateau [23] corresponded to the sport-specific homeostasis (SpSH). Exercise stress can disrupt SpSH1, which induces delayed onset muscle soreness (DOMS) [24]. A successful exercise stress such as a bout of eccentric exercise or high intensity exercise can further establish SpSH2, and its DOMS is self-limited [25]. However, the DOMS might be delayed due to exhaustive eccentric exercise, insulin resistance, or aging.

3.3. Extraordinary Stress and Ordinary Stress. A complicated biosystem is just a network of functions [9]. There are many subfunctions to maintain a normal function/Fmax, FSH/FmaxSH-essential subfunctions (FESs/FmaxESs) and FSH/FmaxSH-nonessential subfunction (FNSs/FmaxNSs). FESs/FmaxESs might be very sparse [6]. This sparse characteristic is also supported by the theoretical study of the steady-state fluctuation. Fluctuations in the abundance of molecules in the living cell may affect their growth and well-being. For regulatory molecules (e.g., signaling proteins or transcription factors), fluctuations in their expression can affect the levels of downstream targets in a metabolic network. Levine et al. have developed an analytic framework to investigate the phenomenon of noise correlation in molecular networks, and they found the steady-state fluctuation in different nodes of the pathways to be effectively uncorrelated for all but one case examined [26]. Consequently, fluctuations in enzyme levels only affect local properties and do not propagate elsewhere into metabolic networks, and intermediate metabolites can be freely shared by different reactions [26].

For a normal function/Fmax, all the FESs/FmaxESs should be in their respective FES/FmaxES-specific homeostasis (FESH/FmaxESH), but some FNSs/FmaxNSs may be allowed far from their respective FNS/FmaxNS-specific homeostasis (FNSH/FmaxNSH). Obviously, the more the FNSs/FmaxNSs in their FNSH/FmaxNSH, the higher their functional fitness. The response of a biosystem to a FSSor disrupting a FESH/FmaxESH or FNSH/FmaxNSH is defined as an extraordinary or ordinary stress of the function in this paper.

Inhibitors of epidermal growth factor receptor (EGFR) signaling might induced an extraordinary stress of tumor cells in their respective PlSH. Chemotherapeutic agents that induce the DNA damage response (DDR) are typically used to kill tumor cells; however, the effects of aberrant growth factor signaling, for example, can lead to resistance. Lee et al. took a systems-level approach to examine the interplay between growth factor signaling and the DDR in triple-negative breast cancer (TNBC) cells [27], which respond poorly to standard therapies. The greatest extent of apoptosis was caused by pretreatment with inhibitors of EGFR signaling before treatment with the DNA-damaging agent doxorubicin; simultaneous treatment with these compounds was not as potent. Prolonged (6 hours) EGFR inhibition led to changes in the expression of many genes, which suggested that the oncogenic potential of some TNBC cells is dependent on EGFR signaling. The staggered application of EGFR inhibitor and doxorubicin induced cell death in lung cancer cell lines in a caspase 8—dependent manner. It was found that the timed application of signaling inhibitors causes the rewiring of signaling pathways in tumor cells and makes them more susceptible to subsequent DDR-inducing therapy.

Obviously, there may be an ordinary stress for a normal function/Fmax, and its functional fitness can be upgraded through its successful ordinary stress. The successful ordinary stress might be mediated by redundant genes/pathways. Genetic redundancy means that two or more genes are performing the same function and that inactivation of one of these genes has little or no effect on the biological phenotype [28]. The two or more genes and their corresponding pathways are redundant genes and redundant pathways, respectively. Fibroblast growth factor (FGF) 1 is the prototype of the 22-member FGF family of proteins and has been implicated in a range of physiological processes, including development, wound healing, and cardiovascular changes. Surprisingly, FGF1 knockout mice display no significant phenotype under standard laboratory conditions. Jonker et al. show that FGF1 is highly induced in adipose tissue in response to a high-fat diet and that mice lacking FGF1 develop an aggressive diabetic phenotype coupled to aberrant adipose expansion when challenged with a high-fat diet [29]. Obviously, FGF1 is a redundant pathway which is induced in response to a high-fat diet. Allison et al. have summarized the potential

impacts of a disturbance on microbial composition and/or ecosystem processes [30]. Consider an increasing disturbance applied to an ecosystem and the microbial communities within it. Microbial composition might be resistant to the very-low-level disturbance and might not change. For a low level disturbance, the community is sensitive and does change, it could be resilient and quickly recover to its initial composition through homeostatic mechanism. For a rather-high level disturbance which induces a successful ordinary stress, a community whose composition is sensitive and not resilient might produce process rates similar to the original community through redundant pathways if the members of the community are functionally redundant. For a high level disturbance which induces a successful extraordinary stress, the community performs differently.

4. Photobiomodulation

Modulation can be classified into low level modulation and high level modulation. Low level modulation cannot directly modulate a normal function, but can modulate a chronic stress. High level modulation can modulate a normal function, which might be a successful stress. It has been found [24] that low level modulation cannot promote the functional recovery of self-limiting DOMS, but high level modulation can. From this viewpoint, PBM was discussed in this section.

PBM is a modulation of laser irradiation or monochromatic light (LI) on biosystems, which stimulates or inhibits biological functions but does not result in irreducible damage. The LI intensity is in the range of 10–1000 mW/cm^2 [31, 32]. As we have classified [6–8], the LI used in PBM is always low intensity LI (LIL), ~10 mW/cm^2, which includes the LI used in the so-called ultra-low-level laser therapy [33], but moderate intensity LI (MIL), 0.10~1.0 W/cm^2, is of PBM if the irradiation time is not so long that it damages organelles or cells. The PBMs of LIL and MIL are denoted as LPBM and MPBM, respectively. The MIL with short irradiation time and LIL are two kinds of low level LI (LLL), and their PBM is a kind of low level modulation and is called low level PBM. The PBM of MIL with long irradiation time is a kind of high level modulation and is called high level PBM.

For a normal function/Fmax, there may be a chronic ordinary stress. Low level PBM cannot directly modulate the normal function/Fmax, but it can modulate the chronic ordinary stress until it is successful and then upgrade the normal function/Fmax. At this point, low level PBM can be divided into two kinds, the direct PBM (dPBM) and indirect PBM (iPBM). Direct PBM cannot directly modulate a normal function, but can modulate a chronic stress. A normal function/Fmax cannot be directly modulated by dPBM, but can be upgraded by iPBM if there is at least a chronic ordinary stress. High level PBM, dPBM, and iPBM will then be detailedly discussed.

4.1. Direct Photobiomodulation. There were no dPBM on human osteosarcoma cell line, SAOS-2 [34], HeLa (epithelial adenocarcinoma) and TK6 (lymphoblast) [35], murine fibroblast 3T3 cells, primary human keloid fibroblast cells [36], and osteogenic cells [37] in 10% FCS. Proliferation in 10% FCS is always normal proliferation so that LLL cannot directly modulate the proliferation. Schwartz-Filho et al. have studied MPBM (685 nm) on osteogenic cells originated from rat calvaria [37]. The cells were irradiated immediately after plating and after each change of culture medium. They found that the MPBM at 3.5 W/cm^2 cannot modulate their proliferation in 10% FCS at 25, 77, and 130 J/cm^2, respectively, at days 1, 4, 7, and 11 but promoted mineralized bone-like nodule formation is only at 25 J/cm^2 at day 14.

Normal erythrocyte deformability is maintained by deformability-specific homeostasis (DeSH). According to Mi et al. [38], the DeSH of pig erythrocytes was maintained in 0 and 0.5 mM $CaCl_2$ so that the MIL at 532 or 632.8 nm cannot directly modulate the deformability, but it was disrupted in 1.0, 1.5, and 2.0 mM $CaCl_2$ or 10 uM A23187 so that the MIL can modulate the deformability.

Many functions of nondiabetic rats may be normal, but the ones of diabetic rats may be dysfunctional. Rabelo et al. have compared diabetic with nondiabetic rats (male Wistar) and found MPBM (632.8 nm) of 15 days has no effects on informatory cells, vessels, and fibroblastic cells of nondiabetic rats but inhibited informatory cells and promoted fibroblastic cells of diabetic rats [39].

Mafra de Lima et al. have found that LIL at 650 nm had no effects on rat lung [40], but attenuated acute lung inflammation induced by aerosol of lipopolysaccharide from Escherichia coli. They found the LIL-inhibited pulmonary edema and endothelial cytoskeleton damage, as well as neutrophil influx and activation. Similarly, the LIL reduced the tumor necrosis factor (TNF) α and IL-1β in lung and bronchoalveolar lavage fluid (BALF). LIL prevented lung intercellular adhesion molecule-1 (ICAM-1) upregulation. The rise of cytokine-induced neutrophil chemoattractant-1 (CINC-1) and macrophage inflammatory protein-2 (MIP-2) protein levels in both lung and BALF, and the lung mRNA expressions for IL-10, were unaffected. Their data suggest that the LIL effect is due to the inhibition of ICAM-1 via the inhibition of TNF-α and IL-1β. Lima et al. also found that MIL at 660 nm had no effects on rat lung but attenuated intestinal ischemia and reperfusion-induced acute lung inflammation which favor the IL-10 production and reduce TNF generation [41].

Although there is dPBM on sleep that has been discussed from 1998 on, the puzzle remains unsolved. Campbell et al. found that 3 h of bright light exposure to the area behind the knee caused phase shifts of the circadian rhythms of both body temperature and saliva melatonin in participants in ambient illumination <50 lux [42]. However, Wright et al. found the absence of circadian phase resetting in response to the same bright light behind the knees of participants in ambient illumination 0 lux [43]. The environmental light is the key point. Sleep is normal if there is no environmental light, but is dysfunctional if the environmental light is rather intensive.

No dPBM on the functional recovery has been found for self-limited DOMS [44, 45]. However, dPBM can promote the functional recovery of delayed DOMS. Exhaustive downhill running was used to induce muscle injury in

rat gastrocnemius muscle. LIL significantly reduced serum creatine kinase (CK) activity at 48 h after exercise [46]. The load-resistance swimming test forced adult male Wistar rats to swim until exhaustion. 40 s MIL treatment lowered CK activity and muscular apoptosis [47].

LPBM on chronic ordinary stress might be mediated by redundant pathways. In our C2C12 studies [11, 12], normal glucose maintained the PlSH in normal glucose (nPlSH). We found that low/high glucose disrupted PlSH and lowered the proliferation, which was completely recovered by red light from light emitting diode array (RLED) at 640 nm so that PlSH in low/high glucose (lPlSH/hPlSH) was established. We further found that high glucose partially activated insulin-like growth factor (IGF) 1, which was promoted by RLED at 640 nm so that IGF-1 was completely activated [12]. Obviously, IGF-1 is the redundant pathway mediating the successful ordinary stress from nPlSH to hPlSH.

4.2. High Level Photomodulation. Xu et al. have studied the effects of laser irradiation at 810 nm and doses 1~7 (0.33, 1.338, 2.646, 5.338, 8.220, 11.22, and 14.16 J/cm^2) on the reactive oxygen species (ROS) metabolism and mitochondrial function of C2C12 myotubes [48]. They found that the LI at doses 1~5 had no effects on the mitochondrial function, but the one at doses 6&7 induced mitochondrial dysfunction; and the LI at doses 1~3 had no effects on the ROS metabolism, but the one at doses 4~7 increased ROS level. In this case, the mitochondrial function-specific homeostasis (MiSH) holds for the LI at doses 1~5, but breaks up for the LI at doses 6&7; and ROS metabolism-specific homeostasis (RoSH) holds for the LI at doses 1~3, but breaks up for the LI at doses 4~7. They further found that the electrical stimulation at 20 ms, 5 Hz, and 45 V for 75 min broke up MiSH and RoSH, and the LI at dose 1 promoted RoSH establishment and the one at doses 1~5 promoted MiSH establishment.

Ilic et al. have studied the effects of laser irradiation at 808 nm and 7.5, 75, 375, and 750 mW/cm^2 in either continuous wave (CW) or pulse modes for 2 min on the intact brain of healthy male Sprague-Dawley rats, respectively, and found that the only rats showing an adverse neurological effect were those in the 750 mW/cm^2, CW mode group, and there was no significant difference between the LI group and the control group for the each other dose [49].

Lacjaková et al. found that LIL at 670 nm improved wound healing in nonsteroid rats, but was not effective after methylprednisolone treatment [50]. However, MIL at 392.9 mW/cm^2 and 240 s was found to accelerate wound healing of the steroid rats, acting as a biostimulative coadjutant agent, balancing the undesirable effects of cortisone on the tissue healing process [51].

4.3. Successful Stress. DPBM cannot modulate a successful stress such as self-limited conditions. DPBM can modulate a chronic stress, but dPBM is not sensitive to LI parameters if the successful stress is established because the stress is in its homeostasis.

Iyomasa et al. found no significant differences in the area of newly formed bone between the groups of the MIL at 780 nm in a single application in contact with the skin surface on the critical bone defect and nonirradiated groups, 14 days after induction of critical bone defect, because the greatest stimulus for bone formation involved application of the recombinant human bone morphogenetic protein 2 (rhBMP-2) [52]. In this case, rhBMP-2 has established a successful stress.

The recovery of cells isolated from animal model is self-limited. Osteoblast-like cells isolated from fetal rat calvariae were irradiated once with an LIL (830 nm) in four different irradiation modes: continuous irradiation (CI) and 1-, 2-, and 8-Hz pulsed irradiation (PI-1, PI-2, and PI-8). Ueda et al. found no significant differences on alkaline phosphatase activity between the control group, CI, PI-1, PI-2, and PI-8 on 18th and 21st day [53]. Bone marrow derived mesenchymal stem cells (BMSCs) were harvested from rat fresh bone marrow and exposed to a 635 nm diode laser (60 mW; 0, 0.5, 1.0, 2.0, or 5.0 J/cm^2). 10 days after the isolation, there were no significant proliferation difference between the control and irradiation groups [54].

Inflammation is always self-limited. Gingivitis was induced in ten female dental students by refraining from all oral hygiene measures for 28 days. On days 21 and 24 the marginal gingiva, buccal to one of the lateral mandibular incisors, was exposed to 4 minutes of laser irradiation (total dose = 1 J). Rydén et al. found that the difference between sites at day 28 was not statistically significant. Their results suggest that LLL does not influence the inflammatory reaction of the gingiva [55].

de Souza et al. have studied the effects of daily MIL at 685 nm for 1 (MIL1) and 3 (MIL3) min on amputated worms [56]. They found that MIL1 more strongly promoted stem-cell proliferation than MIL3 on the 4th day, but there were no significant differences between the control, MIL1, and MIL3 on the 7th and 15th day.

Wound healing of healthy animal or human is always self-limited. Patients presenting with a total of 12 wounds after minor surgical procedures (partial/total nail avulsions/electrosurgery) were recruited from the Podiatry Teaching Clinic, Northern Ireland. Wound assessment and recording of pain levels were conducted weekly. Lagan et al. have found no statistically significant differences between weekly MIL (830 nm) and control groups neither for wound closure nor for pain levels reported, and no differences between MPBM of 11 weeks and control groups neither for wound closure nor for pain levels reported [57]. Low level gallium aluminium arsenide (GaAlAs) laser irradiation was administered to full-thickness skin wounds (3 × 3 cm) induced surgically on the dorsal aspect of the metacarpophalangeal joints of 6 crossbred horses in a randomised, blind, and controlled study. There were no wound complications. Petersen et al. have found no significant differences in wound contraction or epithelialization between the laser treated and the control wounds [58]. Pugliese et al. found no dPBM on collagen and elastic fibers of punched healthy rats. Cutaneous wounds were inflicted on the back of healthy Wistar rats [59]. Medrado et al. found no significant differences between the control group, LIL at 4 J/cm^2, and LIL at 8 J/cm^2 on the 14th day. Two standardized 1.27 cm^2 abrasions were

induced on the anterior forearm of healthy youth [60]. Hopkins et al. used a randomized, triple-blind, and placebo-controlled design with 2 within-subjects factors (wound and time) and 1 between-subjects factor (group) and found that the MIL group had smaller wounds than the sham group for both the treated and the untreated wounds on days 6, 8, and 10, but had no significant differences on day 20 [61]. Bayat et al. have found no acceleration of healing of deep second-degree burns in healthy rats after treatment with LIL at energy densities of 1.2 or 2.4 J/cm^2 although the LIL therapy caused significant decrease in the number of macrophage, depth of new epidermism, and incidence of *S. epidermidis* and *S. aureus* [62]. Prabhu et al. have studied the effects of the LIL at 632.8 nm and human placental extract (HPE) on full-thickness excision wounds on Swiss albino mice of diameter 15 and found the wounds exposed to the LIL at 2 J/cm^2 immediately after wounding showed considerable contraction on days 5, 9, 12, 14, 16, and 19 of postirradiation compared with the controls and other treatment schedules, but there were no significant differences between LIL, HPE, and the control 30 days after the wound [63]. Medrado et al. found that the MIL group of Wistar rats exhibited significantly more smooth muscle alpha-actin-positive staining cells 7 days after punch biopsy, more desmin-positive staining cells on day 10 around blood vessels, and higher numbers of NG2-positive staining cells, especially on days 3 and 7 post-biopsy, but there were no significant differences between the MIL group and the control group 14 days after punch biopsy [64].

Diabetic wound might be also self-limited. Akyol et al. found that MIL promoted the healing of the wound of streptozotocin- (STZ-) induced diabetes of female Wistar rats on 10th day, but did not on 20th day [65]. Ma et al. found that LIL promoted the healing of the wound of STZ-induced diabetes of male Wistar rats before 9th day, but did not on 14th day. As a fact, even type 2 diabetes might be self-limited [66]. Lim et al. found that normalisation of both beta cell function and hepatic insulin sensitivity in type 2 diabetes was achieved by dietary energy restriction alone [67].

Musculoskeletal conditions like temporomandibular disorders (TMD) are of the self-limiting feature [68, 69]. The factors causing sports injuries can be grouped in 2 separate broad categories: extrinsic and intrinsic factors. However, the great majority of injuries which are sustained are minor and self-limiting, suggesting that children and youth sports are safe [70]. Among them, DOMS is a common but self-limiting condition that usually requires no treatment [71]. Most exercise enthusiasts are familiar with its symptoms. However, where a muscle has been immobilised or debilitated, it is not known how that muscle will respond to exercise, especially eccentric activity [71]. There were no significant differences between the 30 days therapeutic effects of transcutaneous electrical nerve stimulation (TENS) and the ones of laser therapy on TMD [69], and no significant differences between the 30 days therapeutic effects of the microelectronic neurostimulation (MENS) and the ones of laser therapy on TMD [68].

LPBM modulates chronic stress until the successful stress is established. The successful stress is in a kind of homeostasis so that the LPBM might be dose/intensity-independent if the successful stress is established. Al-Watban et al. have studied the acceleration effects of the LIL at 532, 633, 810, and 980 nm on streptozotocin-induced diabetic rats (male Sprague-Dawley) [72]. Their results suggested that the LPBM of 21 days was dose-independent for each laser irradiation. For the LPBM on round full-thickness skin wounds in nonsteroid rats [73], the LPBM of 2 or 6 days was intensity-dependent, but the one of 14 days was intensity-independent. For the LPBM on round full-thickness skin wounds in steroid rats [73], the LPBM of 14 days was still intensity-dependent. After 14 days, the wounds completely recovered in nonsteroid rats so that the successful stress was established, but methylprednisolone inhibited wounds in steroid rats were still far from successful stress. Prabhu et al. have studied the effects of the LIL at 632.8 nm on full-thickness excision wounds on Swiss albino mice of diameter 15 and found that the LPBM of 30 days was dose independent [63]. Morais et al. have studied the anti-inflammatory LPBM on zymosan-induced arthritis and found that there were no significant difference between the effects of the LIL at 685 nm and the ones at 830 nm in increasing vascular permeability and reducing the edema 3 h after zymosan injection and in reducing paw elevation time 4 h after zymosan injection [74].

4.4. Indirect Photobiomodulation. In 10% FCS, the normal proliferation in its PlSH is the normal Fmax, but other functions are dysfunctional. LLL cannot directly affect the normal proliferation, but can modulate the other dysfunctional functions whose normalization does not resist normal proliferation. He-Ne irradiation elicits PBM in mitochondria processes, which involve Jun N-terminal kinase/activator protein-1 activation and enhanced the release of growth factors such as IL-8 and transforming growth factor (TGF) beta1, and ultimately lead to enhanced A2058 cell proliferation in 10% FCS [75]. The normal proliferation and normal procollagen of fibroblasts antagonized against each other [76]. Yamamoto et al. found that LIL cannot affect the procollagen synthesis of the fibroblasts in PlSH, but promoted the procollagen synthesis of the fibroblasts far from PlSH [77]. Coombe et al. have found that a single or daily MIL at 830 nm on SAOS-2 cells in 10% FCS has no effects on the cell viability or proliferation, protein expression, and alkaline phosphatase activity, but it has heat shock response, and increased intracellular calcium [34]. Frigo et al. found the MPBM (660 nm) for 60 s once a day for three days inhibited the death of primary human keloid fibroblast cells in 10% FCS at 630 mW/cm^2 only at day 2, but cannot modulate the proliferation of murine fibroblast 3T3 cells and primary human keloid fibroblast cells in 10% FCS at 260 mW/cm^2 at days 1, 2, and 3, and the death of primary human keloid fibroblast cells in 10% FCS at days 1 and 3 and murine fibroblast 3T3 cells in 10% FCS at days 1, 2, and 3 at 630 mW/cm^2 [78]. In this case, death inhibition maintains proliferation.

For cells in their respective PlSH, the functions which promote proliferation may be promoted with LLL. Cultured NIH3T3 fibroblasts from normal mice in 10% FCS were irradiated by RLED at 627 nm and 25 mW/cm^2 twice, first

at subculture and 24 h later. At day 2, Komine et al. observed the RLED promoted cell growth of NIH3T3 fibroblasts and increased the expression of platelet-derived growth factor (PDGF)-C, but did not affect the expression of PDGF-A, PDGF-B, and TGF-beta [79]. As Komine et al. have pointed out [79], one possible mechanism of fibroblast proliferation induced by RLED involves an increase of PDGF-C expression and activation of the ERK pathway through phosphorylation of the PDGF receptor.

Proliferation of tumor cells in 10% FCS or tumor growth is always normal. Frigo et al. have studied the effects of the MIL at 660 nm and 2.5 W/cm^2 in vitro for 3 days and in vivo for 10 days [78]. They found that the MIL once a day for three days did not modulate the proliferation of melanoma cells (B16F10) in 10% FCS, but promoted their apoptosis. They have used the in vivo mouse model (male Balb C) of melanoma to analyze the effects of the MIL once a day for ten days on tumor volume and histological characteristics. They found that the outcome measures for the 150 J/cm^2 dose group were not significantly different from controls, but there were significant increases in tumor volume, blood vessels, and cell abnormalities compared to the other groups for the 1050 J/cm^2 dose group. The MIL did not modulate a normal function so that it is a LLL and it should not modulate normal growth. The tumor is a complicated system. Its other functions such as telomere function [80] might be dysfunctional so that they may be modulated to promote its growth. Telomerase reactivation following telomere dysfunction yields murine prostate tumors with bone metastases [81]. It needed ten days for the tumor growth to be promoted by the MIL at 1050 J/cm^2. It suggested that the MIL promotion might be mediated by some protein synthesis. At this point, the tumor itself should not be irradiated with LLL.

A normal Fmax can be enhanced by iPBM if there is at least a chronic ordinary stress. iPBM might be mediated by redundant pathways because successful ordinary stress is mediated by redundant pathways. In our C2C12 studies [13], The Fmax of C2C12 myoblasts in normal glucose is the normal proliferation, and its FmaxSH is nPlSH. We found that RLED at 640 nm promoted the normal proliferation of C2C12 myoblasts from 4 days on and IGF-1/FOXO3a (forkhead box O family 3a) was completely activated/inhibited. In other words, the redundant pathways IGF-1 and FOXO3a mediated the iPBM enhancement.

5. Enhanced Recovery

Enhanced recovery after surgery (ERAS) has proven efficacious in improving the quality and efficiency of surgical care [82]. ERAS encompasses a systematic and evidence-based appraisal of all interventions performed in an episode of care. They have been associated with a reduction in duration of hospital stay, readmissions, and reoperations, together with decreased mortality and morbidity, improved pain control, better cost containment, and improved patient satisfaction. Obviously, recovery after surgery is just a stress, and the most rapid recovery is just a successful stress. Therefore, LLL can be used to promote ERAS.

The function recovery of a person suffering from an FSS depends on his/her initial state. The function recovery of the person who initially has a normal related function is more rapid than the one of the person who initially has a dysfunctional related function. Patients with major depressive disorder (MDD) had slower heart rate recovery 1 min after exercise stress than non-MDD patients [83]. MDD is accompanied by a dysregulation in autonomic control of exercise-related cardiovascular recovery, suggesting that depressed individuals have a slow parasympathetic recovery from exercise. Major League Baseball players of body mass index (BMI) 26.2 kg/m^2 demonstrated a significantly higher return-to-play rate from surgery for lumbar disc herniations than National Football League players of BMI 32.1 kg/m^2 did [84]. Efendiev et al. found that preliminary influencing upon the site of a future incision with the infrared laser radiation in constant regime within the range of 1 to 150 mW (dosage of radiation per 1 field of 0.06–9.3 J/cm^2) facilitated pronounced stimulation of the processes of collagen formation and significant increase in strength of a forming scar [85].

Moreover, the higher the functional fitness of a normal related function before operation, the more rapid his postoperation recovery. The higher the level of heat shock protein (HSP), the higher the functional fitness [4, 86]. Using a pulsed diode laser (1850 nm, 2 ms, 50 Hz, 7.64 mJ/cm^2), the skin of transgenic mice that contain an HSP70 promoter-driven luciferase was preconditioned 12 hours before surgical incisions were made. Wilmink et al. found that an optimized laser protocol increased HSP70 expression by 10-fold, and the laser-preconditioned incisions were two times stronger than control wounds [87].

LLL cannot modulate a successful stress, but can modulate a chronic stress until it is successful. Derkacz et al. have evaluated the influence of low-power 808 nm laser illumination of coronary vessels after percutaneous angioplasty in preventing restenosis with major adverse cardiac events (MACE) rate at the 6- and 12-month follow-up points and found that the LLL did not affect the MACE rate of patients without restenosis, but significantly reduced the MACE rate of patients with restenosis [88].

6. Discussion

MPBM might be mediated by reactive oxygen species, but LPBM might be mediated by membrane proteins [6, 7]. The plasma membrane delimits the cell, and its integrity is essential for cell survival. Lipids and proteins form domains of distinct composition within the plasma membrane. Membrane stress, for example, induced by either inhibition of sphingolipid metabolism or by mechanically stretching the plasma membrane, redistributes Slm proteins between distinct plasma membrane domains [89]. A cellular function is always related to a kind of membrane protein so that the protein is called function-specific protein (FSP). According to our membrane hypothesis [6, 7], the identical FSPs in the membrane may form coherent states if the function is dysfunctional or random states if the function is normal. The nonresonant interaction of FSPs and LI is so weak that its biological response cannot be observed in random states,

but it can be amplified in coherent states so that the PBM is observed. There are interactions between coherent states of one kind of FSPs and random states of another kind of FSPs so that some FSH cannot be established if it can be resisted by the FmaxSH, but a FmaxNSH can be established because its establishment can upgrade the FmaxSH. Each dysfunctional function in a cell has its FSPs in coherent states so that each action spectroscopy of each PBM on each dysfunctional function might be FSP-specific. This was supported by the reference [90]. Karu et al. found that the action spectroscopy of proliferation PBM was different from the one of adhesion PBM [90].

The iPBM might mainly contribute to the low morbidity or mortality of most diseases in the zone of low latitude or in summer. White light may have no effects on cells, but the skin-decayed sunlight is not white light anymore. As the cold light such as green, blue, or violet decays more rapid than the hot light such as red, orange, or yellow does, the skin-decayed sunlight may mainly be hot light, residual hot light (RHL). A normal function can resist internal/external disturbance, but chronic stress is sensitive to it. As a kind of LIL, RHL can modulate a chronic stress until it is successful. Moreover, as a kind of iPBM, RHL may upgrade the functional fitness of a normal function. Therefore, RHL and then sunlight can enhance the resistances to decrease disease morbidity or mortality.

7. Conclusion

DPBM may modulate a chronic stress. When a biosystem in the FmaxSH, dPBM cannot modulate the normal Fmax, but iPBM can modulate a dysfunctional FmaxNS through redundant pathways until it is normal and the normal Fmax is then upgraded. High level PBM can modulate a normal function and may be also a successful stress.

Acknowledgments

This work was supported by National Science Foundation of China (60878061) and the Opening Project of MOE Key laboratory of Laser Life Science, South China Normal University, Guangzhou, China.

References

[1] W. B. Cannon, *The Wisdom of the Body*, W. W. Norton, New York, NY, USA, 1932.

[2] H. Selye, "Forty years of stress research: principal remaining problems and misconceptions," *Canadian Medical Association Journal*, vol. 115, no. 1, pp. 53–56, 1976.

[3] M. R. Hara, J. J. Kovacs, E. J. Whalen et al., "A stress response pathway regulates DNA damage through β_2-adrenoreceptors and β-arrestin-1," *Nature*, vol. 477, no. 7364, pp. 349–353, 2011.

[4] L. R. Saunders and E. Verdin, "Cell biology: stress response and aging," *Science*, vol. 323, no. 5917, pp. 1021–1022, 2009.

[5] N. Kourtis and N. Tavernarakis, "Cellular stress response pathways and ageing: intricate molecular relationships," *The EMBO Journal*, vol. 30, no. 13, pp. 2520–2531, 2011.

[6] C. Y. Liu and P. Zhu, *Intranasal Low Intensity Laser Therapy*, People's Military Medical Press, Beijing, China, 2009.

[7] T. C. Y. Liu, R. Liu, L. Zhu, J. Q. Yuan, M. Wu, and S. H. Liu, "Homeostatic photobiomodulation," *Front Optoelectron China*, vol. 2, no. 1, pp. 1–8, 2009.

[8] T. C. Y. Liu, D. F. Wu, Z. Q. Gu, and M. Wu, "Applications of intranasal low intensity laser therapy in sports medicine," *Journal of Innovation in Optical Health Science*, vol. 3, no. 1, pp. 1–16, 2010.

[9] I. Lestas, G. Vinnicombe, and J. Paulsson, "Fundamental limits on the suppression of molecular fluctuations," *Nature*, vol. 467, no. 7312, pp. 174–178, 2010.

[10] H. Youk and A. van Oudenaarden, "Growth landscape formed by perception and import of glucose in yeast," *Nature*, vol. 462, no. 7275, pp. 875–879, 2009.

[11] F. H. Li, E. X. Wei, Y. Y. Liu, and T. C. Y. Liu, "Redundant photobiomodulation on low glucose induced dysfunctions of C2C12 myoblasts," *Lasers in Surgery and Medicine*, vol. 44, supplement 24, p. 63, 2012.

[12] F. H. Li, E. X. Wei, Y. Y. Liu, and T. C. Y. Liu, "Redundant photobiomodulation on high glucose induced signal transduction network of C2C12 myoblasts," *Lasers in Surgery and Medicine*, vol. 44, supplement 24, p. 63, 2012.

[13] T. C. Y. Liu, "Indirect photobiomodulation on tumors," *Lasers in Surgery and Medicine*, vol. 44, no. 4, p. 358, 2012.

[14] N. A. Burd, D. W. D. West, A. W. Staples et al., "Low-load high volume resistance exercise stimulates muscle protein synthesis more than high-load low volume resistance exercise in young men," *PLoS ONE*, vol. 5, no. 8, Article ID e12033, 2010.

[15] A. B. Salmon, A. A. Sadighi Akha, R. Buffenstein, and R. A. Miller, "Fibroblasts from naked mole-rats are resistant to multiple forms of cell injury, but sensitive to peroxide, ultraviolet light, and endoplasmic reticulum stress," *Journals of Gerontology A*, vol. 63, no. 3, pp. 232–241, 2008.

[16] J. Bigelow, *A Discourse on Self-Limited Diseases*, Kessinger, Kila, Mont, USA, 1835.

[17] G. D. Schiff, W. L. Galanter, J. Duhig, A. E. Lodolce, M. J. Koronkowski, and B. L. Lambert, "Principles of conservative prescribing," *Archives of Internal Medicine*, vol. 171, no. 16, pp. 1433–1440, 2011.

[18] K. Y. Tsang, D. Chan, D. Cheslett et al., "Surviving endoplasmic reticulum stress is coupled to altered chondrocyte differentiation and function," *PLoS Biology*, vol. 5, no. 3, article e44, 2007.

[19] C. Carter, S. Savic, J. Cole, and P. Wood, "Natural killer cell receptor expression in patients with severe and recurrent Herpes simplex virus-1 (HSV-1) infections," *Cellular Immunology*, vol. 246, no. 2, pp. 65–74, 2007.

[20] F. Bazzoni, M. Rossato, M. Fabbri et al., "Induction and regulatory function of miR-9 in human monocytes and neutrophils exposed to proinflammatory signals," *Proceedings of the National Academy of Sciences of the United States of America*, vol. 106, no. 13, pp. 5282–5287, 2009.

[21] J. F. Puglia, R. P. Brenner, and M. J. Soso, "Relationship between prolonged and self-limited photoparoxysmal responses and seizure incidence: study and review," *Journal of Clinical Neurophysiology*, vol. 9, no. 1, pp. 137–144, 1992.

[22] P. A. Kumar, Y. Hu, Y. Yamamoto et al., "Distal airway stem cells yield alveoli in vitro and during lung regeneration following H1N1 influenza infection," *Cell*, vol. 147, no. 3, pp. 525–538, 2011.

[23] T. Busso, "Variable dose-response relationship between exercise training and performance," *Medicine and Science in Sports and Exercise*, vol. 35, no. 7, pp. 1188–1195, 2003.

[24] K. Cheung, P. A. Hume, and L. Maxwell, "Delayed onset muscle soreness: treatment strategies and performance factors," *Sports Medicine*, vol. 33, no. 2, pp. 145–164, 2003.

[25] T. C. Y. Liu, R. D. Fu, X. G. Liu, and Z. X. Tian, "Laser homeostaticts on delayed onset muscle soreness," *Journal of Physics*, vol. 277, no. 1, Article ID 012021, 2011.

[26] E. Levine and T. Hwa, "Stochastic fluctuations in metabolic pathways," *Proceedings of the National Academy of Sciences of the United States of America*, vol. 104, no. 22, pp. 9224–9229, 2007.

[27] M. J. Lee, A. S. Ye, A. K. Gardino et al., "Sequential application of anticancer drugs enhances cell death by rewiring apoptotic signaling networks," *Cell*, vol. 149, no. 4, pp. 780–794, 2012.

[28] M. A. Nowak, M. C. Boerlijst, J. Cooke, and J. M. Smith, "Evolution of genetic redundancy," *Nature*, vol. 388, no. 6638, pp. 167–171, 1997.

[29] J. W. Jonker, J. M. Suh, A. R. Atkins et al., "A PPARā-FGF1 axis is required for adaptive adipose remodelling and metabolic homeostasis," *Nature*, vol. 485, no. 7398, pp. 391–394, 2012.

[30] S. D. Allison and J. B. H. Martiny, "Resistance, resilience, and redundancy in microbial communities," *Proceedings of the National Academy of Sciences of the United States of America*, vol. 105, supplement 1, pp. 11512–11519, 2008.

[31] E. S. Valchinov and N. E. Pallikarakis, "Design and testing of low intensity laser biostimulator," *BioMedical Engineering Online*, vol. 4, article 5, 2005.

[32] H. Chung, T. Dai, S. K. Sharma, Y. Y. Huang, J. D. Carroll, and M. R. Hamblin, "The nuts and bolts of low-level laser (light) therapy," *Annals of Biomedical Engineering*, vol. 40, no. 2, pp. 516–533, 2011.

[33] L. Baratto, L. Calzà, R. Capra et al., "Ultra-low-level laser therapy," *Lasers in Medical Science*, vol. 26, no. 1, pp. 103–112, 2011.

[34] A. R. Coombe, C. T. Ho, M. A. Darendeliler et al., "The effects of low level laser irradiation on osteoblastic cells," *Clinical Orthodontics and Research*, vol. 4, no. 1, pp. 3–14, 2001.

[35] M. Amognato, F. Squizzato, F. Facchin, L. Zaghetto, and L. Corti, "Cell growth modulation of human cells irradiated in vitro with low-level laser therapy," *Photomedicine and Laser Surgery*, vol. 22, no. 6, pp. 523–526, 2004.

[36] L. Frigo, J. S. S. Luppi, G. M. Favero et al., "The effect of low-level laser irradiation (In-Ga-Al-AsP—660 nm) on melanoma in vitro and in vivo," *BMC Cancer*, vol. 9, article 404, 2009.

[37] H. O. Schwartz-Filho, A. C. Reimer, C. Marcantonio, E. Marcantonio, and R. A. C. Marcantonio, "Effects of low-level laser therapy (685 nm) at different doses in osteogenic cell cultures," *Lasers in Medical Science*, vol. 26, no. 4, pp. 539–543, 2011.

[38] X. Q. Mi, J. Y. Chen, and L. W. Zhou, "Effect of low power laser irradiation on disconnecting the membrane-attached hemoglobin from erythrocyte membrane," *Journal of Photochemistry and Photobiology B*, vol. 83, no. 2, pp. 146–150, 2006.

[39] S. B. Rabelo, A. B. Villaverde, R. A. Nicolau, M. A. C. Salgado, M. D. S. Melo, and M. T. T. Pacheco, "Comparison between wound healing in induced diabetic and nondiabetic rats after low-level laser therapy," *Photomedicine and Laser Surgery*, vol. 24, no. 4, pp. 474–479, 2006.

[40] F. Mafra de Lima, A. B. Villaverde, M. A. Salgado et al., "Low intensity laser therapy (LILT) in vivo acts on the neutrophils recruitment and chemokines/cytokines levels in a model of acute pulmonary inflammation induced by aerosol of lipopolysaccharide from Escherichia coli in rat," *Journal of Photochemistry and Photobiology B*, vol. 101, no. 3, pp. 271–278, 2010.

[41] F. M. de Lima, A. B. Villaverde, R. Albertini et al., "Dual effect of low-level laser therapy (LLLT) on the acute lung inflammation induced by intestinal ischemia and reperfusion: action on anti- and pro-inflammatory cytokines," *Lasers in Surgery and Medicine*, vol. 43, no. 5, pp. 410–420, 2011.

[42] S. S. Campbell and P. J. Murphy, "Extraocular circadian phototransduction in humans," *Science*, vol. 279, no. 5349, pp. 396–399, 1998.

[43] K. P. Wright and C. A. Czeisler, "Absence of circadian phase resetting in response to bright light behind the knees," *Science*, vol. 297, no. 5581, p. 571, 2002.

[44] P. Douris, V. Southard, R. Ferrigi et al., "Effect of phototherapy on delayed onset muscle soreness," *Photomedicine and Laser Surgery*, vol. 24, no. 3, pp. 377–382, 2006.

[45] E. Vinck, B. Cagnie, P. Coorevits, G. Vanderstraeten, and D. Cambier, "Pain reduction by infrared light-emitting diode irradiation: a pilot study on experimentally induced delayed-onset muscle soreness in humans," *Lasers in Medical Science*, vol. 21, no. 1, pp. 11–18, 2006.

[46] X. G. Liu, Y. J. Zhou, T. C. Y. Liu, and J. Q. Yuan, "Effects of low-level laser irradiation on rat skeletal muscle injury after eccentric exercise," *Photomedicine and Laser Surgery*, vol. 27, no. 6, pp. 863–869, 2009.

[47] D. A. Sussai, P. D. T. C. D. Carvalho, D. M. Dourado, A. C. G. Belchior, F. A. Dos Reis, and D. M. Pereira, "Low-level laser therapy attenuates creatine kinase levels and apoptosis during forced swimming in rats," *Lasers in Medical Science*, vol. 25, no. 1, pp. 115–120, 2010.

[48] X. Xu, X. Zhao, T. C. Y. Liu, and H. Pan, "Low-intensity laser irradiation improves the mitochondrial dysfunction of C2C12 induced by electrical stimulation," *Photomedicine and Laser Surgery*, vol. 26, no. 3, pp. 197–202, 2008.

[49] S. Ilic, S. Leichliter, J. Streeter, A. Oron, L. DeTaboada, and U. Oron, "Effects of power densities, continuous and pulse frequencies, and number of sessions of low-level laser therapy on intact rat brain," *Photomedicine and Laser Surgery*, vol. 24, no. 4, pp. 458–466, 2006.

[50] K. Lacjaková, N. Bobrov, M. Poláková et al., "Effects of equal daily doses delivered by different power densities of low-level laser therapy at 670 nm on open skin wound healing in normal and corticosteroid-treated rats: a brief report," *Lasers in Medical Science*, vol. 25, no. 5, pp. 761–766, 2010.

[51] E. S. Pessoa, R. M. Melhado, L. H. Theodoro, and V. G. Garcia, "A histologic assessment of the influence of low-intensity laser therapy on wound healing in steroid-treated animals," *Photomedicine and Laser Surgery*, vol. 22, no. 3, pp. 199–204, 2004.

[52] M. M. Iyomasa, J. P. Mardegan Issa, M. L. de Queiróz Tavares et al., "Influence of low-level laser associated with osteogenic proteins recombinant human BMP-2 and Hevea brasiliensis on bone repair in Wistar rats," *Microscopy Research and Technique*, vol. 75, no. 2, pp. 117–125, 2011.

[53] Y. Ueda and N. Shimizu, "Effects of pulse frequency of low-level laser therapy (LLLT) on bone nodule formation in rat calvarial cells," *Journal of Clinical Laser Medicine and Surgery*, vol. 21, no. 5, pp. 271–277, 2003.

[54] J. F. Hou, H. Zhang, X. Yuan, J. Li, Y. J. Wei, and S. S. Hu, "In vitro effects of low-level laser irradiation for bone marrow mesenchymal stem cells: proliferation, growth factors secretion and myogenic differentiation," *Lasers in Surgery and Medicine*, vol. 40, no. 10, pp. 726–733, 2008.

[55] H. Rydén, L. Persson, H. Preber, and J. Bergström, "Effect of low level energy laser irradiation on gingival inflammation," *Swedish Dental Journal*, vol. 18, no. 1-2, pp. 35–41, 1994.

[56] S. C. de Souza, E. Munin, L. P. Alves, M. A. C. Salgado, and M. T. T. Pacheco, "Low power laser radiation at 685 nm stimulates stem-cell proliferation rate in *Dugesia tigrina* during regeneration," *Journal of Photochemistry and Photobiology B*, vol. 80, no. 3, pp. 203–207, 2005.

[57] K. M. Lagan, B. A. Clements, S. McDonough, and G. D. Baxter, "Low intensity laser therapy (830 nm) in the management of minor postsurgical wounds: a controlled clinical study," *Lasers in Surgery and Medicine*, vol. 28, no. 1, pp. 27–32, 2001.

[58] S. L. Petersen, C. Botes, A. Olivier, and A. J. Guthrie, "The effect of low level laser therapy (LLLT) on wound healing in horses," *Equine Veterinary Journal*, vol. 31, no. 3, pp. 228–231, 1999.

[59] L. S. Pugliese, A. P. Medrado, S. R. Reis, and Z. A. Andrade, "The influence of low-level laser therapy on biomodulation of collagen and elastic fibers," *Pesquisa Odontologica Brasileira*, vol. 17, no. 4, pp. 307–313, 2003.

[60] A. R. A. P. Medrado, L. S. Pugliese, S. R. A. Reis, and Z. A. Andrade, "Influence of low level laser therapy on wound healing and its biological action upon myofibroblasts," *Lasers in Surgery and Medicine*, vol. 32, no. 3, pp. 239–244, 2003.

[61] J. T. Hopkins, T. A. McLoda, J. G. Seegmiller, and G. D. Baxter, "Low-level laser therapy facilitates superficial wound healing in humans: a triple-blind, sham-controlled study," *Journal of Athletic Training*, vol. 39, no. 3, pp. 223–229, 2004.

[62] M. Bayat, M. M. Vasheghani, N. Razavi, S. Taheri, and M. Rakhshan, "Effect of low-level laser therapy on the healing of second-degree burns in rats: a histological and microbiological study," *Journal of Photochemistry and Photobiology B*, vol. 78, no. 2, pp. 171–177, 2005.

[63] V. Prabhu, S. B. S. Rao, N. B. Rao, K. B. Aithal, P. Kumar, and K. K. Mahato, "Development and evaluation of fiber optic probe-based helium-neon low-level laser therapy system for tissue regeneration-an in vivo experimental study," *Photochemistry and Photobiology*, vol. 86, no. 6, pp. 1364–1372, 2010.

[64] A. Medrado, T. Costa, T. Prado, S. Reis, and Z. Andrade, "Phenotype characterization of pericytes during tissue repair following low-level laser therapy," *Photodermatology Photoimmunology and Photomedicine*, vol. 26, no. 4, pp. 192–197, 2010.

[65] U. Akyol and M. Güngörmüş, "The effect of low-level laser therapy on healing of skin incisions made using a diode laser in diabetic rats," *Photomedicine and Laser Surgery*, vol. 28, no. 1, pp. 51–55, 2010.

[66] H. Ma, Y. X. Li, H. L. Chen, Y. X. Cui, and T. C. Y. Liu, "Effects of low-level laser therapy on wound healing in diabetic rats," *International Journal of Photoenergy*, vol. 2012, Article ID 838496, 7 pages, 2012.

[67] E. L. Lim, K. G. Hollingsworth, B. S. Aribisala, M. J. Chen, J. C. Mathers, and R. Taylor, "Reversal of type 2 diabetes: normalisation of beta cell function in association with decreased pancreas and liver triacylglycerol," *Diabetologia*, vol. 54, no. 10, pp. 2506–2514, 2011.

[68] E. M. Kogawa, M. T. Kato, C. N. Santos, and P. C. Conti, "Evaluation of the efficacy of low-level laser therapy (LLLT) and the microelectric neurostimulation (MENS) in the treatment of myogenic temporomandibular disorders: a randomized clinical trial," *Journal of Applied Oral Science*, vol. 13, no. 3, pp. 280–285, 2005.

[69] M. T. Kato, E. M. Kogawa, C. N. Santos, and P. C. R. Conti, "Tens and low-level laser therapy in the management of temporomandibular disorders," *Journal of Applied Oral Science*, vol. 14, no. 2, pp. 130–135, 2006.

[70] N. Maffulli and A. D. G. Baxter-Jones, "Common skeletal injuries in young athletes," *Sports Medicine*, vol. 19, no. 2, pp. 137–149, 1995.

[71] D. L. MacIntyre, W. D. Reid, and D. C. McKenzie, "Delayed muscle soreness. The inflammatory response to muscle injury and its clinical implications," *Sports Medicine*, vol. 20, no. 1, pp. 24–40, 1995.

[72] F. A. H. Al-Watban, X. Y. Zhang, and B. L. Andres, "Low-level laser therapy enhances wound healing in diabetic rats: a comparison of different lasers," *Photomedicine and Laser Surgery*, vol. 25, no. 2, pp. 72–77, 2007.

[73] P. Gál, M. Mokrý, B. Vidinský et al., "Effect of equal daily doses achieved by different power densities of low-level laser therapy at 635 nm on open skin wound healing in normal and corticosteroid-treated rats," *Lasers in Medical Science*, vol. 24, no. 4, pp. 539–547, 2009.

[74] N. C. R. De Morais, A. M. Barbosa, M. L. Vale et al., "Anti-inflammatory effect of low-level laser and light-emitting diode in zymosan-induced arthritis," *Photomedicine and Laser Surgery*, vol. 28, no. 2, pp. 227–232, 2010.

[75] W.-P. Hu, J.-J. Wang, C.-L. Yu, C.-C. E. Lan, G.-S. Chen, and H.-S. Yu, "Helium-neon laser irradiation stimulates cell proliferation through photostimulatory effects in mitochondria," *Journal of Investigative Dermatology*, vol. 127, no. 8, pp. 2048–2057, 2007.

[76] J. G. Clark, D. K. Madtes, and G. Raghu, "Effects of platelet-derived growth factor isoforms on human lung fibroblast proliferation and procollagen gene expression," *Experimental Lung Research*, vol. 19, no. 3, pp. 327–344, 1993.

[77] Y. Yamamoto, T. Kono, H. Kotani, S. Kasai, and M. Mito, "Effect of low-power laser irradiation on procollagen synthesis in human fibroblasts," *Journal of Clinical Laser Medicine and Surgery*, vol. 14, no. 3, pp. 129–132, 1996.

[78] L. Frigo, G. M. Fávero, H. J. Campos Lima et al., "Low-level laser irradiation (InGaAIP-660 nm) increases fibroblast cell proliferation and reduces cell death in a dose-dependent manner," *Photomedicine and Laser Surgery*, vol. 28, supplement 1, pp. S151–S156, 2010.

[79] N. Komine, K. Ikeda, K. Tada, N. Hashimoto, N. Sugimoto, and K. Tomita, "Activation of the extracellular signal-regulated kinase signal pathway by light emitting diode irradiation," *Lasers in Medical Science*, vol. 25, no. 4, pp. 531–537, 2010.

[80] J. A. Hackett and C. W. Greider, "Balancing instability: dual roles for telomerase and telomere dysfunction in tumorigenesis," *Oncogene*, vol. 21, no. 4, pp. 619–626, 2002.

[81] Z. Ding, C. J. Wu, M. Jaskelioff, E. Ivanova et al., "Telomerase reactivation following telomere dysfunction yields murine prostate tumors with bone metastases," *Cell*, vol. 148, no. 5, pp. 896–907, 2012.

[82] M. Adamina, H. Kehlet, G. A. Tomlinson, A. J. Senagore, and C. P. Delaney, "Enhanced recovery pathways optimize health outcomes and resource utilization: a meta-analysis of randomized controlled trials in colorectal surgery," *Surgery*, vol. 149, no. 6, pp. 830–840, 2011.

[83] J. L. Gordon, B. Ditto, K. L. Lavoie et al., "The effect of major depression on postexercise cardiovascular recovery," *Psychophysiology*, vol. 48, no. 11, pp. 1605–1610, 2011.

[84] W. K. Hsu, K. J. McCarthy, J. W. Savage et al., "The Professional Athlete Spine Initiative: outcomes after lumbar disc herniation in 342 elite professional athletes," *Spine Journal*, vol. 11, no. 3, pp. 180–186, 2011.

[85] A. I. Efendiev, P. I. Tolstykh, A. I. Dadashev, and S. A. Azimov, "Increasing the scar strength after preventive skin irradiation

with low-intensity laser," *Klinicheskaya Khirurgiya*, no. 1, pp. 23–25, 1992 (Russian).

[86] S. J. Tonsor, C. Scott, I. Boumaza, T. R. Liss, J. L. Brodsky, and E. Vierling, "Heat shock protein 101 effects in A. thaliana: genetic variation, fitness and pleiotropy in controlled temperature conditions," *Molecular Ecology*, vol. 17, no. 6, pp. 1614–1626, 2008.

[87] G. J. Wilmink, S. R. Opalenik, J. T. Beckham et al., "Molecular imaging-assisted optimization of hsp70 expression during laser-induced thermal preconditioning for wound repair enhancement," *The Journal of investigative dermatology*, vol. 129, no. 1, pp. 205–216, 2009.

[88] A. Derkacz, M. Protasiewicz, R. Poreba, A. Szuba, and R. Andrzejak, "Usefulness of intravascular low-power laser illumination in preventing restenosis after percutaneous coronary intervention," *American Journal of Cardiology*, vol. 106, no. 8, pp. 1113–1117, 2010.

[89] D. Berchtold, M. Piccolis, N. Chiaruttini et al., "Plasma membrane stress induces relocalization of Slm proteins and activation of TORC2 to promote sphingolipid synthesis," *Nature Cell Biology*, vol. 14, no. 5, pp. 542–547, 2012.

[90] T. I. Karu, L. V. Pyatibrat, G. S. Kalendo, and R. O. Esenaliev, "Effects of monochromatic low-intensity light and laser irradiation on adhesion of HeLa cells in vitro," *Lasers in Surgery and Medicine*, vol. 18, no. 2, pp. 171–177, 1996.

Hindawi Publishing Corporation
International Journal of Photoenergy
Volume 2012, Article ID 374861, 7 pages
doi:10.1155/2012/374861

Review Article

Photobiomodulation Process

Yang-Yi Xu,[1,2] Timon Cheng-Yi Liu,[1] and Lei Cheng[1]

[1] *Laboratory of Laser Sports Medicine, South China Normal University, University Town, Guangzhou 510006, China*
[2] *School for Information and Optoelectronic Science and Engineering, South China Normal University, University Town, Guangzhou 510006, China*

Correspondence should be addressed to Timon Cheng-Yi Liu, liutcy@scnu.edu.cn

Received 17 February 2012; Revised 12 April 2012; Accepted 12 April 2012

Academic Editor: Rui Duan

Photobiomodulation (PBM) is a modulation of laser irradiation or monochromatic light (LI) on biosystems. There is little research on PBM dynamics although its phenomena and mechanism have been widely studied. The PBM was discussed from dynamic viewpoint in this paper. It was found that the primary process of cellular PBM might be the key process of cellular PBM so that the transition rate of cellular molecules can be extended to discuss the dose relationship of PBM. There may be a dose zone in which low intensity LI (LIL at different doses) has biological effects similar to each other, so that biological information model of PBM might hold. LIL may self-adaptively modulate a chronic stress until it becomes successful.

1. Introduction

Photobiomodulation (PBM) is a modulation of laser irradiation, monochromatic light, hot color light such as red, orange or yellow, or cold color light such as green, blue or violet (LI) on biosystems. Since its introduction in the early 1960s, laser has transformed phototherapy. Now in its developing years, the PBM field is still experiencing growing pains especially in dose relationship. The dose relationship of PBM is very important topic which has been often underestimated. A paper of excellent results could not been referred because there has been no clear dose relationship. Some international groups always reported negative results of PBM since their inattentive research on dose relationship, which have left other researchers or physicians confused. Many Chinese groups have done the same things so that there almost was no laser acupuncture in clinical applications, and intravascular low energy laser therapy (ILELT) was forbidden by Chinese Health Ministry. The dose relationship of PBM would be discussed from dynamic viewpoint in this paper.

2. Initial States

PBM depends on the initial state of a biosystem. Negative feedback is common in biological processes and can maintain the resistance of biosystems to internal and external perturbations [1]. The PBM was discussed from the viewpoint of negative feedback.

The negative feedback is generally used to maintain internal stability of a biosystem, which is a classical concept of homeostasis [2, 3]. However, circadians or oscillations are found at nearly every level of biology. Homeostasis is too obscure to be deeply studied so that it has been developed as function-specific homeostasis (FSH) in our laboratory. An FSH is a negative-feedback response of a biosystem to maintain the function-specific conditions inside the biosystem so that the function is perfectly performed [4, 5]. A biosystem in an FSH means the function is in its FSH. A biosystem far from an FSH means the function is far from its FSH. A function in its FSH is better performed than all the dysfunction far from the FSH so that the function in its FSH is locally the best performed one.

The negative feedback can be also used to maintain a stress. An FSH can resist internal/external disturbance, but can be disrupted by an FSH-specific stress (FSS). An FSS is also a function of a biosystem so that there is an FSS-specific homeostasis (FSSH) [6]. A FSS in its FSSH is called successful stress, but a FSS far from its FSSH is just a chronic stress.

The LI used in PBM is always low intensity LI (LIL), ~10 mW/cm^2. However, moderate intensity LI (MIL), $10^{2\sim3}$ mW/cm^2, is of PBM if the irradiation time is not so

long that it damages organelles or cells. The PBM of LIL and MIL are denoted as LPBM and MPBM, respectively. It has been found [6] that LIL or MIL with short irradiation time is a low level LI (LLL) so that it cannot directly affect a successful stress or a function in its FSH. However, an LLL can modulate a chronic stress. On the other hands, MIL with long irradiation time is a high level LI so that it can disrupt an FSH/FSSH.

3. Primary Process

The first law of photochemistry (and photophysics) states that light must be absorbed for photochemistry (or photophysics) to occur. This is a simple concept, but it is the basis for performing photobiological experiments correctly. Since photobiological and phototherapeutic effects are initiated by photochemistry (or photophysics), unless light of a particular wavelength is absorbed by a system, no photochemistry (or photophysics) will occur, and no photobiological effects will be observed, no matter how long one irradiates with that light.

The biosystem is very complicated, but it can be studied at cellular level. The primary process of cellular PBM of LI is the interaction of LI with cellular molecules. A molecule in the ground state $|n\rangle$ with energy E_n has been irradiated with LI at angular frequency ω and intensity I for irradiation time t. According to quantum mechanics, the coefficient, $\langle k \mid n\rangle$, of the ground state $|n\rangle$ in the expansion of the wavefunction of the excited state $|k\rangle$ with energy E_k at the time t is calculated by the following equation under the electric-dipole approximation [7, 8]:

$$\langle k \mid n\rangle = \frac{1}{2\hbar}\sqrt{I}D_{kn}\frac{1-\exp[i(\omega_{kn}-\omega)t]}{\omega_{kn}-\omega}, \tag{1}$$

where $\hbar$ is the reduced Plank constant, D_{kn} is the matrix element of the transition from the ground state $|n\rangle$ to the excited state $|k\rangle$, and $\omega_{kn} = (E_k - E_n)/\hbar$. $|\langle k \mid n\rangle|^2$ has been explained to be the transition probability from the ground state $|n\rangle$ to the excited state $|k\rangle$. We then have the transition rate, the transition probability per unit time, of the molecule

$$r = \frac{d}{dt}|\langle k \mid n\rangle|^2 = \frac{1}{2\hbar^2}|D_{kn}|^2 I\frac{\sin(\omega_{kn}-\omega)t}{\omega_{kn}-\omega}. \tag{2}$$

If the identical protein molecules interacting with LI are in the membrane of the cell or their organelles (Figure 1), the identical molecules might cooperate with each other to form coherent states when the related function/FSS is far from its FSH/FSSH, and the transition rate of a cell should be [7]

$$R = \frac{1}{2\hbar^2}C_k N^2|D_{kn}|^2 I\frac{\sin(\omega_{kn}-\omega)t}{\omega_{kn}-\omega}, \tag{3a}$$

where N and C_k are the number of the identical molecules and the quantum constant of the excited $|k\rangle$. For the resonant transition, $\omega_{kn} = \omega$, we have from (2)

$$r_r = \frac{1}{2\hbar^2}|D_{kn}|^2 It. \tag{4a}$$

We then have the reciprocity rule (Bunsen-Roscoe law) [9] that the photochemical response is independent of the intensity I and the irradiation time t when the dose It is kept constant.

According to whether the primary process is resonant or nonresonant, the pathways mediating cellular PBM are classified into two kinds, the specific pathway which is mediated by the resonant interaction of LI with endogenous photosensitizers such as hemoglobin, flavin and nicotinamide adenine dinucleotide phosphate (NADPH) oxidases which consist of the membrane-bound cytochrome b558 [10], the nonspecific pathway which is mediated by the nonresonant interaction of LI with the proteins in the membrane of cells or organelles [7, 8]. Equations (3a) and (4a) hold for nonspecific pathways and specific pathways, respectively.

Obviously, the nonresonant transition rate (2) is extraordinarily small in comparison with resonant transition rate (4a) ($r \ll r_r$) so that the non-specific pathway may be impossible. However, the non-specific pathway may be nonlinearly amplified according to our identical particle model within the frame work of quantum mechanics [7]. In (3a), the number N of the membrane protein molecules (Figure 1) mediating the non-specific pathway is about $10^{3\sim4}$. All the membrane molecules mediating the non-specific pathway are identical. They cooperate with one another to form the coherent states when the related cellular function/FSS is far from its FSH/FSSH. The coherent states can be classified into two kinds, the superradiant state whose transition rate is a nonlinear function of the molecular numbers N so that the ultra-weak nonresonant interaction can be amplified according to (3a), and the subradiant state whose transition rate is zero. It has been easily shown that the function of cells whose molecules mediating the non-specific pathway are in superradiant states is not optimal and the cells are far from its FSH and the function of cells whose molecules are in subradiant states is optimal and the cells are in its FSH [8]. Therefore, the PBM mediated by non-specific pathway should be homeostatic. The PBM of LIL is mainly mediated by the non-specific pathway [8] and then might be homeostatic. This is in agreement with the conclusion in the previous section.

4. Key Process

A complicated process consists of many subprocesses each of which has its rate. The key subprocess is one of the subprocesses whose rate is the smallest one among the subprocesses. There are many processes of PBM from LI absorption to the observed biomedical effect among which one process is called the key process which is very critical for PBM, and its rate determines PBM rate. Through the dynamics of PBM we tried to find the key process, and discuss further the dose relationship of PBM. There is little research on the dynamics of PBM although its phenomena and mechanism have been widely studied, which is in the way of the deep research of PBM mechanism, especially the urgent research on the dose relationship in clinical

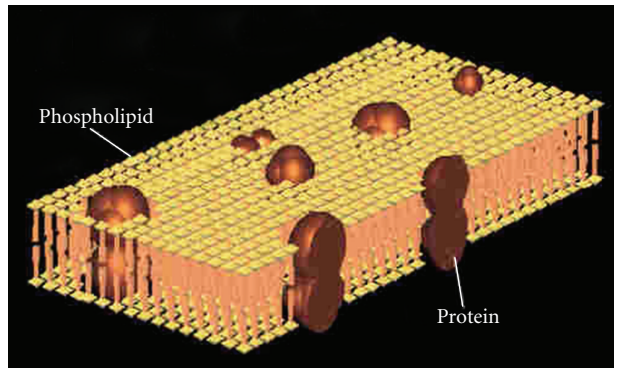

Figure 1: Cellular membrane structure illustration.

applications. The key process of cellular PBM might be studied by comparing the transition rate of its primary process with its dose relationship after reviewing cellular PBM.

The key process is the rate-limiting process. As photodegradation is a key process in governing the residence time and fate of many agrochemicals in top soils [11], the primary process of cellular PBM might be supposed to be the key process of cellular PBM so that the dose relationship of cellular PBM should be decided by transition rate of the primary process, (3a) and (4a), which was called the key process hypothesis of cellular PBM (KPHCP) for convenience. According to KPHCP, (3a) should hold for the non-specific pathway mediated response of light (NSPR):

$$\text{NSPR} \propto I \frac{\sin(\omega_{kn} - \omega)t}{\omega_{kn} - \omega}, \tag{3b}$$

and the reciprocity rule, (4a), should hold for the specific pathway mediated response of light (SPR):

$$\text{SPR} \propto It. \tag{4b}$$

Therefore, (3a), (3b) and (4a), (4b) might be the dose relationship of LPBM and MPBM because LPBM and MPBM may be mainly mediated by non-specific pathways and specific pathways [8], respectively. KPHCP was supported by its applications.

MPBM or photodynamic effects is mainly mediated by SPR so that the reciprocity rule, (4a), (4b), should hold according to KPHCP. Ben-Dov et al. [12] have studied MPBM on satellite cell proliferation in vitro and found that there was a linear relationship of PBM and irradiation time when the intensity was kept constant. Stadler et al. [13] have studied the MIL of whole blood on the lymphocyte proliferation and also found a linear relationship of the PBM and irradiation time when the intensity was kept constant. Obviously, (4a), (4b) hold for MPBM. For ILELT, the changed laser intensity is a kind of MIL, but the irradiation time, the period for blood cells to flow through the cross section of the optical fiber, is a constant. Wang et al. [14] have used ILELT to treat New Zealand rabbits with Alloxan-diabetes and observed the variations of their erythrocyte filtration index (EFI). Their data have been linearized as follows:

$$\begin{aligned} &\text{First day after treatment,} \\ &\quad y_1 = -0.00490x_1 + 0.288, \qquad R_1 = 0.9130, \\ &\text{Third day after treatment,} \\ &\quad y_3 = -0.0492x_3 + 0.386, \qquad R_3 = 0.9300, \end{aligned} \tag{5}$$

where x, y, and R are the intensity, EFI, and the correlation coefficient.

LPBM is mainly mediated by NSPR [8] so that (3a) and (3b) should hold according to KPHCP. In this case, the reciprocity rule, (4a), (4b), should not hold, and LPBM depends on intensity or irradiation time if the dose is kept constant. From the observations of different research groups and their own observations, Sommer et al. [15] concluded that the threshold parameters dose and intensity are biologically independent from each other. The analysis of intensity and irradiation time dependences for the same biological response indicated that the reciprocity rule does not hold when HeLa cells were irradiated with low intensity He-Ne laser irradiation (LHNL) [16, 17]. Although few studies have addressed the validity of the reciprocity rule in experimental and applied photobiology to date, most of these data point to the fact that the rule of reciprocity is invalid or of limited validity for many photobiological reactions, and it has been shown that at a constant total dose, the intensity of the source is a major factor that determines quality and quantity of the response for the effects of LLL [18]. Van Breugel and Bar [19] have found that LHNL at 1.24 mW/145 s can significantly promote the proliferation of human diploid skin fibroblasts in vitro, but the irradiation at 0.55 mW/330 s or 5.98 mW/30 s cannot although their doses are almost the same. Lubart et al. [20] have investigated the effect of LIL on mammalian cells. They found that the induction of fibroblast proliferation at a constant dose depends on the applied intensity in a nonlinear manner. In the research of Li et al. [21], polymorphonuclear neutrophils (PMNs) were irradiated by LHNL at doses of 800, 1,000, 1,800, and 2,000 J/m^2, respectively, and the intensity was changed at each dose. They found that the NADPH oxidase activity was different at different intensity for each dose of

LHNL. Lanzafame et al. [22] have studied the effects of red light at 670 nm from light emitting diode array (RLED 670) on pressure ulcers of C57/BL mice and found varying irradiance and exposure time to achieve a specified energy density affecting phototherapy outcomes.

When the dose of LIL is constant, the reciprocity rule might not hold so that there might be a maximum PBM according to (3a) and (3b). Let T be defined as follows:

$$T = (\omega_{kn} - \omega)t. \tag{6}$$

From (3a), we have

$$R = \frac{1}{2\hbar^2} C_k N^2 |D_{kn}|^2 It \frac{\sin T}{T}. \tag{7}$$

and then

$$\frac{dR}{dt} = \frac{1}{2\hbar^2} I C_k N^2 |D_{kn}|^2 \left(\cos T - \frac{\sin T}{T}\right). \tag{8}$$

Therefore, the transition rate of the primary process and then LPBM arrives at their maximum value, respectively, at $T = T_0$:

$$T_0 \cos T_0 = \sin T_0. \tag{9}$$

Karu [23] has measured DNA synthesis in exponentially growing HeLa cells and proliferation after constant low doses of 632.8 nm (0.01 J/cm^2) and 454 nm (0.3 J/cm^2) laser irradiation applied within different exposure times (i.e., with different intensities), respectively. Her findings pointed to the nonvalidity of the reciprocity rule as the biological response varied clearly with different intensities peaking between 1 mW/cm^2 and 20 mW/cm^2. Karu and Kolyakov [24] also observed dependence of stimulation of DNA synthesis rate on light intensity or irradiation time at a constant dose measured 1.5 h after irradiation of log-phase HeLa cells with a continuous wave dye laser pumped by an argon laser (633 nm, 8 mW/cm^2) at 100 J/m^2 and found the maximum PBM at about 10 s.

Obviously, the optimum T_0 and then the optimum radiation time t_0 are dose-independent according to (6) and (9). We also observed the maximum PBM of low intensity 810 nm GaAlAs laser irradiation at the constant dose 528 and 2130 mJ/cm^2, respectively, on NIH 3T3 fibroblasts [25]. Moreover, the optimum irradiation time 40 s at the maximum PBM has been found dose-independent [25]. This is a direct support to KPHCP.

KPHCP was also supported by the dose relationship when the intensity or the radiation time is kept constant. There are many works on the dose relationship when the intensity is kept constant [9]. In this case, the LPBM should be the SIN function of irradiation time according to KPHCP and (3a) and (3b), which is supported by Al-Watban et al., Brill et al., Karu, Yang et al., Zhang et al., and Zharov et al. [9, 26–36].

There are few works on the dose relationship when the irradiation time is kept constant. In this case, the LPBM should be the linear function of intensity according to KPHCP and (3a) and (3b), which is supported by Cheng et al., Duan et al., Karu, Liang et al., and Xu et al. [9, 37–40].

We have studied RLED 640 promotion on the recovery of differentiated PC12 (dPC12) cells from H_2O_2 cytotoxicity [41]. dPC12 cells were cultured with the medium of H_2O_2 at 150 μmol/L for 30 min and then with fresh medium for 6 h and were then irradiated with RLED 640 at 0.06 mW/cm^2 for 10, 20, 40, and 60 min and 72 mJ/cm^2 for 5, 10, 20, and 40 min, respectively. It was found among the irradiation at 0.06 mW/cm^2 or 72 mJ/cm^2, 10 and 20 min irradiation was the most effective in promoting cellular rehabilitation, respectively. Obviously, (3a) and (3b) may hold.

In a summary, KPHCP has been supported by its applications. In other words, the primary process of cellular PBM might the key process of cellular PBM.

5. Dose Zone

It has been found that there is a dose zone in which LI at different doses has biological effects similar to each other. For example, the dose zones were called dose 1, dose 2, and dose 3 from low dose on so that human skin fibroblast cell (HSF) proliferation was inhibited in dose 1 (16, 24 mJ/cm^2) and promoted in dose 2 (298, 503, 597 mJ/cm^2), and the collagen synthesis was inhibited in dose 2 (401, 526 mJ/cm^2), and promoted in dose 3 (714, 926, 1539 and 1727 mJ/cm^2) [37]. Based on these phenomena, the biological information model of PBM (BIMP) has been put forward [7, 42].

According to traditional Chinese medicine, *yin* and *yang* are antagonistic, but they transform into each other under some condition [43]. It can be extended to other systems such as cells [44]. The cellular signal transduction pathways can be classified into two kinds: pathway 1 mediated by Gs protein mediated pathway, and pathway 2 is mediated by the other pathways mediated by proteins such as G_i protein, G_q protein, or one of receptor-linked enzyme. We then have cellular *yin* and *yang* [44]:

pathway 1 belongs to *yin*, and pathway 2 belongs to *yang*. (10)

The *yin* and *yang* of LIL depend on its dose zone. The dose zones were called dose n from the lowest dose of PBM on. At dose 1 [44],

Hot color light belongs to *yin*, and cold color light belongs to *yang*. (11)

According to *yin-yang* parallel principle [44], we have

Hot color light activates pathway 1, cold color light activates pathway 2. (12)

It is called BIMP1. If the dose is at dose 2 which is larger than the threshold of dose 1, the *yin-yang* properties of LIL will transform into each other according to *yin-yang* inter-transformation [44] so that we have,

Hot color light belongs to *yang*, and cold color light belongs to *yin*. (13)

According to *yin-yang* parallel principle [44], we have from (10) and (13).

Cold color light activates pathway 1, hot color light activates pathway 2. (14)

This is called BIMP2. Generally, we have (13) according to *yin-yang* intertransformation if the dose is at dose $2n$ (n = 1, 2,3,...) which is larger than the threshold of dose $2n - 1$ if it does not damage membrane or cell compartments such as mitochondria, lysosomes, endoplasmic reticulum so that (13) is called BIMP $2n$, and we have (14) according to *yin-yang* inter-transformation if the dose is at dose $2n+1$ (n = 1, 2,3, ...) which is larger than the threshold of dose $2n$ if it does not damage membrane or cell compartments so that (14) is called BIMP $2n + 1$. BIMP n (n = 1,2,3,...) has been supported by its successful application in the cellular level, animal model level, and clinic level [7, 42].

6. Self-Adaptive Photobiomodulation

The LPBM is non-specific so that it can modulate any function far from its respective FSH according to the dosage relationship discussed above. After an FSS disrupts an existing FSH, there are many would-be FSH (wFSH) which might be established. The higher the quality of the wFSH is, the stronger it resists the disturbances of the other functions far from their respective wFSH so that only the wFSH of highest quality is established by a successful stress [6]. Therefore, LIL can modulate a chronic stress until it is successful so that it might be self-adaptive. It is indeed self-adaptive at least according to our recent following progress, but it takes time long enough for a chronic stress to be successful. The observation period of many studies has been too short to observe the self-adaptive property of the PBM.

We have found that RLED 640 self-adaptively modulate high-glucose- (hG-) induced dysfunctions of C2C12 myoblasts [45]. hG increased the ratio of nicotinamide adenine dinucleotide (NAD^+) and its reduced form NADH, NAD^+/NADH, at 4th, 24th, and 36th h, respectively, but decreased it at 72nd h, which were completely reversed by RLED 640. hG decreased the mRNA levels of sirtuin 1 and manganese superoxide dismutase (MnSOD) at 4th, 24th, 48th, and 72nd h, respectively. The hG inhibition on sirtuin 1 mRNA was reversed by RLED 640 partially at 4th and 48th h, respectively, and completely at 72nd h, but wasnot modulated at 24th h. The hG inhibition on MnSOD mRNA was completely reversed by RLED 640 at 72nd h, but were not modulated at 4th, 24th, and 48th h. hG did not modulate the activities of MnSOD at 24th and 48th h and catalase at 4th, 24th, 48th, and 72nd h, respectively, but RLED 640 increased catalase activity only at 48th h. hG decreased MnSOD activity at 4th h, but increased it at 72nd h, which wasnot modulated by RLED 640.

We also found the low intensity gallium aluminum arsenide 635 nm laser irradiation (LIGL) effects on insulin-like growth factor-1 (IGF-1) and transforming growth factor (TGF) beta1 was self-adaptive [46]. LIGL promoted IGF-1 mRNA expression on the 1st, 2nd, 3rd, and 7th d, but inhibited the one on the 14th and 21st d, respectively. LIGL increased IGF-1 level on the 2nd, 3rd, and 7th d, but decreased the one on the 14th and 21st d, respectively. LIGL decreased TGF-beta1 level on the 3rd and 28th d, but increased the one on the 7th and 14th d, respectively.

7. Discussion

The dosage, intensity, or dose discussed above should be the exact dosage at which LI exactly interacts with the target cells. The LI gets weaker and weaker the further from the surface it penetrates so that there may be a difference between the LI dosage of light source and its exact dosage absorbed by the cells especially for the clinical applications. The dosage for PBM should be location-specific in order to get the same exact dosage absorbed by the cells. This LI penetration is on tissue type, pigmentation, and dirt on the skin or membrane. LI can even penetrate bone (as well as it can penetrate muscle tissue). Fat tissue is more transparent than muscle tissue.

8. Conclusion

The primary process of cellular PBM might be the key process of cellular PBM. The specific pathways might mediate MPBM so that the reciprocity rule holds. The non-specific pathways might mediate LPBM so that the reciprocity rule does not hold, the LPBM might be the SIN function of irradiation time when the intensity is kept constant, and the LPBM might be the linear function of intensity when the irradiation time is kept constant. There may be a dose zone in which LIL at different doses has biological effects similar to each other, so that BIMP might hold. LIL may self-adaptively modulate a chronic stress until it becomes successful.

Acknowledgments

This work was supported by National Science Foundation of China (60878061) and the Opening Project of MOE Key Laboratory of Laser Life Science, South China Normal University, Guangzhou, China.

References

[1] I. Lestas, G. Vinnicombe, and J. Paulsson, "Fundamental limits on the suppression of molecular fluctuations," *Nature*, vol. 467, no. 7312, pp. 174–178, 2010.

[2] W. B. Cannon, *The Wisdom of the Body*, W. W. Norton & Company New York, 1932.

[3] G. Recordati and T. G. Bellini, "A definition of internal constancy and homeostasis in the context of non-equilibrium thermodynamics," *Experimental Physiology*, vol. 89, no. 1, pp. 27–38, 2004.

[4] C. Y. Liu and P. Zhu, *Intranasal Low Intensity Laser Therapy*, People's Military Medical Press, Beijing, China, 2009.

[5] T. C. Y. Liu, R. Liu, L. Zhu, J. Q. Yuan, M. Hu, and S. H. Liu, "Homeostatic photobiomodulation," *Frontiers of Optoelectronics in China*, vol. 2, no. 1, pp. 1–8, 2009.

[6] T. C. Y. Liu, E. X. Wei, and F. H. Li, "Photobiomodulation on stress," *International Journal of Photoenergy*. In press.

[7] T. C. Y. Liu, J. L. Jiao, R. Duan, Y. Li, Y. Y. Yeung, and S. H. Liu, "Membrane mechanism of low intensity laser biostimulation on a cell," *Lasers in Medicine, Surgery and Dentistry. Croatia: European Medical Laser Association*, pp. 83–105, 2003.

[8] T. C.-Y. Liu, J.-L. Jiao, X.-Y. Xu, X.-G. Liu, S.-X. Deng, and S.-H. Liu, "Photobiomodulation: phenomenology and its mechanism," in *Proceedings of the Optics in Health Care and Biomedical Optics: Diagnostics and Treatment II*, B. Chance, M. Chen, A. E. T. Chiou, and Q. Luo, Eds., vol. 5630 of *Proceedings of SPIE*, p. 185, Beijing, China, 2005.

[9] T. Karu, *The Science of Low-Power Laser Therapy*, Gordon and Breach, Amsterdam, The Netherlands, 1998.

[10] R. Lubart, M. Eichler, R. Lavi, H. Friedman, and A. Shainberg, "Low-energy laser irradiation promotes cellular redox activity," *Photomedicine and Laser Surgery*, vol. 23, no. 1, pp. 3–9, 2005.

[11] A. Ciani, K. U. Goss, and R. P. Schwarzenbach, "Photodegradation of organic compounds adsorbed in porous mineral layers: determination of quantum yields," *Environmental Science and Technology*, vol. 39, no. 17, pp. 6712–6720, 2005.

[12] N. Ben-Dov, G. Shefer, A. Irinitchev, A. Wernig, U. Oron, and O. Halevy, "Low-energy laser irradiation affects satellite cell proliferation and differentiation in vitro," *Biochimica et Biophysica Acta*, vol. 1448, no. 3, pp. 372–380, 1999.

[13] I. Stadler, R. Evans, B. Kolb et al., "In vitro effects of low-level laser irradiation at 660 nm on peripheral blood lymphocytes," *Lasers in Surgery and Medicine*, vol. 27, no. 3, pp. 255–261, 2000.

[14] Y. Wang, H. Shi, L. Yu, Z. Wang, X. Liu, and N. Lin, "The dosage and time effects of intravascular low level laser irradiation on red cell deformability," *Chinese Journal of Medical Physics*, vol. 13, no. 4, pp. 217–220, 1996.

[15] A. P. Sommer, A. L. B. Pinheiro, A. R. Mester, R. P. Franke, and H. T. Whelan, "Biostimulatory windows in low-intensity laser activation: lasers, scanners, and NASA's light-emitting diode array system," *Journal of Clinical Laser Medicine and Surgery*, vol. 19, no. 1, pp. 29–33, 2001.

[16] T. I. Karu, G. S. Kalenko, V. S. Letokhov, and V. V. Lobko, "Biological action of low-intensity visible light on hela cells as a function of the coherence, dose, wavelength, and irradiation regime," *Soviet journal of quantum electronics*, vol. 9, no. 9, pp. 1134–1138, 1982.

[17] T. I. Karu, G. S. Kalendo, V. S. Letokhov, and V. V. Lobko, "Biostimulation of HeLa cells by low-intensity visible light," *Il Nuovo Cimento D*, vol. 1, no. 6, pp. 828–840, 1982.

[18] A. Schindl, B. Rosado-Schlosser, and F. Trautinger, "The reciprocity rule in photobiology. A review," *Hautarzt*, vol. 52, no. 9, pp. 779–785, 2001.

[19] H. H. F. I. Van Breugel and P. R. D. Bar, "Power density and exposure time of He-Ne laser irradiation are more important than total energy dose in photo-biomodulation of human fibroblasts in vitro," *Lasers in Surgery and Medicine*, vol. 12, no. 5, pp. 528–537, 1992.

[20] R. Lubart, H. Friedmann, I. Peled, and N. Grossman, "Light effect on fibroblast proliferaton," *Laser Therapy*, vol. 5, no. 2, pp. 55–57, 1993.

[21] Y. L. Li, T. C. Y. Liu, X. G. Liu et al., "Experimental research on the non-resonant interaction of low intensity He-Ne laser irradiation with neutrophils," *Lasers in Surgery and Medicine*, vol. 34, no. 16, p. 40, 2004.

[22] R. J. Lanzafame, I. Stadler, A. F. Kurtz et al., "Reciprocity of exposure time and irradiance on energy density during photoradiation on wound healing in a murine pressure ulcer model," *Lasers in Surgery and Medicine*, vol. 39, no. 6, pp. 534–542, 2007.

[23] T. Karu, "Photobiology of low-power laser effects," *Health Physics*, vol. 56, no. 5, pp. 691–704, 1989.

[24] T. I. Karu and S. F. Kolyakov, "Exact action spectra for cellular responses relevant to phototherapy," *Photomedicine and Laser Surgery*, vol. 23, no. 4, pp. 355–361, 2005.

[25] L. Cheng, *Key process of cellular photo- biomodulation of low intensity laser irradiation*, M.S. thesis, South China Normal University, 2007.

[26] F. A. H. Al-Watban and B. L. Andres, "The effect of He-Ne laser (632.8 nm) and Solcoseryl in vitro," *Lasers in Medical Science*, vol. 16, no. 4, pp. 267–275, 2001.

[27] A. G. Brill, B. Shenkman, G. E. Brill et al., "Blood irradiation by He-Ne laser induces a decrease in platelet responses to physiological agonists and an increase in platelet cyclic GMP," *Platelets*, vol. 11, no. 2, pp. 87–93, 2000.

[28] T. J. Karu, G. S. Kalendo, and V. S. Letokhov, "Control of RNA synthesis rate in tumour cell HeLa by action of a low- intensity visible light of copper laser," *Lettere Al Nuovo Cimento Series 2*, vol. 32, no. 2, pp. 55–59, 1981.

[29] T. I. Karu, L. V. Pyatibrat, and G. S. Kalendo, "Donors of NO and pulsed radiation at λ = 820 nm exert effects on cell attachment to extracellular matrices," *Toxicology Letters*, vol. 121, no. 1, pp. 57–61, 2001.

[30] T. I. Karu, L. V. Pyatibrat, and G. S. Kalendo, "Cell attachment modulation by radiation from a pulsed light diode (λ = 820 nm) and various chemicals," *Lasers in Surgery and Medicine*, vol. 28, no. 3, pp. 227–236, 2001.

[31] T. I. Karu, L. V. Pyatibrat, and G. S. Kalendo, "Cell attachment to extracellular matrices is modulated by pulsed radiation at 820 nm and chemicals that modify the activity of enzymes in the plasma membrane," *Lasers in Surgery and Medicine*, vol. 29, no. 3, pp. 274–281, 2001.

[32] T. I. Karu, L. V. Pyatibrat, and T. P. Ryabykh, "Melatonin modulates the action of near infrared radiation on cell adhesion," *Journal of Pineal Research*, vol. 34, no. 3, pp. 167–172, 2003.

[33] T. I. Karu, L. V. Pyatibrat, and G. S. Kalendo, "Photobiological modulation of cell attachment via cytochrome c oxidase," *Photochemical and Photobiological Sciences*, vol. 3, no. 2, pp. 211–216, 2004.

[34] X. H. Yang, C. Y. Liu, S. J. Liu et al., "Photobiomodulation on chondrocyte proliferation: in vitro evaluation," *Zhongguo Jiguang/Chinese Journal of Lasers*, vol. 33, no. 12, pp. 1692–1697, 2006.

[35] Y. Zhang, S. Song, C. C. Fong, C. H. Tsang, Z. Yang, and M. Yang, "cDNA microarray analysis of gene expression profiles in human fibroblast cells irradiated with red light," *Journal of Investigative Dermatology*, vol. 120, no. 5, pp. 849–857, 2003.

[36] V. P. Zharov, T. I. Karu, Y. O. Litvinov, and O. P. Tiphlova, "Biological effect of radiation of a semiconductor laser in near infrared region," *Soviet Journal of Quantum Electronics*, vol. 17, no. 11, pp. 1361–1362, 1987.

[37] L. Cheng, T. C. Y. Liu, J. Q. Chi, Y. Li, and H. Jin, "Photobiomodulation on the proliferation and collagen synthesis of normal human skin fibroblast cells," in *International Commission for Optics: Biomedical Optics*, vol. 6026 of *Proceedings of SPIE*, August 2005.

[38] R. Duan, T. C. Y. Liu, Y. Li, H. Guo, and L. B. Yao, "Signal transduction pathways involved in low intensity He-Ne laser-induced respiratory burst in bovine neutrophils: a potential

mechanism of low intensity laser biostimulation," *Lasers in Surgery and Medicine*, vol. 29, no. 2, pp. 174–178, 2001.

[39] J. Liang, T. C. Y Liu, X. H. Yang, and S. H. Liu, "Collagen synthesis mediated photobiomodulation on chondrocyte proliferation in vitro," *Lasers in Surgery and Medicine*, vol. 40, no. 20, p. 78, 2008.

[40] X. Xu, X. Zhao, T. C. Y. Liu, and H. Pan, "Low-intensity laser irradiation improves the mitochondrial dysfunction of C2C12 induced by electrical stimulation," *Photomedicine and Laser Surgery*, vol. 26, no. 3, pp. 197–202, 2008.

[41] T. C. Y. Liu, L. Zhu, X. Y. Li, and S. H. Liu, "Red light promotion on the recovery of hydrogen peroxide pretreated differentiated PC12," *Lasers in Surgery and Medicine*, vol. 42, no. 22, pp. 57–58, 2010.

[42] T. C. Liu, Y. Q. Gao, and S. H. Liu, "Light-cell interaction: quasi-hormone model and time theory," in *Proceedings of the SPIE*, vol. 2887, pp. 140–151, November 1996.

[43] H. H. Yin and X. Z. Shuai, *Fundamentals of Traditional Chinese Medicine*, Foreign Languages Press, Beijing, China, 1992.

[44] T. C. Y. Liu, J. L. Jiao, X. Y. Xu, J. Lu, X. Y. Deng, and S. H. Liu, "Process Theory—The Bridge of the Eastern and Western Culture," in *Science, Medicine and Culture: Festschrift for G. Fritz Wallner*, M. J. Jandl and K. Greiner, Eds., pp. 165–175, Peter Lang GmbH, Frankfurt, Germany, 2005.

[45] Y. Y. Liu, F. H. Li, E. X. Wei, and T. C. Y. Liu, "Self-adaptive photobiomodulation on high glucose induced dysfunctions of C2C12 myoblasts," *Lasers in Surgery and Medicine*, vol. 44, no. S24, p. 63, 2012.

[46] T. C. Y. Liu, L. Luo, and L. Zhang, "Self-adaptive effects of low intensity laser irradiation in prophylaxis of muscular fibrosis," *Lasers in Surgery and Medicine*, vol. 43, no. S23, p. 975, 2011.

Hindawi Publishing Corporation
International Journal of Photoenergy
Volume 2012, Article ID 290796, 5 pages
doi:10.1155/2012/290796

Research Article

Efficacy of Proliferation of HeLa Cells under Three Different Low-Intensity Red Lasers Irradiation

H. Q. Yang, Y. H. Wang, J. X. Chen, X. G. Chen, Y. M. Huang, H. Li, S. S. Xie, and L. Q. Zheng

Key Laboratory of Optoelectronic Science and Technology for Medicine of Ministry of Education, Provincial Key Laboratory for Photonics Technology, Institute of Laser and Optoelectronics Technology, Fujian Normal University, Fuzhou 350007, China

Correspondence should be addressed to S. S. Xie, ssxie@fjnu.edu.cn

Received 16 January 2012; Revised 3 May 2012; Accepted 15 May 2012

Academic Editor: Timon Cheng-Yi Liu

This study was intended to compare the efficacy of proliferation of HeLa cells under three different low-intensity laser irradiation (LIL), that is, 633 nm, 658 nm, and 785 nm. The time-dependent responses of proliferation of HeLa cells after the red laser irradiation and the influence of fetal bovine serum (FBS) at 1%, 2%, 5%, or 10% on the proliferation of cells were also investigated. The results indicated that the proliferation of HeLa cells in 10% FBS was in proliferation-specific homeostasis (PSH) so that it was not modulated with LIL; the proliferation in FBS at 1%, 2%, or 5% was far from PSH so that it may be wavelength dependently modulated with LIL, and the maximum proliferation promotion was conducted with LIL at 633 nm amongst the three different LIL. It was concluded the wavelength-dependent photobiomodulation of LIL on proliferation of HeLa cells may be homeostatic.

1. Introduction

The interaction between low-intensity laser irradiation (LIL) and biological system or tissue has attracted much attention and motivated LIL therapy, an interdisciplinary branch of photomedicine in the past several decades, which involved the studies and applications of LIL in health care and disease treatment. This therapeutic approach has primarily been shown to be useful in the short-term treatment of acute pain caused by rheumatoid arthritis [1], osteoarthritis [2] and in the treatment of both acute and chronic neck pain [3], although it is still unclear how it works. Many kinds of photobiomodulation (PBM) may be involved when biological systems or cells are irradiated with LIL [4–6]. Amongst these effects, PBM on proliferation can happen to various types of cells, such as, fibroblasts, osteoblasts, lymphocytes, stem cells, endothelial cells, lung adenocarcinoma cancer cells, and HeLa cells. PBM on proliferation is the basis of LIL on wound healing, which has been explored and encouraged to be used as an alternative noninvasive method [7]. And researchers have made much progress for decades in the cellular and molecular mechanism of phototherapy or PBM [8–15], especially cellular responses to visible and near infrared radiation related to the mitogenic effects promoted by LIL, such as, absorption of light by mitochondrial enzymes [16], photon absorption by flavins and cytochromes in the mitochondrial respiratory chain affecting electron transfer [4], and photoactivation of calcium channels resulting in increased intracellular calcium concentration and cellular proliferation [17]. The mechanism underlying PBM is still elusive. In addition, not all of LIL studies supported the positive efficacy of PBM. For example, LIL from a gallium aluminum arsenide laser failed to increase proliferation, migration, or adhesion of cultured keratinocytes or fibroblasts [18]. LIL on wounds created in X-ray-treated skin failed to improve wound healing and inhibited healing with the increase of fluence [19]. These varied results prompt that many important factors, including laser parameters (e.g., wavelength, power density, fluence, or irradiation time) and cell types may influence significantly the stimulated effects.

Studies have found that red lights could modulate the maximum cell proliferation [16, 20]. However, few reports involved the comparison of cell proliferation modulated by different red lights in different environment conditions. This study was intended to investigate the efficacy of proliferation of HeLa cells in different concentrations of fetal bovine serum (FBS) under the irradiation of three red lasers

at 633 nm, 658 nm, and 785 nm, respectively. The time-dependent responses of proliferation of HeLa cells after LIL were also studied.

2. Materials and Methods

2.1. Cell Culture. The human cervical carcinoma HeLa cells were maintained in Dulbecco's modified Eagle medium (DMEM) supplemented with 10% FBS, 100 U/mL penicillin, and 100 μg/mL streptomycin, in a humidified incubator with 5% CO_2 under 37°C condition. The cells were digested with 0.125% trypsin every three days and then subcultured into 100 mm culture dishes.

2.2. Lasers Irradiation. HeLa cells at 1.5×10^4 cells/mL were seeded in 96-well microplates using plain DMEM supplemented with 1%, 2%, 5%, and 10% FBS, respectively (total of nine plates in each group). The plates were maintained in the humidified incubator with 5% CO_2 and 95% air at 37°C for 24 hours. The three red lasers used in this study were 633 nm He-Ne laser (Melles Griot, USA), 658 nm diode laser (LQC. Newport, USA), and 785 nm diode laser (LQC. Newport, USA), respectively. The laser power density was 10 W/m^2 and its irradiation time was 100 s. After irradiation, the cells were returned to the incubator. The control groups without LIL were exposed to the same environmental and stress conditions, such as, temperature, humidity, and FBS concentrations. The cell viability of each group was tested at the time of 24, 48, and 72 h, respectively after LIL turning off. All of the measurements were carried out at least in triplicate. In addition, in order to determine a better LIL dose, four different irradiation fluences 100, 300, 600, and 1000 J/m^2 of 633 nm He-Ne laser irradiation were chosen. The laser power density was 10 W/m^2 and the irradiation time was 10, 30, 60, and 100 s, respectively. The cells were cultured in plain DMEM supplemented with 5% FBS. The other procedures were performed according to the above method.

2.3. MTT Assay for Cell Proliferation. MTT(3-(4,5-dimethylthiazol-2-yl)-2,5-diphenyltetrazolium bromide) assay was used to analyze the cell proliferation. It is a laboratory test and standard colorimetric assay for measuring cellular viability and proliferation. Each well of 96-well microplate was added 20 μL of MTT solution (5 mg/mL sterile PBS) and incubated in dark environment at 37°C for 4 hours. Then the cultured medium with the MTT solution was removed and 150 μL/well of dimethylsulfoxide (DMSO) was added to dissolve the formazan crystals. The absorbance was measured via a multimode reader fluorimeter (Mithras LB 940, Germany) and the excitation wavelength was 490 nm. The MTT absorbance value was proportional to the number of viable cells and the cell proliferation.

2.4. Statistical Analysis. Data was given in the format of mean ± standard error. Student's t-test method was used to evaluate the statistical difference. The statistical value $P < 0.05$ means significantly statistical difference and $P < 0.01$ means obviously statistical difference.

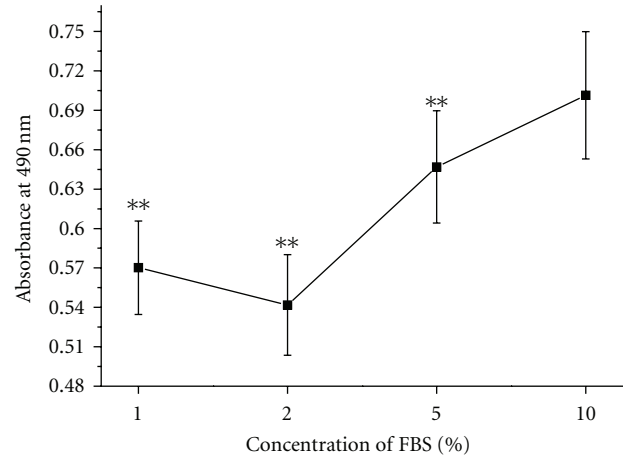

Figure 1: The cell proliferation of HeLa cells in different FBS concentrations without laser irradiation. Error bars were from three independent experiments. $^{**}P < 0.01$.

3. Results

The proliferation of cells varied with FBS concentrations. Figure 1 gave the relationship between HeLa cell viability and FBS concentrations (1%, 2%, 5%, and 10%). Herein, the cell viability was given in the format of absorbance. HeLa cells viability was nonlinearly dependent on FBS concentration. The lowest of cell viability was at 2% FBS. When the FBS concentration was more than 2%, cell viability increased with FBS concentration, and it reached the highest at 10% FBS. The cell growth in 1%, 2%, 5% FBS was significantly lower than that in 10% FBS, respectively ($P < 0.01$).

The proliferation response to laser irradiation fluence of 100, 300, 600, and 1000 J/m^2 was shown in Figure 2. The measurements were carried out at 24, 48, and 72 h after LIL. The cell viability was given in the ratio of the value of LIL group to that of the control group. As shown in Figure 2, the irradiation fluence influenced the proliferation response of HeLa cells. The cell viability increased with LIL fluence, and LIL group of 100, 300, 600 J/m^{2}did not differ statistically from that of 1000 J/m^2 ($P > 0.05$). The values of all the LIL groups were higher than the ones of their control groups, that is, the relative viability was higher than 1. Moreover, the proliferation of HeLa cells at 48 h was the most obvious one. Therefore, the fluence of 1000 J/m^2 was chosen in the following experiments.

The proliferation responses of HeLa cells in 1%, 2%, 5%, and 10% FBS to 633 nm, 658 nm, and 785 nm irradiation at 1000 J/m^2 were given in Figures 3, 4, and 5, respectively. The assessments were carried out at 48 h after laser irradiation. Control groups without LIL were also investigated at the same time. The proliferation difference in 5% FBS was significant between LIL groups of 633 nm ($P < 0.01$), 658 nm ($P < 0.05$), and 785 nm ($P < 0.01$) and their corresponding control groups, respectively. The proliferation difference in 1% FBS was also significant between control group and LIL group of 785 nm ($P < 0.01$). For the other concentrations of FBS, the LIL group did not differ statistically from

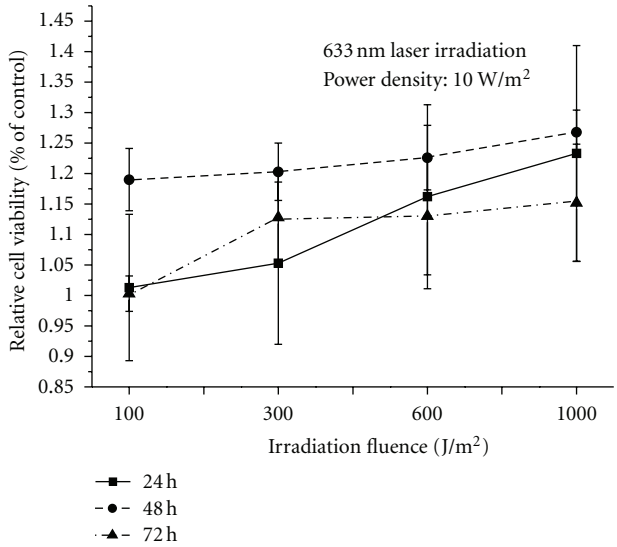

Figure 2: The viability of HeLa cells irradiated with LIL at 633 nm in 5% FBS. The laser power density was 10 W/m^2. Error bars were from three independent experiments.

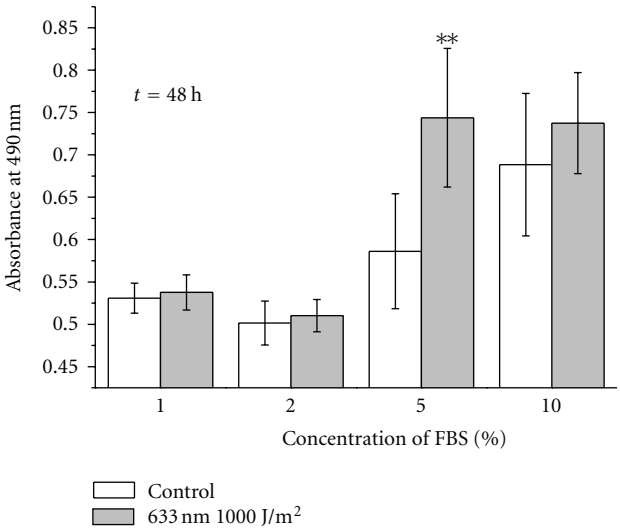

Figure 3: The proliferation of HeLa cells in different FBS concentrations (laser wavelength $\lambda = 633$ nm, energy density 1000 J/m^2, irradiation time 100 s). The absorbance value was assessed at 48 h after laser irradiation. Error bars were from three independent experiments, $^{**}P < 0.01$.

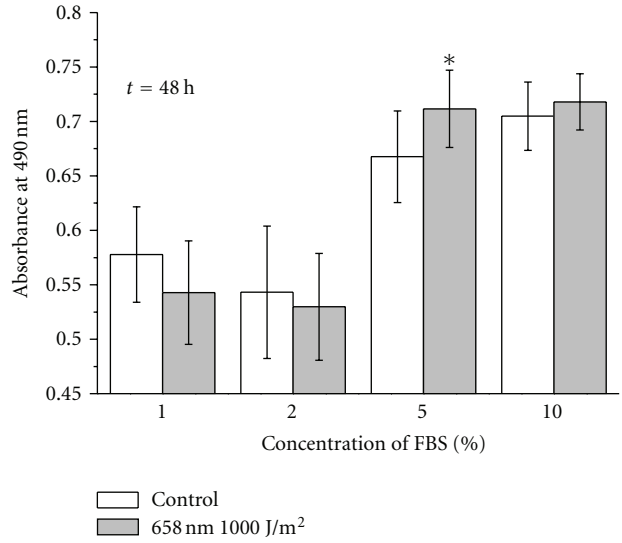

Figure 4: The proliferation of HeLa cells in different FBS concentrations (laser wavelength $\lambda = 658$ nm, energy density 1000 J/m^2, irradiation time 100 s). The absorbance value was assessed at 48 h after laser irradiation. Error bars were from three independent experiments, $^{*}P < 0.05$.

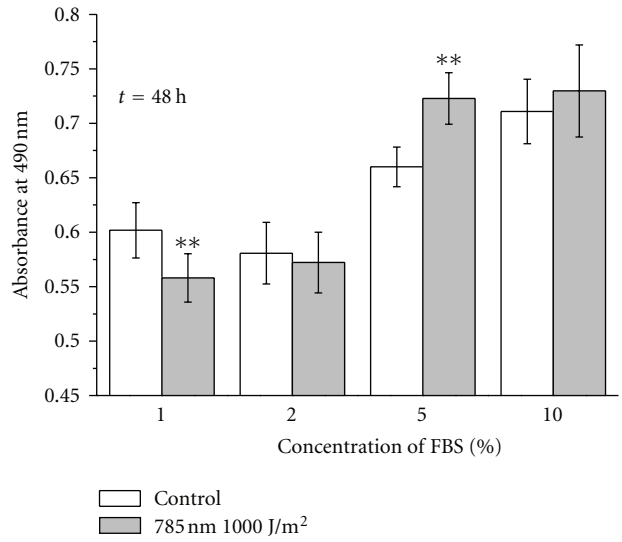

Figure 5: The proliferation of HeLa cells in different FBS concentrations (laser wavelength $\lambda = 785$ nm, energy density 1000 J/m^2, irradiation time 100 s). The absorbance value was assessed at 48 h after laser irradiation. Error bars were from three independent experiments, $^{**}P < 0.01$.

the respective control group ($P > 0.05$). Furthermore, for the control groups, the cell growth in 5% FBS was significantly lower than that in 10% FBS ($P < 0.01$). When the cells were irradiated with LIL, the cell growth in 5% FBS did not differ statistically from that in 10% FBS ($P > 0.05$). This means that LIL completely recovered the proliferation of cells in 5% FBS.

The time-dependent responses of proliferation of HeLa cells in 5% FBS after the three red laser irradiation at 633 nm, 658 nm, and 785 nm were compared in Table 1, in which the cell viability of control groups was 100%. The cell viability was assessed at 24 h, 48 h, and 72 h after lasers irradiation. Obviously, the proliferation of HeLa cells was wavelength-dependent, and the response of proliferation to LIL was obviously time-dependent. At 24 h, 48 h and 72 h after laser irradiation, the proliferation difference was significant between LIL groups of 633 nm and 658 nm ($P < 0.01$) or 785 nm ($P < 0.05$), but there was no significant difference between LIL group of 658 nm and 785 nm ($P > 0.05$). The three red laser irradiations might promote cells proliferation,

Table 1: The time-dependent responses of proliferation of HeLa cells in 5% FBS after three red lasers stimulation (Laser energy density and its irradiation time were 1000 J/m^2 and 100 s, resp.).

Time	Wavelength		
	633 nm	658 nm	785 nm
24 h	1.230 ± 0.082^a	1.034 ± 0.022^c	1.064 ± 0.067^a
48 h	1.269 ± 0.110^a	1.049 ± 0.083^b	1.105 ± 0.071^a
72 h	1.140 ± 0.094^c	1.003 ± 0.030^c	1.014 ± 0.054^c

Notes: The values were the ratio of laser irradiation group to control group (%) ($^aP < 0.01$; $^bP < 0.05$; $^cP > 0.05$).

respectively, and all the three proliferation peaks were at 48 h after laser irradiation.

4. Discussion

LIL may modulate the cell proliferation, which was dependent on many factors, such as, laser wavelength, dose, or intensity as well as FBS concentrations. Among them, the FBS concentration was the key factor. It could be used as a mean to produce different cell growth states. In this study, 1%, 2%, 5%, and 10% FBS were chosen and PBM on cell proliferation was investigated and compared under these nutritional conditions. Cells in 10% FBS were in normal culture state, while cells in 1%, 2%, 5% FBS were in nutritional stress. Many studies have found no PBM on proliferation in 10% FBS, so that it was stated that the proliferation in 10% FBS may be in proliferation-specific homeostasis (PSH) which is a negative feedback to maintain proliferation at its local peak [21]. There was no PBM on proliferation in PSH, but there was PBM on proliferation far from PSH. It was supported in this study. There was no significant PBM on HeLa cells proliferation in 10% FBS. All the three concentrations of FBS, 1%, 2%, and 5%, inhibited proliferation in comparison with proliferation in PSH, respectively. This means that the concentrations of FBS, 1%, 2%, and 5%, can reduce the cell growth rate and make the cell far away from PSH. As the results shown, there may be PBM on proliferation in FBS at 1% and 5%, respectively. LIL at 785 nm inhibited the proliferation in 1% FBS, but all the three kinds of LIL completely recovered 5% FBS-inhibited proliferation in comparison with the proliferation in PSH. In other words, the proliferation may be in PSH in 10% FBS or in 5% FBS under LIL. This is a redundant phenomenon. LIL might promote proliferation in 5% FBS through redundant pathways, which will be further studied [22]. The result was in accordance with the finding of Almeida-Lopes et al. [23] and Tagliani et al. [24]. However, it should be pointed out that 1% and 2% FBS were so low that it can not maintain proliferation and may cause some harmful cell stress. In this case, cells did not produce a satisfactory proliferation response to laser irradiation or may cause other stimulation effects. In our study, we found that LIL didn't promote the proliferation of HeLa cells in 1% and 2% FBS, and LIL at 785 nm inhibited the proliferation in 1% FBS. The reason may be that the LIL at 785 nm might promote other cellular functions except proliferation, such as, in G0 phase so that the proliferation was inhibited. All in all, cellular proliferation in FBS at 1%, 2%, or 5% are far from PSH, so that it can be modulated with LIL. This was also a support to the viewpoint of homeostatic PBM [21].

This study compared the proliferation of HeLa cells modulated by three different LIL at 633 nm, 658 nm, and 785 nm. Among them, the best proliferation effect was at 633 nm. The results indicated that laser wavelength was an important factor that influenced the PBM. This may be due to different wavelength absorption by cellular chromophores, which modulated cell functions differently. The suitable wavelength at 633 nm may be absorbed well by the photoreceptor, such as, chromophores in cytochrome c oxidase or porphyrins, which could lead to second messenger activity resulting in functional changes and cell proliferation. The other possible reason was in relation to the type of lasers. The 633 nm laser used in this study was gas laser, which has longer coherence length and more obvious biological effects than the diode laser (658 nm, 785 nm) [25]. Our results agreed with Moore's work [16]. It is a possible reason why 633 nm He-Ne laser has been widely used in wound healing in clinical application.

5. Conclusions

The proliferation of HeLa cells in 10% FBS was in PSH so that it was not modulated with LIL. The proliferation in FBS at 1%, 2%, or 5% was far from PSH so that it may be wavelength dependently modulated with LIL. The maximum proliferation promotion was conducted with LIL at 633 nm amongst the three kinds of LIL, 633 nm, 658 nm, and 785 nm. This study provided helpful experimental data and shed new light on the research of LIL therapy and its mechanism.

Authors' Contribution

H. Q. Yang and Y. H. Wang contributed equally to this work.

Acknowledgments

This work was supported by the National Natural Science Foundation of China under Grant no. 60978071, Program for Changjiang Scholars and Innovative Research Team in University under Grant no. IRT1115, Natural Science Foundation of Fujian Province under Grant no. 2010J01322, and Fujian Province Educational Project B under Grant no. JB10021 and no. JB11023.

References

[1] L. Brosseau, V. Welch, G. Wells et al., "Low level laser therapy (Classes I, II and III) for treating osteoarthritis," *Cochrane Database of Systematic Reviews*, no. 3, Article ID CD002046, 2004.

[2] G. Jamtvedt, K. T. Dahm, A. Christie et al., "Physical therapy interventions for patients with osteoarthritis of the knee: an overview of systematic reviews," *Physical Therapy*, vol. 88, no. 1, pp. 123–136, 2008.

[3] R. T. Chow, M. I. Johnson, R. A. Lopes-Martins, and J. M. Bjordal, "Efficacy of low-level laser therapy in the management of neck pain: a systematic review and meta-analysis of randomised placebo or active-treatment controlled trials," *The Lancet*, vol. 374, no. 9705, pp. 1897–1908, 2009.

[4] T. Karu, "Photobiology of low-power laser effects," *Health Physics*, vol. 56, no. 5, pp. 691–704, 1989.

[5] R. Duan, T. C. Y. Liu, Y. Li, H. Guo, and L. B. Yao, "Signal transduction pathways involved in low intensity He-Ne laser-induced respiratory burst in bovine neutrophils: a potential mechanism of low intensity laser biostimulation," *Lasers in Surgery and Medicine*, vol. 29, no. 2, pp. 174–178, 2001.

[6] T. Karu, "Low-power laser therapy," in *Biomedical Photonics Handbook*, V. D. Tuan, Ed., pp. 4801–4825, CRC Press, Boca Raton, Fla, USA, 2003.

[7] W. Posten, D. A. Wrone, J. S. Dover, K. A. Arndt, S. Silapunt, and M. Alam, "Low-level laser therapy for wound healing: mechanism and efficacy," *Dermatologic Surgery*, vol. 31, no. 3, pp. 334–340, 2005.

[8] D. Hawkins and H. Abrahamse, "Influence of broad-spectrum and infrared light in combination with laser irradiation on the proliferation of wounded skin fibroblasts," *Photomedicine and Laser Surgery*, vol. 25, no. 3, pp. 159–169, 2007.

[9] D. Hawkins-Evans and H. Abrahamse, "Efficacy of three different laser wavelengths for in vitro wound healing," *Photodermatology Photoimmunology and Photomedicine*, vol. 24, no. 4, pp. 199–210, 2008.

[10] X. G. Liu, Y. J. Zhou, T. C. Y. Liu, and J. Q. Yuan, "Effects of low-level laser irradiation on rat skeletal muscle injury after eccentric exercise," *Photomedicine and Laser Surgery*, vol. 27, no. 6, pp. 863–869, 2009.

[11] T. I. Karu, "Mitochondrial signaling in mammalian cells activated by red and near-IR radiation," *Photochemistry and Photobiology*, vol. 84, no. 5, pp. 1091–1099, 2008.

[12] H. O. Schwartz-Filho, A. C. Reimer, C. Marcantonio, E. Marcantonio, and R. A. C. Marcantonio, "Effects of low-level laser therapy (685 nm) at different doses in osteogenic cell cultures," *Lasers in Medical Science*, vol. 26, no. 4, pp. 539–543, 2011.

[13] X. Gao and D. Xing, "Molecular mechanisms of cell proliferation induced by low power laser irradiation," *Journal of Biomedical Science*, vol. 16, no. 1, article 4, 2009.

[14] T. Kushibiki, T. Tajiri, Y. Ninomiya, and K. Awazu, "Chondrogenic mRNA expression in prechondrogenic cells after blue laser irradiation," *Journal of Photochemistry and Photobiology B*, vol. 98, no. 3, pp. 211–215, 2010.

[15] J. Liebmann, M. Born, and V. Kolb-Bachofen, "Blue-light irradiation regulates proliferation and differentiation in human skin cells," *Journal of Investigative Dermatology*, vol. 130, no. 1, pp. 259–269, 2010.

[16] P. Moore, T. D. Ridgway, R. G. Higbee, E. W. Howard, and M. D. Lucroy, "Effect of wavelength on low-intensity laser irradiation-stimulated cell proliferation in vitro," *Lasers in Surgery and Medicine*, vol. 36, no. 1, pp. 8–12, 2005.

[17] H. Breitbart, T. Levinshal, N. Cohen, H. Friedmann, and R. Lubart, "Changes in calcium transport in mammalian sperm mitochondria and plasma membrane irradiated at 633 nm (HeNe laser)," *Journal of Photochemistry and Photobiology B*, vol. 34, no. 2-3, pp. 117–121, 1996.

[18] M. A. Pogrel, J. W. Chen, and K. Zhang, "Effects of low-energy galliumaluminum-arsenide laser irradiation on cultured fibroblasts and keratinocytes," *Lasers in Surgery and Medicine*, vol. 20, no. 4, pp. 426–432, 1997.

[19] A. S. Lowe, M. D. Walker, M. O. Byrne, G. D. Baxter, and D. G. Hirst, "Effect of low intensity monochromatic light therapy (890 nm) on a radiation-impaired wound-healing model in murine skin," *Lasers in Surgery and Medicine*, vol. 23, no. 5, pp. 291–298, 1998.

[20] H. Yang, Y. Wang, J. Chen, L. Zheng, and S. Xie, "Low level laser irradiation in the visible spectra induces HeLa proliferation," *Spectroscopy and Spectral Analysis*, vol. 32, no. 4, pp. 1024–1027, 2012.

[21] T. C. Y. Liu, R. Liu, L. Zhu, J. Yuan, M. Hu, and S. Liu, "Homeostatic photobiomodulation," *Frontiers of Optoelectronics in China*, vol. 2, no. 1, pp. 1–8, 2009.

[22] T. C. Y. Liu and Y. Liu, "Redundant photobiomodulation," *Personal Communication*. In press.

[23] L. Almeida-Lopes, J. Rigau, R. A. Zângaro, J. Guidugli-Neto, and M. M. M. Jaeger, "Comparison of the low level laser therapy effects on cultured human gingival fibroblasts proliferation using different irradiance and same fluence," *Lasers in Surgery and Medicine*, vol. 29, no. 2, pp. 179–184, 2001.

[24] M. M. Tagliani, C. F. Oliveira, E. M. M. Lins et al., "Nutritional stress enhances cell viability of odontoblast-like cells subjected to low level laser irradiation," *Laser Physics Letters*, vol. 7, no. 3, pp. 247–251, 2010.

[25] D. Hawkins-Evans and H. Abrahamse, "Efficacy of three different laser wavelengths for in vitro wound healing," *Photodermatology Photoimmunology and Photomedicine*, vol. 24, no. 4, pp. 199–210, 2008.

Hindawi Publishing Corporation
International Journal of Photoenergy
Volume 2012, Article ID 167425, 11 pages
doi:10.1155/2012/167425

Research Article

Low-Dose UVA Radiation-Induced Adaptive Response in Cultured Human Dermal Fibroblasts

Zhongrong Liu, Hulin Chen, Huilan Yang, Jie Liang, and Xuemei Li

Department of Dermatology, Guangzhou General Hospital of Guangzhou Military Command (Liuhuaqiao Hospital), Guangzhou 510010, China

Correspondence should be addressed to Zhongrong Liu, pfklzr@163.com

Received 12 February 2012; Revised 6 April 2012; Accepted 3 May 2012

Academic Editor: Timon Cheng-Yi Liu

Objective. To investigate the mechanism of the adaptive response induced by low-dose ultraviolet A (UVA) radiation. *Methods.* Cultured dermal fibroblasts were irradiated by a lethal dose of UVA (86.4 J/cm^2) with preirradiation of single or repetitive low dose of UVA (7.2 J/cm^2). Alterations of cellular morphology were observed by light microscope and electron microscope. Cell cycle and cellular apoptosis were assayed by flow cytometer. The extent of DNA damage was determined by single-cell gel electrophoresis (SCGE). *Results.* The cultured dermal fibroblasts, with pretreatment of single or repetitive irradiation of 7.2 J/cm^2 UVA relieved toxic reaction of cellular morphology and arrest of cell cycle, decreased apoptosis ratio, reduced DNA chain breakage, and accelerated DNA repair caused by subsequent 86.4 J/cm^2 UVA irradiation. Compared with nonpretreatment groups, all those differences were significant ($P < 0.01$ or $P < 0.05$). *Conclusions.* The adaptation reaction might depend on the accumulated dose of low-dose UVA irradiation. Low-dose UVA radiation might induce adaptive response that may protect cultured dermal fibroblasts from the subsequent challenged dose of UVA damage. The duration and protective capability of the adaptive reaction might be related to the accumulated dose of low-dose UVA Irradiation.

1. Introduction

All the organisms on the Earth are constantly under the impact of environment. Generally, the organisms adapt to the various environmental factors by natural selection. The nature of adaptive response depends upon the different environmental factors, subject to the evolutionary development and functional status of the organisms, while a few others depend on the nature and the dose of the environmental factors [1].

The lethal dose of the environmental factors often leads to serious injury, or even death of the organisms. However, when the intensity of the environmental factor was not life-threatening, it might induce an adaptive response to reduce the damage caused by a subsequent attack by a lethal dose of the same factor within a certain duration. The nature of the adaptive response to low intensity or dose of the environmental factors is one of the hot areas of research [2].

The adaptive response of organisms or cells induced by low-dose ionization radiation (IR), also termed as low-dose radiation hormesis, was described as the reduced damaging effect of a lethal radiation dose when pretreated by a low priming dose [3]. In the last 30 years, the adaptive response to low-dose IR has been widely investigated. It has been observed *in vitro* and *in vivo* using various indicators of cellular damage, such as cell lethality, chromosomal aberrations, mutation induction, radiosensitivity, and DNA repair [4–6], although its precise mechanisms remained to be further elucidated. All the ubiquitous adaptive response phenomena entail the conservation of programmed adaptability of organic evolution [7].

The Sun emits a wide spectrum of electromagnetic waves from IR to microwaves. Photobiomodulation (PBM) of laser irradiation or monochromatic light (LI) were widely studied as well [8]. Several observations showed that even low-energy visible light (LEVL) might recover the rate of healing of wounds or bone defects [9, 10], the fertilizing capability of sperm cells [11], and proliferation of cultured cells such as fibroblasts [12], keratinocytes [13], and lymphocytes [14].

Although exposure to ultraviolet (UV) light is often viewed as pathogenic owing to its role in the genesis of skin cancer and skin aging [15–17], growing epidemiological

evidence suggests that such exposure may decrease the risk for a number of more serious cancers. Aside from having a favorable impact on blood pressure and vascular health, it may help to prevent certain autoimmune disorders, in addition to its well-known influence on bone density [18, 19]. These beneficial effects may relate to the adaptive response of UV radiation.

It has been widely reported that high doses of UV radiation induce cellular adaptive response, including photoreactivation, UV damage excision repair (UVER) [20], recombination repair, and SOS reaction [21]. The thickening and pigmentation of the epidermis caused by long-term UV radiation are regarded as a type of adaptive response of the organisms against UV radiation [22, 23]. However, the adaptive response induced by low-dose UV radiation has yet to be fully investigated.

As the major component of solar UV, UVA (320~400 nm) mainly produces reactive oxygen species (ROS) through interaction with endogenous photosensitizers. These ROS in turn damage DNA (indirect DNA damage), proteins and membranes [24]. Through direct damage to tissue cells and proteins, and the induction of proteolytic pathways, UVA causes cellular damage similar to IR [25]. However, whether the low-dose UV radiation induces adaptive response like low-dose IR will be investigated in this paper.

2. Material and Methods

2.1. Fibroblast Culture. The cell culture media and chemicals were purchased from Gibco Life Technologies (Cergy Pontoise, France) and Sigma (St. Louis). Skin specimens were collected from healthy neonatal foreskin, and primarily cultured with basal medium (DMEM medium containing 10% fetus calf serum (FCS), 10 mM N-2 HEPES, 1.5 g/L sodium bicarbonate, 0.3 g/L, 100 U/mL glutamine, penicillin, and 100 μg/mL streptomycin). Cells were maintained at 37°C in 5% CO_2, 95% air in a humidified chamber, and then dermal fibroblasts were harvested successfully and stocked in nitrogen canister based on the methods used to establish diploid cell lines [26].

2.2. UVA Irradiation and Low-Dose Determination. Human dermal fibroblasts were thawed and inoculated (250,000 cells/dish), and grown to 70% confluence in a 10-cm plastic culture dish (Corning Costar, Cambridge, MA, USA). To avoid toxicity induced by UV exposure of the culture medium, irradiation was achieved in PBS (phosphate buffered saline, 0.01 mM, pH 7.2). The cells were then exposed under desktop device (Sigma Aldrich), which releases UVA. UVA intensity was 60 mW/cm^2 at 15 cm exposure distance. The dosage of single exposure was calculated by UVA intensity (mW/cm^2) × time (s). After irradiation, the PBS was removed and the fibroblasts were incubated in the medium at 37°C and 5% CO_2 for varying durations. Control cells were treated similarly but without irradiation [27].

Cytotoxicity of UVA irradiation and low-dose modulation were assessed by MTT (3-(4,5-dimethylthiazol-2-yl)-2,5-diphenyltetrazolium bromide). Cultured dermal fibroblasts were transferred into 96-well plates with a density of 1×10^3 cells/well, and irradiated by different doses of UVA (0, 7.2, 14.4, 28.8, 43.2, 64.8, 86.4, and 108 J/cm^2). Each radiation group had 6 repeated wells. Cells in the control group were covered with a tin foil. At the six different time points of 3 h, 6 h, 12 h, 24 h, 48 h, and 72 h after irradiation, MTT solution (5 g/L, 20 μL, 4°C) was added to each well and the plate was incubated for 4 h. Subsequently, the medium was discarded, and 150 μL dimethylsulfoxide (DMSO) was added into each well. After shaking for 10 min, the absorbance value at the wavelength of 570 nm (A_{570}) was determined by Microplate EL 309 Reader. The survival rate (%) was calculated as [(A_{570} of the sample − A_{570} of the blank)/(A_{570} of the control − A_{570} of the blank)] × 100% [28, 29].

2.3. Experimental Groups. Cells cultured for 5~10 generations were divided into 4 groups as follows (Table 1): sham-irradiated group (SIG), normal cultured cells with the same number of doublings compared with the irradiation group were sham irradiated after similar manipulation; low-dose group (LDG), the cultured cells irradiated by 7.2 J/cm^2 UVA (60 mW/cm^2 for 120 s) once a day were divided into LDG1 to LDG5 according to the different accumulated doses 7.2, 14.4, 28.8, 57.6, and 115.2 J/cm^2, respectively; high-dose group (HDG), the cultured cells were only irradiated by 86.4 J/cm^2 UVA (60 mW/cm^2 for 1440 s); adaptive response group (ARG), the cultured cells preirradiated by low-dose UVA, and then irradiated by high-dose 86.4 J/cm^2 UVA. The cells were also divided from ARG1 to ARG5 according to the different accumulated low doses of UVA: 7.2, 14.4, 28.8, 57.6, and 115.2 J/cm^2, respectively, and then irradiated by high dose of 86.4 J/cm^2 UVA after preirradiation for 6 h, 12 h, 24 h, 48 h, 72 h, 7 d, and 14 d, respectively.

2.4. Morphological Observations. Cellular and morphological alterations in different groups were observed at different times under inverted transmission electron microscopy (TEM, JEM-2000EX, Japan) and scanning electron microscopy (SEM, S-520, Japan). Alterations of superficial membrane microvilli and intracellular mitochondria were prominently identified.

2.5. Detection of Cell Cycle and Apoptosis with Flow Cytometry. Cells cultured for 5~10 generations were inoculated into a 6-well culture plate by different grouping manipulations, rinsed once with 1 mL D-Hank's liquid, digested with 0.25% dispase, and then centrifuged and supernatant removed. Cells were separated with 0.5 mL D-Hank's and rinsed twice with 0.01 M PBS (pH 7.4). Cell suspension was prepared with 190 μL binding buffer and the density adjusted to 1×10^6/mL. Annexin V-FITC and PI (1 μg/mL) were added to the cell suspension. Cells were stored for 10 min away from light and rinsed once with binding buffer. Cell cycle and apoptosis were assayed by flow cytometer (FCM). (Elite ESP flow cytometry, Beckman Coulter, Inc.). FCM analysis was done using a single argon ion laser. The wavelength of excited light was 488 nm, and the wavelengths of emitted light were 515–545 nm for annexin V-FITC and 563–607 nm for DNA-PI. Each specimen was measured using 15000 to 20000 cells.

Table 1: UVA intensity, exposure time, and dosage.

Experiment grouping		Intensity (mW/cm^2)	Exposure time (s)	Dosage (J/cm^2)
Shamed irradiation group (SIG)		0	0	0
High-dose group (HDG)		60	1440	86.4
Low-dose group (LDG)	LDG1	60	120 × 1	7.2
	LDG2		120 × 2	14.4
	LDG3		120 × 3	28.8
	LDG4		120 × 4	57.6
	LDG5		120 × 5	115.2
Adaptive response group (ARG)	ARG1	60	120 × 1 s for preirradiation	7.2 (preirradiated dose)
			1440 s for challenged irradiation	86.4 (challenged dose)
	ARG2		120 × 2 s for pre irradiation	14.4 (preirradiated dose)
			1440 s for challenged irradiation	86.4 (challenged dose)
	ARG3		120 × 3 s for pre irradiation	28.8 (preirradiated dose)
			1440 s for challenged irradiation	86.4 (challenged dose)
	ARG4		120 × 4 s for pre irradiation	57.6 (preirradiated dose)
			1440 s for challenged irradiation	86.4 (challenged dose)
	ARG5		120 × 5 s for pre irradiation	115.2 (preirradiated dose)
			1440 s for challenged irradiation	86.4 (challenged dose)

The detection rate was about 500 cells/s. Lantastic software was used for data analysis [30].

2.6. Single-Cell Gel Electrophoresis (SCGE). According to the methods reported [27, 31], SCGE was carried out on all the experimental groups 60 min after UVA irradiation. Cell proportion of DNA migration was counted under the fluorescence microscope: 100 cells were counted per sample randomly, and 3 samples were observed per group. The diameter of nuclear DNA and the length of DNA migration were measured: 6∼10 cells were observed per sample randomly, and 40 cells were surveyed per group.

2.7. Statistical Analysis. Data were expressed as mean ± standard deviation ($x \pm S$) and analyzed by SPSS 13.0 software. One-way ANOVA was used for intergroup comparison and single factor analysis of variance was used for group comparison. $P < 0.05$ was considered statistically significant.

3. Results

3.1. Cytotoxicity of UVA Irradiation. Spindle-shaped fibroblasts were observed after primary culture for 24 h to 48 h. With continued culture, fibroblasts aggregated. The test was carried out with cells after 5∼10 passages. Fibroblasts were irradiated by UVA at 0, 7.2, 14.4, 28.8, 43.2, 64.8, 86.4, and 108 J/cm^2, respectively. Cell survival rates were tested by MTT at 3 h, 6 h, 12 h, 24 h, 48 h, and 72 h, respectively, and the growth curves were drawn, respectively, as shown in Figure 1 [32].

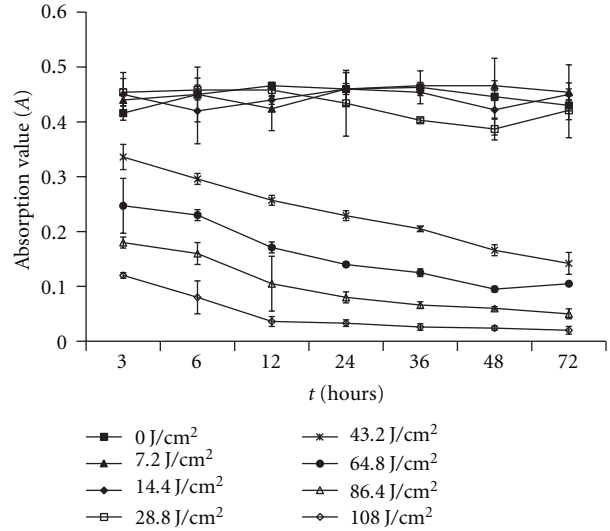

Figure 1: Viability of normal human fibroblasts after UVA irradiation. Normal human fibroblasts were irradiated with UVA at the indicated dosage (J/cm^2), and then cell viability was determined using MTT method at the indicated time (h). No change in cell viability under 7.2, 14.4, and 28.8 J/cm^2 UVA irradiation was seen in comparison with the sham-irradiated cells ($P > 0.05$; One-way ANOVA) and no difference among the three dosages was seen ($P > 0.05$, One-way ANOVA). Decrease in cell viability was observed with the UVA dose over 43.2 J/cm^2. Twenty-four hours after 86.4 J/cm^2 UVA treatment, cell viability only reached 19.7%, in multiple comparisons with the LSD method. Significant difference among 43.2, 64.8, 86.4, and 108 J/cm^2 UVA irradiation was observed.

3.2. Low-Dose UVA Preirradiation Effects on Fibroblast Synthesis and Cellular Senescence, and Its Protection against Subsequent Lethal Dose Showing. Alterations in cellular morphology and proliferation of cultured dermal fibroblasts treated with single irradiation of 7.2 J/cm^2 UVA were not observed clearly under inverted microscope. With increasing irradiation, cells showed slight inhibition of proliferation and enlarged cell volume. At a cumulative dosage up

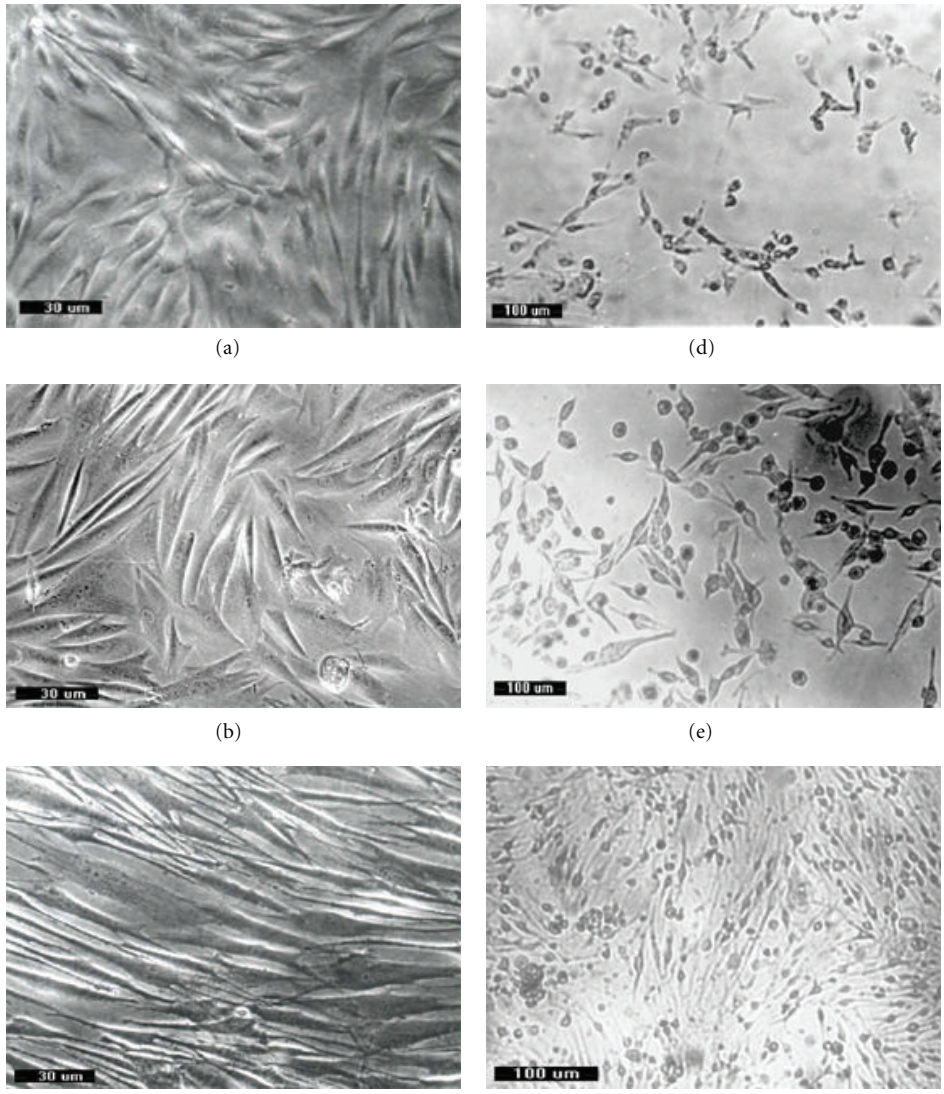

Figure 2: Morphological changes in cultured fibroblasts recorded by light microscopy. (a) SIG, normal fibroblasts showed active cell proliferation. (b) LDG1, single irradiation of 7.2 J/cm^2 UVA caused no significant effect on cell morphology and cell proliferation. (c) LDG5, repetitive irradiation of 7.2 J/cm^2 UVA at a total dose of 115.2 J/cm^2 caused large cell volume, increased intracellular particles, and inhibited cell proliferation. (d) HDG, 12 h after 86.4 J/cm^2 UVA irradiation: massive apoptotic death was observed. (e) ARG1, 3 h after single low-dose UVA preirradiation: atomic and death of fibroblasts caused by sequential 86.4 J/cm^2 UVA irradiation was reduced. (f) ARG5, 3 h after repetitive irradiation of 7.2 J/cm^2 UVA at a cumulative dosage of 115.2 J/cm^2, death of fibroblasts caused by subsequent 86.4 J/cm^2 UVA irradiation was reduced significantly.

to 115.2 J/cm^2, the cells were transferred into the six-well culture plate at 1×10^6 cells/mL. Under scanning electron microscope (SEM), normal cellular morphology was observed in the cells irradiated once with low-dose UVA. With a UVA dosage of over 28.8 J/cm^2, increasing and lengthening of apophysis and abundance of microvilli with normal intracellular structure were observed. Compared with normal cells, an abundance of rough endoplasmic reticulum (RER) and mitochondria were observed in the cultured fibroblasts without significant cytotoxicity. However, along with additional exposure to low-dose UVA irradiation, fibroblasts showed characteristic changes in morphology and cytology of cell senescence including delayed doubling time and enlarged volume, cellular granulation, augmented volume of mitochondria and so on. Massive apoptotic death of cultured cells irradiated with 86.4 J/cm^2 UVA was observed after 3 h, reaching a peak at about 12 h. Evidence of acute toxic reaction under SEM included membrane vacuolization, dendrite shrinkage, necrocytosis, intracellular edema, endoplasmic reticulum extension, mitochondrial edema, membrane destruction, and apoptosis (nuclear loss of volume, chromatin concentration, crescents-like nuclear formation, and microvillus of membrane vanished). In ARG, the time of acute toxic reaction was delayed with high-dose UVA irradiation after the single low-dose UVA preirradiation in two phases in 12 h (3 h, 6 h). The degree of acute toxic

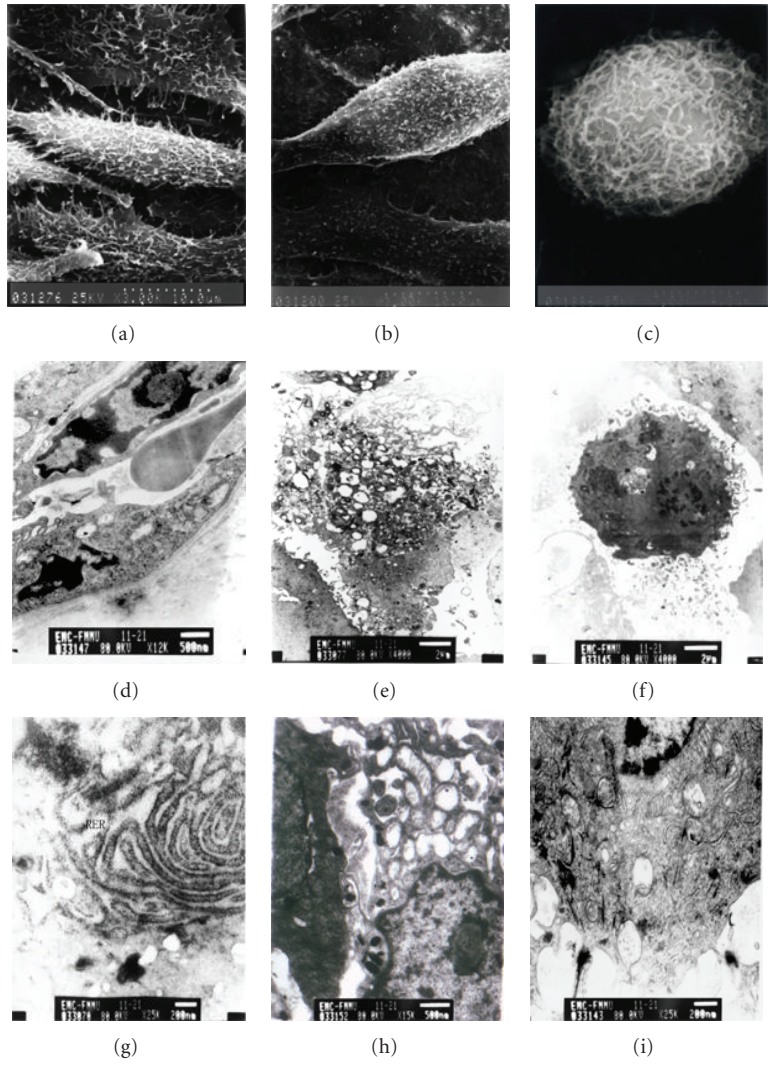

Figure 3: Ultrastructural changes of cultured fibroblasts. (a) SIG, normal morphology of fibroblast showed rich microvilli on cell surface (SEM). (b) HDG, 30 min after irradiation by 86.4 J/cm^2 UVA, microvilli disappeared on cell surface (SEM). (c) ARG3, preirradiated with repetitive irradiation of 7.2 J/cm^2 UVA for a total dosage of 28.8 J/cm^2; 30 min after irradiation by 86.4 J/cm^2 UVA, fibroblasts showed apoptosis (SEM). (d) SIG, normal morphology of fibroblast showed normal mitosis (TEM). (e) HDG, 30 min after irradiation by 86.4 J/cm^2 UVA, cells with vacuolization showed necrosis (TEM). (f) ARG3, preirradiated with repetitive irradiation of 7.2 J/cm^2 UVA with a cumulative dosage of 28.8 J/cm^2, and then 30 min after irradiation by 86.4 J/cm^2 UVA, fibroblasts showed apoptosis (TEM). (g) LDG3, after irradiation with repetitive irradiation of 7.2 J/cm^2 UVA for a cumulative dosage of 28.8 J/cm^2, fibroblasts showed plenty of RER (TEM). (h) LDG3, after irradiation with repetitive irradiation of 7.2 J/cm^2 UVA for a cumulative dosage 28.8 J/cm^2, fibroblasts showed increased number of mitochondria (TEM). (i) LDG5, after irradiation with repetitive irradiation of 7.2 J/cm^2 UVA for a cumulative dosage 115.2 J/cm^2, fibroblasts showed aging of mitochondria (TEM).

response was reduced under light microscope and SEM. However, the protective effects disappeared in phases at 12 h and 24 h with a lethal dose of UVA. When the low-dose UVA increased to over 28.8 J/cm^2, the protective effects due to alterations in cellular morphology caused by lethal-dose UVA irradiation were still apparent, even 14 days later. The changes in cellular morphology in different groups were shown in Figures 2 and 3.

3.3. Low-Dose UVA Preirradiation Induced Fibroblast Cell Cycle Arrest, Reduced Apoptosis due to Subsequent Lethal Dose Irradiation. In our studies, cell cycle and apoptosis of fibroblasts were detected by flow cytometry. Propidium iodide staining using single parameter histogram represented the cell cycle changes in every group. DNA histogram offered peak distribution. The ordinate represented cell number, the abscissa in the 2C represented diploid cells in the G0/G1 phase and in the 4C represented cells with DNA four times in the G2/M period. The peak distribution between 2C and 4C denoted cells with DNA, diploid to four times in S phase and that before 2C denoted apoptosis in cells with hypodiploid DNA [33].

The results showed that the proportion of cells increased in the G0/G1 phase and in the S phase but decreased in the

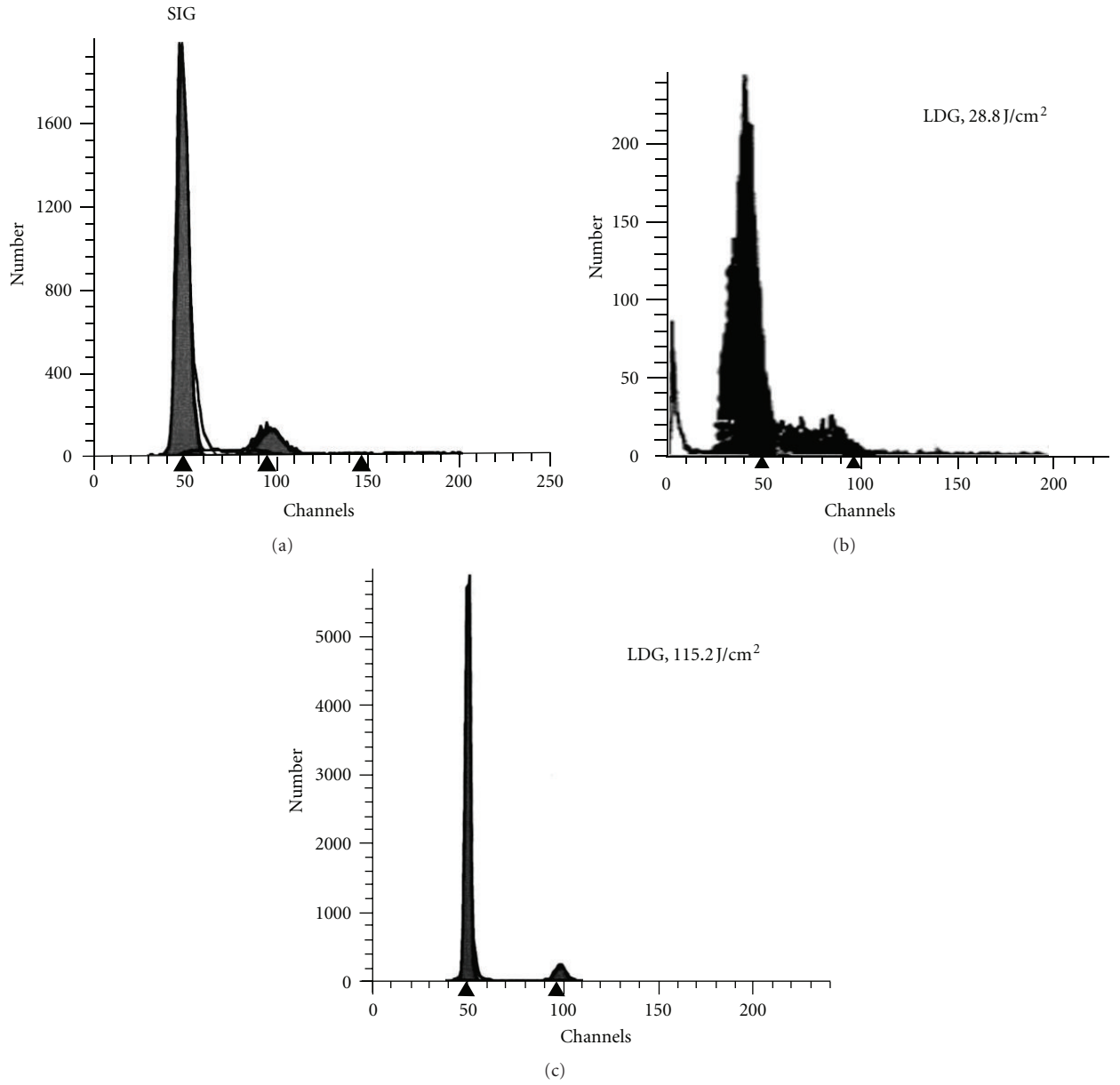

Figure 4: Effects of low-dose UVA on fibroblast cell cycle. PI staining using single parameter histogram represented the change of cell cycle in each group. DNA histogram offered peak distribution. The ordinates represented cell number, and the abscissa represented PI intensity. The DNA peak near 50 (2C) in the abscissa represented the diploid G0/G1 phase; the DNA peak near 100 (4C) in the abscissa represented the tetraploid G2/M phase; the DNA peak between 2C and 4C represented diploid to tetraploid S phase; the DNA peak before 2C represented hypodiploid DNA fragments indicating cell apoptosis. (a) Phase distribution of cell cycle of SIG fibroblasts. The proportions of G0/G1 phase, S phase, and G2/M phase were 85.01%, 6.49%, and 8.49%, respectively. (b and c) Repeated low-dose UVA irradiation altered the phase distribution of cell cycle. When the dosage accumulated to 28.8 J/cm^2, the proportions of G0/G1 phase, S phase, and G2/M phase were 84.09%, 12.95%, and 1.95%, respectively (b); when the dosage accumulated to 115.2 J/cm^2, the inhibition of cell cycle was observed apparently. The proportions of G0/G1 phase, S phase, and G2/M phase were 93.97%, 5.37%, and 0.66%, respectively (c).

G2/M phase along with the cumulative dose after irradiation with single low-dose UVA. However, all of these did not show apoptosis peak markedly and the subsequent inhibition of cell cycle. The distribution of fibroblasts in different phases of the cell cycle with different cumulative doses of low-dose UVA irradiation, are shown in Figure 4, and Table 2.

Annexin V/PI staining and two-dimensional scatter diagram showed the percentage of different cells: normal, apoptosis, injured, and dead. A dot-plot of annexin V-FITC versus PI showed four separate clusters: cells negative for Annexin V-FITC and PI were viable (left inferior quadrant), those positive for Annexin V-FITC but negative for PI were apoptotic (right inferior quadrant), those positive for Annexin V-FITC and PI were necrotic (right superior quadrant) and those negative for Annexin V-FITC but positive for PI were injured (left superior quadrant).

Table 2: Effects of low-dose UVA on fibroblast cell cycle ($x \pm S\%$, $n = 4$).

Group/cell cycles	SIG	LDG (J/cm^2)				
		7.2[a]	14.4[b]	28.8[c]	57.6[d]	115.2[e]
G0/G1	83.4 ± 1.01	84.4 ± 0.65	84.6 ± 0.36	84.4 ± 1.59	92.7 ± 0.97$^{\Delta}$	93.9 ± 0.63$^{\Delta}$
S	9.08 ± 0.28	10.7 ± 0.72$^{\Delta}$	12.3 ± 0.91$^{\Delta}$	13.1 ± 1.09$^{\Delta}$	6.30 ± 1.07$^{\Delta}$	4.90 ± 0.65$^{\Delta}$
G2 + M	6.63 ± 0.89	4.18 ± 0.38$^{\Delta}$	2.60 ± 0.55$^{\Delta}$	1.68 ± 0.37$^{\Delta}$	0.73 ± 0.28$^{\Delta}$	0.63 ± 0.22$^{\Delta}$

$^{\Delta}P < 0.01$, compared with SIG, proportion of G0/G1 phase, S phase, and G2/M phase of fibroblasts of each LDG differences were extremely significant (t_a were −3.440, 3.280, t_b were −9.662, 7.319, t_c were −4.025, 9.316, t_d were −5.788, 10.78, 23.44, t_e were −7.461, 10.58, 4.869); linear regression analysis, the cell cycle distribution of the low-dose group were closely related to cumulative doses of UVA irradiation, respectively, $r = 0.906$, $F = 30.68$, $P < 0.001$.
One-way ANOVA, the proportions of respective phases of cell cycle showed no difference among the 7.2 J/cm^2, 14.4 J/cm^2, and 28.8 J/cm^2 dosages, $P > 0.05$; The t-test also showed no difference between the dosages of 57.6 J/cm^2 and 115.2 J/cm^2, $P > 0.05$.

Detection also showed that the apoptosis peak was markedly observed in the fibroblasts of HDG after 12 h irradiation. After preirradiation with low-dose UVA irradiation at 7.2, 14.4, 28.8, 57.6, and 115.2 J/cm^2, respectively, and then subjected to UVA irradiation at 86.4 J/cm^2 in 6 h, 12 h, 24 h, 48 h, 72 h, 7 d, and 14 d, the proportion of apoptotic cells in every ARG showed differential decrease, relative to the accumulated dose of low-dose preirradiation and time interval of subsequent high-dose irradiation. With 86.4 J/cm^2 UVA irradiation following single 7.2 J/cm^2 UVA preirradiation, proportions of necrosis and apoptosis decrease in ARG cells of 6-h phase were assayed. But the effects vanished in 12-h phase. Low-dose preirradiation accumulated to over 28.8 J/cm^2, necrosis and apoptosis were still reduced even at 14 d with high-dose irradiation. Simultaneously, after low dose preirradiation, the extent of necrosis and apoptosis was reduced by preirradiation. When the cumulative dose was less than 57.6 J/cm^2, the effect was directly proportional to the low cumulative dose. However, the response was weak with the cumulative preirradiation dose up to 115.2 J/cm^2 [34]. The degree of necrosis and apoptosis in different groups was assayed quantitatively by AnnexinV/PI staining. Apoptosis and necrosis were caused by different cumulative doses of preirradiation and high-dose irradiation at different time points subsequently. The results of this radiation effect were shown in Figure 5. Changes in apoptosis in every group were caused by high- dose irradiation at different time intervals after different cumulative doses of preirradiation. The static assayed result was expressed in Table 3.

3.4. Low-Dose UVA Preirradiation Conferred DNA Protective Effects, against Subsequent Lethal-Dose UVA Exposure. Single-cell gel electrophoresis (SCGE) was carried out on every group 30 min after UVA irradiation. After 5 μg/mL ethidium bromide dyeing, the orange-yellow cells were observed under fluorescence microscope. Four types were identified as follows. (1) Type I: undamaged, with no obvious tail; (2) type II: with a tail shorter than the diameter of the head (nucleus); (3) type III: with a tail longer but less wider than the diameter of the head; (4) type IV: with a tail longer and wider than the diameter of the head (Figure 6). Table 4 shows the proportion of DNA migration in cultured fibroblasts and the diameter and the length of DNA migration in the comet assay. The proportion of DNA migration in cultured fibroblasts was 6.50%. The length of DNA migration in cultured cells was 110.7 ± 4.00 (μm). Significant differences in DNA migration and the length of DNA migration with different cumulative doses in RAG and single HDG after 6 h with low-dose preirradiation were determined by t-test. A positive correlation between DNA protection and the accumulated dose were observed.

4. Discussion

In the present study, we demonstrated the changes in morphology, cell cycle, apoptosis and DNA damage due to low-dose UVA-irradiation on dermal fibroblasts and the protective effects of low-dose UVA preirradiation that prevented the cultured dermal fibroblasts from damage caused by subsequent lethal-dose UVA irradiation.

The LI used in PBM might be low intensity LI (LIL) (about 10 mW/cm^2), or moderate intensity LI (MIL) ($10^2 \sim 10^3$ mW/cm^2) [8, 35]. The UVA at 60 mW/cm^2 in our experiments was a kind of MIL which PBM is mediated by ROS [8]. The PBM on a function is dependent on whether it is in its function-specific homeostasis (FSH). FSH is just a negative feedback response for a function to be fully performed. There is no PBM of MIL for short irradiation time on a function in its FSH, but MIL for long irradiation time can disrupt a FSH [8]. The survival rate of fibroblasts was not affected significantly with 7.2 J/cm^2, 14.4 J/cm^2, and 28.8 J/cm^2 UVA. At a dose above 43.2 J/cm^2 ($\geq$720 s), cell survival rate obviously decreased in a dose-dependent fashion: the survival rate of fibroblasts was 19.7 percent after exposure to 86.4 J/cm^2 UVA for 24 hours. The fibroblasts in 10% FCS were in proliferation-specific homeostasis (PSH) so that the UVA at 7.2 J/cm^2, 14.4 J/cm^2 and 28.8 J/cm^2 cannot modulate the proliferation [8, 36, 37]. The UVA at increased doses disrupted the PSH, causing extensive, dose-dependent inhibition or cell death. Therefore, in our experiments, low-dose UVA was termed as a dose that does not affect morphology and growth of fibroblasts. Cultured dermal fibroblasts were irradiated with a low-dose 7.2 J/cm^2 UVA preirradiation and by a subsequent lethal dose of 86.4 J/cm^2 UVA.

Cellular morphology and proliferation of cultured dermal fibroblasts treated with single irradiation of 7.2 J/cm^2 UVA were not altered, but when irradiation dosage increased to more than 28.8 J/cm^2, cells showed dose-dependent inhibition of proliferation. With further low-dose UVA

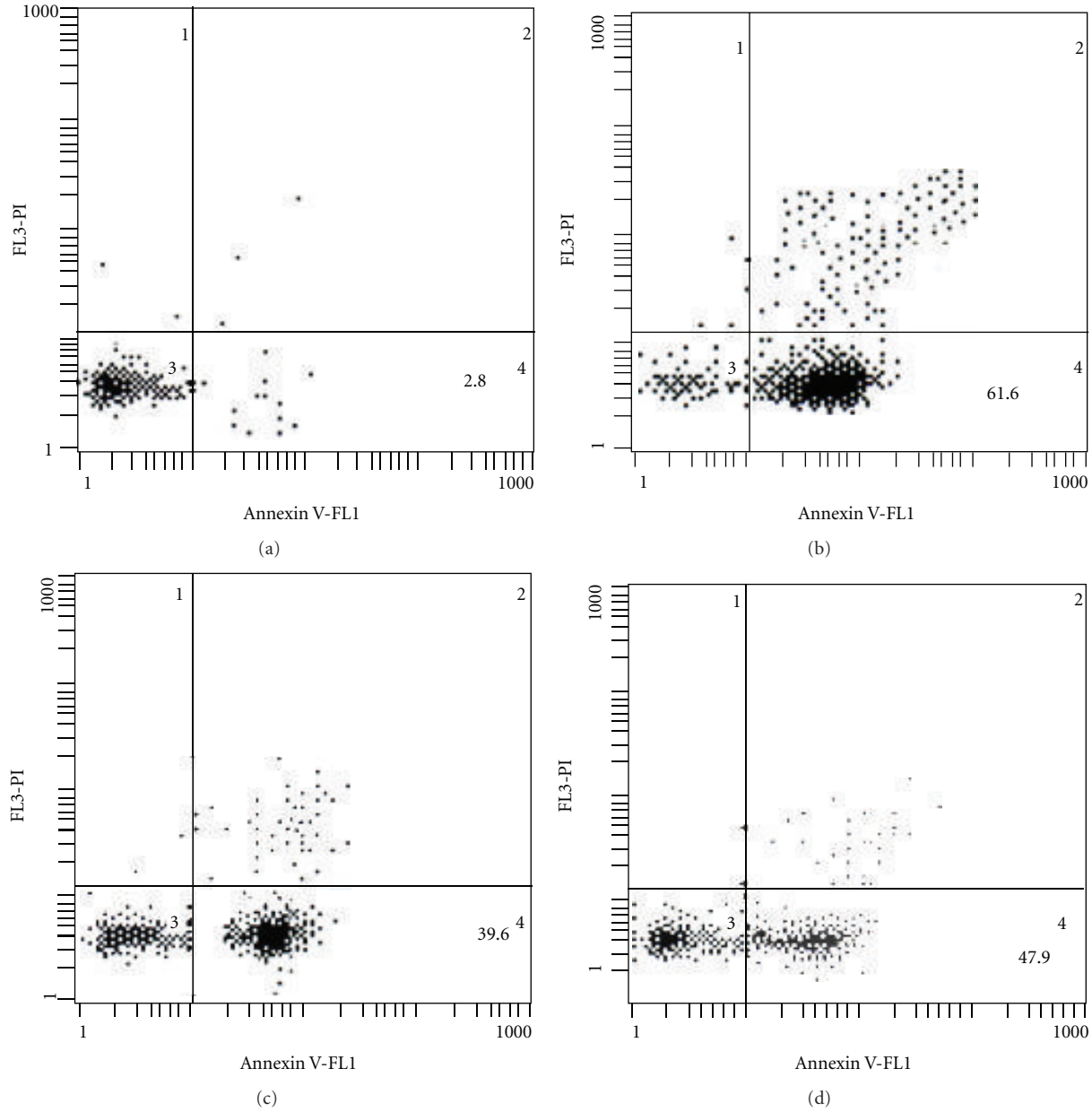

Figure 5: Detection of apoptosis in fibroblasts by flow cytometry. (a) Most of the fibroblasts in the SIG were alive, with only 2.8% of apoptotic cells. (b) The high-dose UVA irradiation (86.4 J/cm^2) strongly induced cellular apoptosis in cultured fibroblasts, with 61.6% apoptotic cells. (c and d) Preirradiation of low-dose UVA reduced cellular apoptosis induced by the subsequent lethal dose of UVA irradiation. Irradiation with 86.4 J/cm^2 UVA 6 h and 72 h after preirradiation with a cumulative dose of 28.8 J/cm^2, reduced the proportion of apoptotic cells to 39.6% (c), and 47.9% (d), respectively.

irradiation exposure, fibroblasts showed characteristic morphological and cytological changes in cellular senescence such as delayed doubling time and enlarged cell volume, cellular granulation, augmented volume of mitochondria and so on. Massive apoptosis and death of 86.4 J/cm^2 UVA-irradiated cultured cells were observed after 3 h and reached a peak about 12 h, showing evidence of acute toxic reaction. In the ARG, the low-dose UVA preirradiation relieved toxic response in morphology induced by the subsequent lethal dose of UVA irradiation. Interestingly, the fibroblasts of LDG not only displayed plenty of RER (rough endoplasmic reticulum) that suggested decreased cell synthesis, but also features of cellular senescence with further exposure to low-dose UVA irradiation. These results showed that repeated exposure of human fibroblasts to low-dose UVA induced fibroblast senescence [38], but also suggested that senescence might be some kind of adaptive response induced by low-dose UVA irradiation, serving as a cellular mechanism to escape from stress-induced death.

Apoptosis or programmed cell death is a key function in regulating skin development, homeostasis, and tumorigenesis [39]. UV-triggered apoptotic signaling has been

Table 3: Effects of lethal irradiation on fibroblast apoptosis after UVA preirradiation at different time intervals ($x \pm S\%$, $n = 4$).

Group/time	SIG	HDG[a]	ARG (J/cm^2)				
			7.2	14.4	28.8	57.6	115.2
3 h	2.38 ± 0.47	55.3 ± 6.17	50.2 ± 4.15[b]	35.0 ± 4.87[c]	39.4 ± 2.21[d]	35.2 ± 3.82[e]	37.3 ± 3.95[f]
6 h	2.68 ± 0.33	54.7 ± 4.11	49.3 ± 4.92[b]	42.5 ± 3.93[c]	43.9 ± 3.33[d]	38.5 ± 2.87[e]	41.4 ± 3.02[f]
12 h	2.60 ± 0.56	61.9 ± 6.47	55.4 ± 9.26	41.1 ± 3.61[c]	45.6 ± 1.05[d]	42.0 ± 1.15[e]	43.4 ± 4.09[f]
24 h	2.70 ± 0.27	59.0 ± 2.81	55.7 ± 6.29	47.8 ± 9.71[c]	47.9 ± 4.65[d]	45.9 ± 5.45[e]	44.8 ± 2.66[f]
48 h	2.78 ± 0.25	55.3 ± 5.36	52.9 ± 3.77	56.1 ± 6.00	49.0 ± 6.35[d]	48.2 ± 3.34[e]	44.1 ± 2.95[f]
72 h	2.68 ± 0.33	57.0 ± 3.60	57.5 ± 4.19	54.8 ± 5.19	45.2 ± 4.22[d]	49.2 ± 2.44[e]	45.9 ± 3.40[f]
7 d	2.25 ± 0.45	59.4 ± 5.78	58.1 ± 7.04	56.6 ± 9.56	46.8 ± 7.94[d]	48.4 ± 2.44[e]	46.6 ± 3.71[f]
14 d	2.10 ± 0.46	61.4 ± 3.53	55.1 ± 3.36	60.5 ± 8.16	48.3 ± 6.34[d]	47.3 ± 3.82[e]	46.8 ± 4.72[f]

[a] $P < 0.001$, compared with SIG, differences were significant ($t = -53.52$), [b] $P < 0.01$, compared with HDG, differences in corresponding phase points were significant ($t = 13.68, 16.34$), [c] $P < 0.01$, compared with HDG, differences in corresponding phase points were significant ($t_{3\,h} = 18.84$, $t_{6\,h} = 13.00$, $t_{12\,h} = 4.645$); [d] $P < 0.01$, compared with HDG, differences in corresponding phase points were significant (t value in phases, resp., were 7.654, 12.64, 17.69, 21.24, 14.81, 13.21, and 15.84); [e] $P < 0.01$, compared with HDG, differences in corresponding phase points were significant (t value in phases, resp., were 5.279, 11.63, 7.698, 13.55, 12.85, 4.281, 4.845, and 24.88) [f] $P < 0.01$, compared with HDG, differences in corresponding phase points were significant (t value in phases, resp., were 6.774, 7.386, 5.047, 24.02, 3.792, 5.146, 9.548, and 16.49).

One-way ANOVA, the proportion of apoptotic fibroblasts showed no difference among the ARG1 (7.2 J/cm^2), ARG2 (14.4 J/cm^2), and ARG3 (28.8 J/cm^2), $P > 0.05$; t-test, no difference observed between ARG4 (57.6 J/cm^2) and ARG3 (115.2 J/cm^2), $P > 0.05$.

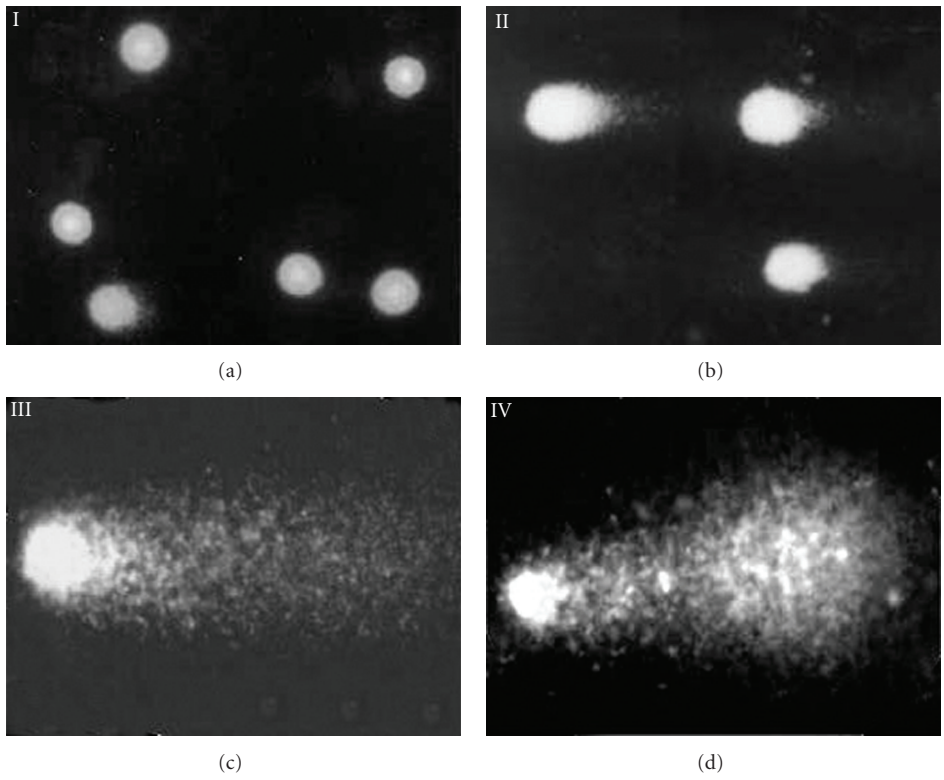

Figure 6: Fluorescence microscopic detection of four types of cellular DNA separated by SCGE. (a) Type I: undamaged, with no obvious tail; (b) type II: with a tail shorter than the diameter of the head (nucleus); (c) type III: with a tail longer but less wider than the diameter of the head; (d) type IV: with a tail length and width both longer than the diameter of the head.

well documented, whereas UV-induced survival effects have received little attention. Our results suggested that low-dose UVA preirradiation induced fibroblast cell cycle arrest, reduced cellular apoptosis induced by the subsequent lethal-dose UVA irradiation. In the low-dose group, the proportion of fibroblasts in the G0/G1 phase and in the S phase was increased with the cumulative dose addition after single low-dose UVA irradiation once a day, but no differences among fibroblasts of LDG1 (7.2 J/cm^2), LDG2 (14.4 J/cm^2) and LDG3 (28.8 J/cm^2) were observed. It might suggest that fibroblasts cultured in 10% FCS were in PSH, but with the dosages increasing to 57.6 J/cm^2 and 115.2 J/cm^2, fibroblasts were arrested in the G0/G1 phase, cell synthesis and proliferation were inhibited remarkably, which suggested

Table 4: Effects of low-dose UVA preirradiation on fibroblast DNA damage ($x \pm S$, $n = 4$).

Groups		The percentage of DNA migration (%)	t value	Average length of DNA migration (μm)	t value
SIG		7.50 ± 1.29		11.8 ± 3.49	
HDG		90.8 ± 4.35$^{\bullet\bullet}$	−36.41	102 ± 29.4$^{\bullet\bullet}$	−11.98
ARG (J/cm^2)	7.2	82.5 ± 6.81$^{\triangle}$	3.794	88.4 ± 19.1	1.596
	14.4	75.0 ± 2.94$^{\triangle}$	10.97	77.3 ± 19.6$^{\triangle}$	12.78
	28.8	68.5 ± 3.87$^{\triangle\triangle}$	11.52	65.3 ± 18.5$^{\triangle\triangle}$	14.38
	57.6	57.9 ± 5.38$^{\triangle}$	8.568	49.3 ± 14.5$^{\triangle\triangle}$	16.76
	115.2	51.0 ± 5.48$^{\triangle}$	10.93	42.9 ± 11.4$^{\triangle\triangle}$	17.90

t-test, compared with SIG, differences were extremely significant $^{\bullet\bullet}P < 0.001$; compared with HDG, differences were extremely significant $^{\triangle\triangle}P < 0.001$, and significant $^{\triangle}P < 0.01$; linear regression analysis of internal ARG, the percentage of DNA migration ($r = 0.764$, $F = 25.25$, $t = -5.025$, and $P < 0.001$) and average length of DNA migration ($r = 0.603$, $F = 44.55$, $t = -6.674$, and $P < 0.001$) were both close related to accumulated doses.
One-way ANOVA, the percentage of DNA migration, and the average length of DNA migration were no different among the ARG1 (7.2 J/cm^2), ARG2 (14.4 J/cm^2), and ARG3 (28.8 J/cm^2), $P > 0.05$; t-test, there also was no difference between ARG4 (57.6 J/cm^2) and ARG3 (115.2 J/cm^2), $P > 0.05$.

that fibroblasts were in resting-specific homeostasis [8] that was better than PSH in resisting apoptosis of fibroblasts induced by a lethal dose of UVA irradiation.

UVA mainly produces ROS through interaction with endogenous photosensitizers. These ROS can in turn damage DNA indirectly [24, 25]. It was established that UVA irradiation was most likely to cause single-strand breaks in fibroblast DNA [40]. The SCGE was therefore used to detect the DNA damage caused by UVA in our study. Single-strand DNA breaks in fibroblasts were likely to reach their peak 1 h after UVA irradiation, and therefore immediately subjected to SCGE [27]. Our results showed that, compared with SIG, no further DNA damage of human skin fibroblasts exposed to low-dose UVA radiation as detected by SCGE. The low dose UVA preirradiation induced significant protective effects against DNA damage associated with the subsequent lethal dose of UVA irradiation, with 7.2 J/cm^2, 14.4 J/cm^2 and 28.8 J/cm^2 ($P < 0.05$) or between 57.6 J/cm^2 and 115.2 J/cm^2 ($P < 0.05$). The mechanisms might involve DNA repair and temporary cell cycle arrest induced by low-dose UVA irradiation. This protective response not only inhibited the damage, but also increased the resilience of cells against a subsequent UV dose, leading to increased survival of cells that maintain their DNA repair capability [23].

The beneficial effects of ultraviolet radiation on human are well known. In recent years, growing epidemiological evidence suggests that exposure to ultraviolet radiation may decrease risk for a number of serious cancers including prostate cancer. The beneficial biological effects may be associated with PBM induced by low-dose irradiation. Further research on PBM including adaptive responses may have great medical significance in terms of exposure to ultraviolet radiation.

5. Conclusions

Our results suggested that low-dose UVA radiation might induce adaptive response protecting cultured dermal fibroblasts from damage due to subsequent lethal dose of UVA. The degree of protection and duration of the response might be clearly related to the accumulated doses of low-dose UVA radiation.

Acknowledgments

This work was supported by the National Natural Science Foundation of China (Grant no. 30972652), and the National Natural Science Foundation of Guangdong Province (Grant no. 915100100200020). Liu and his collaborators report no conflicts of interest relating to any manufacturers or distributors in this paper. The authors would also like to thank Professor Timon Chengyi LIU for his excellent and professional revision of this paper.

References

[1] A. P. Moczek, S. Sultan, S. Foster et al., "The role of developmental plasticity in evolutionary innovation," *Proceedings of the Royal Society B*, vol. 278, no. 1719, pp. 2705–2713, 2011.
[2] M. P. Mattson, "Hormesis defined," *Ageing Research Reviews*, vol. 7, no. 1, pp. 1–7, 2008.
[3] S. Tapio and V. Jacob, "Radioadaptive response revisited," *Radiation and Environmental Biophysics*, vol. 46, no. 1, pp. 1–12, 2007.
[4] L. A. Sagan, G. Chairman, and J. J. Cohen, "Biological effects of low-dose radiation: overview and perspective," *Health Physics*, vol. 59, no. 1, pp. 11–13, 1990.
[5] M. Pollycove and L. E. Feinendegen, "Radiation-induced versus endogenous DNA damage: possible effect of inducible protective responses in mitigating endogenous damage," *Human and Experimental Toxicology*, vol. 22, no. 6, pp. 290–306, 2003.
[6] S. Z. Liu, "Biological effects of low level exposures to ionizing radiation: theory and practice," *Human and Experimental Toxicology*, vol. 29, no. 4, pp. 275–281, 2010.
[7] J. Fu, C. G. Woods, E. Yehuda-Shnaidman et al., "Low-level arsenic impairs glucose-stimulated insulin secretion in pancreatic beta cells: involvement of cellular adaptive response to oxidative stress," *Environmental Health Perspectives*, vol. 118, no. 6, pp. 864–870, 2010.
[8] T. C. Y. Liu, R. Liu, L. Zhu, J. Q. Yuan, M. Hu, and S. H. Liu, "Homeostatic photobiomodulation," *Frontiers of Optoelectronics in China*, vol. 2, no. 1, pp. 1–8, 2009.
[9] M. J. Conlan, "Biostimulation of wound healing by low-energy laser irradiation: a review," *Journal of Clinical Periodontology*, vol. 23, no. 5, pp. 492–496, 1996.
[10] G. A. Guzzardella, M. Fini, P. Torricelli, G. Giavaresi, and R. Giardino, "Laser stimulation on bone defect healing: an in

vitro study," *Lasers in Medical Science*, vol. 17, no. 3, pp. 216–220, 2002.

[11] N. Cohen, R. Lubart, S. Rubinstein, and H. Breitbart, "Light irradiation of mouse spermatozoa: stimulation of in vitro fertilization and calcium signals," *Photochemistry and Photobiology*, vol. 68, no. 3, pp. 407–413, 1998.

[12] M. Kreisler, A. B. Christoffers, H. Al-Haj, B. Willershausen, and B. D'Hoedt, "Low level 809-nm diode laser-induced in vitro stimulation of the proliferation of human gingival fibroblasts," *Lasers in Surgery and Medicine*, vol. 30, no. 5, pp. 365–369, 2002.

[13] N. Grossman, N. Schneid, H. Reuveni, S. Halevy, and R. Lubart, "780 nm low power diode laser irradiation stimulates proliferation of keratinocyte cultures: involvement of reactive oxygen species," *Lasers in Surgery and Medicine*, vol. 22, no. 4, pp. 212–218, 1998.

[14] J. S. Chen, H. C. Chiu, C. J. Hsu et al., "Low-energy visible light irradiation modulates immune responses induced by epicutaneous sensitization with protein antigen," *Journal of Investigative Dermatology*, vol. 129, no. 9, pp. 2258–2264, 2009.

[15] V. Molho-Pessach and M. Lotem, "Ultraviolet radiation and cutaneous carcinogenesis," *Current Problems in Dermatology*, vol. 35, pp. 14–27, 2007.

[16] L. P. Massari, M. Kaštelan, and F. Gruber, "Epidermal malignant tumors: pathogenesis, influence of UV light and apoptosis," *Collegium Antropologicum*, vol. 31, no. 1, pp. 83–85, 2007.

[17] T. Henriksen, A. Dahlback, S. H. Larsen, and J. Moan, "Ultraviolet-radiation and skin cancer. Effect of an ozone layer depletion," *Photochemistry and photobiology*, vol. 51, no. 5, pp. 579–582, 1990.

[18] D. Bodiwala, C. J. Luscombe, S. Liu et al., "Prostate cancer risk and exposure to ultraviolet radiation: further support for the protective effect of sunlight," *Cancer Letters*, vol. 192, no. 2, pp. 145–149, 2003.

[19] M. F. McCarty, "A moderately low phosphate intake may provide health benefits analogous to those conferred by UV light—a further advantage of vegan diets," *Medical Hypotheses*, vol. 61, no. 5-6, pp. 543–560, 2003.

[20] W. P. Jeeves and A. J. Rainbow, "U.V. enhanced reactivation of U.V.- and γ-irradiated adenovirus in normal human fibroblasts," *International Journal of Radiation Biology*, vol. 43, no. 6, pp. 599–623, 1983.

[21] H. S. Murphy, V. A. Palejwala, M. Sayeedur Rahman, P. M. Dunman, G. Wang, and M. Zafri Humayun, "Role of mismatch repair in the Escherichia coli UVM response," *Journal of Bacteriology*, vol. 178, no. 23, pp. 6651–6657, 1996.

[22] G. E. Costin and V. J. Hearing, "Human skin pigmentation: melanocytes modulate skin color in response to stress," *FASEB Journal*, vol. 21, no. 4, pp. 976–994, 2007.

[23] D. Decraene, K. Smaers, D. Maes, M. Matsui, L. Declercq, and M. Garmyn, "A low UVB dose, with the potential to trigger a protective p53-dependent gene program, increases the resilience of keratinocytes against future UVB insults," *Journal of Investigative Dermatology*, vol. 125, no. 5, pp. 1026–1031, 2005.

[24] K. Scharffetter-Kochanek, M. Wlaschek, P. Brenneisen, M. Schauen, R. Blaudschun, and J. Wenk, "UV-induced reactive oxygen species in photocarcinogenesis and photoaging," *Biological Chemistry*, vol. 378, no. 11, pp. 1247–1257, 1997.

[25] W. Ma, M. Wlaschek, I. Tantcheva-Poór et al., "Chronological ageing and photoageing of the fibroblasts and the dermal connective tissue," *Clinical and Experimental Dermatology*, vol. 26, no. 7, pp. 592–599, 2001.

[26] K. Kaji, T. Ohta, N. Horie, E. Naru, M. Hasegawa, and N. Kanda, "Donor age reflects the replicative lifespan of human fibroblasts in culture: research article," *Human Cell*, vol. 22, no. 2, pp. 38–42, 2009.

[27] N. Emonet-Piccardi, M. J. Richard, J. L. Ravanat, N. Signorini, J. Cadet, and J. C. Béani, "Protective effects of antioxidants against UVA-induced DNA damage in human skin fibroblasts in culture," *Free Radical Research*, vol. 29, no. 4, pp. 307–313, 1998.

[28] K. Maier, R. Schmitt-Landgraf, and B. Siegemund, "Development of an in vitro test system with human skin cells for evaluation of phototoxicity," *Toxicology in Vitro*, vol. 5, no. 5-6, pp. 457–461, 1991.

[29] M. Chen, G. Zhang, M. Yi et al., "Effect of UVA irradiation on proliferation and NO/iNOS system of human skin fibroblast," *Journal of Central South University*, vol. 34, no. 8, pp. 705–711, 2009.

[30] A. Schindl, G. Klosner, H. Hönigsmann, G. Jori, P. C. Calzavara-Pinton, and F. Trautinger, "Flow cytometric quantification of UV-induced cell death in a human squamous cell carcinoma-derived cell line: cose and kinetic studies," *Journal of Photochemistry and Photobiology B*, vol. 44, no. 2, pp. 97–106, 1998.

[31] C. Alapetite, T. Wachter, E. Sage, and E. Moustacchi, "Use of the alkaline comet assay to detect DNA repair deficiencies in human fibroblasts exposed to UVC, UVB, UVA and γ-rays," *International Journal of Radiation Biology*, vol. 69, no. 3, pp. 359–369, 1996.

[32] J. D. Hoerter, C. S. Ward, K. D. Bale et al., "Effect of UVA fluence rate on indicators of oxidative stress in human dermal fibroblasts," *International Journal of Biological Sciences*, vol. 4, no. 2, pp. 63–70, 2008.

[33] H. Bånrud, T. Stokke, J. Moan, and K. Berg, "S phase arrest and induction of multinucleated cells after exposure to ultraviolet radiation," *Carcinogenesis*, vol. 16, no. 5, pp. 1087–1094, 1995.

[34] Y. Ibuki and R. Goto, "Antiapoptotic effects induced by different wavelengths of ultraviolet light," *Photochemistry and Photobiology*, vol. 75, no. 5, pp. 495–502, 2002.

[35] S. S. Campbell and P. J. Murphy, "Extraocular circadian phototransduction in humans," *Science*, vol. 279, no. 5349, pp. 396–399, 1998.

[36] T. C. Y. Liu, J. L. Jiao, X. Y. Xu, X. G. Liu, S. X. Deng, and S. H. Liu, "Photobiomodulation: phenomenology and its mechanism," in *Optics in Health Care and Biomedical Optics: Diagnostics and Treatment II*, Proceedings of the SPIE, pp. 185–191, chn, November 2004.

[37] X. H. Yang, C. Y. Liu, S. J. Liu et al., "Photobiomodulation on chondrocyte proliferation: in vitro evaluation," *Zhongguo Jiguang/Chinese Journal of Lasers*, vol. 33, no. 12, pp. 1692–1698, 2006.

[38] J. Shin, J. H. Kim, and E. K. Kim, "Repeated exposure of human fibroblasts to UVR induces secretion of stem cell factor and senescence," *Journal of the European Academy of Dermatology and Venereology*. In press.

[39] N. Pustišek and M. Šitum, "UV-radiation, apoptosis and skin," *Collegium Antropologicum*, vol. 35, no. 2, supplement 2, pp. 339–341, 2011.

[40] J. L. Rizzo, J. Dunn, A. Rees, and T. M. Rünger, "No formation of DNA double-strand breaks and no activation of recombination repair with UVA," *Journal of Investigative Dermatology*, vol. 131, no. 5, pp. 1139–1148, 2011.

Hindawi Publishing Corporation
International Journal of Photoenergy
Volume 2012, Article ID 186752, 5 pages
doi:10.1155/2012/186752

Research Article

LED Light-Activated Hypocrellin B Induces Mitochondrial Damage of Ovarian Cancer Cells

Yuan Jiang,[1] Albert Wingnang Leung,[2] Junyan Xiang,[1] and Chuanshan Xu[2]

[1] *Department of Photodynamic and Sonodynamic Therapy, The Second Affiliated Hospital, Chongqing Medical University, Chongqing 400010, China*
[2] *School of Chinese Medicine, The Chinese University of Hong Kong, Shatin, Hong Kong*

Correspondence should be addressed to Albert Wingnang Leung, awnleung@cuhk.edu.hk and Chuanshan Xu, xcshan@163.com

Received 22 December 2011; Revised 1 May 2012; Accepted 7 May 2012

Academic Editor: Timon Cheng-Yi Liu

Objective. Hypocrellin is a natural photosensitizer from a traditional Chinese herb. In the present study, our aim is to investigate the effect of LED light-activated hypocrellin B on mitochondria of ovarian cancer cells. *Material and Methods*. Ovarian cancer HO-8910 cells were incubated with hypocrellin B at the concentration of 2.5 μM for 5 h and then irradiated by blue light from a novel LED source. Cell survival rate of HO-8910 cells was measured using MTT assay 24 h after photodynamic treatment of hypocrellin B. Mitochondrial morphology was observed using transmission electron microscopy (TEM). Mitochondrial membrane potential was measured using flow cytometry with JC-1 staining. *Results*. MTT assay showed that cell survival rate of HO-8910 cells in the photodynamic treatment group has significantly decreased down to $27.22 \pm 1.26\%$ ($P < 0.01$). Light irradiation alone or hypocrellin B alone showed no significant impact. In our TEM mitochondria of the cells after photodynamic treatment of hypocrellin B showed severe damage with swollen mitochondria that had nearly nonexistant cristae. Mitochondrial membrane potential remarkably decreased after photodynamic action of hypocrellin B. *Conclusion*. The findings demonstrated that photodynamic action of hypocrellin B significantly decreased cell proliferation of ovarian cancer HO-8910 cells, caused severe damage to mitochondrial structure, and induced mitochondrial membrane collapse.

1. Introduction

Ovarian cancer is one of the most common cancers threatening the health of women worldwide. Significant advances have been made in therapeutic modalities in the management of ovarian cancer. However, drawbacks exist in some of the commonly used modalities [1, 2]. Therefore, novel and more effective therapeutic strategies are needed for improving the clinical outcomes.

Photodynamic therapy (PDT) can eradicate the unwanted cells/tissues via the generation of reactive oxygen species (ROS) during photodynamic treatment, in which a photosensitizer is activated by light with an appropriate wavelength [3, 4]. The doubly selective advantages, including photosensitizer selectively retaining in tumor tissue and site-directed light irradiation, make PDT become a promising alternative to combat malignancies. Photosensitizer is a key component affecting the efficacy of photodynamic therapy. Hypocrellin B is a natural product isolated from a traditional Chinese Medicine *Hypocrella bambuase* [5, 6]. Growing evidence shows that hypocrellin B has significantly photodynamic activity with high quantum yields of singlet oxygen ($^1O_2$) [7, 8]. Upon light activation hypocrellin B exhibits remarkably photodynamic eradication of cancer cells, virus, and bacteria. Our previous study showed that blue light from a novel LED source in our Lab could activate hypocrellin B, subsequently induced photocytotoxicity of ovarian cancer cells [9]. However, the biological mechanism is still unclear. On considering that mitochondria play an important role in cell growth and death, in the present study we focused on investigating the effect of photodynamic treatment of hypocrellin B on mitochondrial morphology and mitochondrial membrane potential of ovarian cancer cells.

2. Materials and Methods

2.1. Sensitizer. Hypocrellin B was used as a photosensitizer in our present study from Institute of Chemistry, Chinese Academy of Sciences. A stock solution was made in dimethyl

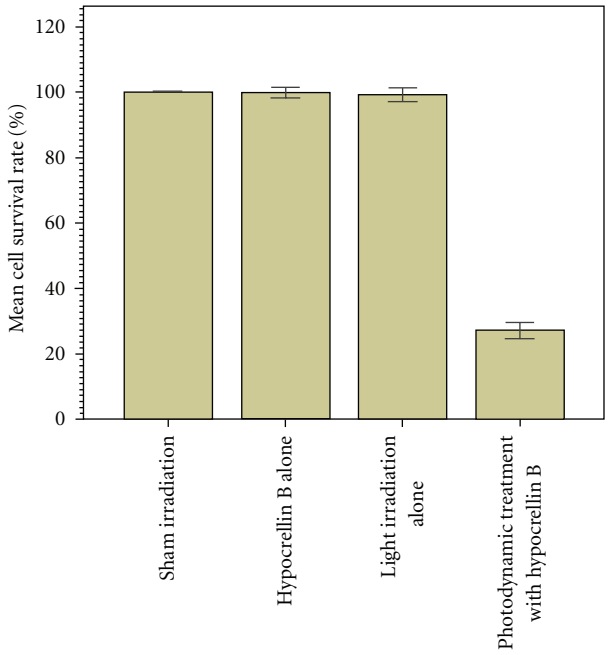

Figure 1: Cell survival rate of HO-8910 cells was measured using MTT 24 h after photodynamic action of hypocrellin B.

sulfoxide (DMSO) at a concentration of 100 mM and kept in the dark at −20°C.

2.2. Cell Culture. Ovarian cancer HO-8910 cells were stored in the Institute of Ultrasound and Medicine Engineering, Chongqing under the approval of the ethics committee of Chongqing Medical University. The cells were grown in RPMI-1640 medium supplemented with 10% fetal calf serum (FCS, Gibco), 50 μg/mL penicillin, 50 μg/mL streptomycin, and 10 μg/mL neomycin.

2.3. Photodynamic Treatment. Photodynamic treatment of hypocrellin B in HO-8910 cells was the same as described by our previous study [9]. In brief, the cells were incubated with hypocrellin B (2.5 μM) at 37°C for 5 h in the dark. Unbound hypocrellin B was washed away and the cells were exposed for 17 s (except for the dark controls) to blue light emitted from LED source system with the wavelength of 470 nm and the power density of 60 mW/cm^2. After light irradiation, the cells were then incubated for analysis. All experiments were randomly divided into 4 groups: photodynamic treatment of hypocrellin B, hypocrellin B treatment alone, light irradiation alone, and sham irradiation. The cells in the photodynamic treatment group were incubated with hypocrellin B before the exposure to light. The cells in light irradiation alone group were irradiated by light without incubation with hypocrellin B. Those in hypocrellin B treatment alone group were incubated with hypocrellin B without light irradiation. The cells in sham radiation group were treated by neither light irradiation nor hypocrellin B.

2.4. Cell Survival Measurement. To measure cell survival rates of ovarian cancer cells treated by photodynamic action of hypocrellin B, HO-8910 cells (2×10^4 cells/well) were cultured overnight in 96-well microplates. Hypocrellin B (2.5 μM) was added into cells in each well and incubated for 5 h in the dark. Unbound hypocrellin B was removed and the cells were exposed (except for the dark controls) to blue light from LED system with the wavelength of 470 nm and the energy density of 1 J/cm^2. After photodynamic action of hypocrellin B the cells were incubated for 20 h at 37°C. After that, 100 μL MTT-containing medium was added into each well (0.5 mg/mL, diluted with medium). After the incubation for 4 h at 37°C, MTT-containing medium was removed and 100 μL DMSO was added into each well. The optical density (OD) was measured using an iEMS Analyzer (Lab-system, Type1401) at the wavelength of 570 nm. The cell survival rate is calculated using the following formula: cell survival rate (%) = OD of the treatment group/OD of the control group $\times$100%.

2.5. Mitochondrial Morphological Observation. Transmission electron microscopy (TEM) was performed to observe mitochondrial morphological changes of ovarian cancer HO-8910 cells. It was carried out 6 hours after hypocrellin B (2.5 μM) had been activated by blue light from LED system with the wavelength of 470 nm and the energy density of 1 J/cm^2. Fixed cells were postfixed in 2% OsO_4, dehydrated in graded alcohol, and flat-embedded in Epon 812 (Electron Microscopy Sciences, Fort Washington, PA, USA). Ultrathin sections (100 nm) were prepared, stained with uranyl acetate and lead citrate, and examined under an electron microscopy (H-600; Hitachi, Japan).

2.6. Mitochondrial Membrane Functional Measurement. Mitochondrial membrane potential was measured using flow cytometry with JC-1 staining. Briefly, HO-8910 cells were incubated with hypocrellin B (2.5 μM) for 5 h. The cells were then irradiated by blue light from LED source with the energy density of 1 J/cm^2 and further incubated for 3 h. Finally, the treated cells were washed 3 times in PBS and stained with JC-1 for 20 min at 37°C in the dark. The washed cells were resuspended in PBS and then analyzed using flow cytometry (SE, Becton Dickinson) with the excitation setting at 488 nm, and signals were acquired at the FL-2 channel. At least 10,000 cells per sample were acquired in histograms and data analyzed by CellQuest software.

2.7. Statistical Analysis. The statistical analysis was performed using SPSS 13.0 for Windows. Differences between groups were analyzed by one-way ANOVA (analysis of variance). A P value <0.05 was considered significantly difference.

3. Results

3.1. Inhibition of Cell Proliferation. MTT assay showed that cell survival rate of the photodynamic treatment group was 27.22 ± 1.26%, which was significantly lower than that of the sham group ($P < 0.01$). Neither hypocrellin B treatment alone nor light irradiation alone had significant effect on cell survival (Figure 1).

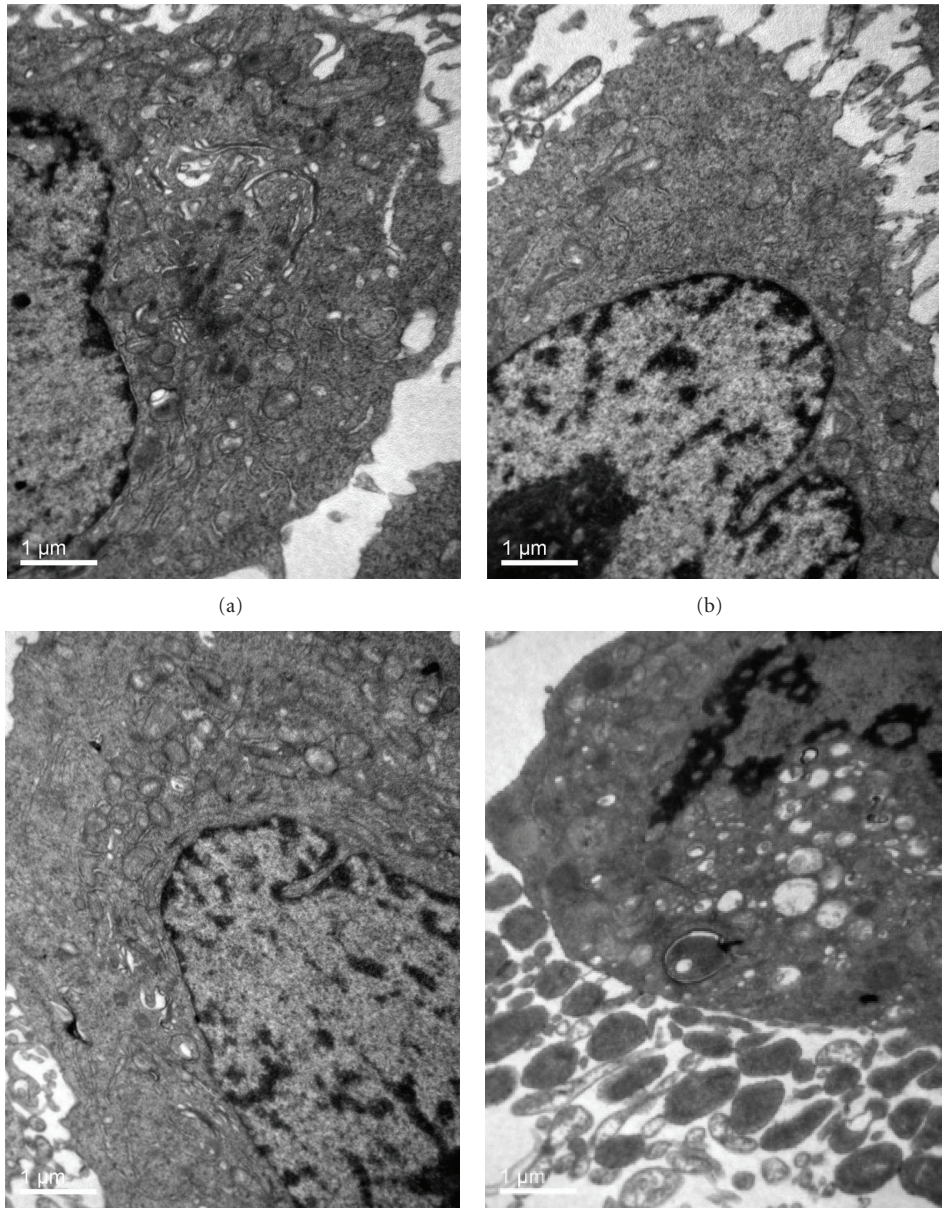

(a) (b)

(c) (d)

Figure 2: Mitochondrial morphological changes in HO-8910 cells were observed using TEM 6 h after photodynamic action of hypocrellin B (×15,000). (a): Sham irradiation; (b): hypocrellin B treatment alone; (c): light irradiation alone; (d): photodynamic action of hypocrellin B.

3.2. Mitochondrial Morphological Changes. Mitochondria which maintained integrity of cell membrane and cristae were observed in ovarian cancer HO-8910 cells after sham irradiation, hypocrellin B treatment alone, and light irradiation treatment alone Figures 2(a), 2(b), and 2(c). After the combined treatment of light irradiation and hypocrellin B, swollen mitochondria were observed and some cells even showed an absence of cristae (Figure 2(d)).

3.3. Changes in Mitochondrial Function. Ovarian cancer HO-8910 cells were sensitized with 2.5 μM hypocrellin B and then irradiated by LED light. After JC-1 staining, flow cytometry was used to analyze the changes of mitochondrial membrane potential. Figure 3 showed that the spectral shift of the fluorescence curve to the left, indicating that mitochondrial membrane depolarization occurred in the treated HO-8910 cells.

4. Discussion

Hypocrellin B from traditional Chinese herb *Hypocrella bambuase* has been confirmed as an efficient singlet oxygen generator upon light irradiation [5, 6, 10, 11]. Growing evidences show that light-activated hypocrellin B can markedly

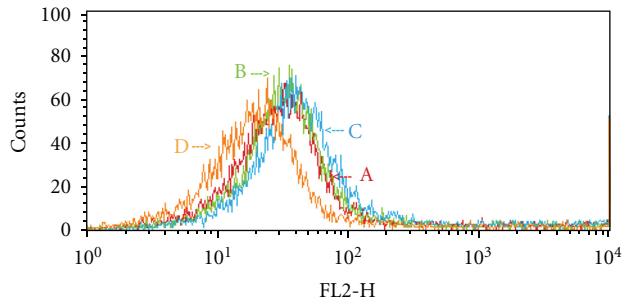

Figure 3: Mitochondrial membrane potential of HO-8910 cells was measured using flow cytometry with JC-1 staining 6 h after photodynamic action of hypocrellin B. The spectral shift of the fluorescence curve to the left indicates mitochondrial membrane depolarization. A: sham irradiation; B: hypocrellin B treatment alone; C: light irradiation alone; D: photodynamic action of hypocrellin B.

kill malignant cells and induce cell apoptosis [8, 9]. Our previous studies observed that hypocrellin B irradiated by blue light from LED source could cause significant damage to ovarian cancer HO-8910 cells [9]. In the present study, MTT assay showed that cell survival rate of HO-8910 cells in the photodynamic treatment group decreased significantly. Hypocrellin B treatment alone or light irradiation alone showed no significant impact. These data demonstrated that photodynamic action of hypocrellin B could decrease cell survival rate of ovarian cancer HO-8910 cells. However, the underlying mechanisms still need to be clarified.

Mitochondria play a central role in the regulation of cell growth and death [12, 13]. Mitochondria affect cellular breathing and energy metabolism directly or indirectly, subsequently decreasing cell proliferation and inducing cell death [14, 15]. In our TEM, we observed mitochondria with well-developed cristae in ovarian cancer HO-8910 cells after sham irradiation, hypocrellin B treatment alone, and light irradiation alone. After photodynamic treatment of hypocrellin B, some mitochondria displayed serious damage and disappearance of cristae. These alterations of mitochondrial structure would directly affect mitochondrial functions. In our present study, flow cytometry analysis with JC-1 staining also found that the spectral shift of the fluorescence curve was to the left, indicating that mitochondrial membrane depolarization occurred in HO-8910 cells treated by photodynamic action of hypocrellin B. The mitochondrial membrane depolarization can induce the release of mitochondrial cytochrome c into cytoplasm to initiate effector caspases such as caspases 3, 6, and 7. These effector Caspases can induce the generation of tBid to cause cell program death [16–18]. These findings suggest that mitochondrial morphological alterations and mitochondrial membrane depolarization are important events in photodynamic action of hypocrellin B on ovarian cancer HO-8910 cells. Hypocrellin B is a very good generator of ROS causing cell damage under light irradiation. It is well known that ROS has a very limited diffuse distance inside the cells; thus, ROS result in intracellular damage often close to the sensitizer localization [19, 20]. Ali and Olivo have reported that hypocrellin B mainly localizes in lysosomes other than mitochondria [21], suggesting that lysosomes are the direct target of photodynamic action of hypocrellin B. Recent studies have observed that there is lysosomal/mitochondrial crosstalk inside the cell [22–25]. The damaged lysosomes can cause lysosomal membrane permeabilization (LMP) and release cathepsins into the cytosol, subsequently inducing the mitochondrial alterations via the bcl-2 family Bid or bax [23–25]. Therefore, hypocrellin B-mediated photodynamic action induced cell death of HO-8910 cells probably through lysosomal-mitochondrial axis.

5. Conclusion

Photodynamic action of hypocrellin B under LED light irradiation significantly decreased cell proliferation and caused damage to mitochondrial morphology and function of ovarian cancer cells, highlighting that mitochondrial damage might be an important event in photodynamic therapy of hypocrellin B on ovarian cancer.

Acknowledgments

This work was supported by the Grants from National Nature Science Foundation of China (30973168) and the Chinese University of Hong Kong (2030446). The authors express their sincere thanks to Mr. Eric Chuck Hey Pun, Professor Faqi Li, Professor Shen Chen, Mr. Jianyong Wu, Mr. Dejiang Chao, and Ms. Qinglin Li for their helpful assistance.

References

[1] L. Y. Han, E. Kipps, and S. B. Kaye, "Current treatment and clinical trials in ovarian cancer," *Expert Opinion on Investigational Drugs*, vol. 19, no. 4, pp. 521–534, 2010.

[2] L. Hu, C. McArthur, and R. B. Jaffe, "Ovarian cancer stem-like side-population cells are tumourigenic and chemoresistant," *British Journal of Cancer*, vol. 102, no. 8, pp. 1276–1283, 2010.

[3] T. J. Dougherty, C. J. Gomer, B. W. Henderson et al., "Photodynamic therapy," *Journal of the National Cancer Institute*, vol. 90, no. 12, pp. 889–905, 1998.

[4] S. Pachydaki, L. Sobrin, and J. W. Miller, "Photodynamic therapy and combination treatments," *International Ophthalmology Clinics*, vol. 47, no. 1, pp. 95–115, 2007.

[5] J. B. Hudson, J. Zhou, J. Chen, L. Harris, L. Yip, and G. H. Towers, "Hypocrellin, from Hypocrella bambuase, is phototoxic to human immunodeficiency virus," *Photochemistry and Photobiology*, vol. 60, no. 3, pp. 253–255, 1994.

[6] D. Zhenjun and J. W. Lown, "Hypocrellins and their use in photosensitization," *Photochemistry and Photobiology*, vol. 52, no. 3, pp. 609–616, 1990.

[7] E. P. Estey, K. Brown, Z. Diwu et al., "Hypocrellins as photosensitizers for photodynamic therapy: a screening evaluation and pharmacokinetic study," *Cancer Chemotherapy and Pharmacology*, vol. 37, no. 4, pp. 343–350, 1996.

[8] Z. J. Diwu, R. P. Haugland, J. Liu et al., "Photosensitization by anticancer agents 21: new perylene- and aminonaphthoquinones," *Free Radical Biology and Medicine*, vol. 20, no. 4, pp. 589–593, 1996.

[9] Y. Jiang, A. W. N. Leung, J. Y. Xiang, and C. S. Xu, "Blue light-activated hypocrellin B damages ovarian cancer cells," *Laser Physics*, vol. 22, no. 1, pp. 300–305, 2012.
[10] S. M. Ali, S. K. Chee, G. Y. Yuen, and M. Olivo, "Hypericin and hypocrellin induced apoptosis in human mucosal carcinoma cells," *Journal of Photochemistry and Photobiology B*, vol. 65, no. 1, pp. 59–73, 2002.
[11] P. Wang, C. S. Xu, J. Xu, X. Wang, and A. W. Leung, "Hypocrellin B enhances ultrasound-induced cell death of nasopharyngeal carcinoma cells," *Ultrasound in Medicine and Biology*, vol. 36, no. 2, pp. 336–342, 2010.
[12] A. Chalah and R. Khosravi-Far, "The mitochondrial death pathway," *Advances in Experimental Medicine and Biology*, vol. 615, pp. 25–45, 2008.
[13] D. J. Smith, H. Ng, R. M. Kluck, and P. Nagley, "The mitochondrial gateway to cell death," *IUBMB Life*, vol. 60, no. 6, pp. 383–389, 2008.
[14] Z. Y. Shen, J. Shen, Q. S. Li, C. Y. Chen, J. Y. Chen, and Y. Zeng, "Morphological and functional changes of mitochondria in apoptotic esophageal carcinoma cells induced by arsenic trioxide," *World Journal of Gastroenterology*, vol. 8, no. 1, pp. 31–35, 2002.
[15] H. C. Lee, P. H. Yin, C. Y. Lu, C. W. Chi, and Y. H. Wei, "Increase of mitochondria and mitochondrial DNA in response to oxidative stress in human cells," *Biochemical Journal*, vol. 348, no. 2, pp. 425–432, 2000.
[16] Y. Wang, C. M. Che, J. F. Chiu, and Q. Y. He, "Dioscin (saponin)-induced generation of reactive oxygen species through mitochondria dysfunction: a proteomic-based study," *Journal of Proteome Research*, vol. 6, no. 12, pp. 4703–4710, 2007.
[17] P. Wang, C. Xu, X. Xia et al., "Mitochondrial damage in nasopharyngeal carcinoma cells induced by ultrasound radiation in the presence of hypocrellin B," *Journal of Ultrasound in Medicine*, vol. 29, no. 1, pp. 43–50, 2010.
[18] S. A. Susin, H. K. Lorenzo, N. Zamzami et al., "Molecular characterization of mitochodrial apoptosis-inducing factor," *Nature*, vol. 397, no. 6718, pp. 441–446, 1999.
[19] J. Morgan and A. R. Oseroff, "Mitochondria-based photodynamic anti-cancer therapy," *Advanced Drug Delivery Reviews*, vol. 49, no. 1-2, pp. 71–86, 2001.
[20] J. Xu, X. Xia, X. Wang et al., "Sonodynamic action of pyropheophorbide-a methyl ester in liver cancer cells," *Journal of Ultrasound in Medicine*, vol. 29, no. 7, pp. 1031–1037, 2010.
[21] S. M. Ali and M. Olivo, "Efficacy of hypocrellin pharmacokinetics in phototherapy," *International journal of oncology*, vol. 21, no. 6, pp. 1229–1237, 2002.
[22] M. J. Sousa, F. Azevedo, A. Pedras et al., "Vacuole-mitochondrial cross-talk during apoptosis in yeast: a model for understanding lysosome-mitochondria-mediated apoptosis in mammals," *Biochemical Society Transactions*, vol. 39, no. 5, pp. 1533–1537, 2011.
[23] M. Ali-Seyed, R. Bhuvaneswari, K. C. Soo, and M. Olivo, "Photolon—photosensitization induces apoptosis via ROS-mediated cross-talk between mitochondria and lysosomes," *International Journal of Oncology*, vol. 39, no. 4, pp. 821–831, 2011.
[24] L. Liu, Z. Zhang, and D. Xing, "Cell death via mitochondrial apoptotic pathway due to activation of Bax by lysosomal photodamage," *Free Radical Biology and Medicine*, vol. 51, no. 1, pp. 53–68, 2011.
[25] G. Yang, S. Wang, L. Zhong et al., "6-Gingerol induces apoptosis through lysosomal-mitochondrialaxis in human hepatoma G2 cells," *Phytotherapy Research*. In press.

Hindawi Publishing Corporation
International Journal of Photoenergy
Volume 2012, Article ID 238468, 6 pages
doi:10.1155/2012/238468

Research Article

Inhibitory Effects of Far-Infrared Ray-Emitting Belts on Primary Dysmenorrhea

Ben-Yi Liau,[1] Ting-Kai Leung,[2] Ming-Chiu Ou,[3] Cheng-Kun Ho,[3] Aiga Yang,[3] and Yung-Sheng Lin[3]

[1] *Department of Biomedical Engineering, Hungkuang University, 34 Chung-Chie road, Shalu, Taichung 443, Taiwan*
[2] *Department of Diagnostic Radiology, Taipei Medical University Hospital & Department of Radiology, School of Medicine, College of Medicine, Taipei Medical University, 250 Wu-Hsing Street, Taipei 110, Taiwan*
[3] *Department of Applied Cosmetology and Master Program of Cosmetic Science, Hungkuang University, 34 Chung-Chie road, Shalu, Taichung 443, Taiwan*

Correspondence should be addressed to Yung-Sheng Lin, linys@sunrise.hk.edu.tw

Received 1 December 2011; Revised 21 May 2012; Accepted 5 June 2012

Academic Editor: Timon Cheng-Yi Liu

This study investigated the therapeutic effect of the far-infrared ray-emitting belt (FIRB) in the management of primary dysmenorrhea in female patients. Forty adolescent females with primary dysmenorrhea were enrolled in the study. Quantitative measurements were taken during the menstruation. Several parameters were measured and compared, including temperature, abdominal blood flow, heart rate variability, and pain assessment. Statistical analysis shows that treatment with FIRB had significant efficiency in increasing regional surface temperature and abdominal blood flow, widening standard deviation of normal-to-normal RR intervals, and reducing VRS and NRS pain scores. The application of an FIRB appears to alleviate dysmenorrhea.

1. Introduction

Dysmenorrhea is one of the gynecological symptoms pertaining obviously to women. Ninety percent of women experienced menstrual pain, with a third to half of the women reporting moderate-to-severe symptoms. Population surveys suggest that, although prevalence rates vary considerably according to geographical locations, complaints of dysmenorrhea are widespread among diverse populations. Symptoms are frequently associated with time lost from school, work, or other activities. Despite the frequency and severity of dysmenorrhea, most women do not seek medical treatment for this condition.

"Dysmenorrhea" is derived from a Greek root word that translates as "difficult menstrual flow." Dysmenorrhea can be divided into the two broad categories of primary and secondary. Primary dysmenorrhea is defined as a cramping pain in the lower abdomen occurring just before or during menstruation, without pelvic abnormalities. Secondary dysmenorrhea is menstrual pain associated with underlying pelvic pathology such as endometriosis.

Primary dysmenorrhea is typically characterized by a menstrual cramp that begins between several hours before and a few hours after onset of menstrual bleeding. Primary dysmenorrhea may be associated with vomiting, fatigue, back pain, headaches, dizziness, and diarrhea. Ninety percent of young women report that the duration of their menstrual cramps is 48 hours or less. Symptoms are relatively repeated from one menstrual period to the next. The pain is characteristically colicky and located in the midline of the lower abdomen. Primary dysmenorrhea arises from the secretion of prostaglandins during the luteal phase and subsequent menstrual flow. Excessive release of prostaglandins increases the amplitude and frequency of uterine contractions and causes vasospasm of the uterine arterioles, resulting in ischaemia and cyclical lower abdominal cramps.

In the United States, dysmenorrhea accounts for 600 billion working hours loss and over US$ 2 billion productivity lost every year [1]. In Taiwan, primary dysmenorrhea is the most common reason adolescent girls consult gynecologists. Dysmenorrhea may lead to severe anxiety;

thus, if pain during menstruation can be relieved, anxiety levels may also be reduced [2]. Many women consider menstrual pain to be inevitable even though the pain is severe and incapacitating. Women suffering from primary dysmenorrhea may not seek medical assistance and frequently do not use available prescription therapies. Anti-inflammatory drugs are generally the first choice of treatment for primary dysmenorrhea. Anti-inflammatory drugs directly inhibit the enzyme of cyclooxygenase (COX-2), indirectly reducing prostaglandin synthesis. However, 20% to 30% of patients with primary dysmenorrhea report that anti-inflammatory drugs are ineffective. In addition, drug therapy provides only temporary relief, and drugs are associated with several gastrointestinal side effects and complications such as anti-inflammatory-induced gastric ulcers or bleeding, and increased load on the kidneys and liver. Thus, an effective alternative therapy without drugs is necessary for the treatment of dysmenorrhea.

Research has shown that electromagnetic waves of far-infrared ray (FIR) especially at 4–14 μm produce both nonthermal and thermal effects [3–9]. Such effects include an increase in microvascular dilation, higher blood flow volume, and an elevation in regional tissue temperature [3–5]. The consensus view is that these wavelengths promote other intracellular effects at the microscopic level, affecting heat transfer in subcutaneous tissues, and other physiobiological processes [5, 6, 10]. Several studies indicated that far-infrared ray irradiation is an effective treatment for chronic pain [10–13]. However, a limited number of studies have used objective parameters to assess the clinical efficacy of FIR, or have attempted to explain its mechanism on a biomolecular basis.

This study investigated the therapeutic effect of an FIR-emitting belt (FIRB) on dysmenorrhea by analyzing objective parameters and attempted to explain the possible mechanisms. In this study, participants were assessed during the dysmenorrheal period, and changes were monitored before and after application of the FIRB. Dysmenorrhea was measured quantitatively by thermography, laser Doppler imaging, standard deviation of normal-to-normal RR intervals (SDNN), verbal rating scale (VRS), and numeric rating scale (NRS).

2. Materials and Methods

2.1. Participants. The clinical trial was approved by an independent ethics committee of the university, with certification by the Institutional Review Board (IRB) approval number HK IRB 98-B-002. We performed this experiment from February 1, 2010 to January 31, 2011.

Participants were recruited for the study cohort from campus. Adolescent female students with dysmenorrhea volunteered as candidates and were screened by the doctor. All of the participants were required to complete a pretest questionnaire on their medical history and pain. The questionnaire investigated possible discomfort and other descriptions. The participants were also required to sign a consent form before any measurements were taken or FIRB was applied. The inclusion criteria for all candidates who participated in this study were as follows: older than 18; self-reported dysmenorrhea; no history of major gynecological disease or secondary dysmenorrhea; no pain medication taken in the 24 hours before receiving treatment. Only subjects on the first-to-third days from the onset of menses could be included in this study to treat with the FIRB. The carefully selected sample included forty young women with primary dysmenorrhea.

Figure 1: The photograph of the carbon fiber belt in this study. The belt controller was set to 50°C for 30 minutes.

2.2. FIR-Emitting Belt. The FIR spectrum of the carbon fiber fabric belt (30 cm × 60 cm as shown in Figure 1, THERMEDIC, LinkWin Technology Co., Ltd., Taiwan) used in this study was determined by a CI SR5000 spectroradiometer at the Industrial Technology Research Institute, Taiwan. The FIR energy generated from the carbon fiber belt at 50°C is 11.34 mW/cm^2 by integrating the intensity of the wavelengths between 4 μm and 16 μm in Figure 2.

2.3. Measurements. All measurements and procedures in this study were performed in a climate-controlled room at a constant temperature and humidity (23°C and 60% relative humidity). Before assessment, participants were required to lie down in this room to acclimatize to these indoor climatic conditions for 30 minutes [14]. Participants were thermographed for the abdominal region by the Fluke Ti25 (Fluke Corporation, Everett, WA, USA). Their abdominal blood flows were measured by the MoorLDI2-IR laser Doppler imaging (Moor Instruments Ltd., Devon, UK) [15]. Subsequently, they were asked to wear the FIRB on the abdominal region. Then FIRB was warmed to a temperature of 50°C to enhance FIR irradiation for 30 minutes. The second measurements of abdominal temperature and blood flow were performed after the application of FIRB.

In addition, ANSWatch wrist monitor (TS-0411, Taiwan Scientific Corp., Taiwan) utilized in studying nervous system regulation [16, 17] was applied to conduct a standard 5-minute heart rate variability (HRV) test with left hand before and after using FIRB for 30 minutes. The cuff with piezoelectrical sensors obtained blood pressure signals produced by the radial artery, with the aid of an air pouch pressure controlled by an air pump and a release valve. The blood pressure waveforms with peak-to-peak intervals were determined in

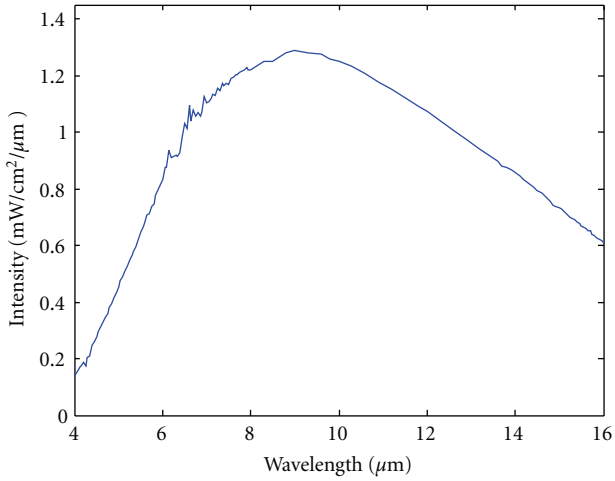

Figure 2: The FIR spectrum of the carbon fiber belt at 50°C. The total intensity of the wavelengths between 4 μm and 16 μm is 11.34 mW/cm^2.

time domain analysis. The HRV analysis followed closely the 1996 International Standard. HRV is total ANS activity index (ms) that equal to standard deviation of normal-to-normal RR intervals defined in the 1996 international standard [18].

2.4. Menstrual Pain Assessment. Before and after the application of FIRB, all the participants were required to complete two pain questionnaires to assess the pain scores associated with their dysmenorrhea. These pain assessments were the five-level verbal rating scale (VRS) and 11-point numeric rating scale (NRS) [19]. The VRS pain scale was classified into grades of none (0), very mild (1), mild (2), moderate (3), severe (4), and very severe (5). The NRS was divided into eleven levels of pain, ranging from no pain (0) to the worst pain (10).

2.5. Statistical Analysis. The data differences between before and after treatment were analyzed using Wilcoxon signed-rank test. A value of $P < 0.05$ was considered statistically significant (*), and $P < 0.01$ was highly significant (**).

3. Results

3.1. Effect of FIRB on Abdominal Temperature. The abdominal temperature was measured by thermography (Fluke Ti25). Results indicated that there was a substantial increase in regional body temperature after participants used FIRB for 30 minutes. It was shown in Figure 3. The average abdominal temperatures of before and after FIRB treatment were 34.6 ± 1.2°C and 37.5 ± 1.2°C, respectively. This temperature increase was safe for skin and did not cause any burns in participants. There was no side effect such as menorrhagia reported in the treatment of primary dysmenorrhea with the FIRB.

3.2. Effect of FIRB on Blood Flow. The abdominal blood flow was measured by the Moor laser Doppler imaging device (MoorLDI2-IR). A significant increase was found in

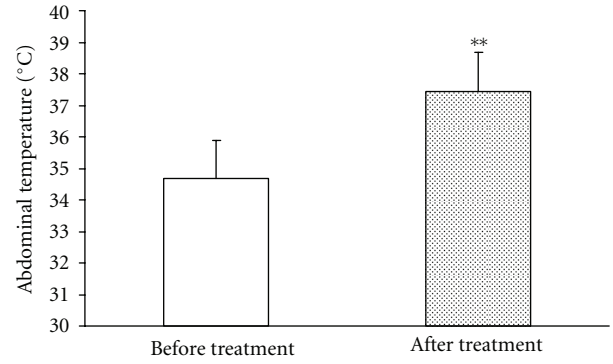

Figure 3: The average abdominal temperatures before and after treatment. Expression values are the mean and standard deviation, and the statistical difference was analyzed by Wilcoxon signed-rank test. Double asterisk mean that this group was highly significantly different from control group ($P < 0.01$).

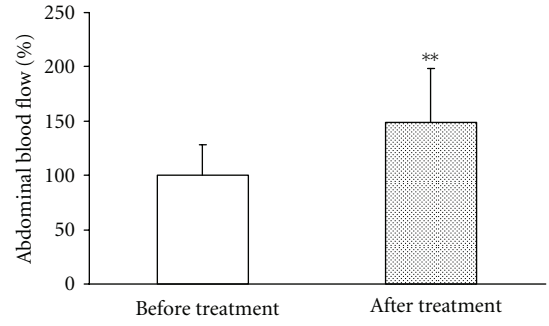

Figure 4: The relative abdominal blood flows before and after treatment. Expression values are the mean and standard deviation, and the difference between groups was tested using Wilcoxon Signed-Rank Test. Double asterisk mean that this group was highly significantly different from control group ($P < 0.01$).

regional blood perfusion after participants' use of FIRB for 30 minutes (Figure 4). There was a 48.7 ± 49.7% increase in the normalized abdominal blood flow after FIRB treatment.

3.3. Effect of FIRB on Physiological Signals. No significant differences emerged in the physiological parameters of the blood pressure and respiration between before and after FIRB treatment conditions. However, the standard deviation of normal-to-normal RR intervals in pulse waveforms increased significantly (Figure 5). The average SDNN values of before and after FIRB treatment were 69.2 ± 42.2 ms and 97.2 ± 72.8 ms, respectively. This finding may imply that the autonomic nervous system became more active with treatment. It seems possible that FIRB may help relieve pain by regulating the autonomic nervous system.

3.4. Effect of FIRB on VRS and NRS Scores. The pain assessments by VRS and NRS showed that treatment with FIRB significantly decreased the participants' subjective ratings of their pain or suffering associated with dysmenorrhea (Figures 6 and 7). The average VRS scores before and after FIRB treatment were 1.89 ± 1.02 and 0.76 ± 0.68,

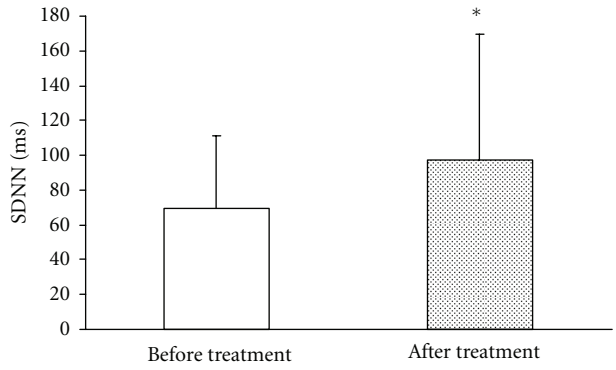

Figure 5: The mean SDNN values before and after treatment. Expression values are the mean and standard deviation, and Wilcoxon Signed-Rank Test was used to test the statistical difference between groups. Asterisk means that this group has statistical difference with control group ($P < 0.05$).

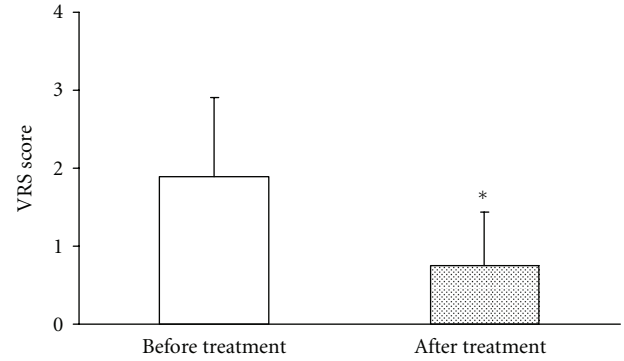

Figure 6: The VRS scores before and after treatment. Expression values are the mean and standard deviation, and the statistical difference was detected by Wilcoxon Signed-Rank Test. Asterisk means that this group has statistical difference with control group ($P < 0.05$).

respectively. The average NRS scores before and after FIRB treatment were 4.57 ± 1.83 and 1.62 ± 1.62, respectively.

4. Discussion

The etiology of primary dysmenorrhea is bounded in a multiplicity of pathological, mechanical, and psychoneurotic disorders. One disorder that has been found to correlate with primary dysmenorrhea is blood flow deprivation with organic and lower abdominal ischemia. The sensation of pain and related biomolecule induction of COX-2 and prostaglandin are strongly related to the severity of primary dysmenorrhea. Previous studies have identified the overproduction of uterine prostaglandins as a contributing factor to primary dysmenorrhea. The most widely used anti-inflammatory drugs for primary dysmenorrhea directly inhibit the cyclooxygenase (COX) enzymes, thereby inhibiting the production of prostaglandins. Prostaglandin synthesis is mediated primarily by two distinct isoforms of cyclooxygenase (COX-1 and COX-2), which catalyze the metabolism of arachidonate to prostaglandin H2. Conventional anti-inflammatory drugs act as nonselective inhibitors of both isoforms of COX. It has been proposed that the therapeutic efficacy of anti-inflammatory drugs is primarily the result of COX-2 inhibition. Cyclooxygenase (including COX-2) inhibitors have been developed clinically as a treatment for dysmenorrhea.

Far-infrared radiation offers a nondrug alternative therapy to relieve inflammation by targeting prostaglandin and COX-2. Our earlier study had investigated a FIR-emitting ceramic material with a focus on basic medical science of cells and animal models. We found that the FIR-emitting ceramic material promoted microcirculation and induced other effects by upregulating calcium-dependent nitric oxide (NO) and calmodulin in different cell lines [5, 6]. We manifested that the FIR ceramic material exerted an antioxidant effect by increasing the hydrogen peroxide-scavenging ability in different cells lines [7, 8]. We also illustrated that FIR induced anti-inflammatory effects by inhibiting prostaglandin (PGE-2) in SW1353 human chondrosarcoma cell line [20]. In addition, our unpublished data show that FIR irradiation had significant inhibition of COX-2 elevation during lipopolysaccharide-induced inflammation in both murine macrophages and human chondrosarcoma cell line.

Ischemia is mainly a consequence of decreased microcirculation or a reduction in local muscle blood flow and perfusion. This scenario has important consequences for cellular metabolic status, with a significantly worsened metabolic and acid-base status while acidosis is accumulated. During dysmenorrhea, the corresponding regional organic ischemia is associated with increased oxidative stress due to increased levels of reactive oxygen species (ROS), such as superoxide and hydrogen peroxide (H_2O_2), which are responsible of destructive processes in organic tissues [7, 8]. Our previously published data indicated that FIR-irradiating ceramic material produced calcium-dependent NO [5, 6]. It is a medical fact that NO is essential to female-related cells such as uterine and placental cells. During menstruation and pregnancy, women need to produce more NO in the related cells. Recent medical research has indicated that diminished levels of NO induce myometrial contractions, while NO can cause uterine relaxation. By using oral glyceryl trinitrate as a source of NO can relax the exaggerated myometrial contractions in primary dysmenorrhea. A recent review concluded that nitroglycerin significantly reduces the pain in primary dysmenorrheal [21].

Several important merits of NO and the NO-related biomolecules suggest the mechanisms by which dysmenorrhea is alleviated. First, NO inhibits platelet aggregation, reducing inflammation and providing pain relief. Second, adequate NO activity can improve microcirculation, which is a protective factor in maintaining the smooth muscle dilation of blood vessels. Because NO increases blood flow, microcirculation in the endometrial tissue is enhanced, thus relieving inflammation and dysmenorrhea. Third, dysmenorrhea is due to rapid and strong uterine contractions. NO helps coordinate and relieve smooth muscle contraction and relaxation [22]. Fourth, NO is involved in the endocrine mechanism by which menstruation is initiated. Finally, an exogenous NO donor, glyceryl trinitrate, is already in use

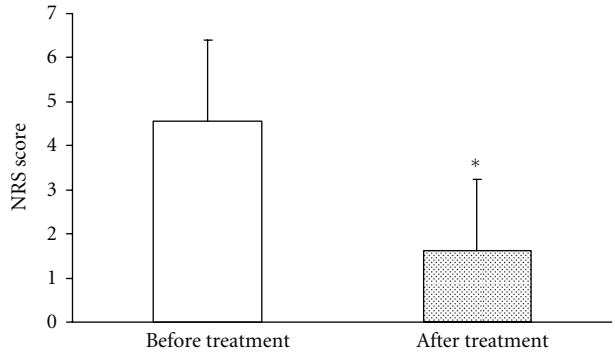

Figure 7: The NRS scores before and after treatment. Expression values are the mean and standard deviation, and the difference between groups was analyzed using Wilcoxon Signed-Rank Test. Asterisk means that this group has statistical difference with control group ($P < 0.05$).

as medication to relieve dysmenorrhea by local application. Glyceryl trinitrate has a relaxing effect on the myometrium and has been shown to have a beneficial effect on primary dysmenorrheal [23, 24].

Primary dysmenorrhea as a psychoneurotic disorder is the most common reason for adolescent girls to consult a gynecologist in Taiwan. Primary dysmenorrhea may lead to severe anxiety. If the dysmenorrheal pain can be relieved, anxiety may also be reduced [2]. Some researchers have suggested using cardiac vagal tone as a novel index of stress and stress-induced pain. The role of the parasympathetic nervous system and particularly the vagus nerve in defining stress has been demonstrated [25]. This study finds that the prolonging of the standard deviation of normal-to-normal RR intervals by FIRB has an effect of relaxation. The relaxation response is controlled by the parasympathetic nervous system and particularly the vagus nerve. This relaxation response is a palliative treatment for pain, and the enhancement of parasympathetic tone is important to apply on different chronic pain control. Automatic nervous system pain regulation by parasympathetic activation via the vagal pathways has been shown to exert a beneficial effect on pain and to produce a relaxation response, included in the treatment of dysmenorrhea [25–28].

The thermal effect of the FIRB is also involved in the treatment of primary dysmenorrhea. Thermal effect individually exhibits some degree of relieving symptoms of dysmenorrhea. One of the mechanisms is warm temperature inhibiting sympathetic nerve activities that are responsible of the pain sensation. Besides, the inhibition of sympathetic nerve activity by warm temperature application on lower abdominal or lumbar region might increase uterine blood flow and remove pain-producing substances [29, 30]. In addition, heat can treat dysmenorrhea through a form of gate control or by altering pain thresholds centrally or through an altered sense of well-being [31].

Although the therapeutic efficacy of the FIRB had been found in this study, there are some limitations in the interpretation of our findings. This is a self-controlled before-and-after experimental study. In spite of the valid physical evidence without a control group, psychological effects may exist in self-report assessments and affect the pain scores. Future studies are suggested to be designed with a larger sample-sized, randomized, and controlled group to further illustrate the psychoneurotic factors.

5. Conclusions

This study demonstrated that FIRB is an effective and safe form of therapy for primary dysmenorrhea. Treatment by FIRB resulted in a significant elevation of temperature and abdominal blood flow as well as effective pain relief assayed by the VRS and NRS. Based on these findings and previous literatures, we speculated that the possible effect of FIR on dysmenorrhea may include NO induction, scavenging oxidative stress, and suppression of COX-2 and PGE2 production. FIRB significantly increased the average SDNN value, reflecting that autonomic tone was modulated for relaxation during menstrual pain. This increase in heart rate variability may explain the effect of FIRB on the relationship between pain, anxiety, and activation of the autonomic nervous system. Therefore, it indicates that FIRB may help relieve dysmenorrhea by regulating the autonomic nervous system.

Conflict of Interests

The authors declare that they have no conflict of interests.

Acknowledgments

This work was supported by a grant from the National Science Council of Taiwan, R.O.C. (NSC99-2622-E-241-004-CC3 and NSC100-2622-E-241-002-CC3). The authors also gratefully acknowledge the help of Roy Sun and Gwo-Diing Lee.

References

[1] H. M. Chen and C. H. Chen, "Effects of acupressure at the Sanyinjiao point on primary dysmenorrhoea," *Journal of Advanced Nursing*, vol. 48, no. 4, pp. 380–387, 2004.

[2] C. Alonso and C. L. Coe, "Disruptions of social relationships accentuate the association between emotional distress and menstrual pain in young women," *Health Psychology*, vol. 20, no. 6, pp. 411–416, 2001.

[3] S. Y. Yu, J. H. Chiu, S. D. Yang, Y. C. Hsu, W. Y. Lui, and C. W. Wu, "Biological effect of far-infrared therapy on increasing skin microcirculation in rats," *Photodermatology Photoimmunology and Photomedicine*, vol. 22, no. 2, pp. 78–86, 2006.

[4] S. Inoue and M. Kabaya, "Biological activities caused by far-infrared radiation," *International Journal of Biometeorology*, vol. 33, no. 3, pp. 145–150, 1989.

[5] T. K. Leung, C. M. Lee, M. Y. Lin et al., "Far infrared ray irradiation induces intracellular generation of nitric oxide in breast cancer cells," *Journal of Medical and Biological Engineering*, vol. 29, no. 1, pp. 15–18, 2009.

[6] T. K. Leung, Y. S. Lin, Y. C. Chen et al., "Immunomodulatory effects of far-infrared ray irradiation via increasing calmodulin

and nitric oxide production in raw 264.7 macrophages," *Biomedical Engineering-Applications, Basis and Communications*, vol. 21, no. 5, pp. 317–323, 2009.

[7] T. K. Leung, Y. S. Lin, C. M. Lee et al., "Direct and indirect effects of ceramic far infrared radiation on the hydrogen peroxide-scavenging capacity and on murine macrophages under oxidative stress," *Journal of Medical and Biological Engineering*, vol. 31, no. 5, pp. 345–351, 2011.

[8] T. K. Leung, H. F. Shang, D. C. Chen et al., "Effects of far infrared rays on hydrogen peroxide-scavenging capacity," *Biomedical Engineering-Applications, Basis and Communications*, vol. 23, no. 2, pp. 99–105, 2011.

[9] T. K. Leung, C. F. Chan, P. S. Lai, C. H. Yang, C. Y. Hsu, and Y. S. Lin, "Inhibitory effects of far-infrared irradiation generated by ceramic material on murine melanoma cell growth," *International Journal of Photoenergy*, vol. 2012, Article ID 646845, 8 pages, 2012.

[10] A. Masuda, Y. Koga, M. Hattanmaru, S. Minagoe, and C. Tei, "The effects of repeated thermal therapy for patients with chronic pain," *Psychotherapy and Psychosomatics*, vol. 74, no. 5, pp. 288–294, 2005.

[11] K. Matsushita, A. Masuda, and C. Tei, "Efficacy of Waon therapy for fibromyalgia," *Internal Medicine*, vol. 47, no. 16, pp. 1473–1476, 2008.

[12] C. H. Lee, J. W. Roh, C. Y. Lim, J. H. Hong, J. K. Lee, and E. G. Min, "A multicenter, randomized, double-blind, placebo-controlled trial evaluating the efficacy and safety of a far infrared-emitting sericite belt in patients with primary dysmenorrhea," *Complementary Therapies in Medicine*, vol. 19, no. 4, pp. 187–193, 2011.

[13] R. M. B. York and I. L. Gordon, "Effect of optically modified polyethylene terephthalate fiber socks on chronic foot pain," *BMC Complementary and Alternative Medicine*, vol. 9, article 10, 2009.

[14] A. M. Hug, T. Schmidts, J. Kuhlmann, D. Segger, G. Fotopoulos, and J. Heinzerling, "Skin hydration and cooling effect produced by the Voltaren vehicle gel," *Skin Research and Technology*, vol. 18, pp. 199–206, 2012.

[15] X. Z. West, N. L. Malinin, A. A. Merkulova et al., "Oxidative stress induces angiogenesis by activating TLR2 with novel endogenous ligands," *Nature*, vol. 467, no. 7318, pp. 972–976, 2010.

[16] K.-M. Chang and C.-W. Shen, "Aromatherapy benefits autonomic nervous system regulation for elementary school faculty in Taiwan," *Evidence-based Complementary and Alternative Medicine*, vol. 2011, Article ID 946537, 7 pages, 2011.

[17] W. C. Liang, J. Yuan, D. C. Sun, and M. H. Lin, "Changes in physiological parameters induced by indoor simulated driving: effect of lower body exercise at mid-term break," *Sensors*, vol. 9, no. 9, pp. 6913–6933, 2009.

[18] T. Force, "Heart rate variability: standards of measurement, physiological interpretation and clinical use. Task force of the european society of cardiology and the north american society of pacing and electrophysiology," *Circulation*, vol. 93, no. 5, pp. 1043–1065, 1996.

[19] A. Fauconnier, E. Dallongeville, C. Huchon, Y. Ville, and B. Falissard, "Measurement of acute pelvic pain intensity in gynecology: a comparison of five methods," *Obstetrics and Gynecology*, vol. 113, no. 2, pp. 260–269, 2009.

[20] T. K. Leung, C. H. Chen, C. H. Lai et al., "Bone and joint protection ability of ceramic material with biological effects," *Chinese Journal of Physiology*, vol. 55, no. 1, pp. 47–54, 2012.

[21] M. Y. Dawood, "Primary dysmenorrhea: advances in pathogenesis and management," *Obstetrics and Gynecology*, vol. 108, no. 2, pp. 428–441, 2006.

[22] I. T. Cameron and S. Campbell, "Nitric oxide in the endometrium," *Human Reproduction Update*, vol. 4, no. 5, pp. 565–569, 1998.

[23] S. Ghazizadeh, T. Dadkhah, and M. Modarres, "Local application of glyceril trinitrate ointment for primary dysmenorrhea," *International Journal of Gynecology and Obstetrics*, vol. 79, no. 1, pp. 43–44, 2002.

[24] C. Lees, S. Campbell, E. Jauniaux et al., "Arrest of preterm labour and prolongation of gestation with glyceryl trinitrate, a nitric oxide donor," *The Lancet*, vol. 343, no. 8909, pp. 1325–1326, 1994.

[25] S. W. Porges, "Cardiac vagal tone: a physiological index of stress," *Neuroscience and Biobehavioral Reviews*, vol. 19, no. 2, pp. 225–233, 1995.

[26] S. D. Schaffer and C. B. Yucha, "Relaxation & pain management: the relaxation response can play a role in managing chronic and acute pain," *The American Journal of Nursing*, vol. 104, no. 8, pp. 75–78, 2004.

[27] M. Sakakibara, S. Takeuchi, and J. Hayano, "Effect of relaxation training on cardiac parasympathetic tone," *Psychophysiology*, vol. 31, no. 3, pp. 223–228, 1994.

[28] T. A. Pellino, D. B. Gordon, Z. K. Engelke et al., "Use of nonpharmacologic interventions for pain and anxiety after total hip and total knee arthroplasty," *Orthopaedic Nursing/National Association of Orthopaedic Nurses*, vol. 24, no. 3, pp. 182–192, 2005.

[29] Y. Nagashima, H. Oda, M. Igaki et al., "Application of heat- and steam-generating sheets to the lumbar or abdominal region affects autonomic nerve activity," *Autonomic Neuroscience*, vol. 126-127, pp. 68–71, 2006.

[30] T. Hosono, Y. Takashima, Y. Morita et al., "Effects of a heat- and steam-generating sheet on relieving symptoms of primary dysmenorrhea in young women," *Journal of Obstetrics and Gynaecology Research*, vol. 36, no. 4, pp. 818–824, 2010.

[31] M. D. Akin, K. W. Weingand, D. A. Hengehold, M. B. Goodale, R. T. Hinkle, and R. P. Smith, "Continuous low-level topical heat in the treatment of dysmenorrhea," *Obstetrics and Gynecology*, vol. 97, no. 3, pp. 343–349, 2001.

Hindawi Publishing Corporation
International Journal of Photoenergy
Volume 2012, Article ID 652040, 8 pages
doi:10.1155/2012/652040

Methodology Report

Assessing the Therapeutic Effect of 630 nm Light-Emitting Diodes Irradiation on the Recovery of Exercise-Induced Hand Muscle Fatigue with Surface Electromyogram

Dandan Yang,[1] Xiaoying Wu,[1] Wensheng Hou,[1] Xiaolin Zheng,[1] Jun Zheng,[2] and Yingtao Jiang[3]

[1] *Key Laboratory of Biorheological Science and Technology of Ministry of Education, Chongqing University, Chongqing 400044, China*
[2] *Department of Computer Science and Engineering, New Mexico Institute of Mining and Technology, Socorro, NM 87801, USA*
[3] *Department of Electrical and Computer Engineering, University of Nevada, Las Vegas, Las Vegas, NV 89154, USA*

Correspondence should be addressed to Wensheng Hou, w.s.hou@cqu.edu.cn

Received 15 October 2011; Revised 24 January 2012; Accepted 27 February 2012

Academic Editor: Rui Duan

This paper aims to investigate the effect of light emitting diode therapy (LEDT) on exercise-induced hand muscle fatigue by measuring the surface electromyography (sEMG) of flexor digitorum superficialis. Ten healthy volunteers were randomly placed in the equal sized LEDT group and control group. All subjects performed a sustained fatiguing isometric contraction with the combination of four fingertips except thumb at 30% of maximal voluntary contraction (MVC) until exhaustion. The active LEDT or an identical passive rest therapy was then applied to flexor digitorum superficialis. Each subject was required to perform a re-fatigue task immediately after therapy which was the same as the pre-fatigue task. Average rectified value (ARV) and fractal dimension (FD) of sEMG were calculated. ARV and FD were significantly different between active LEDT and passive rest groups at 20%–50%, 70%–80%, and 100% of normalized contraction time ($P < 0.05$). Compared to passive rest, active LEDT induced significantly smaller increase in ARV values and decrease in FD values, which shows that LEDT is effective on the recovery of muscle fatigue. Our preliminary results also suggest that ARV and FD are potential replacements of biochemical markers to assess the effects of LEDT on muscle fatigue.

1. Introduction

Muscular fatigue is manifested by a decline in the force-generating capacity during maximal contraction [1] or the incapacity to maintain required or expected muscle force for a period of time [2]. This phenomenon is dependent on the type and intensity of exercise, muscle group involved, duration of the activity, and type and size of muscle fibers [3], which means that fatigue development is a complex and multifaceted process involving physiological, biomechanical and psychological elements [2]. Although the mechanisms of fatigue development, prevention and recovery are not fully understood up to now, fatigue recovery is of great interest to the researchers due to its great significance in rehabilitation medicine, ergonomics and sports science.

In the last decades, a large amount of physical or chemical approaches have been attempted. The positive therapeutic effects of cryotherapy [4, 5], neuromuscular electrical stimulation [6], and antioxidant supplementation [7] were testified for muscle fatigue recovery. Recently, phototherapy or optical irradiation with specific wavelength range was proposed for fatigue development and recovery of skeletal muscle [8–10]. Studies on animal and human revealed that the low level laser therapy (LLLT) significantly promotes the muscle fatigue development and recovery by reducing postexercise blood lactate, decreasing the activity of creatine kinase (CK) and C-reactive protein (CRP), and improving muscle performance [8, 11–14]. Further experiments indicated that the phototherapeutic effects of LLLT were associated with depressing of oxidative stress [15] and reactive oxygen species production [16], improvement of

mitochondrial function [17, 18] and ATP synthesis [19], and enhancement of microcirculation [20]. As an alternative light source, high-power light-emitting diodes (LEDs) exhibited similar phototherapeutic effects, and the decreased muscle fatigue was observed through phototherapy with light-emitting diodes therapy (LEDT) [9, 10, 21, 22]. However, the mechanism for phototherapy in human muscle fatigue recovery is far from clear.

Muscle fatigue is a progressive course of decreasing muscle activity accompanied by physical and chemical change in muscles. Knowledge of these dynamic changes is helpful to evaluate the effects of phototherapy and make better treatment plan. Although the physiochemical changes in CK activity and CRP levels are commonly used as indirect indicators for the estimation of muscle fatigue [10, 23], it is not suitable for continuously monitoring the physiological state of muscle during muscle contraction. Surface electromyography (sEMG) is a widely used electrophysiological technique for muscle activity detection and has been used to characterize the myoelectric properties of muscle fatigue in onset time of mechanical fatigue [24, 25] as well as the neuromuscular properties of muscle fatigue [26]. The average rectified value (ARV) and fractal dimension (FD) of sEMG were successfully used to evaluate the status of muscle fatigue by measuring firing rate of motor unit and its recruitment pattern [2, 27, 28]. The present study is to investigate the effect of phototherapy on hand muscle fatigue recovery by comparing the ARV and FD values of the LEDT and control groups.

2. Materials and Methods

2.1. Subjects. Ten healthy right-handed university students (five males and five females) volunteered to participate in the experiment. The participants' inclusion criteria were (i) healthy with no history of myopathology and neuropathology and (ii) free of intense exercise in 24 hours before the experiment. Experiments were conducted after receiving approval from the local ethics committee. Each participant was given an oral and written summary of the experimental protocol and the purpose of the study and then was required to sign a consent form prior to the experiment.

2.2. Experimental Procedure. Each subject was seated upright in a comfortable chair with his/her hip and knee joint flexed at 90° and their right forearm resting on a supporting armrest. The elbow was positioned in palm downward with the elbow in approximately 120° flexion. The forearm and wrist were stabilized to the armrest with nylon tapes. The subject was asked to produce a force with the combination of four fingers (IMRL, I = index, M = middle, R = ring, and L = little). The exerted forces of individual fingers were recorded by four load cells (linear operation range 0–196 N, JLBS, JinNuo Inc., China), respectively.

The experimental protocol consisted of the following phases.

Phase 1 (Maximal Voluntary Contraction (MVC) of IMRL). MVC was taken as the maximum of three isometric contractions of the right forearm flexors with IMRL. Each contraction lasted 5 seconds with 2-minute recovery period between two successive contractions. Verbal encouragement was provided during MVCs to obtain maximal effort. A 5-minute rest was taken after the maximal contractions.

Phase 2 (Prefatigue). Immediately after Phase 1, the subject was instructed to perform a sustained fatiguing isometric contraction at 30% MVC of IMRL until exhaustion, which was defined as the point at which the force decreased by 5% of the target force for more than 2 seconds [29].

Phase 3 (Therapy). Participants were randomly divided into two equal sized groups, that is, active LEDT group (four males and one female) and passive rest therapy group (one male and four females). The fatigued forearm hand muscle received an active LEDT through photon therapy equipment with a multidiode cluster probe (Carnation66, Shenzhen Lifotronic Tech. Inc., Shenzhen, China) or a passive rest therapy. The therapy started immediately after Phase 2 and ended 120 seconds before Phase 4.

The subject's forearm was positioned in neutral rotation during the therapy. For LEDT, the center of the light spot was located at approximately 50% of landmark line from the medial epicondyle to the styloid process of the ulna, which was the center belly of flexor digitorum superficialis. The subject's forearm maintained the rest state without moving during the therapy.

Irradiation with LEDT (100 LEDs with wavelength 630 nm, spot size 2.5 cm^2, power density 0.048 W/cm^2, and energy density 57.6 J/cm^2) was performed in non-contact mode with the probe held stationary at a vertical distance of 60 mm between light source and skin surface. The total time of therapy was 20 minutes. Opaque goggles were used for all participants during the therapy to protect their eyes from the treatment and assure the blindness of the study.

Phase 4 (Refatigue). Each subject was required to perform the same fatigue task again as that did in Phase 2.

The actual force of IMRL (30% MVC) was recorded by a 12-bit data acquisition card (USB-6008, National Instruments, USA) in Phases 1, 2, and 4. The actual force and the target force were shown on an LCD screen for real-time visual feedback to the subject in Phases 2 and 4. Surface EMG signals were recorded from the right flexor digitorum superficialis during Phases 1, 2, and 4. The skin was prepared by abrading and cleaning the recording area with alcohol. sEMG signals were detected by two disposable ECG electrodes (Shanghai LITU Medical Appliances Co., model LT-601, China) with 20 mm interelectrode distance. The electrodes were centered around the 50% point on the line joining the medial epicondyle to the styloid process of the ulna [29]. A groud electrode was attached on the dorsal surface of the wrist. All force signals and sEMG signals were recorded simultaneously by the multichannel physiological recorder apparatus (RM6280, Chengdu Instrumentation Inc.) at a rate of 2000 samples per second. The force and sEMG signals were band-pass filtered within the frequency ranges of 0–30 Hz and 8–500 Hz, respectively. The quality

of the sEMG signal was visually checked before actual recording.

2.3. Data Analysis. Data analysis was performed off line using MATLAB 7.8 (The MathWorks Inc., Natick, USA). Bipolar signals were band-pass filtered using a seven-order elliptic filter (10 Hz–500 Hz). Bipolar sEMG signals of flexor digitorum superficialis during fatigue were divided into several 10 s segments. For each 10 s segment, a 2048-point sEMG epoch was equally divided into four subepochs to estimate ARV and FD. The ARV and FD values obtained from the 4 subepochs were averaged to get the overall estimations of ARV and FD for each 10 s segment.

The ARV of sEMG signal in the time domain is defined as

$$\mathrm{ARV} = \frac{1}{N}\sum_{i=1}^{N}|x_i|, \tag{1}$$

where x_i is the ith sample of the signal and N is the number of the samples in the epoch.

The FD value of a one-dimensional physiological signal is calculated as the change in length of recursively defined self-similar curves with the measurement scale. The length of curve used in computation was the same as described in the study of Arjunan and Kumar [30]. By plotting the logarithm of the average length of curve versus the logarithm of the time interval, the FD is obtained as the slope of the fitted linear line.

The ARV values were normalized by values obtained at 100% MVC contraction because the absolute level of each parameter differed among the subjects. Because the task time was not the same for each subject, we normalized the contraction time by setting the task time as 100%. The task time of each subject was divided into 10 equal segments. The variables were obtained at every 10% time. If there was no measurement value at the resampled point, an interpolated value was calculated from the nearest sampled values. The ARV and FD values were averaged for all the subjects in the same group.

2.4. Statistical Analysis. Statistical analysis was performed with SPSS 13.0 in our study. Normality of the distributions of ARV and FD values was checked with the Kolmogorov-Smirnov test prior to statistical testing, and the results were positive. The t-test was employed to test if there was a significant difference between the two experimental groups for ARV and FD of prefatigue task at the end of the fatiguing contraction (i.e., 100% of contraction time). The difference between two types of therapies during refatigue task was also assessed by the t-test at each time instant. Changes in ARV and FD over the normalized contraction time were assessed by linear regression analysis. Results were reported as mean and standard deviation (SD) in the text and standard error (SE) in the figures. The level of statistical significance was set at 0.05.

Table 1: Results of linear regression analysis for refatigue task.

sEMG parameter	Group	Slope	P value
ARV	LEDT	0.136	<0.001
	Control	0.227	0.001
FD	LEDT	−0.015	0.085
	Control	−0.04	0.002

3. Results

The average age of participants was 23.7 years (SD ± 1.19). Their average weight and height were 55.6 kg (SD ± 9.38) and 165.5 cm (SD ± 6.70), respectively. For the LEDT group, the average lengths of the prefatigue and refatigue tasks were 815.4 s (SD ± 595.3) and 311.4 s (SD ± 109.5), respectively, and the average lengths of the prefatigue and refatigue tasks for passive rest therapy group were 1000.0 s (SD ± 254.7) and 602.8 s (SD ± 195.8), respectively.

Examples of the sEMG signals recorded from the right flexor digitorum superficialis and the forces generated during the experiment from the two treatment groups are presented in Figure 1. Figures 2 and 3 plot the changes of mean normalized ARV and mean FD along the normalized contraction time, respectively. From Figures 2(a) and 2(c), it can be observed that there are no statistical differences for ARV between the LEDT and control groups at the 100% of the normalized contraction time during prefatigue task ($P > 0.05$). The same observation can be obtained from Figures 3(a) and 3(c) for FD.

The results of linear regression analysis for the refatigue task are summarized in Table 1. The mean ARV value of the two groups increases over contraction time after both therapies as shown in Table 1. Comparing Figure 2(b) with Figure 2(d), the mean ARV values of the LEDT group are significantly smaller than those of the passive rest therapy group. The statistically significant difference between the mean ARV values of the two groups can be found at 10%–50%, 70%–80%, and 100% of the normalized contraction time ($P < 0.05$).

From Figure 3(d), it can be easily observed that the mean FD value decreases over the normalized contraction time for passive rest group, which is confirmed by Table 1 ($P < 0.05$). For active LEDT group, the mean FD value has a trend of decreasing (Figure 3(b)) but not statistically significant ($P = 0.085$ as shown in Table 1). The statistically significant difference between the mean FD values of the two groups can be found at 0% and 20%–100% of the normalized contraction time ($P < 0.05$).

4. Discussion

Unlike biochemical indicators commonly used in previous studies, we attempt to use electrophysiological indicators for assessing the therapeutic effect of LEDT on the recovery of muscle fatigue. The aim of the present study is to verify the effect of LEDT by using two parameters extracted from sEMG: ARV and FD. There was no significant difference between the two groups for both sEMG variables during

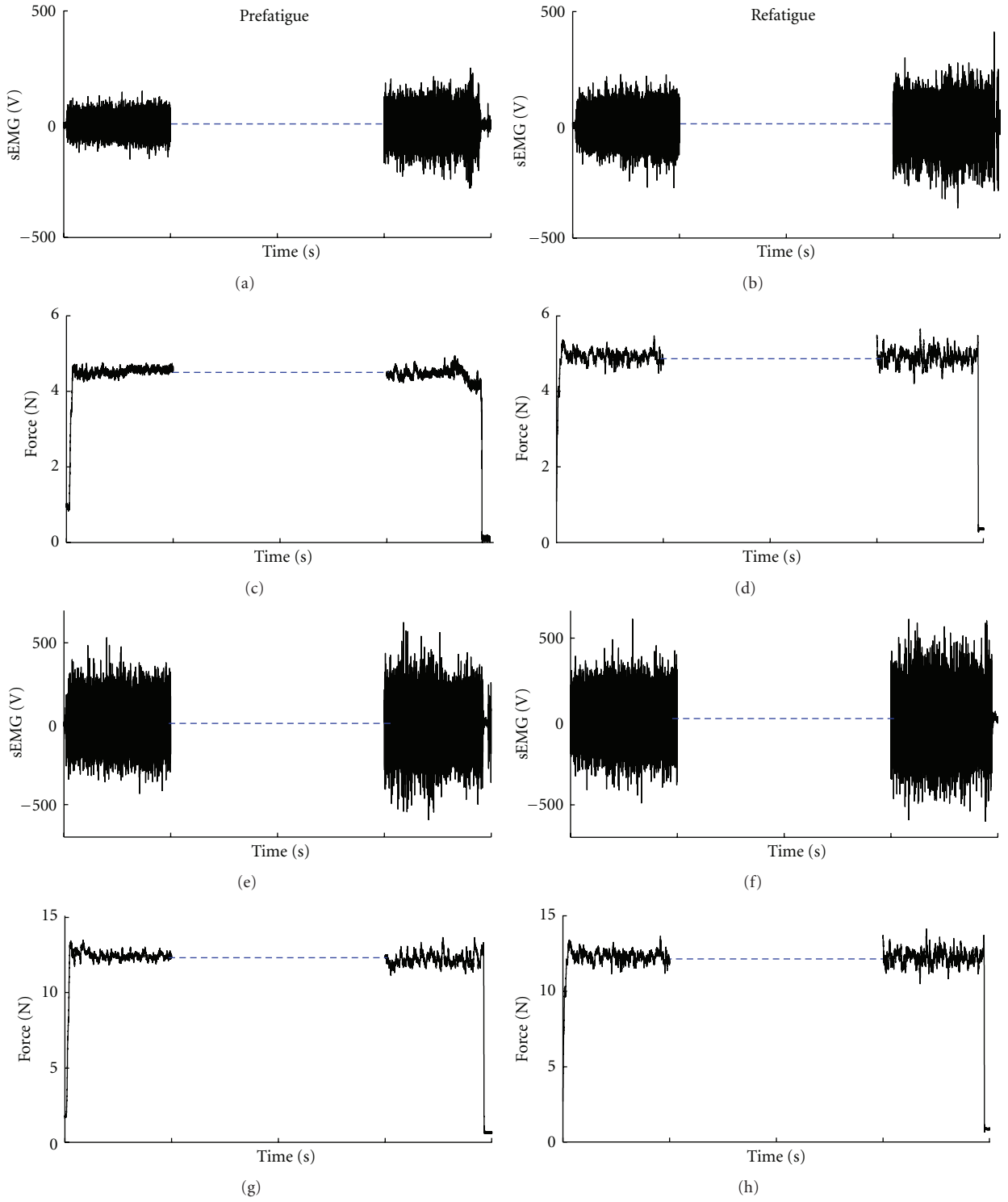

Figure 1: Examples of sEMG signals and the forces recorded during the prefatigue and refatigue tasks until exhaustion for the two types of treatments. (a)–(d) Passive rest therapy, (e)–(h) Active LEDT.

prefatigue task. Therefore, any difference found in ARV and FD between the two groups during the refatigue task cannot be attributed to possible pre-existing uncontrolled differences. Compared with passive rest, irradiation of the flexor digitorum superficialis with active LEDT after muscle fatigue resulted in significantly smaller changes of ARV and FD values along the contraction time, which demonstrates that LEDT is effective at accelerating fatigue recovery.

Compared with passive rest group, smaller increase of the sEMG ARV value along the contraction time was observed

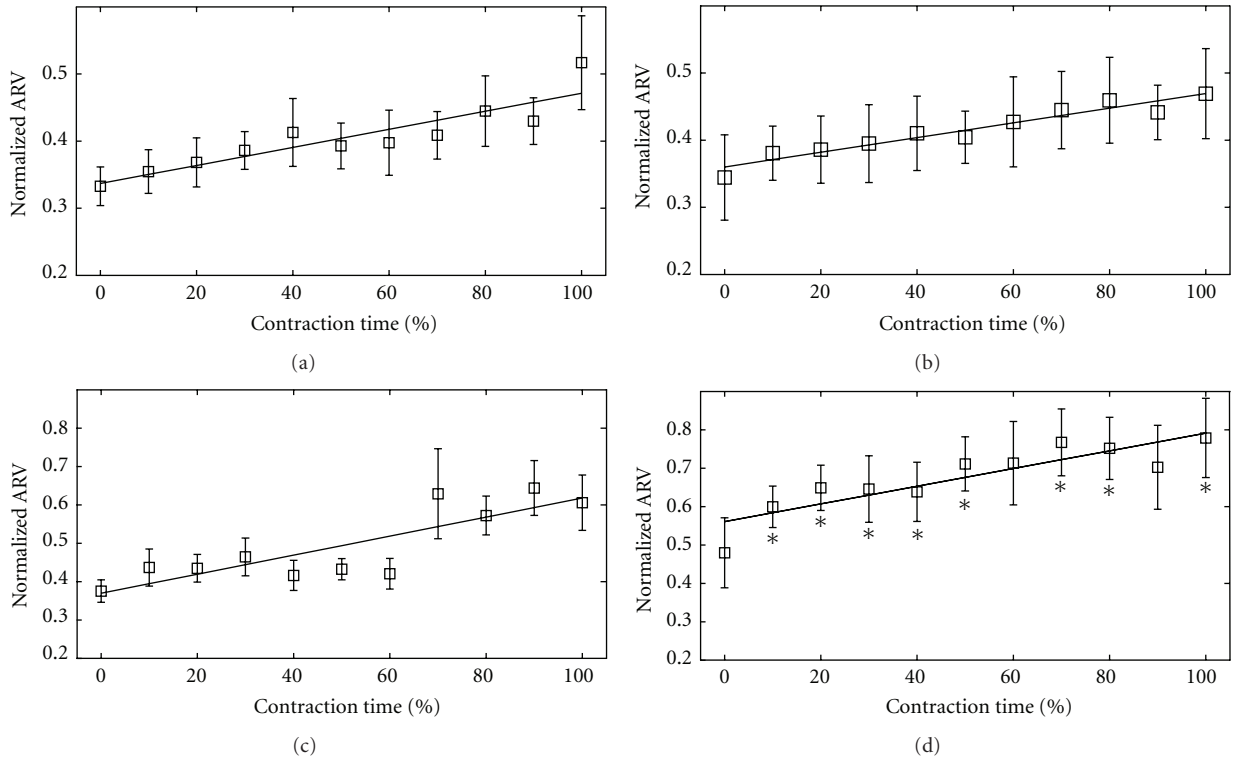

Figure 2: The changes of the mean normalized ARV (±SE) over the normalized contraction time during the prefatigue (a) and refatigue (b) tasks of the LEDT group and the prefatigue (c) and refatigue (d) tasks of the passive rest group. The symbol "∗" indicates that the difference between the mean normalized ARV values of the two groups in the corresponding normalized contraction time is statistically significant.

in LEDT group, indicating that prefatigued muscle tends to return to its initial unfatigue state faster after LEDT. The sEMG ARV reflects the total potential of activating motor units during muscle contraction. Thus, increased ARV value under sustained contraction is mainly a consequence of the recruitment of additional motor units and the decrease of conduction velocity [31]. Hence, if muscle function did not recover completely from prefatigue status, it might need to recruit more new motor units to maintain the desired force, which results in larger and faster increase of sEMG ARV. Previous studies have reported that sEMG amplitude can return to their initial status from fatigue status after appropriate rest [32, 33]. However, 20 min recovery is not enough to enable the flexor digitorum superficialis to fully recover after long fatiguing contraction at low force level [34]. Therefore, the difference of the ARV values between the two groups in our study suggests that LEDT certainly has effect on fatigue recovery and refatigue development.

It can also be observed that although the ARV value increases along the contraction time, it never exceeds 40%–60% of the maximal level for the active LEDT group and 70%–90% of the maximal level for the passive rest group (Figure 2). Moreover, the ARV value at 100% of contraction time is group dependent ($P < 0.05$). Previous studies found that the central fatigue occurred inevitably at lower contraction intensities when muscle fatigue was induced by means of sustained, submaximal isometric contractions of limb and hand muscles [35]. Recent studies also found deficit in average EMG in hand and limb muscles of subjects performing submaximal contractions, which was inversely related to contraction intensity, with much larger deficits in the low-intensity task [36]. In our study, we observed that the LEDT group has smaller sEMG deficits than the control group, suggesting the inhibiting effect of LEDT on driving motor neurons.

Next, significant decrease of FD value over contraction time was observed in the passive rest group in our study. The FD of sEMG signal can be used to quantify the complexity of motor unit recruitment patterns [25, 27]. The decrease in discharge rate of motor unit as well as the increase in duration of motor unit action potentials [37] and the level of synchronism of motor units [38] would account for the decrease of FD during the refatigue task as an adaptation to muscle fatigue. When the task muscle without recovering completely from fatigue status was required to work again, the larger changes of the three aforementioned factors would lead to distinct reduction of FD over contraction time. Many studies reported that the power spectrum of sEMG showed an increased median frequency during recovery [39], which is the opposite process with the development of muscle fatigue. This means that the change of FD for the LEDT group should be smaller than that of the passive rest group, which is in accordance with our results. Moreover, the differences between the two treatment groups occur at all instants except for 10% contraction time, which is another indication of the LEDT effect on skeletal muscle fatigue recovery.

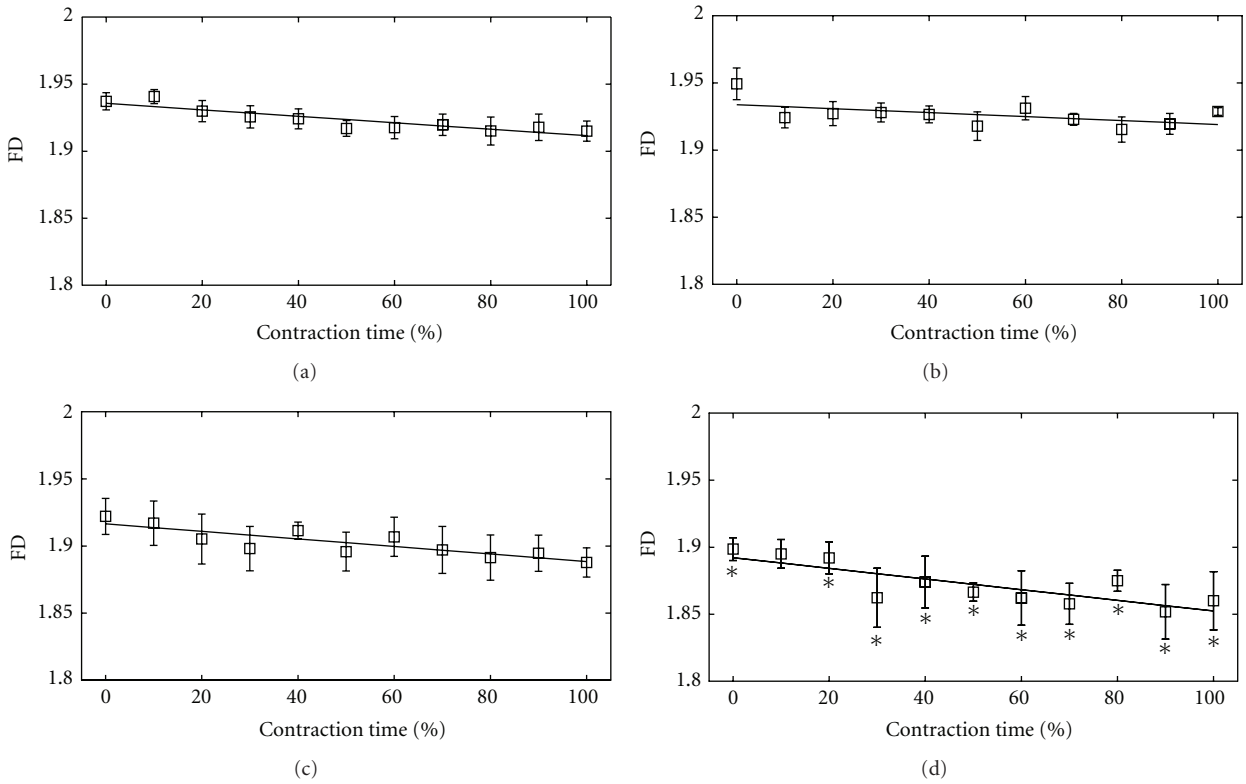

Figure 3: The changes of mean FD (±SE) over the normalized contraction time during the prefatigue (a) and refatigue (b) tasks of the LEDT group and the prefatigue (c) and refatigue (d) tasks of the passive rest group. The symbol "∗" indicates that the difference between the mean FD values of the two groups in the corresponding normalized contraction time is statistically significant.

In addition, it can be observed that the two sEMG parameters show difference in the time instances to be statistically significant different between the two groups. One possible explanation is that the two parameters characterize muscle fatigue from a couple of different perspectives. Compared with FD, ARV is an indicator of sEMG amplitude in the time domain, which is more sensitive to peripheral fatigue [28]. FD is the most promising index of central fatigue and mainly affected by the level of motor unit synchronization and weakly affected by either conduction velocity or fat layer thickness [25, 28]. However, the lack of consistency of EMG amplitude is a common problem to many electromyographic studies. Therefore, it was suggested that myoelectric manifestations of fatigue could be better described by two parameters sensitive to central and peripheral fatigue, respectively [28].

A recent study found that LEDT administrated before exercise could cause a slight delay in the development of skeletal muscle fatigue, decrease blood lactate levels, and inhibit the release of CK and CRP [9]. An other study has also found that LEDT has potential to improve short-term postexercise recovery by inhibiting postexercise increase in blood lactate level and CK activity [10]. Although the exact working mechanism of LEDT remains unknown, some thought that this positive effect might be due to the improved peripheral microcirculation [20], increment in mitochondrial capacity [17, 18], reduced oxidative stress [15], and decreased reactive oxygen species [16] after laser treatment. These changes could improve the muscle fatigue recovery at cellular level [34] and thus affect the physiologic properties of fatigued muscles. If complete blood perfusion is allowed, the metabolic products occurred during muscle fatigue are rapidly washed out so that the muscle fiber membrane function [40] and sEMG spectral content [41] almost completely recover after 5 min rest. Thus, these positive results of LEDT or LLLT indirectly support our findings, suggesting that ARV and FD can be served as valid parameters to investigate the changes of muscle function induced by LLLT or LEDT.

There are several limitations in our study. We investigated the effects of a commercially available LEDT device with red wavelength on muscle fatigue recovery by means of noninvasive sEMG analysis and the preliminary results were encouraging. However, the exact mechanism of how LEDT promotes short-term fatigue recovery cannot be revealed in our study. We also observed that the trend of ARV and FD for one subject was opposite to others, which might be due to the architectural and functional complexity of flexor digitorum superficialis [42] and spatial-dependence center strategy to cope with fatigue [43]. Due to the small sample size, the preliminary results obtained in our study need to be examined with a large-scale study by using both biochemical marks and sEMG parameters.

5. Conclusion

The aim of this study is to use the electrophysiological parameters extracted from sEMG signals instead of biochemical indicators for assessing the effect of light therapies on muscle fatigue recovery. Two electrophysiological parameters used in our experiments, ARV and FD, are sensitive to peripheral and central fatigue, respectively. Our experimental results showed that active LEDT induced smaller increasing rate of ARV and decreasing rate of FD than passive rest over sustained contraction time during the refatigue task, which suggests that active LEDT recovers the muscle fatigue faster than passive rest. In the future, we will conduct a larger-scale study involving more subjects and search for other useful electrophysiological parameters.

Acknowledgments

This work was supported by the National Natural Foundation of China (no. 30770546, 30970758), the Fundamental Research Funds for the Central Universities (no. 10231116), Chongqing Natural Sciences Foundation (no. 2010AB5087, 2010AA5049) and the Third Stage of "211 Project" of Innovation Talent Training Project in Chongqing University (no. S-09104). The authors would like to thank all the volunteers in this study.

References

[1] E. Verburg, H. M. S. Thorud, M. Eriksen, N. K. Vøllestad, and O. M. Sejersted, "Muscle contractile properties during intermittent nontetanic stimulation in rat skeletal muscle," *American Journal of Physiology-Regulatory Integrative and Comparative Physiology*, vol. 281, no. 6, pp. R1952–R1965, 2001.

[2] M. Cifrek, V. Medved, S. Tonković, and S. Ostojić, "Surface EMG based muscle fatigue evaluation in biomechanics," *Clinical Biomechanics*, vol. 24, no. 4, pp. 327–340, 2009.

[3] F. Billaut, F. A. Basset, M. Giacomoni, F. Lemaître, V. Tricot, and G. Falgairette, "Effect of high-intensity intermittent cycling sprints on neuromuscular activity," *International Journal of Sports Medicine*, vol. 27, no. 1, pp. 25–30, 2006.

[4] M. Utsunomiya, K. Nitta, H. Sawagichi et al., "Changes in blood flow, temperature and muscle endurance in association with Cryotherapy," *Journal of Physical Therapy Science*, vol. 22, no. 1, pp. 43–49, 2010.

[5] V. Perciavalle, M. Coco, and L. Gurrisi, "Alternating hot and cold water immersion accelerates blood lactate decrease after maximal anaerobic exercise," *Acta Medica Mediterranea*, vol. 24, no. 1, pp. 19–21, 2008.

[6] N. Babault, C. Cometti, and N. A. Maffiuletti, "Does electrical stimulation enhance post-exercise performance recovery?" *European Journal of Applied Physiology*, vol. 111, no. 1, pp. 2501–2507, 2011.

[7] A. Dutta, K. Ray, V. K. Singh, P. Vats, S. N. Singh, and S. B. Singh, "L-carnitine supplementation attenuates intermittent hypoxia-induced oxidative stress and delays muscle fatigue in rats," *Experimental Physiology*, vol. 93, no. 10, pp. 1139–1146, 2008.

[8] E. C. Pinto Leal Jr., R. A. Brandao Lopes-Martins, L. Frigo et al., "Effects of low-level laser therapy (LLLT) in the development of exercise-induced skeletal muscle fatigue and changes in biochemical markers related to postexercise recovery," *Journal of Orthopaedic & Sports Physical Therapy*, vol. 40, no. 8, pp. 524–532, 2010.

[9] E. C. P. Leal Junior, A. B. Lopes-Martins, B. M. Baroni et al., "Comparison between single-diode low-level laser therapy (LLLT) and LED multi-diode (cluster) therapy (LEDT) applications before high-intensity exercise," *Photomedicine and Laser Surgery*, vol. 27, no. 4, pp. 617–623, 2009.

[10] E. C. Leal Junior, V. de Godoi, J. L. Mancalossi et al., "Comparison between cold water immersion therapy (CWIT) and light emitting diode therapy (LEDT) in short-term skeletal muscle recovery after high-intensity exercise in athletes-preliminary results," *Lasers in Medical Science*, vol. 26, no. 4, pp. 493–501, 2011.

[11] R. Á. B. Lopes-Martins, R. L. Marcos, P. S. Leonardo et al., "Effect of low-level laser (Ga-Al-As 655 nm) on skeletal muscle fatigue induced by electrical stimulation in rats," *Journal of Applied Physiology*, vol. 101, no. 1, pp. 283–288, 2006.

[12] B. M. Baroni, E. C. P. Leal Junior, T. De Marchi, A. L. Lopes, M. Salvador, and M. A. Vaz, "Low level laser therapy before eccentric exercise reduces muscle damage markers in humans," *European Journal of Applied Physiology*, vol. 110, no. 4, pp. 789–796, 2010.

[13] E. C. P. Leal Junior, R. Á. B. Lopes-Martins, B. M. Baroni et al., "Effect of 830 nm low-level laser therapy applied before high-intensity exercises on skeletal muscle recovery in athletes," *Lasers in Medical Science*, vol. 24, no. 6, pp. 857–863, 2009.

[14] E. C. P. Leal Junior, R. Á. B. Lopes-Martins, P. De Almeida, L. Ramos, V. V. Iversen, and J. M. Bjordal, "Effect of low-level laser therapy (GaAs 904 nm) in skeletal muscle fatigue and biochemical markers of muscle damage in rats," *European Journal of Applied Physiology*, vol. 108, no. 6, pp. 1083–1088, 2010.

[15] L. I. Fillipin, J. L. Mauriz, K. Vedovelli et al., "Low-level laser therapy (LLLT) prevents oxidative stress and reduces fibrosis in rat traumatized Achilles tendon," *Lasers in Surgery and Medicine*, vol. 37, no. 4, pp. 293–300, 2005.

[16] Y. Fujimaki, T. Shimoyama, Q. Liu, T. Umeda, S. Nakaji, and K. Sugawara, "Low-level laser irradiation attenuates production of reactive oxygen species by human neutrophils," *Journal of Clinical Laser Medicine and Surgery*, vol. 21, no. 3, pp. 165–170, 2003.

[17] T. Karu, "Mitochondrial mechanisms of photobiomodulation in context of new data about multiple roles of ATP," *Photomedicine and Laser Surgery*, vol. 28, no. 2, pp. 159–160, 2010.

[18] P. C. L. Silveira, E. L. Streck, and R. A. Pinho, "Evaluation of mitochondrial respiratory chain activity in wound healing by low-level laser therapy," *Journal of Photochemistry and Photobiology B*, vol. 86, no. 3, pp. 279–282, 2007.

[19] P. C. L. Silveira, L. A. D. Silva, D. B. Fraga, T. P. Freitas, E. L. Streck, and R. Pinho, "Evaluation of mitochondrial respiratory chain activity in muscle healing by low-level laser therapy," *Journal of Photochemistry and Photobiology B*, vol. 95, no. 2, pp. 89–92, 2009.

[20] F. R. M. Ihsan, "Low-level laser therapy accelerates collateral circulation and enhances microcirculation," *Photomedicine and Laser Surgery*, vol. 23, no. 3, pp. 289–294, 2005.

[21] E. C. P. Leal, R. Á. B. Lopes-Martins, R. P. Rossi et al., "Effect of cluster multi-diode Light Emitting Diode Therapy (LEDT) on exercise-induced skeletal muscle fatigue and skeletal muscle recovery in humans," *Lasers in Surgery and Medicine*, vol. 41, no. 8, pp. 572–577, 2009.

[22] B. M. Baroni, E. C. P. Leal, J. M. Geremia, F. Diefenthaeler, and M. A. Vaz, "Effect of light-emitting diodes therapy (LEDT) on knee extensor muscle fatigue," *Photomedicine and Laser Surgery*, vol. 28, no. 5, pp. 653–658, 2010.

[23] Y. Zhou, Y. Li, and R. Wang, "Evaluation of exercise-induced muscle damage by surface electromyography," *Journal of Electromyography and Kinesiology*, vol. 21, no. 2, pp. 356–362, 2011.

[24] S. Kumar and Y. Narayan, "Spectral parameters of trunk muscles during fatiguing isometric axial rotation in neutral posture," *Journal of Electromyography and Kinesiology*, vol. 8, no. 4, pp. 257–267, 1998.

[25] A. Troiano, F. Naddeo, E. Sosso, G. Camarota, R. Merletti, and L. Mesin, "Assessment of force and fatigue in isometric contractions of the upper trapezius muscle by surface EMG signal and perceived exertion scale," *Gait and Posture*, vol. 28, no. 2, pp. 179–186, 2008.

[26] L. A. C. Kallenberg and H. J. Hermens, "Behaviour of a surface EMG based measure for motor control: motor unit action potential rate in relation to force and muscle fatigue," *Journal of Electromyography and Kinesiology*, vol. 18, no. 5, pp. 780–788, 2008.

[27] Z. Xu and S. Xiao, "Fractal dimension of surface EMG and its determinants," in *Proceedings of the 1997 19th Annual International Conference of the IEEE Engineering in Medicine and Biology Society*, pp. 1570–1573, November 1997.

[28] L. Mesin, C. Cescon, M. Gazzoni, R. Merletti, and A. Rainoldi, "A bi-dimensional index for the selective assessment of myoelectric manifestations of peripheral and central muscle fatigue," *Journal of Electromyography and Kinesiology*, vol. 19, no. 5, pp. 851–863, 2009.

[29] S. Kattla and M. M. Lowery, "Fatigue related changes in electromyographic coherence between synergistic hand muscles," *Experimental Brain Research*, vol. 202, no. 1, pp. 89–99, 2010.

[30] S. P. Arjunan and D. K. Kumar, "Decoding subtle forearm flexions using fractal features of surface electromyogram from single and multiple sensors," *Journal of NeuroEngineering and Rehabilitation*, vol. 7, no. 1, article no. 53, 2010.

[31] D. Farina, F. Leclerc, L. Arendt-Nielsen, O. Buttelli, and P. Madeleine, "The change in spatial distribution of upper trapezius muscle activity is correlated to contraction duration," *Journal of Electromyography and Kinesiology*, vol. 18, no. 1, pp. 16–25, 2008.

[32] F. Danion, S. Li, V. M. Zatsiorsky, and M. L. Latash, "Relations between surface EMG of extrinsic flexors and individual finger forces support the notion of muscle compartments," *European Journal of Applied Physiology*, vol. 88, no. 1-2, pp. 185–188, 2002.

[33] C. Larivière, D. Gravel, A. B. Arsenault, D. Gagnon, and P. Loisel, "Muscle recovery from a short fatigue test and consequence on the reliability of EMG indices of fatigue," *European Journal of Applied Physiology*, vol. 89, no. 2, pp. 171–176, 2003.

[34] D. G. Allen, G. D. Lamb, and H. Westerblad, "Skeletal muscle fatigue: cellular mechanisms," *Physiological Reviews*, vol. 88, no. 1, pp. 287–332, 2008.

[35] T. D. Eichelberger and M. Bilodeau, "Central fatigue of the first dorsal interosseous muscle during low-force and high-force sustained submaximal contractions," *Clinical Physiology and Functional Imaging*, vol. 27, no. 5, pp. 298–304, 2007.

[36] K. Schmitt, C. DelloRusso, and R. F. Fregosi, "Force-EMG changes during sustained contractions of a human upper airway muscle," *Journal of Neurophysiology*, vol. 101, no. 2, pp. 558–568, 2009.

[37] J. W. Chung, C. Kim, and W. D. McCall, "Effect of sustained contraction on motor unit action potentials and EMG power spectrum of human masticatory muscles," *Journal of Dental Research*, vol. 81, no. 9, pp. 646–649, 2002.

[38] R. Merletti and S. Roy, "Myoelectric and mechanical manifestations of muscle fatigue in voluntary contractions," *Journal of Orthopaedic and Sports Physical Therapy*, vol. 24, no. 6, pp. 342–353, 1996.

[39] K. S. Sunnerhagen, U. Carlsson, A. Sandberg, E. Stålberg, M. Hedberg, and G. Grimby, "Electrophysiologic evaluation of muscle fatigue development and recovery in late polio," *Archives of Physical Medicine and Rehabilitation*, vol. 81, no. 6, pp. 770–776, 2000.

[40] R. G. Miller, D. Giannini, H. S. Milner-Brown et al., "Effects of fatiguing exercise on high-energy phosphates, force, and EMG: evidence for three phases of recovery," *Muscle and Nerve*, vol. 10, no. 9, pp. 810–821, 1987.

[41] L. S. Krivickas, S. F. Nadler, M. R. Davies, G. F. Petroski, and J. H. Feinberg, "Spectral analysis during fatigue: surface and fine wire electrode comparison," *American Journal of Physical Medicine and Rehabilitation*, vol. 75, no. 1, pp. 15–20, 1996.

[42] T. L. McIsaac and A. J. Fuglevand, "Motor-unit synchrony within and across compartments of the human flexor digitorum superficialis," *Journal of Neurophysiology*, vol. 97, no. 1, pp. 550–556, 2007.

[43] D. Falla and D. Farina, "Non-uniform adaptation of motor unit discharge rates during sustained static contraction of the upper trapezius muscle," *Experimental Brain Research*, vol. 191, no. 3, pp. 363–370, 2008.

Hindawi Publishing Corporation
International Journal of Photoenergy
Volume 2012, Article ID 848401, 5 pages
doi:10.1155/2012/848401

Research Article

TiO_2 and N-Doped TiO_2 Induced Photocatalytic Inactivation of *Staphylococcus aureus* under 405 nm LED Blue Light Irradiation

Hongfei Chen,[1] Zhong Xie,[1,2] Xiujuan Jin,[2] Chao Luo,[3] Chao You,[1,2] Ying Tang,[2] Di Chen,[2] Zhengjia Li,[2] and Xiaohong Fan[1,2]

[1] *Wuhan National Laboratory for Optoelectronics, Huazhong University of Science and Technology, Hubei, WuHan 430074, China*
[2] *College of Optoelectronics Science and Engineering, Huazhong University of Science and Technology, Hubei, WuHan 430074, China*
[3] *School of Life Science and Technology, Huazhong University of Science and Technology, Hubei, WuHan 430074, China*

Correspondence should be addressed to Xiaohong Fan, xhfan@mail.hust.edu.cn

Received 17 February 2012; Revised 8 May 2012; Accepted 17 May 2012

Academic Editor: Timon Cheng-Yi Liu

Irradiation source has been a serious impediment to induce photocatalytic bacterial inactivation which was taken as an advanced indoor air purification technique. Here we reported the synergistic effects of 405 nm LED light and TiO_2 photocatalyst in inactivation process of *Staphylococcus aureus* (*S. aureus*). In this work, TiO_2 and N-doped TiO_2 particles were, respectively, suspended into the nutrient broth suspension with *S. aureus*. Then, the mixed system was exposed to a 405 nm LED light source with energy density of about 0.2 W/cm^2 for 3 hours. Irradiated suspension was then scanned by UV-vis spectrophotometer for bacteria survive/death rate statistics. Subsequently, the inactivation efficiency was calculated based on the difference of the absorption optical density between experimental and controlled suspensions. Results showed that both TiO_2 and N-doped TiO_2 particles exhibit potential bacterial inactivation effects under similar experimental conditions. Specifically, N-doped TiO_2 with the concentration of 5 g/L displayed enhanced inactivation efficiency against *S. aureus* under 405 nm LED light irradiation. Thus, it is a promising indoor air purification technique by using N-doped TiO_2 particles under the LED light irradiation.

1. Introduction

More and more attention has been paid to indoor air quality which is very important to human health [1]. Microbial contamination, especially from the superbug *S. aureus*, is very dangerous. Usually, *S. aureus* can cause local skin infections and even more serious infections in wounds, bones, lungs, and blood and *S.aureus* can be undetected and carried quite harmlessly until the one suffers [2]. Moreover, superbug *S. aureus* is even resistant to all commonly used antibiotics and infects people in both community and hospitals [3, 4]. As an important defensive strategy, indoor air purifying becomes increasingly popular since its inception more than a decade ago. Several different processes have been used to purify the indoor air, such as ultraviolet germicidal irradiation, purification traps filter, porous material-activated carbon adsorbing, polarized-media electronic, photocatalytic oxidation, ionizer purifiers, liquid ioniser purifiers, ozone generators, and titanium dioxide (TiO_2) technology [5]. Among these processes, heterogeneous photocatalytic oxidation (PCO) is the most promising air purifying technique in outdoor conditions using TiO_2 particles activated under UV light irradiation. However, due to the shortage of UV light irradiation in indoor condition, there is still no effective indoor PCO air purifier in our daily life at present.

Chung et al. have reported photocatalytic inactivation of *S.aureus* with various light sources on titanium dioxide thin film. They found that the bactericidal effect on *S. aureus* under UV or fluorescent light irradiation was better than that under visible light irradiation [6]. The inactivation effect of modified TiO_2 sample activated under visible light (Vis) or LED light irradiation has been intensely studied recently. The valence band of TiO_2 can be changed by different dopants and the spectral response of TiO_2 can be extended from the UV into the visible light region [7–10]. Up to now, the visible-light-induced photocatalytic inactivation of human pathogens by modified TiO_2 has been studied deeply by many research groups around the world. Wong et al. have reported photocatalytic inactivation of *Escherichia coli* cell

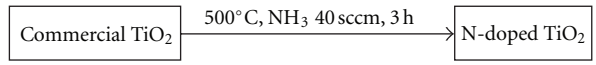

Figure 1: The manufacturing process of N-doped TiO_2.

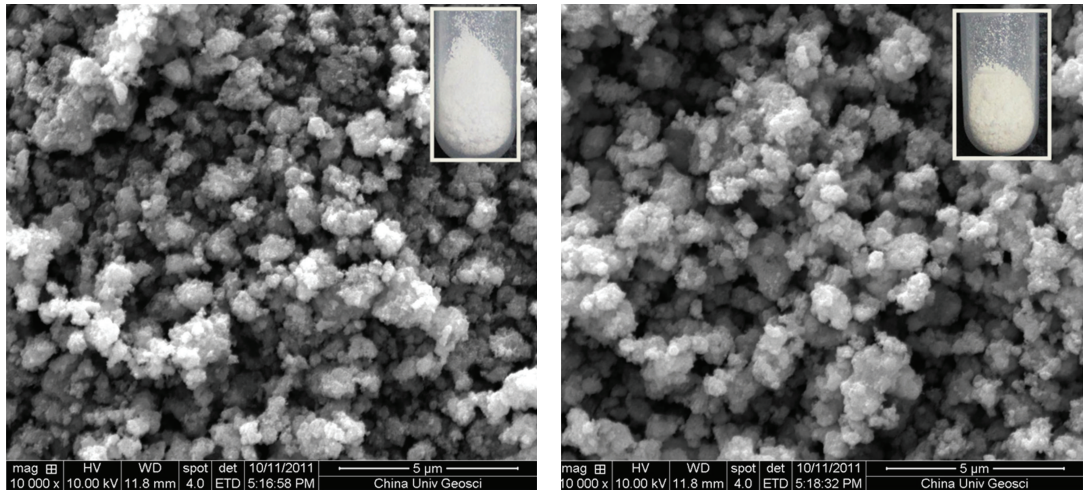

(a) (b)

Figure 2: SEM image of commercial TiO_2 (a) and N-doped TiO_2 (b) samples.

using N-doped TiO_2 under an incandescent lamp [11]. However, incandescent lamp, with limited working time and low electrooptical conversion efficiency, produces a continuous spectrum of light from near ultraviolet to deep into the infrared. Enwemeka et al. have reported the photo-destroys methicillin-resistant *Staphylococcus aureus* (MRSA) *in vitro* using visible 405 nm LED [12]. Those reports directed our attentions to LED light, which may enhance the catalytic efficiency of TiO_2 and has many unique advantages, such as narrow bandwidth, long life span, incredible reliability, and high electrooptical conversion efficiency over incandescent lamp and other visible light source. In addition, bactericidal effect of 405 nm light exposure have been evidenced in many other studies [13, 14], recently.

In this work, we demonstrated the photocatalytic inactivation of the target organisms, *S. aureus* in nutrient broth suspension, using commercial and modified TiO_2 nanoparticles activated under 405 nm LED blue light. Experimental results confirmed that modified TiO_2 nanoparticles activated under 405 nm LED blue light is an ideal indoor purification method.

2. Experimental

2.1. Preparation of N-Doped TiO_2 Nanoparticles and Experimental Suspensions. N-doped TiO_2 was prepared from the vapor phase process (illustrated in Figure 1), using commercial anatase TiO_2 nanoparticles with diameter of 60 nm as the precursor.

Yellow colony of *S. aureus* on a nutrient broth agar plate, cultured at 37°C for 24 hours, was diluted into 500 mL nutrient broth suspension and broken up into 50 equal bacteria suspension samples. Those samples were divided into five groups equally. Then certain weight of TiO_2 or N-doped TiO_2 nanoparticles will be suspended into the samples of each group. At last, we obtained five different groups with concentration of 1 g/L TiO_2, 5 g/L TiO_2, 1 g/L N-TiO_2, 5 g/L N-TiO_2 and 0 g/L, there were 10 samples in each group. Nutrient broth suspensions with the same concentration of bacteria in the absence of photocatalyst were prepared for contrast experiments.

2.2. Photocatalytic Inactivation Experiment. The obtained suspensions with various concentrations of suspended nanoparticles were transferred into cell culture plate for the photocatalytic inactivation experiments. Cell culture plate was directly exposed to the 405 nm LED light, which was vertically fastened right above and cooled with circulating water. The power density of the LED light irradiation was about 0.2 W/cm^2. After 3 hours exposure to LED light, the suspensions were collected and characterized by UV-vis spectrophotometer. The absorption optical density of each sample was measured at wavelength region from 240 nm to 800 nm, while the evaluation of activities of TiO_2 and N-doped TiO_2 at inactivation of *S. aureus* was the decrease in OD_{600} values. In practice, nutrient broth suspensions with the same concentration of photocatalyst in the absence of bacteria were prepared for baseline liquid to eliminate the influence of light scattering by nanoparticles suspending in experimental suspensions.

2.3. Characterization. The obtained samples were characterized by scanning electron microscopy (SEM) and UV-vis spectrophotometer (UV-2500, Shimadzu). As shown in Figure 2, commercial TiO_2 powder is white while N-doped

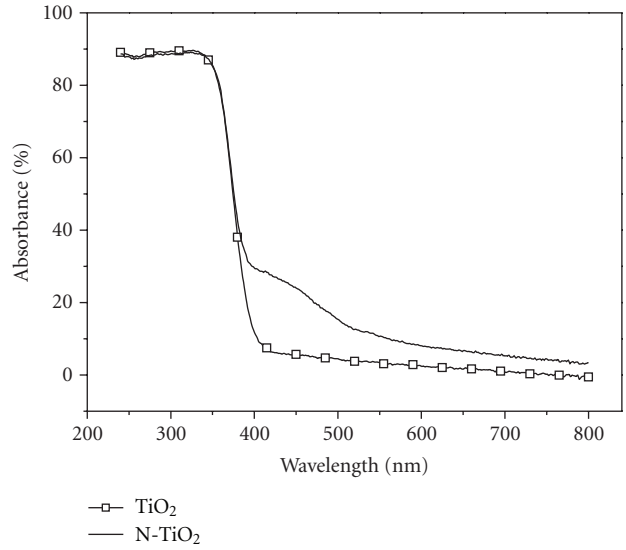

Figure 3: UV-vis absorbance spectra of commercial TiO_2 and N-doped TiO_2 samples.

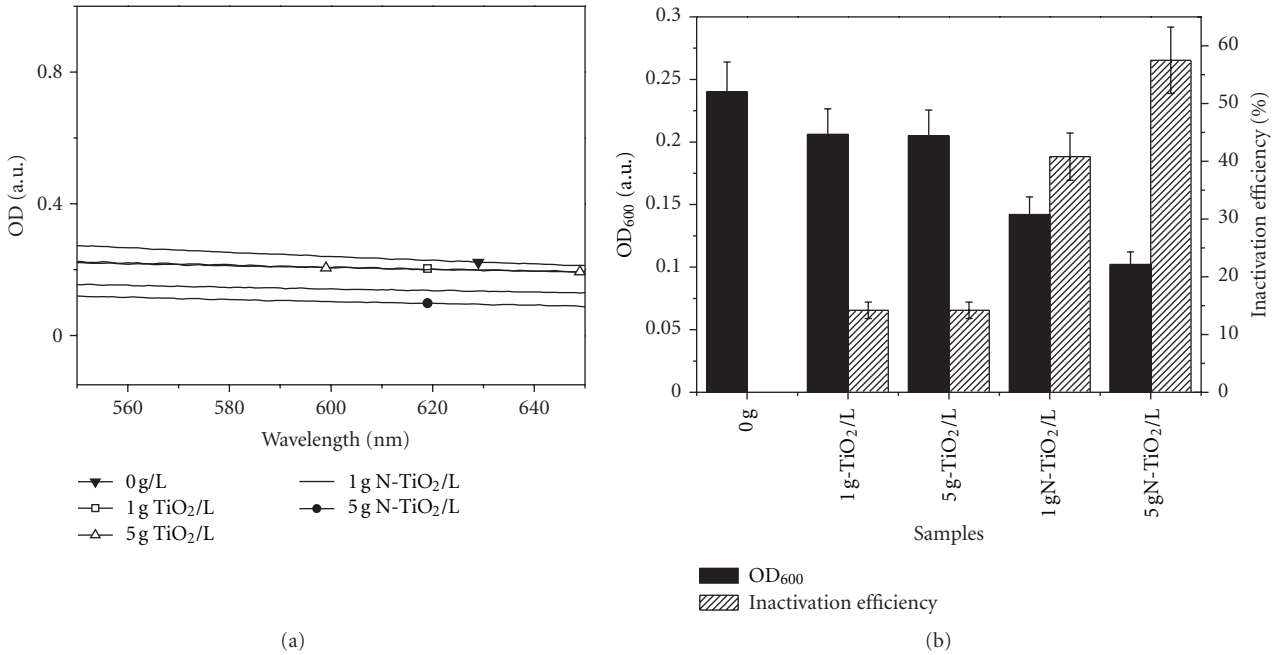

Figure 4: Inactivation efficiency of commercial TiO_2 and N-doped TiO_2.

TiO_2 power has a pale yellow color, and both samples are anatase crystalline phase.

The UV-vis absorption spectra of two samples were shown in Figure 3. Clearly, pure TiO_2 particle showed only a strong absorption in UV light region, while the absorption of N-doped TiO_2 particle extended into visible light region.

3. Results and Discussions

3.1. Results. The absorption optical density of experimental and control suspensions were measured in the wavelength ranged from 550 nm to 650 nm and showed in Figure 4(a). The OD_{600} values of suspensions were the evaluation of activities of commercial TiO_2 and N-doped TiO_2 photocatalyst in inactivation of bacteria. Depended upon the principle of nephelometery [15], the photocatalytic inactivation efficiency (sterilization efficiency) is determined by following formula.

$$R = \frac{A_0 - A_x}{A_0} * 100\%, \quad (1)$$

where R is the photocatalytic inactivation efficiency, A_0 is the OD_{600} value of the control suspension in absence of photocatalyst, and A_x is the OD_{600} of each experimental suspension with photocatalyst. Here in order to eliminate the influencing of light scattering of nanoparticles, A_x was the

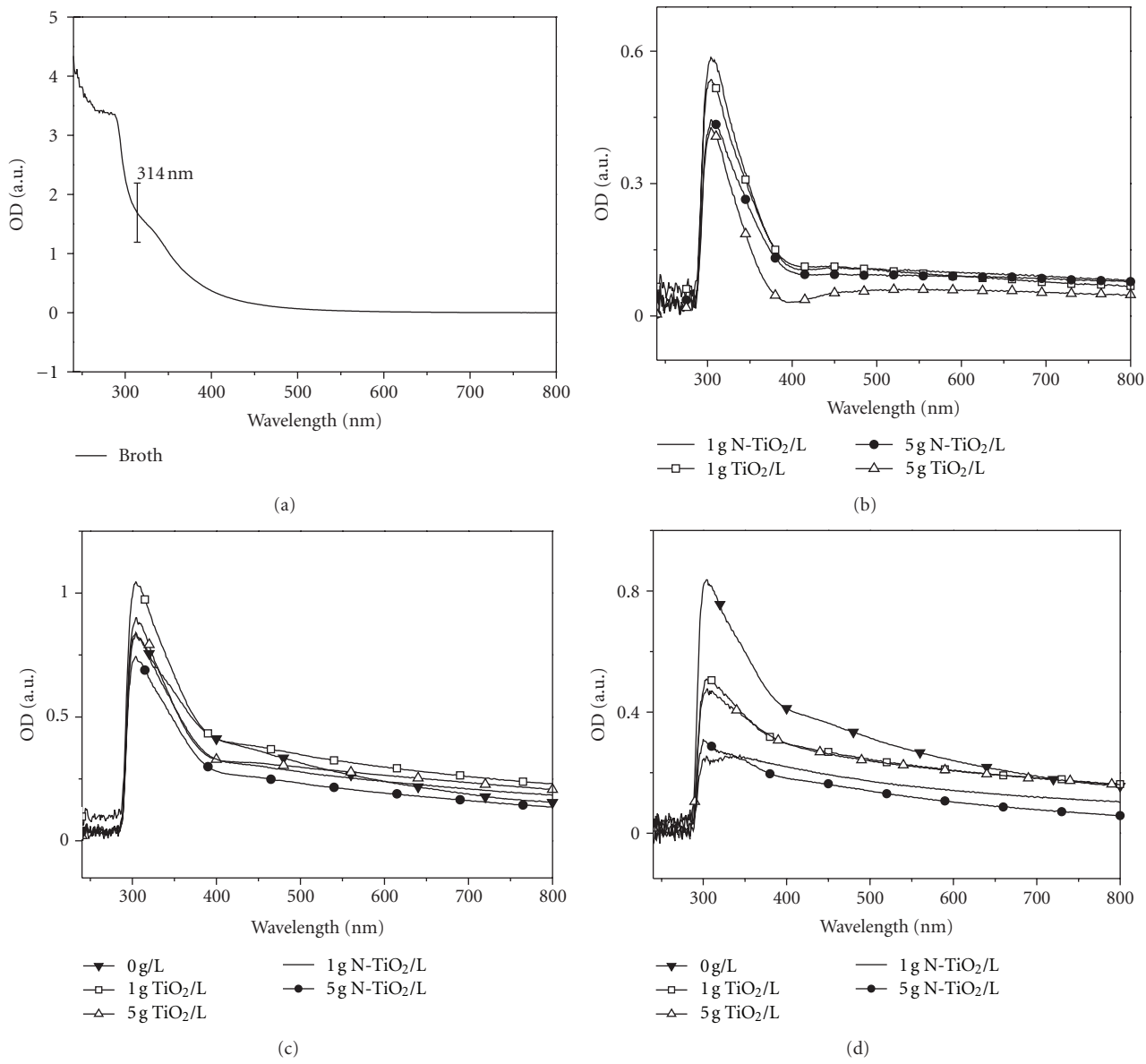

Figure 5: The optical density of nutrient broth (a), nutrient with photocatalyst (b), and experiment suspensions (c) exposed to 405 nm LED (0.2 W/cm^2) for 3 hours (employed bare nutrient broth for reference axis), (d) is the difference value between (b) and (c).

difference between the OD_{600} values of each experimental sample and the nutrient broth suspension with suspended nanoparticles at corresponding concentration but in absence of bacteria.

The inactivation efficiency of both commercial TiO_2 and N-doped TiO_2 at different concentrations was shown in Figure 4(b) ($P < 0.05$). According to Figure 4(b), N-doped TiO_2 nanoparticles suspended at 5 g/L exhibits the best inactivation effect, with an inactivation efficiency of about 57.5%, on *S. aureus* under 405 nm LED light irradiation for 3 hours in this work. It's visible that the efficiency was enhanced as the concentration changed from 1 g/L (about 40.8%) to 5g/L (about 57.5%). Refer to Figure 4(b), the commercial TiO_2 nanoparticles also exhibit inactivation effect on *S. aureus* but with a limited and much lower inactivation efficiency of about 14.2% than that of N-doped TiO_2 under the same experiment condition. It is due to the different absorption of TiO_2 and N-doped TiO_2 nanoparticles at wavelength 405 nm, where TiO_2 has no absorption but N-doped TiO_2 has (see Figure 3). Although 5 g/L N-doped TiO_2 displayed a very good inactivation effect with an efficiency of about 57.5% in this case, it is still far from the requirement of application in air-purifying and needed to be improved. Nevertheless, energy-efficient LED light source photocatalysis is promising.

3.2. Discussions. The absorption optical density of nutrient broth (Figure 5(a)), nutrient broth suspension with only photocatalyst (Figure 5(b)), and nutrient broth bacteria suspensions (Figure 5(c)) measured from 240 nm to 800 nm was illustrated in Figure 5. Figure 5(d) was the difference between the value of photocatalyst suspension with bacteria

(Figure 5(c)) and without bacteria (Figure 5(b)), in order to eliminate the influence of light scattering of nanoparticles in experiment suspension. According to Figures 5(a)–5(d), all nutrient broth suspension measured showed an absorption peak in 315 nm. The OD value of the nutrient broth suspensions was bigger than 1 even up to 4 at the UV region (refer to Figure 5(a)), which was far beyond the liner region (0–0.4), and both TiO_2 and N-doped nanoparticles have high absorption in UV region (Figure 3). In addition, the nutrient broth was used as the baseline liquid of measurement and there were nanoparticles in the experimental suspension, the high OD value in UV region may influence the measurement accuracy. Thus the OD value in UV region cannot be the evaluation. There were crosses between curves according to Figure 5(c), and the crosses were eliminated in Figure 5(d). Thus, it is necessary to use OD value in Figure 5(d) for inactivation efficiency calculation.

At inactivation of *S. aureus* under 405 nm LED light in our case, the N-doped TiO_2 is much better than TiO_2 but the inactivation efficiency of which is still far from the requirement of application in air-purifying. Although it is feasible to enhance photocatalyst inactivation efficiency of N-doped TiO_2 under 405 nm irradiation by increasing the concentration of photocatalytic, it is wasteful and not environment-friendly to use too much nanoparticles. There is also another way to enhance the photocatalyst inactivation efficiency, which is to increase the N-doped concentration [10]. Of course, there are other factors, such as types of the crystal surfaces [16], types of photocatalytic, and strains of bacteria [17], influencing the inactivation efficiency besides the photocatalytic activity.

4. Conclusions

In summary, we investigated the inactivation effects of pure TiO_2 and N-doped TiO_2 products over *S. aureus* under the irradiation of 405 nm LED light. Under similar conditions, N-doped TiO_2 powder with the increased absorption ability to light shows enhanced activities for inactivation of *S. aureus* than pure TiO_2. Thus, using photocatalytic process with the assistance of LED light is a promising air purification technique in future.

Acknowledgments

The authors gratefully appreciate the help from Professors Di Chen and her group in Wuhan National Laboratory. Also, they thank the Analytical and Testing Center of Huazhong University Science and Technology for the samples measurements.

References

[1] Q. L. Yu and H. J. H. Brouwers, "Indoor air purification using heterogeneous photocatalytic oxidation. Part I: experimental study," *Applied Catalysis*, vol. 92, no. 3-4, pp. 454–461, 2009.

[2] MRSA information for patients[Z], http://www.rcn.org.uk/ipc/.

[3] A. Bogut, M. Kozioł-Montewka, I. Baranowicz et al., "Community-acquired methicillin-resistant *Staphylococcus aureus* (CA-MRSA) in Poland: further evidence for the changing epidemiology of MRSA," *New Microbiologica*, vol. 31, no. 2, pp. 229–234, 2008.

[4] X. X. Ma, T. Ito, C. Tiensasitorn et al., "Novel type of staphylococcal cassette chromosome mec identified in community-acquired methicillin-resistant *Staphylococcus aureus* strains," *Antimicrobial Agents and Chemotherapy*, vol. 46, no. 4, pp. 1147–1152, 2002.

[5] http://en.wikipedia.org/wiki/Air_purifier.

[6] C. J. Chung, H. I. Lin, C. M. Chou et al., "Inactivation of *Staphylococcus aureus* and *Escherichia coli* under various light sources on photocatalytic titanium dioxide thin film," *Surface & Coatings Technology*, vol. 203, no. 8, pp. 1081–1085, 2009.

[7] Slamet, H. W. Nasution, E. Purnama, S. Kosela, and J. Gunlazuardi, "Photocatalytic reduction of CO_2 on copper-doped Titania catalysts prepared by improved-impregnation method," *Catalysis Communications*, vol. 6, no. 5, pp. 313–319, 2005.

[8] F. Peng, Y. Liu, H. J. Wang, H. Yu, and J. Yang, "Synthesis and characterization of novel N-doped TiO_2 photocatalyst with visible light active," *Chinese Journal of Chemical Physics*, vol. 23, no. 4, pp. 437–441, 2010.

[9] C. L. Luu, Q. T. Nguyen, and S. T. Ho, "Synthesis and characterization of Fe-doped TiO_2 photocatalyst by the sol-gel method," *Advances in Natural Sciences*, vol. 2010, Article ID 015008, 5 pages, 2010.

[10] T. M. D. Dang, D. D. Le, V. T. Chau, and M. C. Dang, "Visible-light photocatalytic activity of N/SiO_2-TiO_2 thin films on glass," *Advances in Natural Sciences*, vol. 2010, Article ID 015004, 5 pages, 2010.

[11] M. S. Wong, W. C. Chu, D. S. Sun et al., "Visible-light-induced bactericidal activity of a nitrogen-doped titanium photocatalyst against human pathogens," *Applied and Environmental Microbiology*, vol. 72, no. 9, pp. 6111–6116, 2006.

[12] C. S. Enwemeka, D. Williams, S. Hollosi, D. Yens, and S. K. Enwemeka, "Visible 405 nm SLD light photo-destroys methicillin-resistant *Staphylococcus aureus* (MRSA) *in vitro*," *Lasers in Surgery and Medicine*, vol. 40, no. 10, pp. 734–737, 2008.

[13] J. S. Guffey and J. Wilborn, "*In vitro* bactericidal effects of 405 nm and 470 nm blue light," *Photomedicine and Laser Surgery*, vol. 24, no. 6, pp. 684–688, 2006.

[14] J. S. Guffey and J. Wilborn, "Effects of combined 405 nm and 880 nm light on *Staphylococcus aureus* and *Pseudomonas aeruginosa in vitro*," *Photomedicine and Laser Surgery*, vol. 24, no. 6, pp. 680–683, 2006.

[15] D. Wei, B. X. Wang, K. M. Li, M. Y. Pei, X. L. Li, and G. Z. Wang, "Determination of concentration of anthrax vaccine by spectrophotometry," *Chinese Journal of Biologicals*, vol. 23, no. 8, pp. 894–905, 2010.

[16] S. R. Sousa, P. Moradas-Ferreira, and M. A. Barbosa, "TiO_2 type influences fibronectin adsorption," *Journal of Materials Science*, vol. 16, no. 12, pp. 1173–1178, 2005.

[17] C. L. Cheng, D. S. Sun, W. C. Chu et al., "The effects of the bacterial interaction with visible-light responsive titania photocatalyst on the bactericidal performance," *Journal of Biomedical Science*, vol. 16, no. 7, 10 pages, 2009.

Hindawi Publishing Corporation
International Journal of Photoenergy
Volume 2012, Article ID 584079, 5 pages
doi:10.1155/2012/584079

Research Article

Nd:YAG Lasers Treating of Carious Lesion and Root Canal In Vitro

Danqing Xia,[1,2] Zenggui Mo,[3] Gang Zhao,[4] Fei Guo,[1,2] Chao You,[1,2] Ze Chen,[1,2] Xiao Zhu,[1,2] Zhengjia Li,[1,2] Di Chen,[1,2] and Xiaohong Fan[1,2]

[1] *Wuhan National Laboratory for Optoelectronics, Huazhong University of Science and Technology, Hubei 430074, Wuhan, China*
[2] *College of Optoelectronics Science and Engineering, Huazhong University of Science and Technology, Hubei 430074, Wuhan, China*
[3] *Affiliated Hospital, Huazhong University of Science and Technology, Hubei 430074, Wuhan, China*
[4] *Department of Stomatology, The People's Hospital of Huangzhou District, Hubei 438000, Huanggang, China*

Correspondence should be addressed to Xiaohong Fan, xhfan@mail.hust.edu.cn

Received 14 February 2012; Revised 29 April 2012; Accepted 7 May 2012

Academic Editor: Timon Cheng-Yi Liu

Dental caries is a transmissible bacterial disease process, with cavities at the end, and caused by acids from bacterial metabolism. The essence of dental treatment is to clean and disinfect bacterial contamination from the tooth. In this work, we tried to demonstrate the cleaning and disinfecting effects of Nd:YAG laser irradiation on dental carious lesion and root canal in vitro. Acousto-optic Q-switched quasicontinuous and Cr^{3+}:YAG crystal Q-switched pulse Nd:YAG lasers were employed to treat caries lesion and the root canal, respectively. Results showed that acousto-optic Q-switched quasicontinuous Nd:YAG laser irradiation and Cr^{3+}:YAG crystal Q-switched pulse Nd:YAG laser irradiation could rapidly clean decayed material and bacterial contamination from dental carious lesion and the narrow tail end of root canal with minimally invasive in vitro, respectively. It was concluded that acousto-optic Q-switched quasicontinuous laser irradiation may be a rapid and effective alternative caries treatment, and Cr^{3+}:YAG crystal Q-switched pulse Nd:YAG laser irradiation may be an effective method for canal cleaning and disinfecting during root canal therapy.

1. Introduction

Dental caries is the most prevalent disease among preschool children (early child caries) [1], although it has been reported to be a declining incidence worldwide in the last decades [2]. Almost 76% of children aged 5 in China [3] and about 30% aged 2 to 5 in America [4] were affected by dental caries, and the percent is in rise. Dental caries is a transmissible bacterial disease process and caused by acids from bacterial metabolism. Cariogenic bacterial, feeding on the carbohydrates in food, can be easily transferred to babies from mothers or caregivers before the teeth erupts [5–7] and colonize teeth as dental plaque when teeth erupts. Acids produced by bacteria in dental plaque rapidly diffuse in all directions through the pores of enamel or dentine and into the underlying tissue to dissolve acid soluble mineral, and finally cavity was formed in the tooth after many months or years. Usually, dental caries can be inhibited and even reversed in its early stages of process by removing cariogenic bacteria from teeth. Unfortunately, it is often not self-limiting and progresses without proper care until the tooth is destroyed with cavities. Then, it is more difficult to remove bacteria from rough, cavitated surfaces, which quicken the dental caries progress. In addition, bacterial contamination in root canal is also considered the principle etiologic factor for the development of pulpal and periapical lesions [7, 8].

Dental treatment can prevent and inhibit the dental caries by cleaning and disinfecting the bacterial contamination in tooth or enhancing the caries resistance of tooth at the very beginning of dental caries process [9]. For those small lesions, enhancing the caries resistance to prevent caries normally by topical fluoride is the focal point of treatment [10]. Mentionable, laser has been widely used in dentistry for decades, which is well known to increase enamel resistance to acids dissolving, and Nd:YAG laser irradiation combined with topical fluoride treatment can induce an even greater increase in caries resistance [11]. However, there is no doubt that removal of plaque is the most effective way to help prevent periodontal disease and caries processing due to the

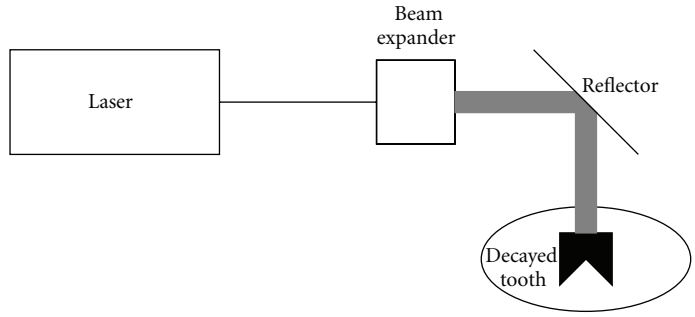

Figure 1: The sketch of quasicontinuous laser system.

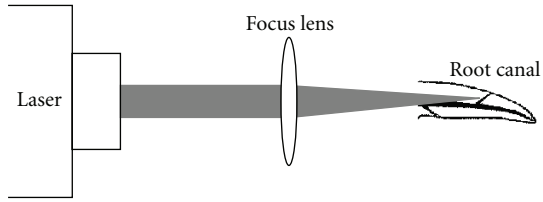

Figure 2: The sketch of Q-switched laser system.

well-known harm of fluoride [12, 13]. Many types of lasers have been used for dental caries prevention, and Nd:YAG laser is the most studied one [11, 14–16]. For larger lesions, cleaning and disinfecting the bacterial contamination in tooth to inhibit the caries is the essence of treatment. Aiming to preserve tooth structures and prevent further destruction of the tooth, large portions of decayed material is removed from the tooth by a dental drill and cleaned carefully by a spoon during traditional caries treatment [17], which is with great invasive and painful even terrifying for patient especially preschool children. Moreover, it is impossible to completely remove pulp tissue, debris, and bacteria which cause secondary caries and pain.

Thus, it is necessary to develop an alternative caries treatment, which can remove the bacterial containment painless with minimally invasive. Present work is to demonstrate the ability of acousto-optic Q-switched quasicontinuous Nd:YAG lasers and Cr^{3+}:YAG crystal Q-switched pulse Nd:YAG lasers in cleaning of decayed material (pulp and others) speedily and disinfecting of bacteria completely of human tooth in vitro. Laser irradiation treatment may be an ideal alternative dental caries treatment especially preschool children aged 2 to 5 years.

2. Materials and Methods

2.1. Laser System. Quasicontinuous laser beam with wavelength of 1064 nm provided by an acousto-optic Q-switched Nd:YAG laser system (Figure 1) was vertically delivered to the carious lesion on tooth surface. Comparing to continuous-wave laser, acousto-optic Q-switched quasicontinuous laser has a relative higher peak power, which is better for bacterial disinfecting, and a shorter half-height pulse width, which will be beneficial to avoid overheating. This laser system was normally set with 30 W peak average output power and 600 Hz frequency. The peak power density of the laser irradiation was about 152.86 W/cm^2 with a diameter of about 0.5 cm and beam area of approximate 0.196 cm^2.

The Q-switched laser beam, provided by a Cr^{3+}:YAG crystal Q-switched laser system (Figure 2), was vertically focused on the canal directly. The focused Q-switched pulse laser irradiation has a smaller diameter, a higher peak power, and energy density, which is better for cleaning and disinfecting of narrow canal gap. This laser system was normally set with 100 mJ single-pulse energy, 1/3/5 Hz frequency, and about 100 ns half-height pulse width.

2.2. Materials. Human teeth with carious lesion on crown surface (one was shown at Figure 3(a)) were collected from the affiliated hospital to reveal the cleaning and disinfecting effect of quasicontinuous acousto-optic Q-switched Nd:YAG laser irradiation for decayed material from caries lesion. The tail end of root canal (one is shown at Figure 3(b)), which is the most narrow part and the difficult point of cleaning and disinfecting in root canal system, was prepared in the affiliated hospital to reveal the cleaning and disinfecting effect of Cr^{3+}:YAG crystal Q-switched laser irradiation for tissue and bacterial contamination in tooth canal.

2.3. Experiment. To demonstrate the cleaning effect of laser treatment, carious lesion tooth samples were exposed to acousto-optic Q-switched quasicontinuous laser irradiation, and tooth canal samples were exposed to Cr^{3+}:YAG crystal Q-switched pulse Nd:YAG laser irradiation, respectively. The cleaning efficiency is evaluated from the difference between pictures of lesion surface before and after laser treated. The disinfecting effect and efficiency of laser treatment is evaluated from the colony counts loss of samples. The experiment samples were scrubbed by swabs with sterile physiological saline before and after laser treatment, respectively. Then, the

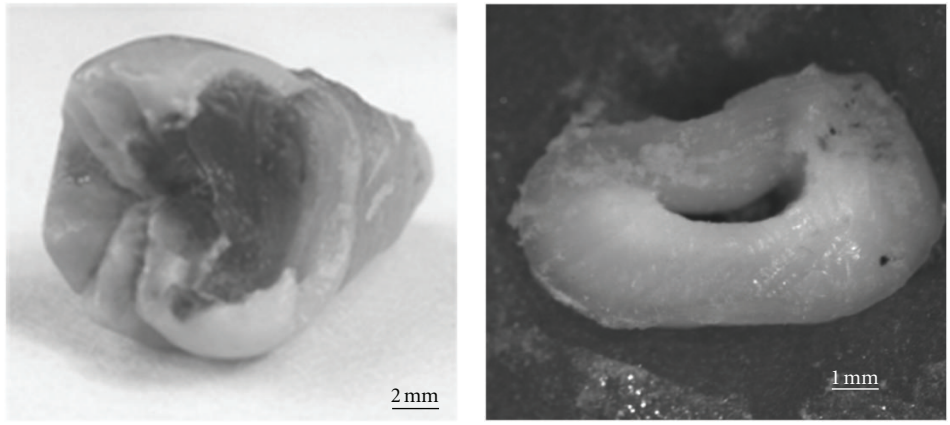

(a) (b)

Figure 3: Stereomicroscope images of (a) tooth with carious lesion and (b) tail end of root canal.

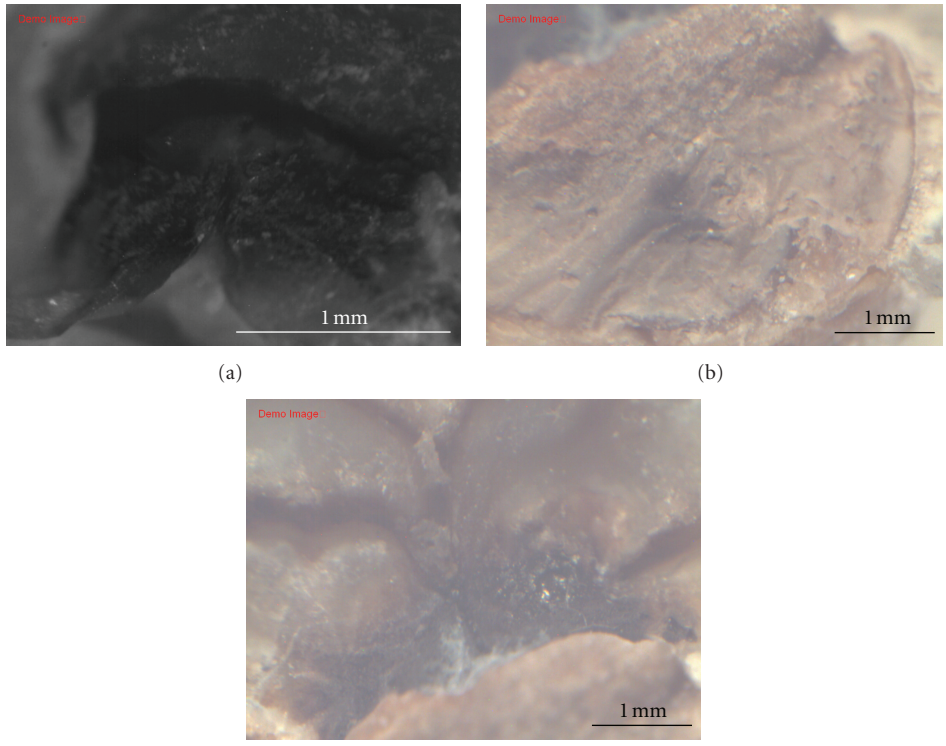

(a) (b)

(c)

Figure 4: Stereomicroscope images of decayed tooth surface (a) before and (b, c) after acousto-optic Q-switched Nd:YAG quasicontinuous laser treatment.

infected physiological saline of each sample was inoculate to 3 parallel agar dishes and cultivated at 37°C for 24 hours. In order to prevent the bacterial contamination from hands, the medical rubber gloves were necessary during the whole experiment.

3. Results and Discussion

3.1. Cleaning and Disinfecting Effects. Figure 4 showed the stereomicroscope images of carious lesion on the surface of tooth before (Figure 4(a)) and after laser treatment (Figures 4(b) and 4(c)). It was clear that decayed material in caries lesion was cleared away by laser irradiation without any visible damages to surrounding normal tooth tissues after no more than 2-second quasicontinuous laser irradiation. However, there was little carbonization in the treated area, carbonization indicated that laser treatment with less power density or shorter irradiation time would be better for caries material cleaning. The obvious change of caries in tooth before and after laser treatment indicated that the

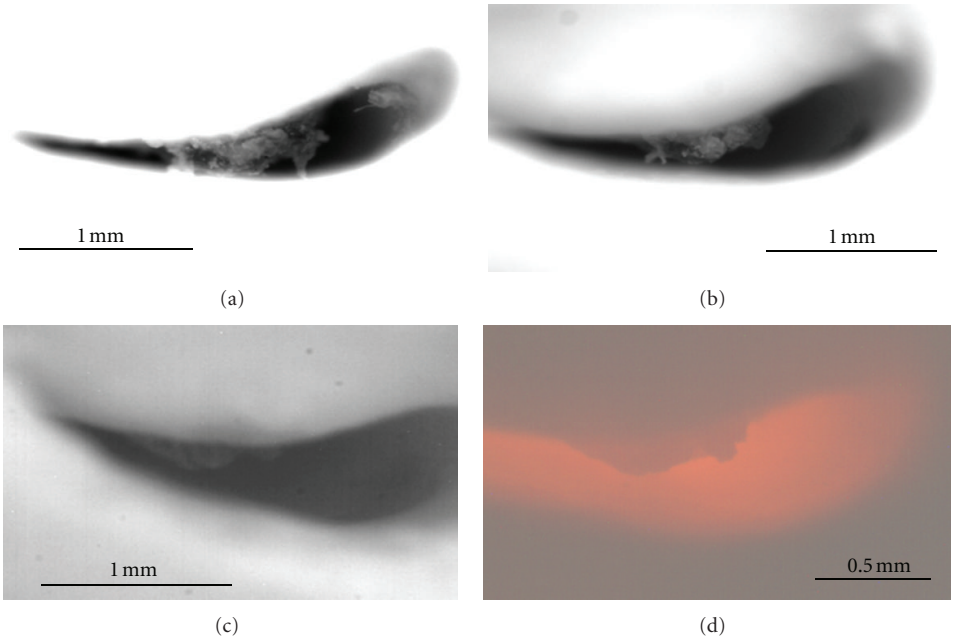

Figure 5: Stereomicroscope images of organisms in untreated (a), 20 pulses (b), and 40 pulses (c, d) laser irradiation-treated root canal gap.

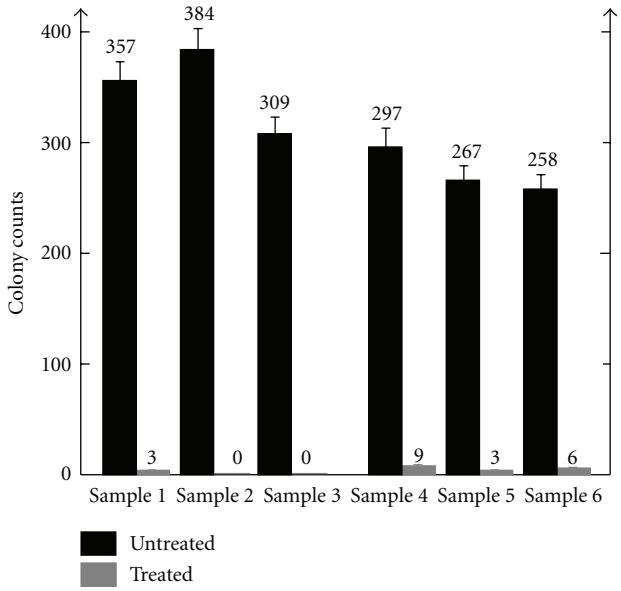

Figure 6: The colony counts of carious lesions (samples 1–3) and root canals (samples 4–6).

acousto-optic Q-switched Nd:YAG quasicontinuous laser irradiation was a speedy and efficient cleaning method and treatment for carious lesion.

Figure 5 shows the images of root canal sample before (Figure 5(a)) and after 20 pulses (Figure 5(b)), 40 pulses laser-treated by Cr^{3+}:YAG crystal Q-switched laser. (Figures 5(c) and 5(d)) comparing Figure 5(a) to Figure 5(b), it was clear that much portion of the tissue in canal was removed and almost cleared away after 40-pulse laser treatment. Particularly, there was almost no byproduct in tooth canal after laser treatment according to Figures 5(c) and 5(d). These results indicated that Cr^{3+}:YAG Q-Switched laser irradiation might clean up the root canal after more than 40 pulses, and Cr^{3+}:YAG Q-switched laser treatment may be an ideal method for tooth canal cleaning.

The colony counts of experiment tooth samples before and after laser treatment were shown in Figure 6 ($P < 0.05$). Samples 1–3 refer to the tooth samples with carious lesion, and samples 4–6 refer to root canal samples. According to decrement colony counts of untreated and treated samples, the disinfecting effect was obvious and the disinfecting efficiency was high, approximately 100% and 98.5% for

caries and root canal disinfecting, respectively. The results indicated that Q-switched laser irradiation treatment was a very effective disinfecting method for caries treatment, even root canal.

4. Discussions

It is an advantage to choose laser beam with less power density, or less repeated frequency for tooth treatment, because the carbonization showed in Figure 4(b) was due to overheat of acousto-optic Q-switched quasicontinuous laser irradiation. In addition, those experimental samples used in this work were only with carious lesion on the crown surface, but majority of patients in clinics have caries lesion deeply inside the tooth. Thus our further work will aim at laser holing for cleaning material in deep carious lesion.

Acousto-optic Q-switched quasicontinuous laser irradiation with big beam size, high average energy density, and repeated frequency was effective for caries lesion treatment, and Cr^{3+}:YAG crystal Q-switched laser irradiation with smaller beam size, shorter pulse width, and higher peak energy density is effective for root canal treatment without any obvious byproducts as carbonization appeared in caries lesion laser treatment. Both acousto-optic Q-switched quasicontinuous laser irradiation and Cr^{3+}:YAG crystal Q-switched laser irradiation had advantages over each other in dental caries treatment and had common advantages such as no pain, no vibrating, overtraditional treatment with drill and spoon. Laser irradiation treatment was very friendly for patient especially for the preschool children patients. It will be a good alternative for early child caries inhibition and readiness to be accepted by child patients.

5. Conclusions

In conclusion, acousto-optic Q-switched quasicontinuous laser irradiation may be a rapid and effective alternative caries treatment, and Cr^{3+}:YAG crystal Q-switched pulse Nd:YAG laser irradiation may be an effective method for canal cleaning and disinfecting during root canal therapy.

Acknowledgments

The authors gratefully appreciate the generous help of laser system and stereomicroscope from Professors Xiao Zhu and Pengcheng Li in Wuhan National Laboratory for Optoelectronics.

References

[1] J. A. Aas, A. L. Griffen, S. R. Dardis et al., "Bacteria of dental caries in primary and permanent teeth in children and young adults," *Journal of Clinical Microbiology*, vol. 46, no. 4, pp. 1407–1417, 2008.

[2] R. A. Bagramian, F. Garcia-Godoy, and A. R. Volpe, "The global increase in dental caries. A pending public health crisis," *American Journal of Dentistry*, vol. 22, no. 1, pp. 3–8, 2009.

[3] B. A. Dye, S. Tan, V. Smith et al., "Trends in oral health status: United States, 1988–1994 and 1999–2004," *Vital and Health Statistics*, no. 248, pp. 1–92, 2007.

[4] H. Y. Wang, P. E. Petersen, J. Y. Bian, and B. X. Zhang, "The second national survey of oral health status of children and adults in China," *International Dental Journal*, vol. 52, no. 4, pp. 283–290, 2002.

[5] J. D. B. Featherstone, "Dental caries: a dynamic disease process," *Australian Dental Journal*, vol. 53, no. 3, pp. 286–291, 2008.

[6] R. J. Berkowitz, "Acquisition and transmission of mutans streptococci," *Journal of the California Dental Association*, vol. 31, no. 2, pp. 135–138, 2003.

[7] Y. Kawashita, M. Kitamura, and T. Saito, "Early childhood caries," *International Journal of Dentistry*, vol. 2011, Article ID 725320, 7 pages, 2011.

[8] A. S. Garcez, S. C. Nuñez, M. R. Hamblin, and M. S. Ribeiro, "Antimicrobial effects of photodynamic therapy on patients with necrotic pulps and periapical lesion," *Journal of Endodontics*, vol. 34, no. 2, pp. 138–142, 2008.

[9] C. H. Hu, J. He, R. Eckert et al., "Development and evaluation of a safe and effective sugar-free herbal lollipop that kills cavity-causing bacteria," *International Journal of Oral Science*, vol. 3, no. 1, pp. 13–20, 2011.

[10] R. R. Breaker, "New insight on the response of bacteria to fluoride," *Caries Research*, vol. 46, no. 1, pp. 78–81, 2012.

[11] D. M. Zezell, H. G. D. Boari, P. A. Ana, C. D. P. Eduardo, and G. L. Powell, "Nd:YAG laser in caries prevention: a clinical trial," *Lasers in Surgery and Medicine*, vol. 41, no. 1, pp. 31–35, 2009.

[12] J. M. Broadbent, W. M. Thomson, J. V. Boyens, and R. Poulton, "Dental plaque and oral health during the first 32 years of life," *Journal of the American Dental Association*, vol. 142, no. 4, pp. 415–426, 2011.

[13] R. P. Allaker and C. W. I. Douglas, "Novel anti-microbial therapies for dental plaque-related diseases," *International Journal of Antimicrobial Agents*, vol. 33, no. 1, pp. 8–13, 2009.

[14] P. Rechmann, D. Fried, C. Q. Le et al., "Caries inhibition in vital teeth using 9.6-μm CO_2-laser irradiation," *Journal of Biomedical Optics*, vol. 16, no. 7, Article ID 071405, 2011.

[15] C. S. Castellan, A. C. Luiz, L. M. Bezinelli et al., "In vitro evaluation of enamel demineralization after Er:YAG and Nd:YAG laser irradiation on primary teeth," *Photomedicine and Laser Surgery*, vol. 25, no. 2, pp. 85–90, 2007.

[16] H. G. D. Boari, P. A. Ana, C. P. Eduardo, G. L. Powell, and D. M. Zezell, "Absorption and thermal study of dental enamel when irradiated with Nd:YAG laser with the aim of caries prevention," *Laser Physics*, vol. 19, no. 7, pp. 1463–1469, 2009.

[17] http://en.wikipedia.org/wiki/Dental_caries .

Hindawi Publishing Corporation
International Journal of Photoenergy
Volume 2012, Article ID 730351, 4 pages
doi:10.1155/2012/730351

Research Article

Laser Acupuncture Reduces Body Fat in Obese Female Undergraduate Students

Xiao-Guang Liu, Juan Zhang, Jian-Liang Lu, and Timon Cheng-Yi Liu

Laboratory of Laser Sports Medicine, South China Normal University, Guangzhou 510006, China

Correspondence should be addressed to Xiao-Guang Liu, tygx@jnu.edu.cn

Received 8 February 2012; Revised 19 April 2012; Accepted 21 April 2012

Academic Editor: Rui Duan

The purpose of this study was to investigate the efficacies of laser acupunctures with different laser irradiation doses for body weight loss and body fat reduction in obese persons. Twentyeight subjects with simple obesity were divided into four groups receiving laser acupunctures at 0, 358, 478, and 597 J/cm^2, respectively, which were applied to the acupoints of Cv 8, St 25, and Sp 15, six times per week for four weeks. Body weight (BW), body mass index (BMI), body fat mass (BFM), body fat percent, waist girth, hip girth, and waist-to-hip ratio (WHR) were measured before and after treatment. The laser groups receiving 358 and 597 J/cm^2 showed significant reductions in BW, BMI, BFM, waist girth, hip girth, and WHR after treatment compared with the placebo group. The percent reductions of BFM in the laser groups receiving 358 and 597 J/cm^2 were 4.29% and 3.94%, respectively, and the corresponding values of BW were 1.99% and 1.63%, respectively. In conclusion, laser acupuncture could reduce body fat mass and lower body weight in a dose-dependent manner in obese persons. Among the doses of 358, 478, and 597 J/cm^2, both the 358 and 597 J/cm^2 doses were effective in the 4-week trial.

1. Introduction

With economic growth and constant urbanization, the prevalence of obesity has been increasing in many countries. Obesity is associated with many chronic diseases, including cardiovascular diseases, diabetes, musculoskeletal diseases, and some cancers. Common intervention methods for obesity include low-calorie diet, exercise, behavioral modification, and slimming drugs [1]. Also acupuncture has shown good therapeutic results in the treatment of obesity [2].

Over the last 30 years, low-level laser therapy has been applied in many medical fields, and low-level laser irradiation has been adopted in acupuncture [3]. Laser acupuncture was found to be effective in the treatment of visceral postmenopausal obesity when combined with low-calorie diet [4]. A recent clinical observation showed that laser acupuncture alone could reduce body weight (BW) and body mass index (BMI) in obese persons [5], but the study lacked a placebo control. Moreover, the influence of laser acupuncture on body composition was unclear, and further scientific evidence for the efficacy of laser acupuncture for obesity should be presented.

In this study, we conducted a blinded clinical trial to investigate the efficacies of laser acupunctures with GaAlAs laser irradiation at different doses for body weight loss and body fat reduction in obese humans.

2. Materials and Methods

The study protocol was approved by the ethics committee of the Faculty of South China Normal University, Guangzhou, China. Informed consent was obtained from each participant prior to the start of treatment.

2.1. Subjects and Groups. Twentyeight female undergraduate students with simple obesity aged 19~25 years were enrolled in this study at the Laboratory of Laser Sports Medicine of South China Normal University in Guangzhou. Based on the obesity criteria in the Asian-Pacific region recommended by the World Health Organization [6], inclusion criteria for

Table 1: Body weight and body mass index data in the placebo group and the three laser groups before and after treatment.

Measurement	Group	Pretreatment	Posttreatment	Change over time
BW (kg)	Placebo	64.43 ± 5.79	64.51 ± 5.89	−0.09 ± 0.72
	Low-dose laser	71.76 ± 13.34	70.33 ± 12.37*	1.43 ± 1.37$^{\Delta}$
	Medium-dose laser	71.64 ± 11.24	70.83 ± 11.45*	0.81 ± 0.76
	High-dose laser	77.49 ± 16.91	76.23 ± 16.36*	1.26 ± 1.33$^{\Delta}$
BMI (kg/m^2)	Placebo	26.94 ± 1.62	27.00 ± 1.83	−0.06 ± 0.28
	Low-dose laser	28.31 ± 3.53	27.68 ± 3.38*	0.63 ± 0.51$^{\Delta\Delta}$
	Medium-dose laser	27.93 ± 3.54	27.61 ± 3.67*	0.31 ± 0.31
	High-dose laser	29.44 ± 5.13	28.91 ± 4.92*	0.53 ± 0.57$^{\Delta}$

BW: body weight, BMI: body mass index. Asterisks indicate significant differences from pretreatment ($^*P < 0.05$). Triangles indicate significant differences from the placebo group ($^{\Delta}P < 0.05$, $^{\Delta\Delta}P < 0.01$).

the subjects were determined as body mass index (BMI) ≥ 25 kg/m^2 and body fat percent ≥30%. All subjects were randomly divided into four groups, namely, placebo group, low-dose laser group, medium-dose laser group, and high-dose laser group, seven in each group. Each subject was asked not to change her diet or exercise habits during the trial.

2.2. Laser Acupuncture. A GaAlAs laser (Model LD-1, Guangzhou, China) with 810 nm wavelength, 0~500 mW adjustable and continuous power output, and with 0.4 cm beam diameter was used. The subjects in the placebo group, the low-dose group, the medium-dose group, and the high-dose group were treated with the laser at the doses of 0, 358, 478, and 597 J/cm^2 (powers: 0, 150, 200, and 250 mW; intensity: 0, 1194, 1592, and 1990 mW/cm^2; irradiation time: 5 min/point, 25 min in total), respectively, six times per week for four weeks. The following abdominal acupuncture points were irradiated: Cv 8 (Shenque), St 25 (Tianshu, bilateral), and Sp 15 (Daheng, bilateral). The laser irradiations were applied directly to the skin of the points with a perpendicular beam.

2.3. Outcome Measures. BW, BMI, body fat mass (BFM), body fat percent, waist girth, hip girth, and waist-to-hip ratio (WHR) were measured at baseline and the end of treatment. BW, BMI, BFM, and body fat percent were measured using the body composition analyzer (Model Inbody 3.0, Republic of Korea). Waist girth was measured at the level of the umbilicus, and hip girth was measured at the level of maximum extension of the buttocks. WHR was calculated as waist girth divided by hip girth.

2.4. Statistical Analysis. Data were expressed as mean ± standard deviation. Differences between before and after treatment in each group were analyzed by paired t-tests. Differences between group means were analyzed using one-way ANOVA with post hoc test. The statistical level of significance was set at $P < 0.05$.

3. Results

3.1. Body Weight and Body Composition. There were no significant differences in BW, BMI, BFM, and body fat percent at baseline between any groups (Tables 1 and 2). After the four weeks of treatment, the three laser groups exhibited significant drops in BW, BMI, and BFM except the medium-dose group in BFM, while the placebo group exhibited no significant changes. Mean BWs in the low-dose group, the medium-dose group, and the high-dose group were reduced by 1.43, 0.81, and 1.26 kg (percent reductions: 1.99%, 1.13%, and 1.63%), respectively. Mean BMIs in the three laser groups decreased by 0.63, 0.31, and 0.53 kg/m^2, respectively (Table 1). Mean BFMs in the three laser groups were reduced by 1.16, 0.69, and 1.16 kg (percent reductions: 4.29%, 2.60%, and 3.94%), respectively (Table 2). The changes in BW, BMI, and BFM in the low-dose and high-dose groups were greater than those in the placebo group with statistical significance, but there were no significant differences between the medium-dose group and the placebo group. There were no significant differences in body weight and body composition after treatment between any laser groups. In addition, each laser group showed a nonsignificant drop in body fat percent after treatment.

3.2. Waist Girth and Hip Girth. There were no significant differences in waist girth, hip girth, and WHR at baseline between any groups (Table 3). After the four weeks of treatment, the low-dose and high-dose groups showed significant drops in waist girth and WHR. Each laser group also showed a nonsignificant drop in hip girth after treatment. Mean waist girths in the low-dose group and the high-dose group were reduced by 2.34 and 2.14 cm, respectively. Mean WHR in each laser group decreased by 0.01. The changes in waist girth, hip girth, and WHR in the low-dose and high-dose groups were greater than those in the placebo group with statistical significance, but there were no significant differences between the medium-dose group and the placebo group. There were no significant differences in both the girths after treatment between any laser groups.

4. Discussion

Obesity is a result of disturbance of energy homeostasis. Acupuncture and low-level laser irradiation with their homeostatic activities may give a chance to primarily compensate for the condition. According to traditional Chinese medicine,

Table 2: Body fat mass and body fat percent data in the placebo group and the three laser groups before and after treatment.

Measurement	Group	Pretreatment	Posttreatment	Change over time
BFM (kg)	Placebo	24.00 ± 3.84	23.97 ± 3.58	0.03 ± 0.66
	Low-dose laser	27.06 ± 7.60	25.90 ± 6.87*	1.16 ± 1.11$^{\triangle}$
	Medium-dose laser	26.57 ± 7.36	25.88 ± 7.50	0.69 ± 0.97
	High-dose laser	29.47 ± 10.53	28.31 ± 9.92*	1.16 ± 1.02$^{\triangle}$
BF%	Placebo	37.07 ± 2.89	37.07 ± 2.62	0.00 ± 0.80
	Low-dose laser	37.34 ± 4.33	36.48 ± 4.19	0.86 ± 0.94
	Medium-dose laser	36.64 ± 5.47	36.04 ± 5.54	0.60 ± 1.04
	High-dose laser	37.14 ± 5.13	36.44 ± 5.06	0.70 ± 0.73

BFM: body fat mass, BF%: body fat percent. Asterisks indicate significant differences from pretreatment ($^{*}P < 0.05$). Triangles indicate significant differences from the placebo group ($^{\triangle}P < 0.05$).

Table 3: Waist girth, hip girth, and waist-to-hip ratio data in the placebo group and the three laser groups before and after treatment.

Measurement	Group	Pretreatment	Posttreatment	Change over time
WG (cm)	Placebo	87.71 ± 6.10	88.21 ± 6.53	−0.50 ± 1.22
	Low-dose laser	90.77 ± 12.23	88.43 ± 11.07*	2.34 ± 1.96$^{\triangle\triangle}$
	Medium-dose laser	90.03 ± 7.57	88.64 ± 7.88	1.39 ± 1.92
	High-dose laser	91.59 ± 12.13	89.44 ± 11.61*	2.14 ± 1.75$^{\triangle\triangle}$
HG (cm)	Placebo	101.71 ± 5.64	101.93 ± 5.41	−0.21 ± 0.70
	Low-dose laser	104.79 ± 6.47	103.93 ± 5.83	0.86 ± 0.94$^{\triangle}$
	Medium-dose laser	105.64 ± 9.16	105.14 ± 9.13	0.50 ± 0.50
	High-dose laser	105.93 ± 9.68	105.29 ± 9.55	0.64 ± 0.85$^{\triangle}$
WHR	Placebo	0.86 ± 0.05	0.87 ± 0.06	0.00 ± 0.01
	Low-dose laser	0.86 ± 0.07	0.85 ± 0.07*	0.01 ± 0.01$^{\triangle}$
	Medium-dose laser	0.85 ± 0.04	0.84 ± 0.04	0.01 ± 0.02
	High-dose laser	0.86 ± 0.04	0.85 ± 0.04*	0.01 ± 0.01$^{\triangle}$

WG: waist girth, HG: hip girth, WHR: waist-to-hip ratio. Asterisks indicate significant differences from pretreatment ($^{*}P < 0.05$). Triangles indicate significant differences from the placebo group ($^{\triangle}P < 0.05$, $^{\triangle\triangle}P < 0.01$).

all afflictions of obesity primarily originate from energy deficiency in the meridians St (stomach) and Sp (spleen). With classic needle stimulating some acupoints in the meridians St and Sp, many acupuncture therapies for obesity have shown good results [7–9].

Laser acupuncture integrates the positive effects of acupuncture and low-level laser irradiation. Compared with classic needle acupuncture, laser acupuncture manifests many advantages: aseptic and painless stimulation of acupoints, possibility of application to some needle-forbidden acupoints such as Cv 8 (Shenque) with no subsequent transient erythema, and lack of tissue traumatization. Only a few papers dealing with laser acupuncture referred to its application in the treatment of obesity. Wozniak et al. [4] administered laser acupuncture at the acupoints of Cv 12 (Zhongwan), St 25 (Tianshu), and St 36 (Zusanli) in postmenopausal women with visceral obesity and found that laser acupuncture could increase the efficacy of low-calorie diet for obesity. Hu et al. [5] treated 95 patients of simple obesity with laser acupuncture at the acupoints of Cv 9 (Shuifen), St 25 (Tianshu), St 28 (Shuidao), St 40 (Fenglong), and Sp 15 (Daheng) with 785 nm pulse laser irradiation. In the trial, they did not use placebo control, and their results showed that laser acupuncture alone could reduce both BW and BMI without restrictive diet. Adopting a placebo control, we presented convincing evidence for the efficacy of laser acupuncture alone for obesity in this study. According to the pathogeny of simple obesity in traditional Chinese medicine and clinical data of acupuncture therapy for obesity, we chose Cv 8, St 25, and Sp 15 to treat obesity in the laser acupuncture research. Our results showed that laser acupuncture with the doses of 358 and 597 J/cm^2 significantly reduced both BW and BMI in obese subjects compared with the placebo control. In this study, the effect of laser acupuncture on body composition in female obese undergraduate students was investigated. Our results showed that the laser acupuncture with 810 nm GsAlAs laser irradiation at both the low dose of 358 J/cm^2 and the high dose of 597 J/cm^2 significantly reduces BFM as well as BW in obese subjects. In the low-dose and high-dose groups, the percent reduction was greater in BFM than in BW (in the low-dose group, 4.29% versus 1.99%; in the high-dose group, 3.94% versus 1.63%). This result indicated that laser acupuncture lowered BW primarily by reducing BFM, but not water. The mechanism by which laser acupuncture reduced BFM may include the systemic response and local response. Acupoint of Cv 8 is located at the centre of the umbilicus, which is underlain by the inferior epigastric artery and vein. When laser acupuncture

was applied at Cv 8, low-level laser irradiation may exert a systemic regulating effect on fat metabolism through influencing the blood in the inferior epigastric artery and vein. In this study, hip girth losses in the low-dose and high-dose groups were probably a consequence of systemic regulation of body fat by laser acupuncture. Neira et al. [10] in 2002 reported that low-level laser therapy could release stored fat in adipocytes by the opening of cell membrane-associated pores after a few minutes treatment. Caruso-Davis et al. [11] confirmed the finding of Neira et al. [10] in the investigation of the efficacy of low-level laser therapy for spot fat reduction and at the same time found that low-level laser irradiation over the waist could significantly reduce waist girth in healthy adults, which is a typical phenomenon of indirect photobiomodulation [12]. Acupoints of St 25 and Sp 15 are located in abdominal area with thicker fat at the level the umbilicus. Therefore, waist girth losses after laser acupuncture at St 25 and Sp 15 may partly result from the direct effect of low-level laser irradiation on fat tissue in this study.

We also observed the dose-response relationship of laser acupuncture therapy for obesity in this study. Based on data of several trials of GaAlAs laser therapy [13, 14], we adopted the doses of 358, 478, and 597 J/cm^2 to conduct the laser acupuncture research. The irradiations at both 358 J/cm^2 and 597 J/cm^2 significantly reduced all the measurements except body fat percent compared with placebo irradiation, whereas the irradiation at 478 J/cm^2 nonsignificantly did. Among the three doses, the lowest dose of 358 J/cm^2 appeared to be the best efficient in the laser acupuncture therapy, but there were no significant differences in all the measurements between any laser groups. There are various factors which may influence the efficacy of laser acupuncture therapy for obesity, including laser parameters, skin properties, and subjects' behavior of exercise. Thus, more studies were required to definitely show the dose-response pattern of laser acupuncture therapy for obesity. In addition, the irradiations at all the three doses nonsignificantly reduced body fat percent. The nonsignificant changes in the three laser groups might become significant with the extension of treatment period according to the self-adaptive property of low-level laser irradiation [15]. Of course, it should be further verified.

5. Conclusion

Laser acupuncture could reduce body fat mass and lower body weight in a dose-dependent manner in obese persons. Among the doses of 358, 478, and 597 J/cm^2, both the 358 and 597 J/cm^2 doses were effective in the 4-week trial.

Conflict of Interests

The authors declare that there is no conflict of interests.

Acknowledgments

This work was supported by the Science and Technology Planning Foundation of Guangdong Province, China (2011B031600006) and National Natural Science Foundation of China (60878061).

References

[1] R. H. Eckel, "Clinical practice. Nonsurgical management of obesity in adults," *The New England Journal of Medicine*, vol. 358, no. 18, pp. 1886–1950, 2008.

[2] S. H. Cho, J. S. Lee, L. Thabane, and J. Lee, "Acupuncture for obesity: a systematic review and meta-analysis," *International Journal of Obesity*, vol. 33, no. 2, pp. 183–196, 2009.

[3] P. Whittaker, "Laser acupuncture: past, present, and future," *Lasers in Medical Science*, vol. 19, no. 2, pp. 69–80, 2004.

[4] P. Wozniak, G. Stachowiak, A. Piêta-Doliñska, and P. Oszukowski, "Laser acupuncture and low-calorie diet during visceral obesity therapy after menopause," *Acta Obstetricia et Gynecologica Scandinavica*, vol. 82, no. 1, pp. 69–73, 2003.

[5] W. L. Hu, C. H. Chang, and Y. C. Hung, "Clinical observations on laser acupuncture in simple obesity therapy," *American Journal of Chinese Medicine*, vol. 38, no. 5, pp. 861–867, 2010.

[6] World Health Organization, Western Pacific Region, and International Association for the Study of Obesity, *The Asia-Pacific Perspective: Redefining Obesity and Its Treatment*, Health Communications Australia Pty Limited, Sydney, Australia, 2000.

[7] Q. Shan, "Acupuncture therapy for 130 cases of simple obesity," *Journal of Acupuncture and Tuina Science*, vol. 4, no. 2, pp. 121–122, 2006.

[8] M. J. Mu and Y. Q. Yuan, "Clinical study on simple obesity treated with abdomen acupuncture," *Journal of Acupuncture and Tuina Science*, vol. 6, no. 3, pp. 165–168, 2008.

[9] Y. Shi, C. Zhao, and X. Y. Zuo, "Clinical study on treatment of simple obesity due to spleen deficiency by acupuncture-moxibustion," *Journal of Acupuncture and Tuina Science*, vol. 6, no. 6, pp. 352–355, 2008.

[10] R. Neira, J. Arroyave, H. Ramirez et al., "Fat liquefaction: effect of low-level laser energy on adipose tissue," *Plastic and Reconstructive Surgery*, vol. 110, no. 3, pp. 912–922, 2002.

[11] M. K. Caruso-Davis, T. S. Guillot, V. K. Podichetty et al., "Efficacy of low-level laser therapy for body contouring and spot fat reduction," *Obesity Surgery*, vol. 21, no. 6, pp. 722–729, 2011.

[12] T. C. Y. Liu, E. X. Wei, and F. H. Li, "Indirect photobiomodulation on tumors," *Lasers in Surgery and Medicine*, vol. 44, supplement 24, 2012.

[13] R. T. Chow, L. B. Barnsley, and G. Z. Heller, "The effect of 300 mW, 830 nm laser on chronic neck pain: a double-blind, randomized, placebo-controlled study," *Pain*, vol. 124, no. 1-2, pp. 201–210, 2006.

[14] U. Dundar, D. Evcik, F. Samli, H. Pusak, and V. Kavuncu, "The effect of gallium arsenide aluminum laser therapy in the management of cervical myofascial pain syndrome: a double blind, placebo-controlled study," *Clinical Rheumatology*, vol. 26, no. 6, pp. 930–934, 2007.

[15] T. C. Y. Liu, L. Luo, and L. Zhang, "Self-adaptive effects of low intensity laser irradiation in prophylaxis of muscular fibrosis," *Lasers in Surgery and Medicine*, vol. 43, supplement 23, article 975, 2011.

Hindawi Publishing Corporation
International Journal of Photoenergy
Volume 2012, Article ID 275209, 5 pages
doi:10.1155/2012/275209

Research Article

Aquaporin-1-Mediated Effects of Low Level He-Ne Laser Irradiation on Human Erythrocytes

Gang-Yue Luo,[1,2,3,4] Li Sun,[5] and Timon Cheng-Yi Liu[1,2,3]

[1] *Laboratory of Laser Sports Medicine, South China Normal University, Guangzhou 510631, China*
[2] *School of Life Science, South China Normal University, Guangzhou 510631, China*
[3] *The Key Laboratory of Ministry of Education of China in Laser Life Science, South China Normal University, Guangzhou 510631, China*
[4] *School of Information and Optoelectronic Science and Engineering, South China Normal University, Guangzhou 510631, China*
[5] *Medical School, Jinan University, Guangzhou 510632, China*

Correspondence should be addressed to Timon Cheng-Yi Liu, liutcy@scnu.edu.cn

Received 30 January 2012; Revised 12 April 2012; Accepted 12 April 2012

Academic Editor: Rui Duan

The role of membrane aquaporin-1 (APQ-1) in the photobiomodulation (PBM) on erythrocyte deformability will be studied in this paper with human dehydrated erythrocytes as echinocytic shape alterations lead to decreased cellular deformability. Human dehydrated erythrocytes were irradiated with low intensity He-Ne laser irradiation (LHNL) at 0.9, 1.8, 2.7, and 4.4 mW/cm^2 for 5, 15, and 30 min, respectively, and APQ-1 inhibitor, 0.2 μmol/L $HgCl_2$, was used to study the role of APQ-1 in mediating PBM with LHNL at 4.4 mW/cm^2 for 5 min. Comprehensive morphological parameters of an intact cell such as contact area, perimeter, roundness and erythrocyte elongation index (EEI) were measured to characterize erythrocyte deformability with fast micro multi-channel spectrophotometer. It was observed that the dosage of LHNL improvement of the morphological parameters of dehydrated erythrocytes was morphological-parameter-dependent, but the Bunsen-Roscoe rule did not hold for roundness. The LHNL at 4.4 mW/cm^2 for 5 min significantly improved the contact area ($P < 0.05$) and EEI ($P < 0.05$) of the dehydrated erythrocytes, but the improvement was significantly inhibited by 0.2 μmol/L $HgCl_2$ ($P < 0.05$). It was concluded that AQP-1 might mediate the effects of LHNL on erythrocyte deformability, which supports the membranotropic mechanism of PBM.

1. Introduction

Photobiomodulation (PBM) is a modulation of laser irradiation, monochromatic light, hot color light such as red, orange, or yellow, or cold color light such as green, blue or violet (LI) on biosystems, which stimulates or inhibits biological functions but does not result in irreducible damage. The LI used in PBM is always low intensity LI (LIL), ~10 mW/cm^2. However, moderate intensity LI (MIL), $10^{2\sim3}$ mW/cm^2, is of PBM if the radiation time is not so long that it damages organelles or cells. The PBM of LIL/MIL (LPBM/MPBM) has been widely used to ameliorate hemorheologic behavior of patients [1], but the mechanism of PBM on red blood cells (RBCs) has not been cleared up. MPBM might be mediated by reactive oxygen spices (ROS) [1, 2]. Kujawa et al. found MIL promoted at 200 mW but inhibited at 400 mW Na^+-K^+-ATPase activity in isolated RBC membranes [3]. Mi et al. found that the deformability of RBCs from pathological samples and Ca^{2+}-treated samples was improved after MIL [4]. They further found that MIL can reduce the hemoglobin (Hbm) contents in RBCs, and the 532 nm laser was more efficient at lowering Hbm than the 632.8 nm laser, consistent with the absorption spectrum of Hbm [5].

However, LPBM mechanisms have not been well understood. It has been suggested that LPBM might be mediated by cytochrome c oxidase in mitochondria [6], which has been supported by Wong-Riley et al. [7]; however, there has been the LPBM on RBCs with no mitochondria. RBC solution samples from healthy volunteers were assigned to three groups: the aliquots in Group 1 were irradiated with LIL within 2 h after sampling, and the aliquots in Group 2

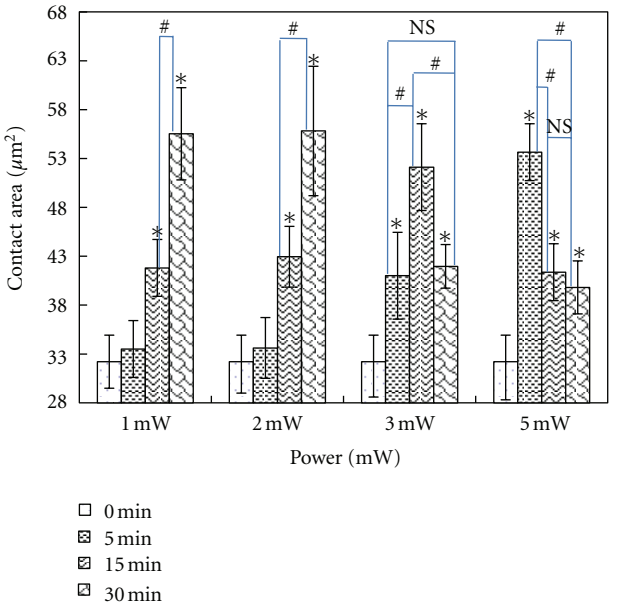

Figure 1: Effects of laser irradiation on the contact area of dehydrated erythrocytes. Data are means ± SD. $N = 100$. $^*P < 0.05$ versus the no irradiation group as control, $^\#$indicate significant differences between the two groups, $^\#P < 0.05$, and NS indicate no significant differences between the two groups.

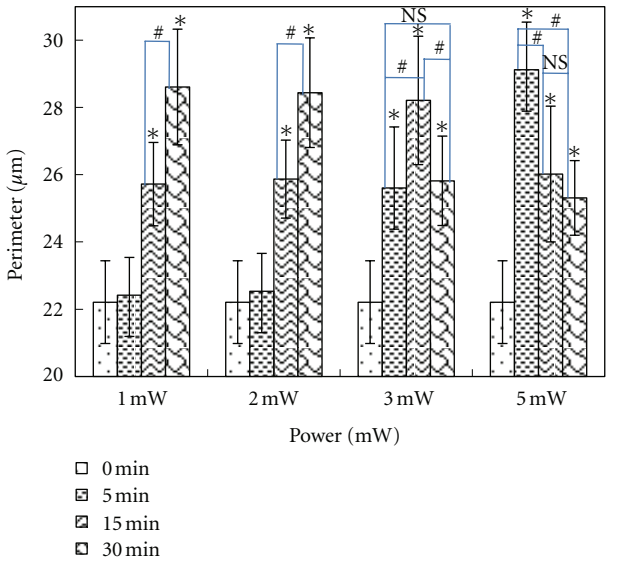

Figure 2: Effects of laser irradiation on the perimeter of dehydrated erythrocytes. Data are means ± SD. $N = 100$. $^*P < 0.05$ versus the no irradiation group as control, $^\#$indicate significant differences between the two groups, $^\#P < 0.05$, and NS indicate no significant differences between the two groups.

and Group 3 were stored at 5°C for 24 and 36 h, respectively, and received LIL after 12 h (in both groups), 24 h (in Group 2), and 36 h (in Group 3) from sampling. Iijima et al. found that the deformability was unchanged in Group 1 (fresh cell group) from the control value, but improved significantly in Groups 2 and 3 (damaged cell groups) after the LIL [8]. Spodaryk found no effects of LIL on the erythrocyte elongation index (EEI) of RBCs from healthy volunteers [9]. Kujawa et al. found LIL promoted Na^+-K^+-ATPase activity in isolated RBC membranes [3].

Function-specific homeostasis (FSH) developed from homeostasis is a negative-feedback response of a biosystem to maintain the function-specific conditions inside the biosystem so that the function is perfectly performed [1, 2]. A biosystem in an FSH means the function is in its FSH so that it is perfectly performed. A biosystem far from a FSH means the function is far from its FSH so that it is dysfunctional. The deformability of RBCs from healthy volunteers [4, 9] is in deformability-specific homeostasis (DSH), but the deformability of RBCs from pathological samples [4], Ca^{2+}-treated samples [4], or damaged cell groups [8] is far from DSH. As discussed above, LIL has no direct effects on RBC deformability in its DSH, but modulates the deformability far from its DSH. This homeostatic LPBM has been supposed to be mediated by membrane proteins [1, 2]. This membranotropic hypothesis has been supported by the LPBM on Na^+-K^+-ATPase activity in isolated RBC membranes [3]. In order to test the membranotropic hypothesis, the role of the membrane aquaporin-1 (APQ-1) in human RBCs in LPBM on RBC deformability far from its DSH was studied in this paper.

2. Materials and Methods

2.1. Blood Samples. Fresh blood from young healthy donors was immediately treated with anticoagulant heparin in tubes. Erythrocytes were collected in the bottom part of the tube after separated from the blood by centrifuging at 1200 xg for 5 min and moving out the blood plasma in the upper part of the centrifuging tube. Some of the erythrocytes were taken out and suspended in isotonic 4-(2-hydroxyethyl)-1-piperazineethanesulfonic acid buffer (HEPES) at 5% hematocrit, and the others were washed out with hypertonic solution (138 mmol/L NaCl, 5 mmol/L KCl, 10 mmol/L HEPES, and pH 7.35). It was done three times with centrifuging at 1000 xg for 10 min each time. The dehydrated erythrocytes were suspended in the hypertonic solution with 5 mmol/L glucose inside at 5% hematocrit.

2.2. Laser Irradiation. Low intensity He-Ne laser irradiation (LHNL) with 632.8 nm wavelength, 0–5 mW adjustable and continuous power output, and 12 mm beam diameter (MODEL 500-C, Guangzhou Research Institute of Laser Technology, China) were used. LHNL was applied vertically with the powers of 1.0, 2.0, 3.0 and 5.0 mW (intensities: 0.9, 1.8, 2.7, and 4.4 mW/cm^2), and radiation times of 5, 15, and 30 min, respectively.

2.3. Measurements of Morphological Parameters and Erythrocyte Elongation Index. After stereo and phase-contrast images of living RBCs were observed by a multidimensional microscope [10], their morphological parameters such as contact area, perimeter, and roundness were determined for one hundred erythrocytes [11, 12], and the EEI was calculated [9].

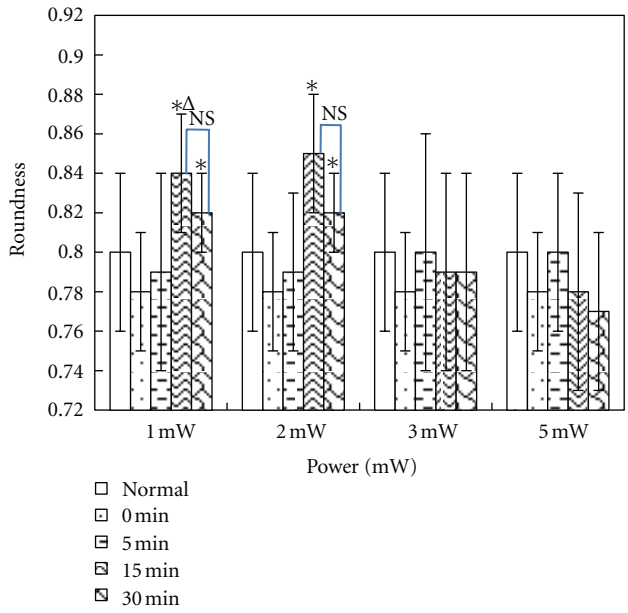

Figure 3: Effects of laser irradiation on roundness of dehydrated erythrocytes. Data are means ± SD. $N = 100$. $^*P < 0.05$ versus the no irradiation group as control. Triangles indicate significant differences between the group of 15 min × 1 mW and the group of 5 min × 3 mW, $^{\Delta}P < 0.05$, and NS indicate no significant differences between the two groups.

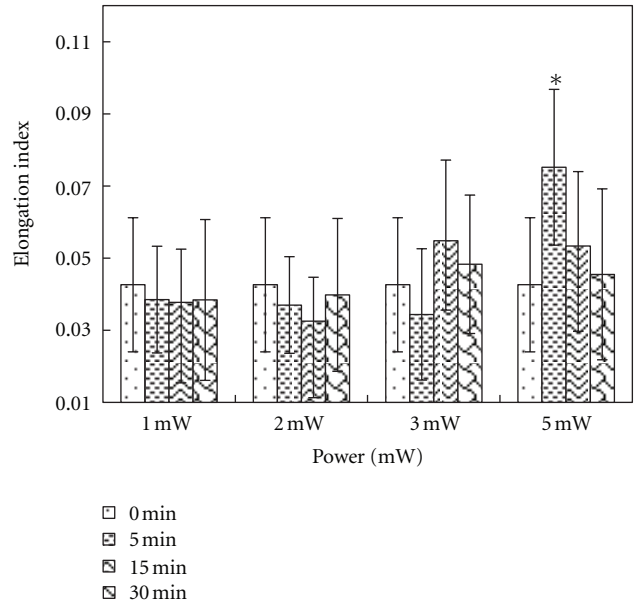

Figure 4: Effects of laser irradiation on elongation index of dehydrated erythrocytes. Data are means ± SD. $N = 100$. $^*P < 0.05$ versus the no irradiation group as control.

2.4. Erythrocytes Were Dehydrated through AQP-1 When Treated with Hypertonic Solution. To testify if normal erythrocytes were dehydrated through water channel AQP-1 when treated with the hypertonic solution, the specific inhibitor of AQP-1, $HgCl_2$ [13], was added. Normal erythrocytes were treated with $HgCl_2$ (0.2 μmol/L) [13] and then with the hypertonic solution.

2.5. Aquaporin-1 Mediated the Effects of Laser Irradiation. The dehydrated erythrocytes were treated with 0.2 μmol/L $HgCl_2$ [13] the specific blockers of AQP-1, and incubated in the hypertonic solution for 10 min at 25°C, then irradiated with LHNL at 5 mW for 5 min.

2.6. Statistical Analysis. Data are expressed as means ± standard (SD). The statistical significance was evaluated by covariance analysis and by Student's t-test with software SPSS 13.0.

3. Results

3.1. Effects of Laser Irradiation on the Morphology of Erythrocytes. The erythrocyte contact area and perimeter are positively relative with cell volume. As shown in Figures 1 and 2, the contact areas and perimeter were increased by the LHNL at 1.0, 2.0, 3.0, and 5.0 mW for 15 and 30 min, and at 3 and 5 mW for 5 min, respectively ($P < 0.05$). Among them, the best radiation time was 30 min for LHNL at 1.0 mW, 30 min for LHNL at 2.0 mW, 15 min for LHNL at 3.0 mW, and 5 min for the LHNL at 5.0 mW.

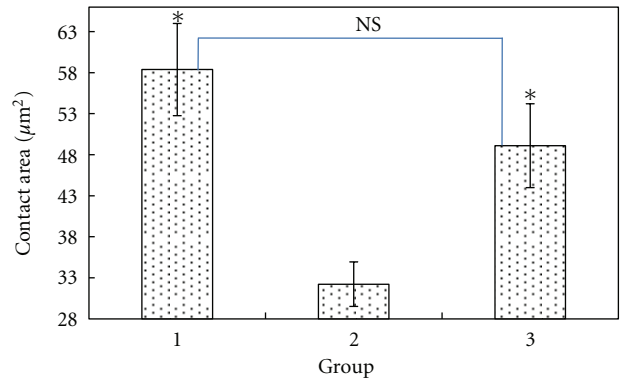

Figure 5: Effects of $HgCl_2$ on the erythrocyte section area: (1) normal erythrocytes, (2) normal erythrocytes were treated with hypertonic solution, and (3) normal erythrocytes were treated with $HgCl_2$ then the hypertonic solution. Data are means ± SD. $N = 100$. $^*P < 0.05$ versus the group 2 as control, and NS indicate no significant differences between the two groups.

The roundness represents the shape of erythrocytes. The more the roundness is close to 1, the more the cell is likely to be spherical. As shown in Figure 3, LHNL increased the roundness at 1 and 2 mW for 15 and 30 min, respectively ($P < 0.05$), but has no effects at 3 and 5 mW. Among them, the best radiation time was 15 min for LHNL at 1 and 2 mW, respectively.

EEI indicates the deformability of erythrocytes. As shown in Figure 4, LHNL increased EEI only at 5 mW for 5 min ($P < 0.05$).

3.2. $HgCl_2$ Inhibited the Effects of Hypertonic Solution on the Deformability of Erythrocytes. $HgCl_2$ is a specific inhibitor

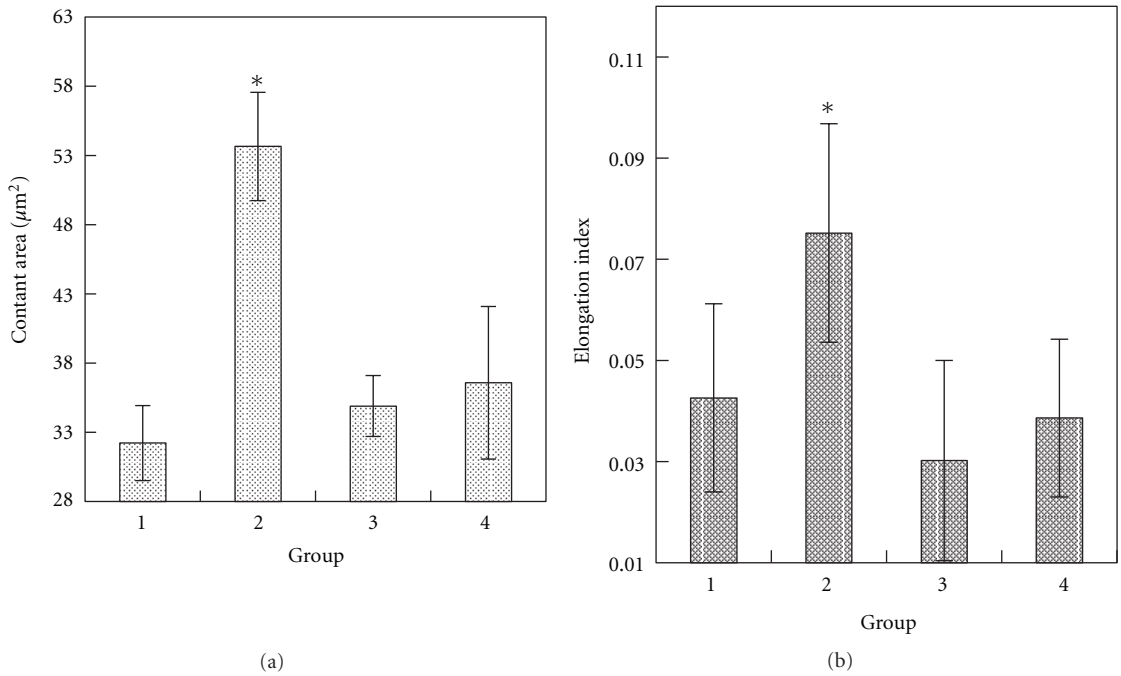

FIGURE 6: Effects of laser irradiation at 5 mW for 5 min on erythrocyte section area (a) and elongation index (b) with and without 0.2 μmol/L $HgCl_2$: (1) dehydrated erythrocytes in the hypertonic solution, (2) the dehydrated erythrocytes were irradiated with laser irradiation at 5 mW for 5 min, (3) the dehydrated erythrocytes were treated with $HgCl_2$, and (4) the dehydrated erythrocytes were treated with $HgCl_2$, then irradiated with laser irradiation at 5 mW for 5 min. Data are means ± SD. $N = 100$. $^*P < 0.05$ versus group 1 as control.

of AQP-1 [13]. In Figure 5, hypertonic solution decreased erythrocyte contact area ($P < 0.05$), but failed to do it when treated with 0.2 μmol/l $HgCl_2$.

As Figures 1–4, and previous paper [8] have shown, LHNL may improve the RBC deformability far from its DSH. In Figure 6, LHNL at 5 mW for 5 min increased the contact area and EEI of dehydrated erythrocytes ($P < 0.05$), but failed to do it when treated with 0.2 μmol/l $HgCl_2$.

4. Discussion

The present study demonstrated that LHNL may improve the deformability of human RBCs in the hypertonic solution, and the improvement might be mediated by membrane APQ-1. These results supported the membranotropic hypothesis of LPBM.

The LPBM on erythrocyte deformability has been found to be homeostatic. By using filter filtration rate, Iijima et al. found LHNL improved the erythrocyte deformability far from its DSH, but had no effects on erythrocyte deformability in its DSH [8]. By using EEI, Spodaryk found no LPBM on erythrocyte deformability in its DSH [9]. The erythrocyte deformability was induced far from its DSH in hypertonic solution in this study. By using contact area, perimeter, roundness, and EEI, we found the dosage of LPBM was morphological parameter dependent.

The reciprocity rule, Bunsen-Roscoe rule [6], should not hold, and LPBM should depend on intensity or radiation time if the dose is kept constant. From the observations of different research groups and their own observations, Sommer et al. concluded that the threshold parameters dose and intensity are biologically independent from each other [14]. Lanzafame et al. have studied the effects of red light at 670 nm from light emitting diode array on pressure ulcers of C57/BL mice, and found varying irradiance and exposure time to achieve a specified energy density affects phototherapy outcomes [15]. The reciprocity rule does not hold in our experiment in Figure 3. The two protocols (5 min × 3 mW and 15 min × 1 mW) gave the same dosage of LIL, but induced different changes in the roundness of erythrocyte ($P < 0.05$), the former one (5 min × 3 mW) caused no significant difference from the control group, but the later one (15 min × 1 mW) has significant differences from control group.

Normal erythrocytes contract and expand reversibly when hypertonic and hypotonic solution are added, but the deformability was far from its DSH when these two solutions were added [16] and even erythrocytolysis can be caused [17]. Specific water channel AQP-1 in erythrocyte membrane can mediate fast and active transport of water molecular through membranes. In numerous physiology responses, this transfer of water molecular through erythrocyte membrane by AQP-1 can have a lasting effect and cause the change of endoplasm viscosity [18]. $HgCl_2$, an inhibitor of AQP-1, can inhibit the transportation mentioned above [13]. As Figure 5 has shown, normal erythrocytes become small in hypertonic solution, but $HgCl_2$-pretreated normal erythrocytes do not. It is worth noting that PBM can inhibit erythrocytolysis in hypotonic solution [16]. In this study, by using multiparameter dynamic measurement of elastic

properties of human erythrocyte and water channel AQP-1 inhibitor $HgCl_2$, we investigated the mechanism of modulation of dehydrated erythrocyte morphological character by LHNL, and found that $HgCl_2$ can inhibit the LPBM of dehydrated erythrocyte. As Figure 6 has shown, dehydrated erythrocytes become large after LHNL, but $HgCl_2$-pretreated dehydrated erythrocytes do not. This suggests that the LPBM of dehydrated erythrocyte morphological might be mediated by AQP-1.

5. Conclusion

AQP-1 might mediate the effect of LHNL on human erythrocyte deformability, which supports the membranotropic mechanism of LPBM.

Authors' Contribution

G.-y. Luo and L. Sun are contributed equally to this work.

Acknowledgments

This work was supported by the National Science Foundation of China (60278012, 60878061), the National 973 basic project (2005CB523502), and the Opening Project of MOE Key Laboratory of Laser Life Science, South China Normal University, Guangzhou, China.

References

[1] T. C. Y. Liu and P. Zhu, Eds., *Intranasal Low Intensity Laser Therapy*, People's Military Medical Press, Beijing, China, 2009.

[2] T. C. Y. Liu, R. Liu, L. Zhu et al., "Homeostatic photobiomodulation," *Frontiers of Optoelectronics in China*, vol. 2, no. 1, pp. 1–8, 2009.

[3] J. Kujawa, L. Zavodnik, I. Zavodnik, V. Buko, A. Lapshyna, and M. Bryszewska, "Effect of low-intensity (3.75–25 J/cm2) near-infrared (810 nm) laser radiation on red blood cell ATPase activities and membrane structure," *Journal of Clinical Laser Medicine and Surgery*, vol. 22, no. 2, pp. 111–117, 2004.

[4] X. Q. Mi, J. Y. Chen, Z. J. Liang, and L. W. Zhou, "In vitro effects of helium-neon laser irradiation on human blood: blood viscosity and deformability of erythrocytes," *Photomedicine and Laser Surgery*, vol. 22, no. 6, pp. 477–482, 2004.

[5] X. Q. Mi, J. Y. Chen, and L. W. Zhou, "Effect of low power laser irradiation on disconnecting the membrane-attached hemoglobin from erythrocyte membrane," *Journal of Photochemistry and Photobiology B*, vol. 83, no. 2, pp. 146–150, 2006.

[6] T. Karu, *The Science of Low-Power Laser Therapy*, Gordon and Breach Science Publishers, Amsterdam, The Netherlands, 1998.

[7] M. T. T. Wong-Riley, H. L. Liang, J. T. Eells et al., "Photobiomodulation directly benefits primary neurons functionally inactivated by toxins: role of cytochrome c oxidase," *The Journal of Biological Chemistry*, vol. 280, no. 6, pp. 4761–4771, 2005.

[8] K. Iijima, N. Shimoyama, M. Shimoyama, and T. Mizuguchi, "Effect of low-power He-Ne laser on deformability of stored human erythrocytes," *Journal of Clinical Laser Medicine and Surgery*, vol. 11, no. 4, pp. 185–189, 1993.

[9] K. Spodaryk, "The influence of low-power laser energy on red blood cell metabolism and deformability," *Clinical Hemorheology and Microcirculation*, vol. 25, no. 3-4, pp. 145–151, 2001.

[10] Y. X. Huang, "A novel multi-dimensional microscope and its applications to nano-material measurements," *Current Applied Physics*, vol. 5, no. 5, pp. 553–556, 2005.

[11] C. Yao, Y. Huang, X. Li, and P. Ruan, "Effects of pH on structure and function of single living erythrocyte," *Chinese Science Bulletin*, vol. 48, no. 13, pp. 1342–1346, 2003.

[12] X. Y. Chen, Y. X. Huang, W. J. Liu, and Z. J. Yuan, "Membrane surface charge and morphological and mechanical properties of young and old erythrocytes," *Current Applied Physics*, vol. 7, supplement 1, pp. e94–e96, 2007.

[13] J. Voigtlaender, B. Heindl, and B. F. Becker, "Transmembrane water influx via aquaporin-1 is inhibited by barbiturates and propofol in red blood cells," *Naunyn-Schmiedeberg's Archives of Pharmacology*, vol. 366, no. 3, pp. 209–217, 2002.

[14] A. P. Sommer, A. L. B. Pinheiro, A. R. Mester, R. P. Franke, and H. T. Whelan, "Biostimulatory windows in low-intensity laser activation: lasers, scanners, and NASA's light-emitting diode array system," *Journal of Clinical Laser Medicine and Surgery*, vol. 19, no. 1, pp. 29–33, 2001.

[15] R. J. Lanzafame, I. Stadler, A. F. Kurtz et al., "Reciprocity of exposure time and irradiance on energy density during photoradiation on wound healing in a murine pressure ulcer model," *Lasers in Surgery and Medicine*, vol. 39, no. 6, pp. 534–542, 2007.

[16] C. Feo and W. M. Phillips, "The influence of suspension osmolarity and erythrocyte volume on cell deformability," *Nouvelle Revue Francaise d'Hematologie*, vol. 24, no. 5, pp. 295–299, 1982.

[17] K. Iijima, N. Shimoyama, M. Shimoyama, and T. Mizuguchi, "Red and green low-powered He-Ne lasers protect human erythrocytes from hypotonic hemolysis," *Journal of clinical laser medicine & surgery*, vol. 9, no. 5, pp. 385–389, 1991.

[18] M. A. Knepper, "The aquaporin family of molecular water channels," *Proceedings of the National Academy of Sciences of the United States of America*, vol. 91, no. 14, pp. 6255–6258, 1994.

Hindawi Publishing Corporation
International Journal of Photoenergy
Volume 2012, Article ID 489713, 5 pages
doi:10.1155/2012/489713

Research Article

Randomized, Double-Blind, and Placebo-Controlled Clinic Report of Intranasal Low-Intensity Laser Therapy on Vascular Diseases

Timon Cheng-Yi Liu,[1,2] Lei Cheng,[1] Wen-Juan Su,[3] Yi-Wen Zhang,[3] Yun Shi,[3] Ai-Hong Liu,[3] Li-Li Zhang,[3] and Zhuo-Ya Qian[3]

[1] *Laboratory of Laser Sports Medicine, South China Normal University, Guangzhou 510006, China*
[2] *Ministry of Education of China Key Laboratory of Laser Life Science, South China Normal University, Guangzhou 510006, China*
[3] *Medicine Department, Shanghai Pudong District Cancer Prevention and Cure Hospital, Pudong District, Shanghai 200126, China*

Correspondence should be addressed to Timon Cheng-Yi Liu, liutcy@scnu.edu.cn

Received 27 January 2012; Revised 21 March 2012; Accepted 27 March 2012

Academic Editor: Rui Duan

The intranasal low intensity GaInP/AlGaInP diode 650 nm laser therapy (ILGLT) might improve blood lipid and hemorheologic behavior of patients in view of its previous research, but it should be further supported by a randomized, double-blind, and placebo-controlled clinical study. In this paper, 90 patients with coronary heart disease or cerebral infarction were randomly divided into two groups, 60 in the treatment group and 30 in the control group, and were blindly treated with ILGLT at 8.38 and 0 mW/cm^2 for 30 min each time once a day ten days each session for two sessions between which there were three days for rest, respectively. Fasting blood lipid such as total cholesterol and low/high-density lipoprotein cholesterol and hemorheologic behavior such as blood viscosity, plasma viscosity, redox viscosity and red blood cell aggregation were assessed before the first treatment and after the two sessions and were found to be significantly improved by ILGLT. It was concluded that ILGLT may improve blood lipid and hemorheologic behavior of patients with coronary heart disease or cerebral infarction.

1. Introduction

Photobiomodulation (PBM) is a modulation of laser irradiation or monochromatic light (LI) on biosystems, which stimulates or inhibits biological functions but does not result in irreducible damage [1]. The LI used in PBM is always low-intensity LI (LIL), ~10 mW/cm^2, which includes the LI used in the so-called ultralow level laser therapy [2]. From 1989 on, many Russian groups have studied the therapeutic effects of intranasal LIL on the local inflammation in vasomotor rhinitis [3, 4] and acute and chronic maxillary sinusitis [5]. In the mainland of China, intranasal LIL has been studied to treat internal diseases and the special treatment was called intranasal low intensity laser therapy (ILILT) since 1998 [6, 7]. ILILT has been applied to treat hyperlipidemia, the blood-stasis syndrome of coronary heart disease (CHD), myocardial infarction, and brain diseases such as insomnia, intractable headache, Alzheimer's disease, Parkinson's disease, poststroke depression, ache in head or face, migraine, cerebral thrombosis, diabetic peripheral neuropathy, cerebral infarction (CI), acute ischemic cerebrovascular disease, brain lesion, schizophrenia, cerebral palsy, and mild cognitive impairment [6, 7]. The studies indicated that serum amyloid β protein, malformation rate of erythrocytes, plasma cholecystokinin-octapeptide, the level of viscosity at lower shear rate (3/s), hematocrit (HCT), and serum lipid decreased, respectively, and melatonin productionred cell deformability, superoxidase dismutase activity, and β endorphin increased, respectively; blood circulation was improved, and immunity was regulated after ILILT [6, 7].

ILILT might be a systemic effect. Nose-mediated therapeutics in traditional Chinese medicine (TCM) has been a very old system [8]. The nasal cavity has long been hypothesized to play an important role in climatic adaptation. The bony nasal cavity appears mostly associated with temperature, and the nasopharynx with humidity [9]. The nose might play more roles in disease treatment [6–9]. There are five possible pathways mediating the ILILT, olfactory nerve, nasal bone, blood cells, meridians in TCM and autonomic nervous system (ANS) [6, 7]. As Wilson et al. have reviewed [10], some impaired olfaction in old age is associated with postmortem evidence of neurodegenerative disease, particularly neurofibrillary tangles and Lewy bodies. These associations, which are present even in the absence of dementia, may explain why olfactory impairment predicts important consequences of neurodegenerative conditions including cognitive decline, incidence of mild cognitive impairment and dementia, incidence of Parkinson's disease, worsening parkinsonian gait, and neuropsychiatric complications of Parkinson's disease [10]. Mesenchymal stem cells/marrow stromal cells (MSCs) in nasal bone might mediate ILILT. MSCs present a promising tool for its cell therapy and are currently being tested in US FDA-approved clinical trials for MI, stroke, meniscus injury, limb ischemia, graft-versus-host disease, autoimmune disorders, and so on. They have been extensively tested and proven effective in preclinical studies for these and many other disorders. It has been found that the therapeutic effects of bone marrow irradiation with LIL on rat MI have been more significant than the ones of MI irradiation, and the effects have been mediated by MSCs [11]. Blood cells mediate the therapeutic effects of intranasal PBM on the local inflammation. Tulebaev et al. have found the LIL-treated patients with vasomotor rhinitis showed a significant increase of T lymphocytes and a higher capacity of T cells to form the migration inhibition factor [3]. Shevrygin et al. have shown that LIL is effective in correction of microcirculatory disorders and tissue mechanisms of homeostasis in children with neurovegetative vasomotor rhinitis [4]. Kruchinina et al. have studied therapeutic effect of LIL on microcirculation of nasal mucosa in children with acute and chronic maxillary sinusitis, and found that laser therapy produced a positive effect on microcirculation and reduced the potential of relapses [5]. As it has been indicated in this paper, ILILT might improve blood cells. There are six meridians inside/around nose, *stomach* meridian of foot *yang-ming*, *du* meridian, *yin-jiao* meridian, *yang-jiao* meridian, *large intestine* meridian of hand *yang-ming*, and *small intestine* meridian of hand *tai-yang*. These six meridians can be irradiated by intranasal LIL through intranasal multiple reflex. They were supposed to mediate some of the therapeutic effects of ILILT. The central ANS functions at maintaining cardiovascular hemodynamics. There is crosstalk between nasal ANS and central ANS [12]. The central ANS activities significantly correlated with changes to the nasal airway during postural change. The central ANS, especially the sympathetic nervous system, may play a role in controlling nasal airway during postural change. Therefore, nasal ANS might mediate ILILT.

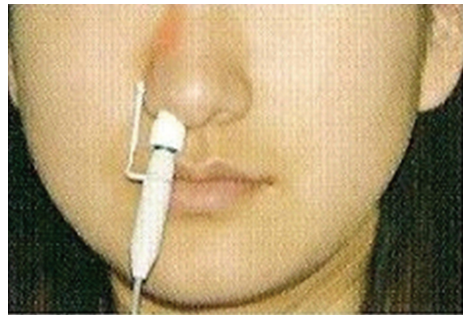

Figure 1: The setup of ILGLT at 650 nm and 8.38 mW/cm^2.

As it has been discussed above, ILILT might be a systemic effect. However, its studies have not been randomized, double-blind, and placebo-controlled. In this paper, a randomized, double-blind, and placebo-controlled clinical study was designed to assess the effects of intranasal low intensity GaInP/AlGaInP diode 650 nm laser therapy (ILGLT) on the blood lipid and hemorheologic behavior of patients with CHD or CI.

2. Materials and Methods

The study protocol was approved by the ethics committee of the Faculty of Medicine, Shanghai Pudong District Cancer Prevention and Cure Hospital, Shanghai, China. Informed consent was obtained from each participant prior to the start of treatment.

2.1. Patients. The 90 clinic patients, 49 men and 41 women, with CHD or CI in Shanghai Pudong District Cancer Prevention and Cure Hospital from January to March in 2008, were approached to participate in this study. By conventional WHO criteria, CHD was diagnosed in terms of electrocardiogram and coronary angiography, and CI was diagnosed in terms of coronal computer tomography appearance. The patients were divided randomly into treatment group with 60 patients and control group with 30 patients. There were no significant differences of gender, age, and type of disease between the two groups ($P > 0.05$) (Table 1).

2.2. Laser Irradiation. BLOODCARE Medical Laser Device manufactured with GaInP/AlGaInP diode 650 nm laser by Shanghai Taicheng (TCM) Technology and Development Co. Ltd. It has been applied to irradiate the patients intranasally (Figure 1) 30 min each time once a day ten days each session for two sessions between which there were 3 days for rest. The treatment group and the control group were irradiated at 8.38 mW/cm^2 (the spot area is 0.358 cm^2) and 0 mW/cm^2, respectively, and no other treatments have been done.

2.3. Blood Viscosity Assays. There were no dietary restrictions on the patients, but the patients fasted before their blood was drawn. Blood samples were collected according to routine clinical protocol. Venous blood was withdrawn to detect the hemorheological indexes, using an automatic analyzer

Table 1: General Information of the two groups ($X \pm$ S.E.M).

Group	Patients (n)	Gender		Age (years)	CHD (n)	CI (n)	CHD and CI (n)
		Male	Female				
Treatment Group	60	34	26	76.6 ± 7.81	21	20	19
Control Group	30	15	15	75.5 ± 9.52	13	14	3
Value		0.358		0.561*		5.157	
P		>0.05		>0.05		>0.05	

Note: *for t value and the rest for x^2 value.

(Zhongchiweiye, ZL9000plus), including blood viscosity and redox viscosity at low (3/s) and high (200/s) shear rates, plasma viscosity at low shear rate (3/s), HCT, and erythrocyte aggregation index. The equipment was operated according to the protocols by the technicians at the Department of Clinical Laboratory in Shanghai Pudong District Cancer Prevention and Cure Hospital.

2.4. Blood Lipid Assays. Blood lipid profile was determined with Hitachi 7600 biochemistry automatic analyzer (Hitachi, Tokyo, Japan). Triglyceride (TG), total cholesterol (TC), and high-density lipoprotein cholesterol (HDL-c) were measured with enzymatic methods. Low-density lipoprotein-cholesterol (LDL-c) was calculated according to the Friedewald formula. Apolipoprotein A-I (ApoA-I) and Apolipoprotein B (ApoB) were determined by immunoturbidimetric assays.

2.5. Statistical Analysis. Data are expressed as mean ± S.E.M. Differences between means were tested for statistical significance by a t-test or x^2-test. The statistical level of significance was set at $P < 0.05$.

3. Results

3.1. Changes of Blood Viscosity. As shown in Table 2, blood viscosity (high shear rate at 200/s) ($P < 0.05$), plasma viscosity (low shear rate at 3/s) ($P < 0.05$), and red blood cell aggregation ($P < 0.01$) decreased significantly after the therapy in the treatment group, but there were no significant changes in the control group. It was also shown that blood viscosity (low shear rate at 3/s) kept unchanged ($P > 0.05$), and blood redox viscosity (high shear rate at 200/s or low shear rate at 3/s) decreased significantly ($P < 0.01$) after ILILT in the treatment group when the corresponding blood parameters became worse in the control treatment.

3.2. Changes of Blood Lipid Metabolite. As shown in Table 3, TC decreased significantly ($P < 0.05$) in the treatment group but there were no significant changes in the control group, LDL-c decreased significantly ($P < 0.05$) in the treatment group although LDL-c increased significantly ($P < 0.001$) in the control group, and HDL-c increased significantly ($P < 0.01$) from 1.07 mmol/L to 1.20 mmol/L but there were no significant changes in the control group. It was also shown that there were no changes in TG, ApoA-I, ApoB, and the ratio of ApoA-I to ApoB either in the treatment group or in the control group.

4. Discussion

The above results indicated that ILGLT improved blood lipid and hemorheologic behavior of patients with CHD or CI. These phenomena would be discussed from homeostatic viewpoint.

Homeostasis is one of the most remarkable and most typical properties of a highly complex open biosystem [13, 14]. It is a negative feedback response of a biosystem to maintain constant conditions inside the biosystem. This is a classic concept in physiology. However, oscillations are found at nearly every level of biology. It is too obscure to be studied so that it has been developed as function-specific homeostasis (FSH) [1, 6]. FSH is a negative-feedback response of a biosystem to maintain the function-specific fluctuations inside the biosystem so that the function is perfectly performed. A biosystem in a FSH means the function is in its FSH so that it is perfectly performed. A biosystem far from a FSH means the function is far from its FSH so that it is dysfunctional. A health person is in homeostasis so that all of his/her physiological functions are in their respective FSH, and we have physiological function-specific homeostasis (PhFSH) in which the physiological function can completely perform. A pathological function defined as a disease-specific physiological function which is far from the corresponding PhFSH, but may be in its pathological function-specific homeostasis (PaFSH).

There was no direct PBM of LIL (LPBM) on a function in its FSH [1, 6]. A function in its FSH can resist against weak disturbance such as LIL so that LIL cannot directly modulate a function in its FSH. Tables 2 and 3 suggested that the HCT, TG, Apo A-I, and Apo B of the patients with CHD or CI were in HCT-specific homeostasis (HSH), TG-specific homeostasis (TSH), Apo A-I-specific homeostasis (AaSH), and Apo B-specific homeostasis (AbSH), respectively. Among these four kinds of FSH, the HSH, AaSH, and AbSH may be a kind of PhFSH [15, 16], but the TSH might be a kind of PaFSH [16].

There was LPBM on a function far from its FSH [1, 6], but the modulation mechanism of different functions may be different. One of the pathways mediating ILILT might be melatonin [7]. It has been found that ILILT can increase serum melatonin level [6, 7]. Hoyos et al. have investigated the effect of melatonin, at pharmacological doses, on serum lipids of rats fed with a hypercholesterolemic

Table 2: Blood viscosity index (mean ± S.E.M).

BV	Treatment group (n)		Verified statistics		Control group (n)		Verified statistics	
	Before	After	T	P	Before	After	T	P
BV(l)	8.34 ± 1.91	8.15 ± 1.91	0.545	>0.05	6.54 ± 1.75	7.87 ± 1.99	2.735	<0.05
BV(h)	4.23 ± 0.82	3.94 ± 0.74	2.020	<0.05	3.56 ± 0.65	4.02 ± 1.64	1.428	>0.05
PV	1.23 ± 0.02	1.14 ± 0.22	2.233	<0.05	1.23 ± 0.18	1.23 ± 0.01	—	—
HCT	39.88 ± 7.72	41.66 ± 4.79	1.526	>0.05	37.92 ± 6.04	38.55 ± 6.52	0.388	>0.05
RV(l)	17.35 ± 4.03	15.24 ± 2.82	3.323	<0.01	14.09 ± 3.26	16.88 ± 4.04	2.944	<0.01
RV(h)	6.99 ± 0.75	6.63 ± 0.55	2.120	<0.05	6.27 ± 1.17	7.21 ± 1.54	2.662	<0.05
RBCA	2.15 ± 0.41	1.95 ± 0.24	3.263	<0.01	1.77 ± 0.35	1.92 ± 0.23	1.961	>0.05

BV: blood viscosity, WBV: Whole blood viscosity, PV: plasma viscosity at low shear rate (3/s), RV: redox viscosity, RBCA: red blood cell aggregation, HCT: hematocrit, h: high shear rate at 200/s, l: low shear rate at 3/s.

Table 3: Blood lipid index (mean ± S.E.M).

BL	Treatment group (n)		Verified statistics		Control group (n)		Verified statistics	
	Before	After	T	P	Before	After	T	P
TC (mmol/L)	4.44 ± 1.72	3.78 ± 0.95	2.603	<0.05	4.10 ± 1.15	4.07 ± 1.26	0.096	>0.05
TGs (mmol/L)	1.88 ± 0.67	1.70 ± 0.77	1.366	>0.05	1.85 ± 0.71	1.87 ± 0.70	0.110	>0.05
HDL-c(mmol/L)	1.07 ± 0.27	1.20 ± 0.24	2.790	<0.01	1.00 ± 0.31	1.17 ± 0.41	1.812	>0.05
LDL-c (mmol/L)	2.73 ± 0.76	2.48 ± 0.51	2.115	<0.05	1.39 ± 0.70	2.33 ± 0.93	4.424	<0.001
ApoA-I (g/L)	1.29 ± 0.29	1.35 ± 0.27	1.367	>0.05	1.24 ± 0.26	1.22 ± 0.34	0.256	>0.05
ApoB (g/L)	0.89 ± 0.29	0.81 ± 0.19	1.788	>0.05	0.81 ± 0.29	0.86 ± 0.33	0.125	>0.05
A/B	1.58 ± 0.43	1.64 ± 0.42	0.733	>0.05	1.54 ± 0.44	1.55 ± 0.49	0.083	>0.05

BL: blood lipid, TC: total cholesterol, TGs: triglycerides, HDL-c(LDL-c): high(low)-density lipoprotein cholesterol, ApoA-I(ApoB): Apolipoprotein A-I(Apolipoprotein B), A/B: ApoA-I/ApoB.

diet [17]. Different groups of animals were fed with either the regular Sanders Chow diet or a diet enriched in cholesterol. Moreover, animals were treated with or without melatonin in the drinking water for 3 months. They found that melatonin treatment did not affect the levels of cholesterol or triglycerides in rats fed with a regular diet. However, the increase in TC and LDL-c induced by a cholesterol-enriched diet was reduced significantly by melatonin administration. On the other hand, melatonin administration prevented the decrease in HDL-c induced by the same diet. However, no differences in the levels of TGs were found. Obviously, ILGLT and melatonin play roles similar to each other on TGs, HDL-c, and LDL-c as Table 3 has shown.

Nicotinamide adenine dinucleotide (NAD^+) might also be one of the pathways mediating ILILT [7]. ILILT can increase serum melatonin level [6, 7] and then NAD^+ level [18]. ILILT might directly increase the ratio of intracellular NAD^+ level and the intracellular level of its reduced form NADH, NAD^+/NADH. Karu has studied the cellular response of LIL from the viewpoint of cellular redox potential and suggested that the cellular response is absent when the redox potential is optimal, and stronger when the redox potential of the target cell is initially shifted to a more reduced state [19]. The cellular redox potential might be represented by NAD^+/NADH [19]. A normally functioning cell in its FSH has its specific redox potential and NAD^+/NADH, respectively, which are referred as the FSH-specific redox potential (FSR) and the FSH-specific NAD^+/NADH (FSN), respectively. A dysfunctional cell far from its FSH is initially shifted to a more reduced state with lowered NAD^+/NADH. In terms of Karu's suggestion [19], the magnitude of LPBM is determined by redox potential or NAD^+/NADH of the cell at the moment. LPBM may enhance the redox potential and NAD^+/NADH, respectively, in cells far from their FSH. The lower the redox potential below the FSR is, the lower the NAD^+/NADH below FSN will be, and the stronger the LPBM will finally be in terms of Karu's suggestion [19]. There is connexin 43 (Cx43), a NAD^+ transporter, in the cellular membrane so that there is bidirectional NAD^+ transport across cellular membrane [20]. ILILT may enhance NAD^+ level in the irradiated blood cells, and then in the blood through Cx43, and then in the unirradiated cells through Cx43, which increase NAD^+/NADH in both the irradiated cells and the un-irradiated cells. Niacin is a precursor of NAD^+ and, as such, may increase NAD^+/NADH [21]. Montefusco et al. have investigated whether acipimox, a nicotinic acid analog, improved hemorheological parameters [22]. 21 patients (17 Males, 4 Females) with asymptomatic hypertriglyceridemia were treated with acipimox (250 b.i.d.) for 30 days. They found that blood viscosity decreased ($P <$ 0.05 and < 0.01) (range of reduction 6–20%) at all shear rates examined (from $2.25\,s^{-1}$ to $450\,s^{-1}$) and plasma viscosity was significantly reduced only at lower shear rates (2.25 and $4.50\,s^{-1}$). In type 2 hypertensive diabetes patients, niceritrol, a pentaerythritol ester containing four niacin residues and aspirin (162/mg per day) that reduced blood viscosity at low ($37.6\,s^{-1}$) and high ($376\,s^{-1}$) shear rates, did not modulate HCT [23]. Obviously, ILGLT and niacin played roles similar

to each other on blood and plasma viscosity as Table 2 has shown.

5. Conclusion

ILGLT may improve blood lipid and hemorheologic behavior of patients with CHD or CI.

Conflict of Interests

No competing financial interests exist.

Acknowledgments

This work was supported by National Science Foundation of China (60878061), and the Opening Project of MOE Key laboratory of Laser Life Science, South China Normal University, Guangzhou, China.

References

[1] T. C. Y. Liu, R. Liu, L. Zhu, J. Q. Yuan, M. Hu, and S. H. Liu, "Homeostatic photobiomodulation," *Frontiers of Optoelectronics in China*, vol. 2, no. 1, pp. 1–8, 2009.

[2] L. Baratto, L. Calzà, R. Capra et al., "Ultra-low-level laser therapy," *Lasers in Medical Science*, vol. 26, no. 1, pp. 103–112, 2011.

[3] R. K. Tulebaev, S. B. Sadykov, V. A. Romanov, and G. K. Khalitova, "Indicators of the activity of the immune system during laser therapy of vasomotor rhinitis," *Vestnik Otorinolaringologii*, no. 1, pp. 46–49, 1989 (Russian).

[4] B. V. Shevrygin, S. V. Rybalkin, F. F. Pekli, and L. V. Feniksova, "Correction of microcirculatory disorders with low-energy laser radiation in children with vasomotor rhinitis," *Vestnik Otorinolaringologii*, no. 2, pp. 31–33, 2000 (Russian).

[5] I. Kruchinina, L. V. Feniksova, S. V. Rybalkin, and F. F. Pekli, "Therapeutic effect of helium-neon laser on microcirculation of nasal mucosa in children with acute and chronic maxillary sinusitis as measured by conjunctival biomicroscopy," *Vestnik Otorinolaringologii*, no. 3, pp. 26–30, 1991 (Russian).

[6] C. Liu and P. Zhu, *Intranasal Low Intensity Laser Therapy*, People's Military Medical Press, Beijing, China, 2009.

[7] T. C. Y. Liu, D. F. Wu, Z. Q. Gu, and M. Wu, "Applications of intranasal low intensity laser therapy in sports medicine," *Journal of Innovation in Optical Health Science*, vol. 3, no. 1, pp. 1–16, 2010.

[8] S. Gao, *Nose Therapy*, Huaxia Publishing House, Beijing, China, 1994.

[9] M. L. Noback, K. Harvati, and F. Spoor, "Climate-related variation of the human nasal cavity," *American Journal of Physical Anthropology*, vol. 145, no. 4, pp. 599–614, 2011.

[10] R. S. Wilson, L. Yu, and D. A. Bennett, "Odor identification and mortality in old age," *Chemical Senses*, vol. 36, no. 1, pp. 63–67, 2011.

[11] H. Tuby, L. Maltz, and U. Oron, "Induction of autologous mesenchymal stem cells in the bone marrow by low-level laser therapy has profound beneficial effects on the infarcted rat heart," *Lasers in Surgery and Medicine*, vol. 43, no. 5, pp. 401–409, 2011.

[12] J. H. Ko, T. B. J. Kuo, and G. S. Lee, "Effect of postural change on nasal airway and autonomic nervous system established by rhinomanometry and heart rate variability analysis," *American Journal of Rhinology*, vol. 22, no. 2, pp. 159–165, 2008.

[13] W. B. Cannon, *The Wisdom of the Body*, W. W. Norton, New York, NY, USA, 1932.

[14] D. S. Jones, *Textbook of Functional Medicine*, The Institute for Functional Medicine, Gig Harbor, Wash, USA, 2006.

[15] T. Kunnas, T. Solakivi, K. Huuskonen, A. Kalela, J. Renko, and S. T. Nikkari, "Hematocrit and the risk of coronary heart disease mortality in the TAMRISK study, a 28-year follow-up," *Preventive Medicine*, vol. 49, no. 1, pp. 45–47, 2009.

[16] G. Walldius and I. Jungner, "Apolipoprotein B and apolipoprotein A-I: risk indicators of coronary heart disease and targets for lipid-modifying therapy," *Journal of Internal Medicine*, vol. 255, no. 2, pp. 188–205, 2004.

[17] M. Hoyos, J. M. Guerrero, R. Perez-Cano et al., "Serum cholesterol and lipid peroxidation are decreased by melatonin in diet-induced hypercholesterolemic rats," *Journal of Pineal Research*, vol. 28, no. 3, pp. 150–155, 2000.

[18] M. Bubis and N. Zisapel, "A role for NAD^+ and cADP-ribose in melatonin signal transduction," *Molecular and Cellular Endocrinology*, vol. 137, no. 1, pp. 59–67, 1998.

[19] T. Karu, *The Science of Low-Power Laser Therapy*, Gordon and Breach Science Publishers, Amsterdam, The Netherlands, 1998.

[20] S. Bruzzone, L. Guida, E. Zocchi, L. Franco, and A. De Flora, "Connexin 43 hemi channels mediate Ca^{2+}-regulated transmembrane NAD^+ fluxes in intact cells," *FASEB Journal*, vol. 15, no. 1, pp. 10–12, 2001.

[21] R. S. Rosenson, "Antiatherothrombotic effects of nicotinic acid," *Atherosclerosis*, vol. 171, no. 1, pp. 87–96, 2003.

[22] S. Montefusco, G. Iannaci, A. Gnasso, C. Cortese, F. Lamenza, and A. Postiglione, "Blood and plasma viscosity after acipimox treatment in hypertriglyceridemic patients," *International Journal of Clinical Pharmacology Therapy and Toxicology*, vol. 26, no. 10, pp. 492–494, 1988.

[23] T. Hamazaki, K. Hasunuma, and S. Kobayashi, "The effects of lipids, blood viscosity and platelet aggregation of combined use of niceritrol (Perycit) and a low dose of acetylsalicylic acid," *Atherosclerosis*, vol. 55, no. 1, pp. 107–113, 1985.

Hindawi Publishing Corporation
International Journal of Photoenergy
Volume 2012, Article ID 920671, 6 pages
doi:10.1155/2012/920671

Research Article

Light-Emitting Diode-Based Illumination System for *In Vitro* Photodynamic Therapy

Defu Chen, Huifen Zheng, Zhiyong Huang, Huiyun Lin, Zhidong Ke, Shusen Xie, and Buhong Li

Key Laboratory of OptoElectronic Science and Technology for Medicine, Ministry of Education, and Fujian Provincial Key Laboratory for Photonics Technology, Fujian Normal University, Fujian 350007, China

Correspondence should be addressed to Buhong Li, bhli@fjnu.edu.cn

Received 19 October 2011; Revised 20 January 2012; Accepted 24 January 2012

Academic Editor: Timon Cheng-Yi Liu

The aim of this study is to develop a light-emitting diode- (LED-) based illumination system that can be used as an alternative light source for *in vitro* photodynamic therapy (PDT). This illumination system includes a red LED array composed of 70 LEDs centered at 643 nm, an air-cooling unit, and a specific-designed case. The irradiance as a function of the irradiation distance between the LED array and the sample, the homogeneity and stability of irradiation, and the effect of long-time irradiation on culture medium temperature were characterized. Furthermore, the survival rate of the CNE1 cells that sensitized with 5-aminolevulinic acid after PDT treatment was evaluated to demonstrate the efficiency of the new LED-based illumination system. The obtained results show that the LED-based illumination system is a promising light source for *in vitro* PDT that performed in standard multiwell plate.

1. Introduction

Photodynamic therapy (PDT) is an emerging, minimally invasive therapeutic procedure that can selectively destroy the tumor tissue with photosensitizers activated by specific-wavelength light in the presence of oxygen [1, 2]. Upon absorption of the light, the photosensitizer initiates photochemical reactions that result in formation of reactive oxygen species (ROS), particularly singlet oxygen ($^1O_2$), which can cause significant cytotoxicity leading to cell death by apoptosis or necrosis within the target tissue [3, 4]. It is widely known that the irradiated light is one of the primary components of PDT, and thus the choice of light sources is crucial for PDT studies [5].

As for the PDT treatments, a stable, wavelength-specific, homogeneous, and large-area illumination is badly needed. Nowadays, a wide range of laser and nonlaser light sources have been used for PDT [5–9]. Laser light sources are not only very expensive, but also a specifically tailored optical system is required to expand the beam for the irradiation of large area. In particular, for the *in vitro* PDT measurement that performed in the standard multiwell plate, each well has to be irradiated one by one, which is a time-consuming experiment for PDT studies. The nonlaser light sources such as the conventional lamps (e.g., conventional tungsten filament and xenon arc lamps) can be used in conjunction with the optical filters to output specific wavelength for treatment of larger area [2, 6]. However, the irradiation devices based on the conventional lamps may lead to significant thermal effect, which should be avoided during PDT treatments [5, 6].

With the recent developments in high-power light-emitting diodes (LEDs), LEDs have been used as an alternative light source for PDT [5–11]. Compared to other available light sources for PDT, the advantages of LEDs include less expensive, less hazardous, thermally nondestructive, and readily available [11–13]. Moreover, LEDs can be arranged in arrays flexibly to irradiate large area according to the geometry of target area [2, 6, 12]. In this study, an LED based illumination system was developed, and the major properties of the illumination system, such as the irradiance as a function of the irradiation distance between the LED

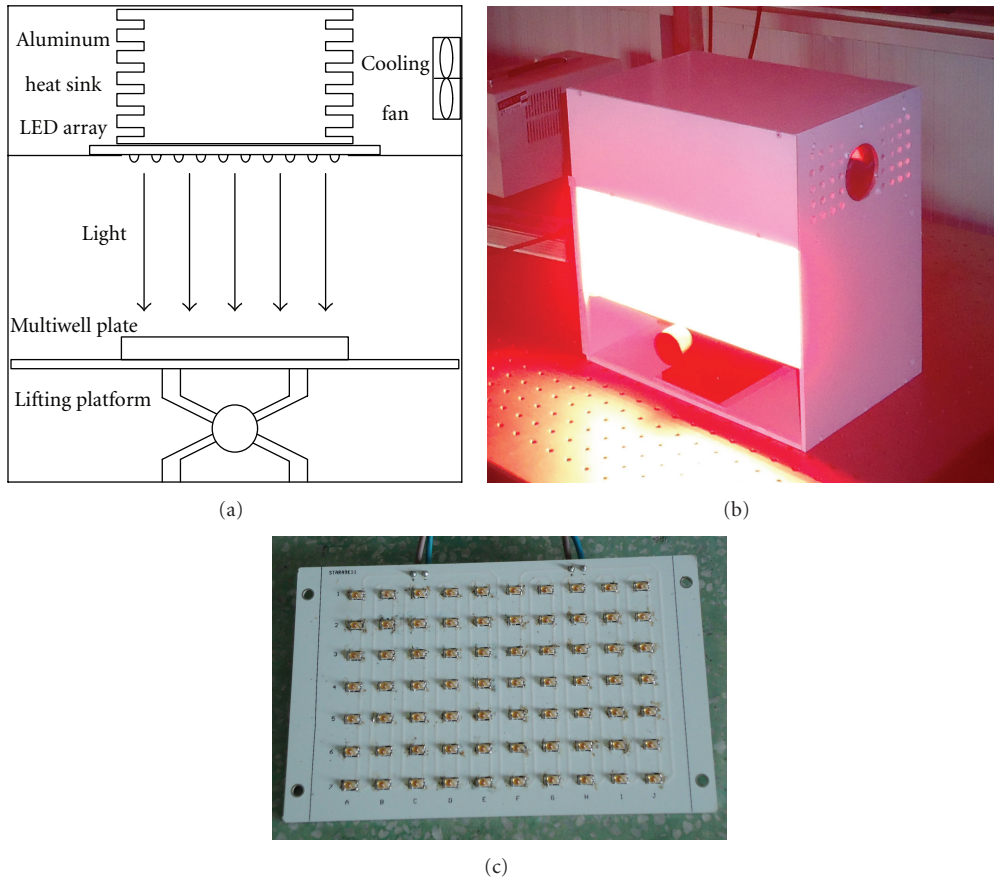

Figure 1: (a) Schematic diagram of the red LED based illumination system. (b) Photograph of the red LED based illumination system for PDT studies. (c) Prototype of the 10 × 7 LED array.

array and the sample, the homogeneity and stability of irradiation, and the effect of long-time irradiation on culture medium temperature, were characterized. In addition, in order to evaluate the efficiency of the illumination system, the survival rate of the CNE1 cells that sensitized with 5-aminolevulinic acid- (5-ALA-) mediated PDT was determined.

2. Experimental Section

2.1. Apparatus Design. A compact LED array-based illumination system with a homogeneous illumination area was proposed specifically for *in vitro* PDT, which usually perform for the cells grown in the standard multiwell plates (6-, 12-, 24-, 96-, or 384-well). The illumination system mainly includes a LED array and a specific case, and the LED array and the standard multiwell plate are both placed into the case. The arrangement of the LED array can be adjusted according to the distance between the LED array and the standard multiwell plate. In order to achieve the desired irradiance and homogeneity for *in vitro* PDT in standard multiwell plates, geometric optics simulation was conducted to optimize the design parameters (e.g., the arrangement of the LED array and the size of the case) for the proposed illumination system. The performances of the illumination system were characterized by evaluating the average irradiance produced on the area of the standard multiwell plate and the corresponding spatial non-homogeneity, which can be defined as the irradiance varied within the target area.

2.2. Construction of the Illumination System. As shown in Figures 1(a) and 1(b), the proposed illumination system includes a red LED array, an air-cooling unit and a specificde-signed case. The LED array composed of 70 LEDs (LXML-PD01-0040, LUXEON Rebel, Philips Lumileds lighting co., San Jose, CA, USA) in a 10 × 7 arrangement, which was illustrated in Figure 1(c), and the distance between the LEDs was 13 mm. Each single LED was soldered into a standard printed circuit board (size 16.3 × 10.3 cm, Fujian Xiangyun Photo-electric Technology Co., Ltd, Fuzhou, China) and connected in series. The LED array was mounted on the interlayer in the custom-designed case that fabricated in aluminum alloy (dimension 30.0 × 20.0 × 31.5 cm), and the LED array could be easily dismounted for exchange if needed. The air-cooling unit consisted of an aluminum heat sink and a cooling fan. In order to achieve the efficient heat transfer, the aluminum heat sink was attached tightly to the back surface of the printed circuit board, while the cooling fan was used to blow air for further dissipating heat. The standard multiwell plate containing samples was placed on a

lifting platform and can be irradiated directly under the LED array. The distance between the LED array and the lifting platform can be precisely adjusted in 1 mm steps vertically.

2.3. Measurement of the Spectrum and Irradiance of the Illumination System. The spectral emission for the red LED array was recorded with a spectrometer (USB4000, Ocean Optics inc., Dunedin, FL, USA) with a spectral resolution of approximately 0.2 nm in a range of 600–700 nm. Meanwhile, a laser power meter (FieldMaxII-Top, Coherent Inc., Santa Clara, CA, USA) with a 1.9 cm diameter circular effective sensing area was used to measure the irradiance.

2.4. Measurement of the Irradiance Homogeneity. The laser power meter was further used to measure the light distribution. The 1.9 cm diameter circular sensor defines the spatial resolution of each measurement. For determination of the homogeneity, the circular sensor was placed on a 1.9 $\times$ 1.9 cm grid, and the intensity was measured for each *x/y* position within the irradiated area.

2.5. Determination of Media Temperature during the Irradiation. 100 μL RPMI 1640 medium was put into each well of the 96-well plates to simulate the PDT *in vitro* experiment. The temperature of the culture medium was continually recorded by using a thermocouple data logger (TC-08, Pico technology Ltd., St Neots, Cambridgeshire, UK) over 20 min upon irradiation at room temperature.

2.6. Cell Lines and Culture Conditions. The CNE1 cell line was purchased from Guangzhou Taisheng Bio-Tech Co., Ltd. (Guangzhou, China). The cells were routinely cultured in RPMI 1640 medium supplemented with 10% new born calf serum (NBCS) and antibiotics (penicillin 200 U/mL and streptomycin 200 μg/mL), and the cells were maintained under the standard culture conditions at 37°C in a humidified 5% CO_2 incubator.

2.7. Cytotoxic Effect of In Vitro PDT. CNE1 cells were seeded into in a 96-well black wall/clear bottom costar plate (COSTAR 3603, Corning Inc., Corning, NY, USA) at a density of approximately 7500 cells per well and left to attach overnight. The medium was replaced with 100 μL serum-free culture medium containing 1 mM 5-ALA (Sigma-Aldrich, St. Louis, MO, USA) and incubated for 4 h. Then the cells were washed twice with PBS and re-fed with fresh culture medium. In order to obtain different light dosages for PDT evaluations, six optical attenuators (size 4 $\times$ 4 cm, Giai Photonics Co., Ltd, Shenzhen, China) with the transmissivity values of 0, 20%, 40%, 60%, 80%, and 100% were put onto the wells of the 96-well plate. Thereafter, the cells were illuminated for 20 min, while the control experiment representing the CNE1 cells incubated with 5-ALA but without light irradiation was performed in parallel. After the treatment, the cells were washed and were kept for 24 h under normal culture conditions for further evaluation of cell viability. Cell survival was determined by using standard MTT assay [14]. The optical density (OD) values were measured with the Mithras LB 940 plate reader (Berthold Technologies, Bad Wildbad, Germany) at 490 nm. Finally, the survival rate of the CNE1 cells under each attenuator was calculated by means of the following formula [15]:

$$\text{Survival rate (\%)} = \frac{\text{mean OD value of the irradiated cells}}{\text{mean OD value of the control cells}} \times 100. \quad (1)$$

2.8. Statistical Analysis. All the measured data were processed and analyzed by using OriginPro 8.0 software (OriginLab Corp., Northampton, MA, USA). Data were presented as means $\pm$ the standard deviation (SD) of three independent measurements.

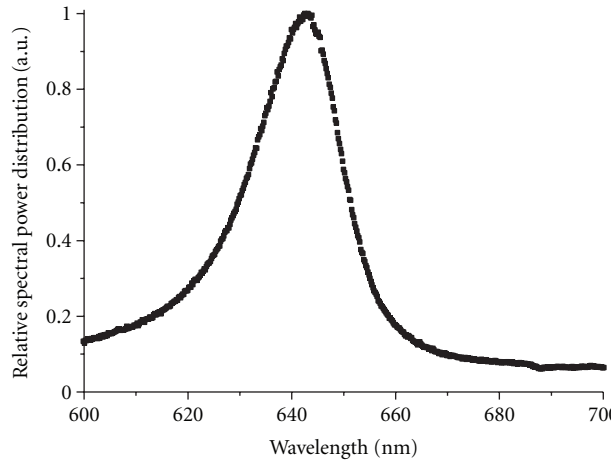

Figure 2: The normalized spectral emission of the LED array.

3. Results

3.1. The Spectrum and Irradiance of the LED-Based Illumination System. The normalized spectral emission for the LED array was shown in Figure 2. Peak power was found at the wavelength of 643 nm with a full width at half maximum (FWHM) of 21 nm. The irradiance emitted by the LED array is depending on the irradiation distance between the LED array and the irradiated sample. As shown in Figure 3, the irradiances were measured at five spots on the lifting platform for each irradiation distance by increasing the irradiation distance from 34 to 174 mm in 10 mm step. The irradiances decreased with the increasing of the irradiation distance and can be continuously adjusted in a range from 18 to 54 mW/cm^2. Moreover, the lower standard deviation of irradiances corresponding to better homogeneity can be found for the larger irradiation distance. Since the most commonly used irradiance is about 20 mW/cm^2 for *in vitro* PDT studies, the optimal irradiation distance can be determined to be about 164 mm for the present illumination system.

3.2. The Irradiance Homogeneity of the Treatment Area. When the irradiation distance was fixed at 164 mm, the irradiance distribution under the LED array was shown in

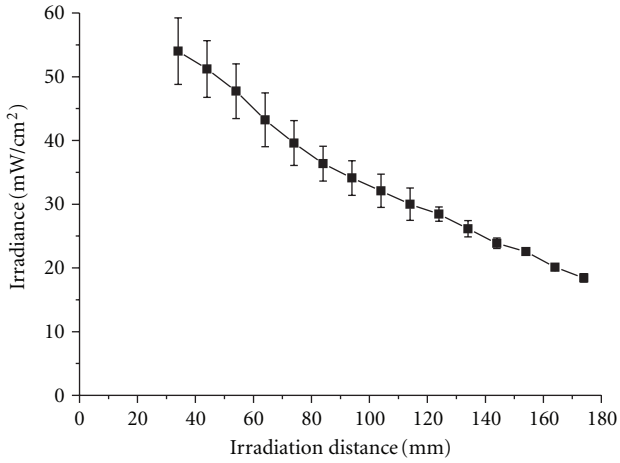

Figure 3: Irradiance as a function of the irradiation distance.

Figure 4(a). The irradiance was found to be good homogeneity within a field of the rectangular area (indicated by the solid line), which is approximately equal to the area of the standard multiwell plate. The average irradiance on the rectangular area was 18.6 mW/cm^2 with a standard deviation of 15%. In order to obtain different irradiances simultaneously, six optical attenuators with the transmissivity values of 0, 20%, 40%, 60%, 80%, and 100% were put onto the wells of the 96-well plate, and the irradiances of the six rectangular areas were shown in Figure 4(b). Different levels of irradiance can be simultaneously obtained with the optical attenuators, and the resulting average irradiances under the six attenuators were 0, 3.2, 7.0, 9.0, 12.7, and 20.3 mW/cm^2, respectively. Moreover, the irradiance almost remains constant during 20 min irradiation, while no significant warming of the LEDs can be detected (data not shown). The variance of irradiance under each attenuator was less than 10%, and there was no statistically significant difference for the cell viability between different wells under each attenuator, which can be found in the following PDT studies. As compared to the system that operates at a single fluence rate, this system would be very efficient for *in vitro* comparative PDT experiments. In particular, all the samples can be maintained in the same circumstance during the measurement.

3.3. The Media Temperature during the Irradiation. The temperature of the media increased when subjected to radiation, and the change in temperature of the culture medium used for *in vitro* PDT was monitored under the six different optical attenuators upon irradiation. In this study, the baseline temperature is about 37°C, which can be obtained directly from the measured prewarming media in the incubator prior to the light irradiation. Although the temperature of culture medium was increasing slowly upon the light irradiation, the increments were less than the maximum value of 1.5°C after 20 min, which caused no significant impact on PDT efficiency, as previously reported by Yang et al. [16].

3.4. CyTotoxic Effect of In Vitro PDT. The phototoxicity of 5-ALA-mediated PDT in CNE1 cells was assessed by MTT assay 24 h after PDT treatment. As shown in Figure 4(b), six different irradiances were simultaneously obtained by using the six optical attenuators. In this case, six different light doses (0, 3.8, 8.4, 10.8, 15.3, and 24.3 J/cm^2) were used for *in vitro* PDT treatment after 20 min of irradiation. The cell survival rates under the different light doses were shown in Figure 5. The survival rate of CNE1 cells was correlated well with the light dose, as expected. In the control groups, the cells incubated with 5-ALA for 4 h but without light irradiation showed no significant dark toxicity (data not shown).

4. Discussion

As for the *in vitro* PDT studies, a compact, low-cost, wavelength-specific, homogeneous, and large-area illumination system is widely desired. The traditional laser light sources can provide a monochromatic and very powerful illumination. Nevertheless, the main limitation of laser light sources is the limited irradiation area. Therefore, additional expanding optical systems are required to widen the beam, and each well in the standard multiwell plate has to be irradiated one by one, which is a relatively complicated and time-consuming experiment for PDT studies. Furthermore, the traditional laser light sources are relatively expensive, and careful maintenances are required. Compared to the laser light sources, the convenient lamps available for PDT have the advantage that they can be spectrally filtered to match the maximum absorption of any photosensitizers for treatment of large area [2, 6]. However, spectral filtering for lamps may lead to the dramatic fluence rates reduction. Additionally, in order to avoid significant thermal effects, the fluence rates have to be limited to the relatively low values [5].

In an effort to overcome the limitations of the current light sources applied in PDT treatments, we have successfully developed an LED array-based illumination system. The performance test suggests that the LED-based illumination system can provide a power-adjustable, wavelength-specific, homogeneous, and large-area illumination for *in vitro* PDT studies, and the survival rate of CNE1 cells was correlated well with the light fluence over a range of treatment conditions. Moreover, no additional optical system is required for achieving a homogeneous and large-area irradiation, which is convenient in operation. In addition, because of the availability of various wavelength LEDs, a LED-based illumination system with an appropriate wavelength can be readily developed as a light source to match the maximal absorption of the photosensitizers used in PDT studies.

5. Conclusions

A LED array based illumination system was successfully developed to provide low-cost, stable, power-adjustable, wavelength-specific, homogeneous, and large-area illumination specifically for *in vitro* PDT experiments. The irradiances can be continuously adjusted in a range from 18 to

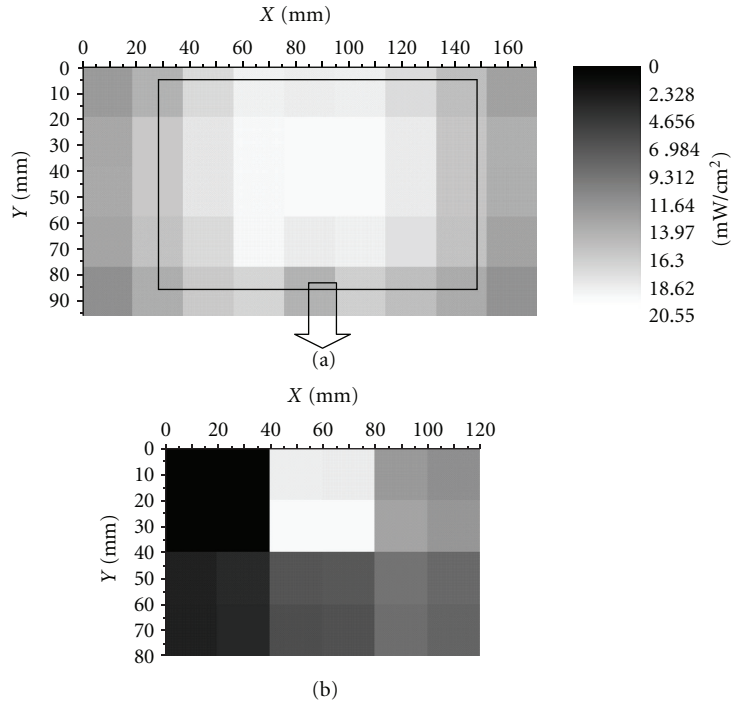

Figure 4: (a) Homogeneity of the irradiance for the irradiation distance of 164 mm between the LED array and treatment area, and the rectangular area is approximately equal to the area of the standard multiwell plate used for PDT studies. (b) Under the six different attenuators, the irradiances of the rectangular areas were 0, 3.2, 7.0, 9.0, 12.7, and 20.3 mW/cm^2, respectively.

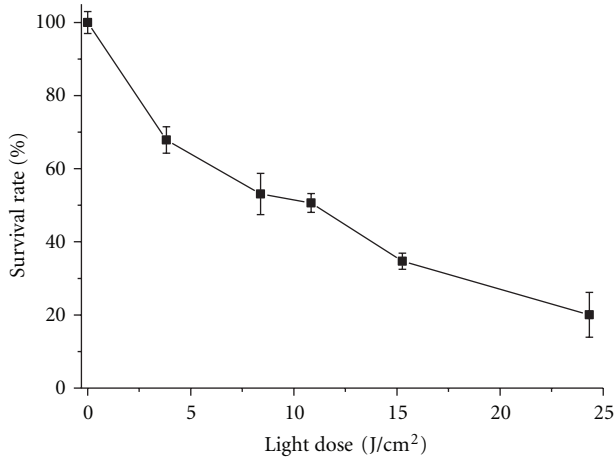

Figure 5: The cell survival rate of CNE1 cells after 5-ALA medicated PDT.

54 mW/cm^2 with an output wavelength centered at 643 nm. Furthermore, different irradiances can be simultaneously available for comparative PDT studies by using different optical attenuators. The efficiency of the illumination system was demonstrated by carrying out the 5-ALA-medicated PDT for CNE1 cells, and the obtained results suggest that the LED-based illumination system is a convenient and promising light source for PDT studies.

Acknowledgments

This work was supported by the National Natural Science Foundation of China (60978070), the Natural Science Foundation for Distinguished Young Scholars of Fujian Province (2011J06022), the program for New Century Excellent Talents in University of China (NCET-10-0012), and the Program for Changjiang Scholars and Innovative Research Team in University (IRT1115).

References

[1] P. Agostinis, K. Berg, K. A. Cengel et al., "Photodynamic therapy of cancer: an update," *CA Cancer Journal for Clinicians*, vol. 61, no. 4, pp. 250–281, 2011.

[2] B. C. Wilson and M. S. Patterson, "The physics, biophysics and technology of photodynamic therapy," *Physics in Medicine and Biology*, vol. 53, no. 9, pp. R61–R109, 2008.

[3] J. P. Celli, B. Q. Spring, I. Rizvi et al., "Imaging and photodynamic therapy: mechanisms, monitoring, and optimization," *Chemical Reviews*, vol. 110, no. 5, pp. 2795–2838, 2010.

[4] Y. Shen, H. Y. Lin, Z. F. Huang, D. F. Chen, B. H. Li, and S. S. Xie, "Indirect imaging of singlet oxygen generation from a single cell," *Laser Physics Letters*, vol. 8, no. 3, pp. 232–238, 2011.

[5] L. Brancaleon and H. Moseley, "Laser and non-laser light sources for photodynamic therapy," *Lasers in Medical Science*, vol. 17, no. 3, pp. 173–186, 2002.

[6] Z. Huang, "A review of progress in clinical photodynamic therapy," *Technology in Cancer Research and Treatment*, vol. 4, no. 3, pp. 283–293, 2005.

[7] T. S. Mang, "Lasers and light sources for PDT: past, present and future," *Photodiagnosis and Photodynamic Therapy*, vol. 1, no. 1, pp. 43–48, 2004.

[8] C. A. Morton, S. B. Brown, S. Collins et al., "Guidelines for topical photodynamic therapy: report of a workshop of the British Photodermatology Group," *British Journal of Dermatology*, vol. 146, no. 4, pp. 552–567, 2002.

[9] P. Babilas, E. Kohl, T. Maisch et al., "*In vitro* and *in vivo* comparison of two different light sources for topical photodynamic therapy," *British Journal of Dermatology*, vol. 154, no. 4, pp. 712–718, 2006.

[10] A. Juzeniene, P. Juzenas, L.-W. Ma, V. Iani, and J. Moan, "Effectiveness of different light sources for 5-aminolevulinic acid photodynamic therapy," *Lasers in Medical Science*, vol. 19, no. 3, pp. 139–149, 2004.

[11] A. Pieslinger, K. Plaetzer, C. B. Oberdanner et al., "Characterization of a simple and homogeneous irradiation device based on light-emitting diodes: a possible low-cost supplement to conventional light sources for photodynamic treatment," *Medical Laser Application*, vol. 21, no. 4, pp. 277–283, 2006.

[12] J. Neupane, S. Ghimire, S. Shakya, L. Chaudhary, and V. P. Shrivastava, "Effect of light emitting diodes in the photodynamic therapy of rheumatoid arthritis," *Photodiagnosis and Photodynamic Therapy*, vol. 7, no. 1, pp. 44–49, 2010.

[13] F. Z. Trindade, A. C. Pavarina, A. P. D. Ribeiro, V. S. Bagnato, C. E. Vergani, and C. A. de Souza Costa, "Toxicity of photodynamic therapy with LED associated to Photogem: an *in vivo* study," *Lasers in Medical Science*, vol. 27, no. 2, pp. 403–411, 2012.

[14] T. Mosmann, "Rapid colorimetric assay for cellular growth and survival: application to proliferation and cytotoxicity assays," *Journal of Immunological Methods*, vol. 65, no. 1-2, pp. 55–63, 1983.

[15] M. Atif, M. Fakhar-E-Alam, S. Firdous, S. S. Z. Zaidi, R. Suleman, and M. Ikram, "Study of the efficacy of 5-ALA mediated photodynamic therapy on human rhabdomyosarcoma cell line (RD)," *Laser Physics Letters*, vol. 7, no. 10, pp. 757–764, 2010.

[16] J. Yang, A. C. Chen, Q. Wu et al., "The influence of temperature on 5-aminolevulinic acid-based photodynamic reaction in keratinocytes *in vitro*," *Photodermatology, photoimmunology & photomedicine*, vol. 26, no. 2, pp. 83–88, 2010.

Hindawi Publishing Corporation
International Journal of Photoenergy
Volume 2012, Article ID 838496, 7 pages
doi:10.1155/2012/838496

Research Article

Effects of Low-Intensity Laser Irradiation on Wound Healing in Diabetic Rats

Hui Ma,[1,2] Ying-xin Li,[2,3] Hong-li Chen,[1,2] Mei-ling Kang,[1,2] and Timon Cheng-Yi Liu[4]

[1] *School of Biomedical Engineering, Tianjin Medical University, Tianjin 300070, China*
[2] *Tianjin Laser Medical Technology Engineering Center, Tianjin 300350, China*
[3] *Institute of Biomedical Engineering, Chinese Academy of Medical Science & Peking Union Medical College, Tianjin 300192, China*
[4] *Laboratory of Laser Sports Medicine, South China Normal University, Guangzhou 510006, China*

Correspondence should be addressed to Ying-xin Li, yingxinli2005@yahoo.com.cn

Received 19 October 2011; Revised 3 December 2011; Accepted 19 December 2011

Academic Editor: Rui Duan

Objective. The effects of low-intensity 630 nm semiconductor laser irradiation at 3.6 J/cm^2 (LISL) on wound healing in diabetic rats were studied in this paper. *Methods.* 36 diabetic rats with dorsal cutaneous excisional wounds were divided into three LISL groups and a control group randomly. The three LISL groups were irradiated with LISL at 5, 10, and 20 mW/cm^2 five times a week for two weeks, respectively. The process of wound healing was assessed by assessing blood glucose, calculating percentage of wound closure, histopathological evaluation, and immunohistochemical quantification. *Results.* Blood glucose of all groups remained at similar levels throughout the experiment. LISL could obviously promote wound contraction, fibroblasts proliferation, and collagen synthesis, alter bFGF and TGF-β1 expression, and reduce inflammatory reaction in the early and middle phases of chronic wound-healing process. However, LISL could not shorten cicatrization time, and the treatment effects were not sensitive to illuminate parameters in the later phase of the experiment. *Conclusions.* LISL might have auxiliary effects in the early and middle phases of wound healing in STZ-induced diabetic rats, but the reciprocity rule might not hold. The wound-healing process of early-phase diabetes rats shows typical characteristics of self-limited disease.

1. Introduction

Diabetes is a complex metabolic disorder involving many body organs and systems and can devastate the lives of affected individuals [1]. It is estimated that global prevalence of diabetes gets to 6.6% (285 million people) in 2010, and the number of people with diabetes will have risen to 438 million or 7.8% of the world's population by 2030 [2]. Impaired wound healing is a complication of diabetes and a serious problem in clinical practice [3]. As many as 15% of people with diabetes will develop foot ulceration and wounds, and 3% will have a lower limb amputation [4, 5].

Photobiomodulation (PBM) is a modulation of laser irradiation (LI) or monochromatic/broad band light on biosystems, which stimulates or inhibits biological functions but does not result in irreducible damage. The LI used in PBM is always low intensity-LI (LIL), ~10 mW/cm^2. However, moderate-intensity LI (MIL), $10^{2\sim3}$ mW/cm^2, is of PBM if the irradiation time is not so long that it damages organelles or cells.

In recent years, PBM has gained considerable recognition and importance among treatment modalities for various medical problems including wound repair processes, musculoskeletal complications, and pain control [6–8]. Many literatures were reported that PBM can promote the healing process by reducing pain and inflammation, promoting cells proliferation, facilitating collagen synthesis, fostering immunity, and increasing wound tensile strength [4, 8–12].

A substantial amount of studies show that PBM with appropriate treatment parameters can promote the chronic wound healing in diabetic rats [13–15]. LI at 630 nm in visible red-light region was generally believed as the optimum wavelength, but significant beneficial effects have also been observed on diabetic rats for LI at 532, 810, and 980 nm [4]. Range of power density options varied considerably (from LIL to MIL). It's worth noting that

Table 1: Groups of experiment and treatment parameters.

	Power density (mW/cm^2)	Irradiation time (min)	Energy density (J/cm^2)	Treatment schedule (times/week)	Number of rats
Control group	0	0	0	0	9
5 mW/cm^2 group	5	12	3.6	5	9
10 mW/cm^2 group	10	6	3.6	5	9
20 mW/cm^2 group	20	3	3.6	5	9

a lately study by Akyol and Güngörmüş [8] suggested that 808 nm MIL at 100 mW/cm^2 has a beneficial effect on the early recovery of skin incisions in female Wistar rats with streptozotocin (STZ)-induced diabetes. There were significant differences between the MIL group and control group in both reepithelialization and inflammation at 10th day. However, the differences disappeared both in inflammation and reepithelialization at 20th day. This is typical of self-limited disease, which indicates that the wound of early phase diabetes can heal completely by itself. Similar phenomenon had been mentioned in conventional wound-healing process [16, 17]. Recently, a research even suggested that diabetes may be also self-limited, and the abnormalities underlying diabetes are reversible [18].

The aims of our paper was to study the effects of low-intensity laser irradiation (LIL) on the wound healing of male Wistar rats with STZ-induced diabetes. With more detailed and comprehensive methods than Akyol et al.'s study, we tried to gain better insight into the healing process more deeply, to verify the characteristics of self-limited disease in the wound-healing process, and to offer an appropriate intensity at 3.6 J/cm^2 for further study.

2. Material and Methods

2.1. Animals. Thirty-six male Wistar rats weighing 220–250 g from the animal house of Institute of Radiation Medicine Chinese Academy of Medical Sciences were used in this study. During the study, the rats were housed 9 per cage, maintained under controlled environmental conditions (12-hours light/dark cycle, temperature 23°C), and provided with standard laboratory food and water *ad libitum*.

2.2. Induction of Diabetes. Diabetes was chemically induced using STZ (Sigma Co., USA), 40 mg/kg, dissolved in citrate buffer (pH 4.4) and administered as tail vein injection in all rats. Seven days after STZ injection, blood glucose levels were measured using a glucometer and test strips (One Touch Ultra; IifeScan Co., USA), and all STZ-injected rats with a blood glucose of 16.5 mmol/L or more were included in the protocol.

2.3. Wound Surgery. Before surgery, the blood glucose level of each rat was checked again. Each rat was anesthetized with 10% chloral hydras (300 mg/kg) intraperitoneally. The hair on the dorsum of all rats was shaved using an electric clipper. The operative site was prepared aseptically. Two incisions (10 mm $*$ 10 mm square) were made on the dorsum of each rat using a steel scalpel (Rockwell number 15). One incision was performed on the left side of the dorsum and the other was on the right.

2.4. Groups of Experiment and Treatment Parameters. Thirty-six rats were randomly divided into 4 groups: 5 mW/cm^2 group, 10 mW/cm^2 group, 20 mW/cm^2 group, and control group, 9 rats per group. The study was performed using a 630 nm continuous semiconductor laser system designed by Laser Medical Laboratory of Institute of Biomedical Engineering, Chinese Academy of Medical Science & Peking Union Medical College. The output power was measured using a laser power meter (SOLO PE; Gentec-EO Inc., Canada). The laser treatment parameters are listed in Table 1. PBM was started immediately after surgery and repeated 5 times/week for two weeks. The laser beam was aligned to cover the entire wound area, including the boundaries.

2.5. Blood Glucose Level. Before surgery and 14 days after wounding, the blood glucose level of each rat was checked.

Average blood glucose was presented as mean blood glucose ± SEM and compared with Matching T test.

2.6. Percentage of Wound Closure. At 3, 6, 9, and 12 days after wounding, the areas of wounds on all rats were recorded with standardized photography, and calculated the percentage of wound closure by ImageJ (http://rsb.info.nih.gov/ij/). Percentage of wound closure was calculated using the following formula [19]: [(Area of 1 Day − Area of X Days)/Area of 1 Day] × 100%. Average wound closure percentage was presented as mean percentage ± SEM and compared with one-way ANOVA with Tukey posttest.

2.7. Histopathological Evaluation. At 4, 8, and 14 days after wounding, 3 rats were chosen from each group randomly and killed by ether inhalation. The tissue specimens were stained with hematoxylin and eosin, examined with a semiquantitative method [10] to evaluate following histological features: polymorphonuclear leukocytes (PMNLs), reepithelization, fibroblasts, new vessels, and collagen synthesis. The sections were studied by two independent observers and evaluated on a scale of 0–4. Observers were blinded for the study of the specimens. Average semiquantitative evaluation score was presented as mean score ± SEM and compared with the nonparametric Kruskal-Wallis test.

2.8. Immunohistochemical Quantification. At 4, 8, and 14 days after wounding, the tissue specimens were fixed for 24

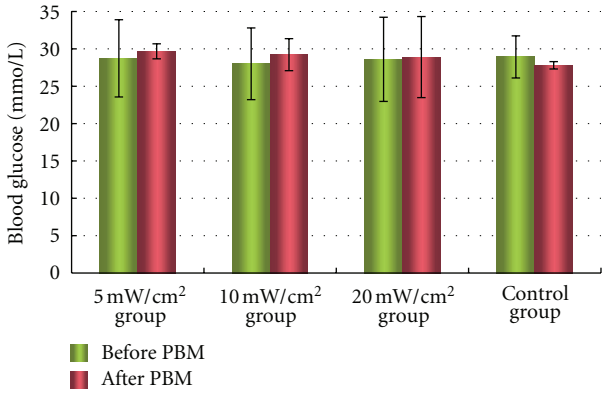

Figure 1: Blood glucose levels of all groups throughout the experiment.

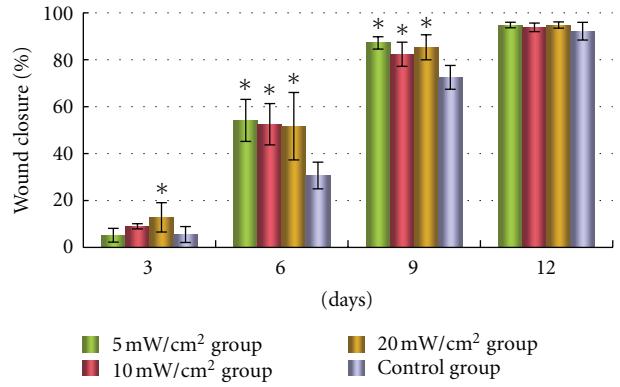

Figure 2: Percentage of wound closure throughout the experiment. Asterisk means that this group has statistical difference with control group ($P < 0.05$).

hours in 4% paraformaldehyde prior to being embedded in paraffin and sectioned (longitudinal section perpendicular to wound surface, 5 μm). The tissue was deparaffinized, rehydrated, and blocked with an appropriate blocking solution. Tissue was incubated at 4°C overnight with an antibody to basic fibroblast growth factor (bFGF) (SC-79; Santa Cruz Inc., USA) or transforming growth factor β1 (TGF-β1) (SC-146; Santa Cruz Inc., USA) followed by incubation with secondary antibody at 37°C for 20 minutes. Choose 5 sections per slide, analysis and read the immunohistochemical score (Image-Pro Plus; Media Cybernetics Inc., USA) using a method modified from that described by Soslow et al. [20]. Average immunohistochemical score (IHS) was presented as mean IHS ± SEM and compared with one-way ANOVA with Tukey posttest.

3. Results

3.1. Blood Glucose Level. There was no significant difference among diabetic rats that had been randomly placed into the 4 groups at the beginning of the experiment ($P > 0.05$). Blood glucose remained at similar levels throughout the experiment, with no significant difference between values before and after PBM ($P > 0.05$). At the end of the experiment, blood glucose of all rats (both control group and three PBM groups) were still in pathological blood glucose range (more than 16.5 mmol/L) with no significant difference ($P > 0.05$) (Figure 1).

3.2. Percentage of Wound Closure. At 3 days after wounding, only wounds of 20 mW/cm^2 group closed significantly faster than control group ($P < 0.05$). Wound closure percentages of other groups showed no significant difference ($P > 0.05$).

At 6 and 9 days after wounding, wounds of all three PBM groups closed significantly faster than control group ($P < 0.05$), but there was no significant difference among 5 mW/cm^2 group, 10 mW/cm^2 group, and 20 mW/cm^2 group ($P > 0.05$).

At 12 days after wounding, percentage of wound closure in all groups remained at similar levels ($P > 0.05$) (Figure 2).

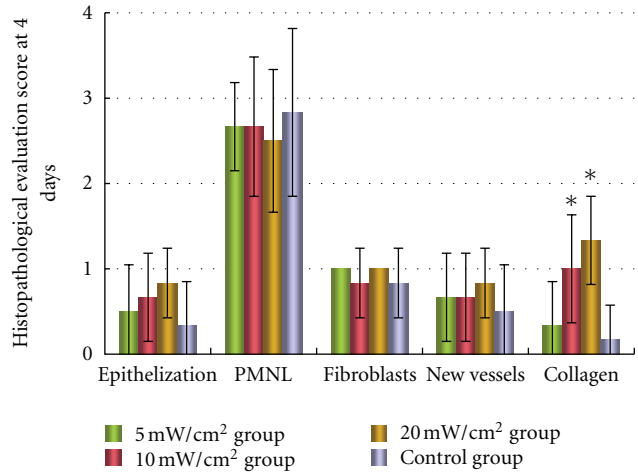

Figure 3: The semiquantitative histopathological evaluation score at 4 days after wounding. Asterisk means that this group has statistical difference with control group ($P < 0.05$).

3.3. Histopathological Evaluation

3.3.1. 4 Days. Remarkable inflammatory exudation and necrotic tissue could be observed in all tissue specimens. Comparable numbers of PMNLs, reepithelization, new vessels, and fibroblasts were recorded in all groups. However, there were significant differences in the creation of new collagen fibers between control group and 10 mW/cm^2 group ($P < 0.05$) or 20 mW/cm^2 group ($P < 0.05$) (Figure 3).

3.3.2. 8 Days. Attenuated inflammation, mature granulation tissue, extensive collagen deposition, and greater reepithelization can be observed in three PBM groups. Control group had more inflammatory exudates and fresh granulation tissue (Figure 4).

The histological evaluation score of reepithelization, numbers of PMNLs, fibroblasts, and new collagen fibers, except for new vessels, shown significant differences between control group and 20 mW/cm^2 group ($P < 0.05$). There were significant differences in extensive fibroblasts and new

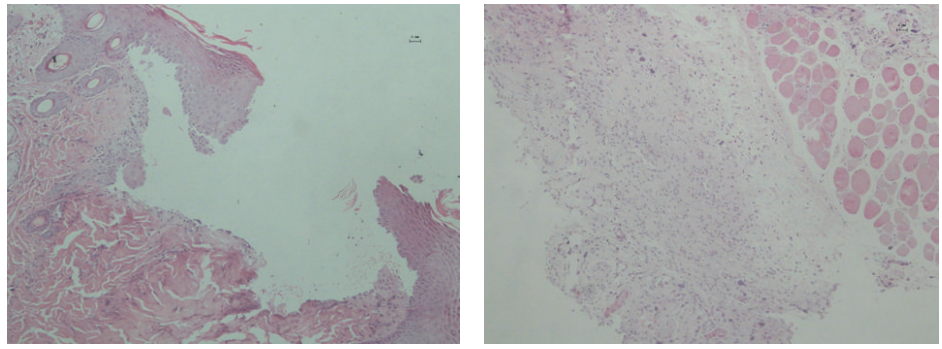

(a) (b)

Figure 4: Photomicrograph of tissue samples from 20 mW/cm^2 group (a) and control group (b) at 8 days after wounding (HE stain × 100).

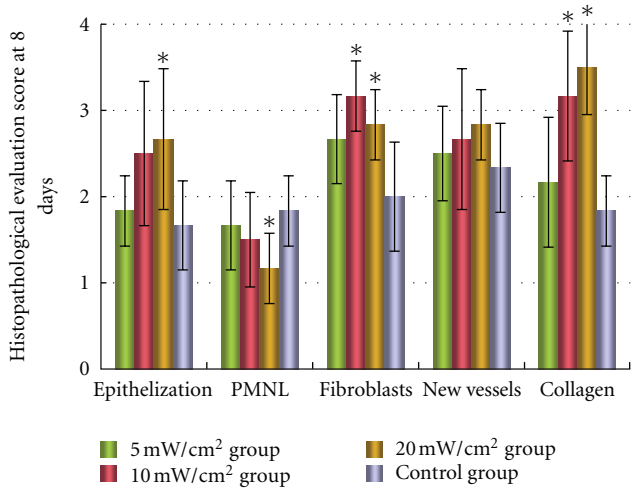

Figure 5: The semiquantitative histopathological evaluation score at 8 days after wounding. Asterisk means that this group has statistical difference with control group ($P < 0.05$).

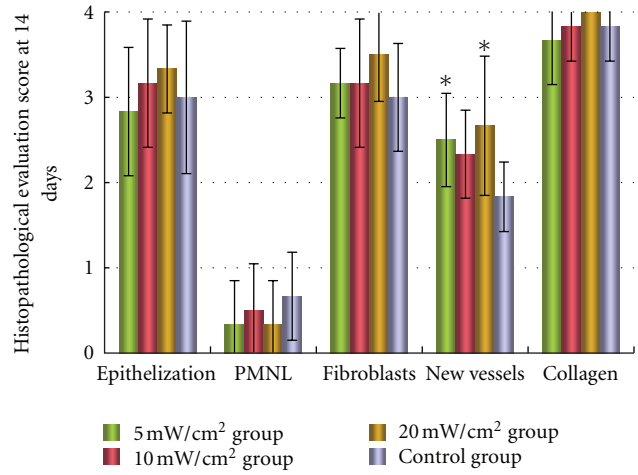

Figure 6: The semiquantitative histopathological evaluation score at 14 days after wounding. Asterisk means that this group has statistical difference with control group ($P < 0.05$).

collagen fibers between control group and 10 mW/cm^2 group ($P < 0.05$). The new vessels in all four groups were at similar level and had no significant differences ($P > 0.05$) (Figure 5).

3.3.3. 14 Days. New epithelial cells of all groups have covered almost all wounds, capillary gradually closed, granulation tissue gradually replaced with fibrous scar, fibroblasts decreased, and intercellular collagen content increased. The progress of wound healing in 4 groups was similar. However, there were significant differences in the evaluation score of new vessels between control group and 5 mW/cm^2 group or 20 mW/cm^2 group ($P < 0.05$), except 10 mW/cm^2 group (Figure 6).

3.4. Immunohistochemical Quantification. bFGF and TGF-β1 protein expression at 4, 8, and 14 days after wounding revealed that growth factors were mainly located in the inflammatory cells (macrophages), granulation tissues (fibroblasts), and the surrounding newly formed capillaries.

IHS analysis revealed that bFGF expression in all PBM groups increased significantly compared with the control group ($P < 0.05$) at 4 days after wounding. 5 mW/cm^2 group had a significant bFGF increase in comparison to control group at 8 days after wounding ($P < 0.05$). There were no significant difference between irradiated groups and control group at 14 days after wounding ($P > 0.05$) (Figure 7).

TGF-β1 protein expression in 10 mW/cm^2 group at 4 days after wounding increased significantly compared with other groups ($P < 0.05$). However, there were no significant differences between PBM groups and control group at 8 and 14 days after wounding ($P > 0.05$) (Figure 8).

4. Discussion

The wound-healing process consists of four highly integrated and overlapping phases: hemostasis, inflammation, proliferation, and tissue remodeling [21]. It is widely accepted that chronic healing of diabetes wounds always accompanied with prolonged inflammation and decreased matrix accumulation [22].

Table 2: The differences of the animal models in two studies.

	Numbers of rats	The gender of rats	Wound surgery	Wound size in length (mm)	Position of control group and LLLT group
Akyol et al.'s study	18	Female	Diode laser	15	On the same rat
Current study	36	Male	Steel scalpel	10	On different rats

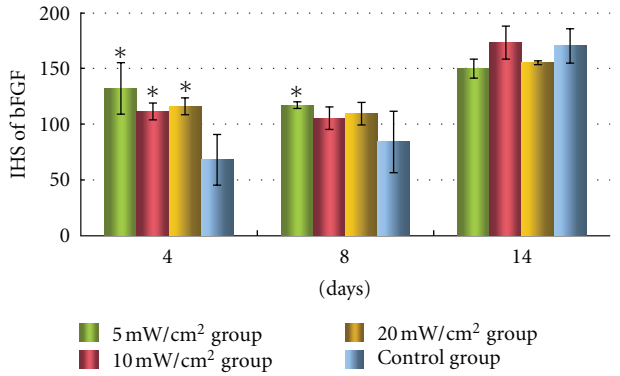

Figure 7: Immunohistochemical score (IHS) of bFGF protein expression throughout the experiment. Asterisk means that this group has statistical difference with control group ($P < 0.05$).

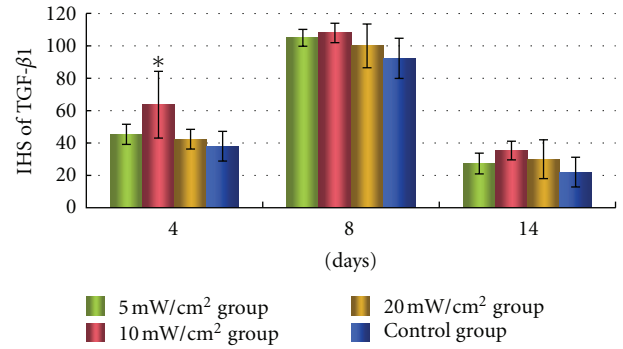

Figure 8: Immunohistochemical score (IHS) of TGF-β1 protein expression throughout the experiment. Asterisk means that this group has statistical difference with control group ($P < 0.05$).

Table 3: The differences of the laser treatment parameters in two studies.

	Wavelength (nm)	Power density (mW/cm^2)	Energy density (J/cm^2)	Total treatment times
Akyol et al.'s study	808	100	2	5
Current study	630	5–20	3.6	10

Our histopathological study found that attenuated inflammation, greater reepithelization, mature granulation tissue (fibroblasts), and extensive collagen deposition can be observed in PBM groups at 8 days after wounding, especially in 20 mW/cm^2 group. At the same time, the control group had more inflammatory exudates and fresh granulation tissue. These phenomena are consistent with the analysis of wound closure percentage data that PBM can obviously promote wound contraction, especially among 6–9 days after wounding. Results from our investigation are also in agreement with some previous published studies [10, 23, 24] that PBM are able to promote wound healing by reducing inflammation without compromising the proliferation of fibroblasts and keratinocytes.

The process of wound healing is precisely executed and regulated by a number of growth factors spatially and temporally. As is known to all, bFGF has potent effects on wound-healing process. It plays a vital role in regulating the synthesis and deposition of various extracellular medium components, increasing keratinocyte motility during reepithelization, and promoting the migration of fibroblasts and collagenase production [25–29]. TGF-β1 has increased expression from the very beginning of injury and is of particular importance to modulate events of wounding healing [25]. TGF-β1 enhances the wound repair by influencing cells proliferation and migration, angiogenesis, extracellular matrix synthesis, and deposition [30, 31].

Our current study investigated that the amount of growth factor productions was significantly altered in diabetic wounds with LIL, especially at 4 days after wounding. The results suggest that LIL promoted wound-healing process by influencing the levels of relevant growth factors, and then promoting cells proliferation and migration, regulating extracellular matrix synthesis and deposition. These are consistent with the aforementioned pathological analysis. It should point out that some growth factors protein expression always decrease in chronic healing wounds [25, 32]. It appeared that the LIL might be a candidate to replace growth factors in clinically treatment [33].

Some literatures have reported that PBM increases bFGF immunolabeling rather than gene expression [19, 34]. It suggested that the observed bFGF immunolabeling increase might derive from bFGF secretion or protein production, instead of de novo synthesis. LIL is capable of activating the latent TGF-β1 complex in vitro, and its expression pattern in vivo suggests that TGF-β1 plays a central role in mediating the accelerated healing response [35]. In this study, LIL at 5 mW/cm^2 increased bFGF protein expression at 4 or 8 days after wounding, LIL at 10 mW/cm^2 increased both bFGF and TGF-β1 protein expression at 4 days after wounding, but LIL at 20 mW/cm^2 increased bFGF protein expression only at 4 days after wounding. The variation of bFGF in the 5 mW/cm^2 group at 8 days is much smaller compared to those of other groups. This may explain why only this group had a statistically significant increase in bFGF compared to the control group. However, the expression pattern of TGF-β1

Table 4: The differences of the evaluate parameters in two studies.

	research methods	Evaluate parameters	Observate time (after wounding)
Akyol et al.'s study	Histopathological evaluation	Reepithelialization; inflammation	10 and 20 days
Current study	Morphology evaluation; histopathological semievaluation; immunohistochemical quantification	Wound closure percentage; PMNLs, reepithelization, fibroblasts, new vessels, and collagen synthesis; bFGF and TGF-β1 protein production	3, 6, 9, and 12 days for morphology evaluation; 4, 8, and 14 days for histopathological and immunohistochemical evaluation

did not show any change after LIL at both 8 and 14 days after wounding in our study. The expression patterns in all PBM groups, both bFGF and TGF-β1, were similar with control group at 14 days after wounding. In an attempt to further understand the impact of LIL on regulating relevant growth factors, further experiments with larger sample size and advanced technologies should be conducted.

According to the reciprocity rule, the same LI dose has the same PBM. It holds for MIL but does not for LIL. The latter was supported in this study. In addition, LIL at the same dose and different power densities exert different regulatory effects on bFGF (8 days after wounding) and TGF-β1 (4 days after wounding) in our study. LIL at 20 mW/cm^2 performed more effective than the one at 5 or 10 mW/cm^2 in the evaluated histological parameters and wound contraction percentage. Moreover, taking the length of the treatment time into consideration, we may choose 20 mW/cm^2 in our further experiments with 630 nm 3.6 J/cm^2 continuous semiconductor laser and consider it as the optimum among the power densities we used.

It is worth noting that no matter what illuminate parameters we used (including control group), the wounds contracted mostly and various evaluated parameters were not sensitive to illuminate parameters (4 groups had similar pathologic and immunohistochemical scores) at 14 days after wounding. In other words, LIL cannot shorten cicatrization time, even though it performed positively in the early and middle phases of wound-healing process, which is similar with the study by Akyol and Güngörmüş [8] using MIL at 100 mW/cm^2. This is typical of self-limited disease, which means that the wound of early-phase diabetes can heal completely by itself without the laser therapy. Similar phenomenon had been mentioned in conventional wound-healing process [16, 17], but rarely reported in healing of diabetes wound. Interestingly, there existed a lot of distinctions between the study of Akyol et al.'s and ours (Tables 2, 3, and 4). Anyway, both LIL and MIL have undeniable effects to facilitate wound healing as an auxiliary treatment by diminishing inflammatory exudation, enhancing wound contraction, avoiding infection, and ameliorating local pain and tumefaction in the early and middle phases.

5. Conclusions

630 nm LIL at 3.6 J/cm^2 might have auxiliary effects in the early and middle phases of wound healing of male Wistar rats with STZ-induced diabetes, but the reciprocity rule did not hold. The wound-healing process of early-phase diabetes rats shows typical characteristics of self-limited disease, and the laser therapy cannot shorten the wound cicatrization time.

Acknowledgment

This work was supported by National Science Foundation of China (60878061).

References

[1] A. K. Khuwaja, L. A. Khowaja, and P. Cosgrove, "The economic costs of diabetes in developing countries: some concerns and recommendations," *Diabetologia*, vol. 53, no. 2, pp. 389–390, 2010.

[2] R. Colagiuri, "Diabetes: a pandemic, a development issue or both?" *Expert Review of Cardiovascular Therapy*, vol. 8, no. 3, pp. 305–309, 2010.

[3] H. Rafehi, A. El-Osta, and T. C. Karagiannis, "Genetic and epigenetic events in diabetic wound healing," *International Wound Journal*, vol. 8, no. 1, pp. 12–21, 2011.

[4] F. A. H. Al-Watban, X. Y. Zhang, and B. L. Andres, "Low-level laser therapy enhances wound healing in diabetic rats: a comparison of different lasers," *Photomedicine and Laser Surgery*, vol. 25, no. 2, pp. 72–77, 2007.

[5] T. Mandrup-Poulsen, "Diabetes," *British Medical Journal*, vol. 316, no. 7139, pp. 1221–1225, 1998.

[6] S. Hagiwara, H. Iwasaka, K. Okuda, and T. Noguchi, "GaAlAs (830 nm) low-level laser enhances peripheral endogenous opioid analgesia in rats," *Lasers in Surgery and Medicine*, vol. 39, no. 10, pp. 797–802, 2007.

[7] A. Schindl, M. Schindl, H. Pernerstorfer-Schön, and L. Schindl, "Low-intensity laser therapy: a review," *Journal of Investigative Medicine*, vol. 48, no. 5, pp. 312–326, 2000.

[8] U. Akyol and M. Güngörmüş, "The effect of low-level laser therapy on healing of skin incisions made using a diode laser in diabetic rats," *Photomedicine and Laser Surgery*, vol. 28, no. 1, pp. 51–55, 2010.

[9] P. Gál, M. Mokrý, B. Vidinský et al., "Effect of equal daily doses achieved by different power densities of low-level laser therapy at 635 nm on open skin wound healing in normal and corticosteroid-treated rats," *Lasers in Medical Science*, vol. 24, no. 4, pp. 539–547, 2009.

[10] K. Lacjaková, N. Bobrov, M. Poláková et al., "Effects of equal daily doses delivered by different power densities of low-level laser therapy at 670 nm on open skin wound healing in normal and corticosteroid-treated rats: a brief report," *Lasers in Medical Science*, vol. 25, no. 5, pp. 761–766, 2010.

[11] M. B. Kreisler, H. Al Haj, N. Noroozi, B. Willershausen, and B. d'Hoedt, "Efficacy of low level laser therapy in reducing postoperative pain after endodontic surgery—a randomized double blind clinical study," *International Journal of Oral and Maxillofacial Surgery*, vol. 33, no. 1, pp. 38–41, 2004.

[12] S. Nakaji, C. Shiroto, M. Yodono, T. Umeda, and Q. Liu, "Retrospective study of adjunctive diode laser therapy for pain attenuation in 662 patients: detailed analysis by questionnaire," *Photomedicine and Laser Surgery*, vol. 23, no. 1, pp. 60–65, 2005.

[13] A. G. Maiya, P. Kumar, and S. Nayak, "Photo-stimulatory effect of low energy helium-neon laser irradiation on excisional diabetic wound healing dynamics in wistar rats," *Indian Journal of Dermatology*, vol. 54, no. 4, pp. 323–329, 2009.

[14] G. K. Reddy, L. Stehno-Bittel, and C. S. Enwemeka, "Laser photostimulation accelerates wound healing in diabetic rats," *Wound Repair and Regeneration*, vol. 9, no. 3, pp. 248–255, 2001.

[15] S. B. Rabelo, A. B. Villaverde, R. A. Nicolau, M. A. Castillo Salgado, M. D. S. Melo, and M. T. T. Pacheco, "Comparison between wound healing in induced diabetic and nondiabetic rats after low-level laser therapy," *Photomedicine and Laser Surgery*, vol. 24, no. 4, pp. 474–479, 2006.

[16] V. Prabhu, S. B. S. Rao, N. B. Rao, K. B. Aithal, P. Kumar, and K. K. Mahato, "Development and evaluation of fiber optic probe-based helium-neon low-level laser therapy system for tissue regeneration-an in vivo experimental study," *Photochemistry and Photobiology*, vol. 86, no. 6, pp. 1364–1372, 2010.

[17] A. R. A. P. Medrado, L. S. Pugliese, S. R. A. Reis, and Z. A. Andrade, "Influence of low level laser therapy on wound healing and its biological action upon myofibroblasts," *Lasers in Surgery and Medicine*, vol. 32, no. 3, pp. 239–244, 2003.

[18] E. L. Lim, K. G. Hollingsworth, B. S. Aribisala, M. J. Chen, J. C. Mathers, and R. Taylor, "Reversal of type 2 diabetes: normalisation of beta cell function in association with decreased pancreas and liver triacylglycerol," *Diabetologia*, vol. 54, no. 10, pp. 2506–2514, 2011.

[19] K. R. Byrnes, L. Barna, M. Chenault et al., "Photobiomodulation improves cutaneous wound healing in an animal model of type II diabetes," *Photomedicine and Laser Surgery*, vol. 22, no. 4, pp. 281–290, 2004.

[20] R. A. Soslow, A. J. Dannenberg, D. Rush et al., "COX-2 is expressed in human pulmonary, colonic, and mammary tumors," *Cancer*, vol. 89, no. 12, pp. 2637–2645, 2000.

[21] S. Guo and L. A. DiPietro, "Factors affecting wound healing," *Journal of Dental Research*, vol. 89, no. 3, pp. 219–229, 2010.

[22] S. E. Thomson, S. V. McLennan, A. Hennessy et al., "A novel primate model of delayed wound healing in diabetes: dysregulation of connective tissue growth factor," *Diabetologia*, vol. 53, no. 3, pp. 572–583, 2010.

[23] P. M. do Nascimento, A. L. B. Pinheiro, M. Â. C. Salgado, and L. M. P. Ramalho, "A preliminary report on the effect of laser therapy on the healing of cutaneous surgical wounds as a consequence of an inversely proportional relationship between wavelength and intensity: histological study in rats," *Photomedicine and Laser Surgery*, vol. 22, no. 6, pp. 513–518, 2004.

[24] P. Gál, B. Vidinský, T. Toporcer et al., "Histological assessment of the effect of laser irradiation on skin wound healing in rats," *Photomedicine and Laser Surgery*, vol. 24, no. 4, pp. 480–488, 2006.

[25] S. Barrientos, O. Stojadinovic, M. S. Golinko, H. Brem, and M. Tomic-Canic, "Growth factors and cytokines in wound healing," *Wound Repair and Regeneration*, vol. 16, no. 5, pp. 585–601, 2008.

[26] Y. Sogabe, M. Abe, Y. Yokoyama, and O. Ishikawa, "Basic fibroblast growth factor stimulates human keratinocyte motility by Rac activation," *Wound Repair and Regeneration*, vol. 14, no. 4, pp. 457–462, 2006.

[27] W. Grellner, T. Georg, and J. Wilske, "Quantitative analysis of proinflammatory cytokines (IL-1β, IL-6, TNF-α) in human skin wounds," *Forensic Science International*, vol. 113, no. 1–3, pp. 251–264, 2000.

[28] G. Di Vita, R. Patti, P. D'Agostino et al., "Cytokines and growth factors in wound drainage fluid from patients undergoing incisional hernia repair," *Wound Repair and Regeneration*, vol. 14, no. 3, pp. 259–264, 2006.

[29] T. Sasaki, "The effects of basic fibroblast growth factor and doxorubicin on cultured human skin fibroblasts: relevance to wound healing," *Journal of Dermatology*, vol. 19, no. 11, pp. 664–666, 1992.

[30] S. M. Safavi, B. Kazemi, M. Esmaeili, A. Fallah, A. Modarresi, and M. Mir, "Effects of low-level He-Ne laser irradiation on the gene expression of IL-1β, TNF-α, IFN-γ, TGF-β, bFGF, and PDGF in rat's gingiva," *Lasers in Medical Science*, vol. 23, no. 3, pp. 331–335, 2008.

[31] Z. Kopecki, M. M. Luchetti, D. H. Adams et al., "Collagen loss and impaired wound healing is associated with c-Myb deficiency," *Journal of Pathology*, vol. 211, no. 3, pp. 351–361, 2007.

[32] M. C. Robson, "The role of growth factors in the healing of chronic wounds," *Wound Repair and Regeneration*, vol. 5, no. 1, pp. 12–17, 1997.

[33] T. I. Karu, "Multiple roles of cytochrome c oxidase in mammalian cells under action of red and IR-A radiation," *IUBMB Life*, vol. 62, no. 8, pp. 607–610, 2010.

[34] H. S. Yu, C. S. Wu, C. L. Yu, Y. H. Kao, and M. H. Chiou, "Helium-neon laser irradiation stimulates migration and proliferation in melanocytes and induces repigmentation in segmental-type vitiligo," *Journal of Investigative Dermatology*, vol. 120, no. 1, pp. 56–64, 2003.

[35] P. R. Arany, R. S. Nayak, S. Hallikerimath, A. M. Limaye, A. D. Kale, and P. Kondaiah, "Activation of latent TGF-β1 by low-power laser in vitro correlates with increased TGF-β1 levels in laser-enhanced oral wound healing," *Wound Repair and Regeneration*, vol. 15, no. 6, pp. 866–874, 2007.